UNIVERSITY OF BELGRADE
FACULTY OF CIVIL ENGINEERING

Isidora N. Jakovljević

DEMOUNTABLE SHEAR CONNECTIONS WITH BOLTS AND WELDED HEADED STUDS IN STEEL-CONCRETE COMPOSITE STRUCTURES

Doctoral Dissertation

Belgrade, 2022

УНИВЕРЗИТЕТ У БЕОГРАДУ

ГРАЂЕВИНСКИ ФАКУЛТЕТ

Исидора Н. Јаковљевић

ДЕМОНТАЖНИ СМИЧУЋИ СПОЈЕВИ ОСТВАРЕНИ ЗАВРТЊЕВИМА И МОЖДАНИЦИМА СА ГЛАВОМ КОД СПРЕГНУТИХ КОНСТРУКЦИЈА ОД ЧЕЛИКА И БЕТОНА

докторска дисертација

Београд, 2022

Supervisors: Prof. Zlatko Marković, PhD civ. eng.

                       University of Belgrade, Faculty of Civil Engineering

                       Associate Prof. Milan Spremić, PhD civ. eng.

                       University of Belgrade, Faculty of Civil Engineering

Committee members: Prof. Emeritus Dragan Buđevac, PhD civ. eng.

                       University of Belgrade, Faculty of Civil Engineering

                       Prof. Milan Veljković, PhD civ. eng.

                       Delft University of Technology, Faculty of Civil Engineering and
                       Geosciences, Department of Engineering Structures

                       Prof. Duško Lučić, PhD civ. eng.

                       Univeristy of Montenegro, Faculty of Civil Engineering in Podgorica

                       Associate Prof. Jelena Dobrić, PhD civ. eng.

                       University of Belgrade, Faculty of Civil Engineering

Defence date: _____

Ментори: др Златко Марковић, редовни професор

Универзитет у Београду, Грађевински факултет

др Милан Спремић, ванредни професор

Универзитет у Београду, Грађевински факултет

Чланови комисије: др Драган Буђевац, професор емеритус

Универзитет у Београду, Грађевински факултет

др Милан Вељковић, редовни професор

Delft University of Technology, Faculty of Civil Engineering and Geosciences, Department of Engineering Structures

др Душко Лучић, редовни професор

Универзитет Црне Горе, Грађевински факултет у Подгорици

др Јелена Добрић, ванредни професор

Универзитет у Београду, Грађевински факултет

Датум одбране: _____

Acknowledgements

DEMOUNTABLE SHEAR CONNECTIONS WITH BOLTS AND WELDED HEADED STUDS IN STEEL-CONCRETE COMPOSITE STRUCTURES

Abstract

The reuse of constructional elements or entire structures is an important approach in the construction industry that follows the concept of sustainable development. Steel-concrete composite structures enable the efficient use of material and savings in material consumption. However, widespread steel-concrete composite beams with welded headed stud shear connectors do not have the demountability feature and therefore cannot be entirely reused. In the past few decades, much research in the field of steel-concrete composite structures has been focused on the development and investigations of demountable floor systems. A further contribution to that field is provided in this thesis. A novel demountable shear connection with bolts and welded headed studs is proposed. The suggested connection is applicable in composite concrete slabs cast in open trough profiled steel sheeting. Welded headed studs are installed in sheeting ribs, whereas bolts are placed between ribs. Implementation of the additional plate or angles between the beam flange and the concrete slab is required. During the building deconstruction, bolts are removed and the composite concrete slab is easily separated from the steel beam with the possibility of being installed again. Destruction methods are avoided and the entire floor structure including concrete slabs and steel beams may be reused in another location in the same configuration as during the first life cycle.

The aim of the study is to promote the novel demountable connection with welded headed studs and bolts. The objectives of the research are to describe the demountable connection response to the shear load at the point of resistance and ductility, to identify failure mechanisms and propose instructions for the design. The developed demountable connection is examined by static push-out tests, conducting experimental and numerical investigations. The experimental work covers 20 push-out test specimens divided into eight series. Different configurations of the demountable steel-concrete connections are experimentally investigated: connections with continuous and discontinuous slabs over the supporting beam, connections with and without stirrup reinforcement around headed studs, connections with the angle between profiled sheeting ribs and the beam of 45°, 60° and 90°. The resistance, ductility and stiffness of demountable connections are compared with corresponding non-demountable connections with welded headed studs. According to the experimental research, the appropriate numerical finite element models are developed and used for a detailed analysis of the connection response and further parametric studies. A range of parameters that might influence the connection response is covered by parametric studies, including the headed stud diameter and height, bolt grade and diameter, concrete class, plate and angle thickness, the distance between the headed stud and slab edge, stirrup reinforcement diameter and position, the angle between sheeting ribs and the beam. The key influential parameters are identified and their effects on the connection performance are quantified. According to the wide set of the obtained data, conclusions regarding the connection response are drawn. Design recommendations for demountable shear connections with bolts and welded headed studs are proposed.

Key words: reusability, headed stud, bolt, shear connection, profiled steel sheeting, steel-concrete composite floor, shear resistance, push-out test, finite element analysis

Scientific field: Structural Engineering

Scientific subfield: Steel Structures

ДЕМОНТАЖНИ СМИЧУЋИ СПОЈЕВИ ОСТВАРЕНИ ЗАВРТЊЕВИМА И МОЖДАНИЦИМА СА ГЛАВОМ КОД СПРЕГНУТИХ КОНСТРУКЦИЈА ОД ЧЕЛИКА И БЕТОНА

Резиме

Принцип поновне употребе конструктивних елемената или целе конструкције у грађевинарству у складу је са концептом одрживог развоја. Спрегнуте конструкције од челика и бетона омогућавају ефикасну употребу материјала и уштеде у потрошњи. Међутим, спрегнуте греде од челика и бетона са завареним можданицима са главом које су у широкој примени, нису демонтажне и не могу се поново употребити. У претходних неколико деценија, многа истраживања у области спрегнутих конструкција бавила су се развојем и испитивањем демонтажних међуспратних конструкција. Допринос наведеној области дат је кроз ову дисертацију. Предложен је нови демонтажни смичући спој са завртњевима и можданицима са главом, као решење применљиво у спрегнутим плочама са трапезним профилисаним лимом. Постављање можданика предвиђено је у ребрима профилисаног лима, док се завртњеви постављају између, у превојима лима. Неопходна је примена додатног челичног лима или угаоника на контакту између ножице челичне греде и бетонске плоче. Током демонтаже, завртњеви се уклањају и спрегнута плоча се једноставно раздваја од челичног профила, уз могућност поновног коришћења. На овај начин, деструктивне методе су избегнуте и комплетна међуспратна контрукција се може поново употребити на другој локацији у истом облику као приликом првог животног циклуса.

Циљ научног истраживања је реализација иновативног демонтажног смичућег споја са можданицима са главом и завртњевима. Циљ је описати понашање демонтажног споја при дејству смичућег оптерећења у погледу носивости и деформабилности, идентификовати механизме лома и дати прорачунске препоруке. Демонтажни смичући спој је испитиван путем тестова смицања применом експерименталних и нумеричких метода. Експериментално испитивање обухвата 20 тестова смицања подељених у осам серија. Испитиване су различите конфигурације демонтажног споја: спојеви са континуалном и дисконтинуалном плочом изнад ослоначке греде, спојеви са и без узенгија постављених око можданика, спојеви са угловима између ребара профилисаног лима и осе носача од 45°, 60° и 90°. Носивост, дуктилност и крутост демонтажних спојева упоређене су са одговарајућим стандардним спојевима са завареним можданицима са главом. На основу експерименталних резултата, формирани су одговарајући нумерички модели, који су потом коришћени за детаљну анализу понашања споја и даљу параметарску анализу. Параметарском анализом обухваћени су различити параметри који би могли утицати на понашање споја, укључујући: пречник и висину можданика, пречник и класу чврстоће завртња, класу бетона, дебљину лима и угаоника, растојање између можданика и ивице бетонске плоче, пречник и позицију узенгија, угао између ребара профилисаног лима и осе носача. Идентификовани су кључни утицајни параметри и њихов ефекат је квантификован. На основу широког скупа добијених резултата, донети су закључци по питању понашања смичућег споја. Такође, дате су препоруке за пројекотовање демонтажног споја са завртњевима и можданицима са главом.

Кључне речи: поновна употреба, можданик, завртањ, смичући спој, профилисани лим, спрегнута међуспратна конструкција, носивост на смицање, тест смицања, метод коначних елемената

Научна област: Грађевинарство

Ужа научна област: Металне конструкције

Table of Contents

ix

List of Figures

xiv

List of Tables

Notation

Roman upper case letters:

A	cross-sectional area of a coupon
A_s	tensile stress area of a bolt
$A_{Wulst,eff}$	effective area of the weld collar of a headed stud [1]
C_1	calibration factor for shear resistance of a headed stud [2]
C_2	calibration factor for shear resistance of a headed stud [2], [3]
D_c	concrete compressive damage variable of concrete damage plasticity model [4]
D_t	concrete tensile damage variable of concrete damage plasticity model [4]
E	modulus of elasticity of steel
E_c	modulus of elasticity of concrete according to [5]
E_{cm}	secant modulus of elasticity of concrete [6]
F_{Rd}	design value of the shear resistance of a bolt [7]
$F_{p,C}$	bolt preloading force
F_u	shear resistance of the high strength bolt
$F_{u,f}$	frictional resistance of the high strength bolt
G_F	fracture energy of concrete [8]
K	ratio of the second stress invariant on the tensile meridian to the compressive meridian in concrete damage plasticity model [9]
L_0	original gauge length of a coupon
M_{pl}	plastic bending resistance of a headed stud [2], [3]
P	shear resistance of a headed stud connector
P_{Rd}	design value of the shear resistance of a headed stud connector [10]
$P_{Rd,c}$	design value of the shear resistance of a headed stud connector for concrete failure [1]
$P_{Rd,s}$	design value of the shear resistance of a headed stud connector for steel failure [1]
$P_{Rd,1}$	design value of the shear resistance of a headed stud connector for concrete failure [2], [3]
$P_{Rd,2}$	design value of the shear resistance of a headed stud connector for steel failure [2], [3]
P_{ult}	ultimate load of the push-out test specimen
$\overline{P}_{ult}$	mean value of the ultimate load of the push-out test specimens
R_g	reduction factor for the resistance of a headed stud in profiled steel sheeting [5]
R_p	reduction factor for the resistance of a headed stud in profiled steel sheeting [5]
W	section modulus of the concrete cone failure surface [2], [3]

Roman lower case letters:

b	width of the concrete slab; width of the flat coupon
b_c	ratio between the plastic and inelastic compressive strain of concrete [11]
b_m	mean width of the rib of open trough profiled steel sheeting or minimum width of the rib of re-entrant profiled steel sheeting [1]
b_{max}	maximum width of the profiled steel sheeting rib [2], [3]
b_t	ratio between the plastic and inelastic tensile strain of concrete [11]
b_{top}	width of the profiled steel sheeting rib at the top surface [2], [3]

b_0	mean width of the rib of open trough profiled steel sheeting or minimum width of the rib of re-entrant profiled steel sheeting [10]
d	diameter of the shank of a headed stud connector; diameter of a round coupon
d_b	bolt diameter
d_0	bolt hole diameter
d_{Wulst}	diameter of the weld collar of a headed stud [1]
e	distance between the rib wall and stud in the direction of shear force (measured at the rib mean width for open trough profiles; measured at the rib minimum width for re-entrant profiles) [1]
e_t	transverse spacing between headed studs inside the rib [3]
e_s	distance between the headed stud and slab edge in the transverse direction
$f_{c,cube}$	compressive strength of concrete cubes [6]
f_{ck}	characteristic value of the cylinder compressive strength of concrete [6]
f_{cm}	mean value of the cylinder compressive strength of concrete [6]
f_{ctk}	characteristic value of the axial tensile strength of concrete [6]
f_{ctm}	mean value of the axial tensile strength of concrete [6]
$f_{ct,sp}$	splitting tensile strength of concrete
f_{cuD}	compressive stress at the point D of the sinusoidal descending part of the concrete stress-strain curve [4]
f_{cuE}	compressive stress at the point E of the sinusoidal descending part of the concrete compressive stress-strain curve [4]
f_{cuF}	final residual strength of concrete [4]
f_c'	specified compressive strength of concrete according to [5]
f_u	ultimate tensile strength of steel
f_y	yield strength of steel
$f_{0.2}$	0.2% proof stress of non-linear material
h	overall depth of a concrete slab
h_A	anchorage length of the headed stud above the profiled steel sheeting [2], [3]
h_p	overall depth of the profiled steel sheeting
h_s	position of the upper plastic hinge in a headed stud [2]
h_{sc}	overall height of a stud connector
h_{Wulst}	height of the weld collar of a headed stud [1]
k_{flex}	reduction factor for the resistance of non-ductile shear connectors [12]
k_l	reduction factor for the resistance of a headed stud in profiled steel sheeting parallel to the supporting beam [10]
k_{sc}	stiffness of a shear connector [10]
k_t	reduction factor for the resistance of a headed stud in profiled steel sheeting transverse to the supporting beam [10]
k_u	correction factor for the shear resistance of a headed stud [3]
k_α	factor for the shear resistance of a headed stud in profiled steel sheeting with the angle between ribs and the beam α
$k_\perp$	reduction factor for the resistance of a headed stud in profiled steel sheeting transverse to the supporting beam [1]
n_r	number of stud connectors in one rib [10]

n_y	number of plastic hinges in a headed stud [2], [3]
t	thickness of profiled steel sheeting; thickness of the flat coupon
t_p	thickness of the plate or angle
w	crack opening [11]
w_c	critical value of the crack opening [11]

Greek letters and symbols:

α	factor for obtaining shear resistance of a headed stud [10]; angle between profiled sheeting ribs and the beam; reduction factor of sinusoidal descending part of the concrete compressive stress-strain curve [4]
α_{ct}	factor accounting for the relaxation in concrete strength [2]
α_{c2}	factor accounting for the relaxation in concrete strength [3]
α_N	factor for obtaining shear resistance of a headed stud [3]
α_{tD}	tangent factor at the point D of the sinusoidal descending part of the concrete compressive stress-strain curve [4]
α_{tE}	tangent factor at the point E of the sinusoidal descending part of the concrete compressive stress-strain curve [4]
β	shape factor for profiled steel sheeting [2]; parameter defining the shape of the stress-strain diagram [13]
γ_c	parameter defining the area under the stress-strain curve [11]
γ_v	partial safety factor for design shear resistance of a headed stud [10]
δ_u	maximum slip measured in a push-out test at the characteristic load level [10]
$\delta_{u,ps}$	maximum slip between the steel plate or angle and concrete slab measured in a push-out test at the characteristic load level
$\delta_{u,bs}$	maximum slip between the steel profile and plate or angle measured in a push-out test at the characteristic load level
ε_c	uniaxial compressive strain in the concrete
ε_c^{pl}	plastic compressive strain in the concrete
ε_{cuD}	compressive strain in the concrete at the point D of the sinusoidal descending part of the concrete compressive stress-strain curve [4]
ε_{cuE}	compressive strain in the concrete at the point E of the sinusoidal descending part of the concrete compressive stress-strain curve [4]
ε_{cuF}	compressive strain in the concrete at the point F at final residual strength of concrete [4]
ε_{c1}	compressive strain in the concrete at the maximum stress f_{cm} [6]
ε_u	tensile strain in the steel at the ultimate strength f_y
μ	slip factor; coefficient of friction; relative coordinate between points D and E on the concrete compressive stress-strain curve [4]
σ_c	uniaxial compressive stress in the concrete
σ_t	uniaxial tensile stress in the concrete
$\varnothing$	diameter of the bar

Subscripts:

anl	value obtained by the analytical expression
D	series D, demountable connection with a continuous slab over the supporting beam, with the angle between profiled sheeting ribs and the beam of 90°
DL	series DL, demountable connection with a discontinuous slab over the supporting beam, with the angle between profiled sheeting ribs and the beam of 90°
DLU	series DLU, demountable connection with a discontinuous slab over the supporting beam and U-bars passing around headed studs, with the angle between profiled sheeting ribs and the beam of 90°
D45	series D45, demountable connection with a continuous slab over the supporting beam, with the angle between profiled sheeting ribs and the beam of 45°
D60	series D60, demountable connection with a continuous slab over the supporting beam, with the angle between profiled sheeting ribs and the beam of 60°
EN	value obtained according to EN 1994-1-1:2004 [10]
exp	experimental value
fea	numerical value obtained through finite element analysis
K	value obtained according to the model proposed by Konrad [1]
NDL	demountable connection with a discontinuous slab over the supporting beam, but in contrast to the connection DL, a vertical angle leg is not present on the slab edge
NDLU	demountable connection with a discontinuous slab over the supporting beam and U-bars passing around headed studs, but in contrast to the connection DLU, a vertical angle leg is not present on the slab edge
nor	normalised value
S	series S, non-demountable connection with a continuous slab over the supporting beam, with the angle between profiled sheeting ribs and the beam of 90°
SC4	value obtained according to the model proposed by the working group CEN/TC250/SC4.PT3 [3]
Sα	non-demountable connection with a continuous slab over the supporting beam, with the angle between profiled sheeting ribs and the beam α
S45	series S45, non-demountable connection with a continuous slab over the supporting beam, with the angle between profiled sheeting ribs and the beam of 45°
S60	series S60, non-demountable connection with a continuous slab over the supporting beam, with the angle between profiled sheeting ribs and the beam of 60°

1 Introduction

1.1 Background

Steel-concrete composite structures are commonly used in construction, as they enable the most efficient use of each material. By connecting a steel and a concrete part, the composite action is realised, increasing the bearing capacities of the structural element. The most common steel-concrete composite system is a downstand composite beam (T-beam) that consists of a steel profile and a concrete slab placed over it. The concrete slab is implemented in one of two ways: as a solid slab or as a composite slab cast in profiled steel sheeting. To join the steel beam and the concrete slab and to prevent vertical separation and enable shear force transfer, shear connectors need to be used. The most often applied mechanical connectors are welded headed studs. Besides those, many novel shear connectors have been investigated in the past decades, including perfobond rib connectors, channel shear connectors, shear connectors fastened with pins, etc.

In the modern age, when a lot of attention is paid to the preservation of the environment, sustainable development is required in all segments of the industry. In the construction industry, new trends include recycling and reusing old construction materials and replacing traditional materials with alternatives whose production is environmentally safe. From the perspective of sustainable development, the reuse of entire constructional elements is highly beneficial. Therefore, the possibility of disassembling a structural system, that is typical for steel structures, is advantageous. However, common steel-concrete composite beams with welded headed stud shear connectors do not have the feature of demountability, implying that they cannot be reused in the second life cycle in the original configuration including concrete slab and steel profile. Accounting for the negative impact that the implementation of concrete has on the environment with the significant release of CO_2 during cement production, the reusability of concrete slabs is highly favourable. This has been confirmed by the recent study on environmental benefits of different composite floor structures that has shown that the demountable steel-concrete floor system leads to the lowest emissions and highest savings of resources in most of the analysed impact categories compared to other traditional steel-concrete composite floor solutions [14]. For those reasons, in the past few decades, much research in the field of steel-concrete composite structures has been turned to developing and investigating demountable steel-concrete composite floor systems, with the focus on shear connectors applicable in those systems.

Various demountable shear connectors have been suggested, experimentally tested and numerically analysed by authors and research groups, often in cooperation with industry partners. Bolted shear connectors have a major role in deconstructability of composite structures, transferring shear force between the steel profile and solid or composite concrete slab by different mechanisms. The most widely investigated are friction-grip bolt connectors, which transfer shear force through friction on the contact between the steel flange and concrete slab. However, due to loss or overcoming of pretension force in friction-grip bolts, a sudden slip occurs, followed by additional deformations of the beam. On the other hand, the implementation of bolt shear connectors that are not preloaded influences the slip at the initial loading stage, induced by bolt-to-hole clearances, whose presence is necessary from the execution point. Consequently, the initial stiffness of the connector is reduced, leading to the incomplete steel-concrete composite action. Injection of the resin in holes of the steel flange prevents the initial bolt slip inside the hole and provides sufficient stiffness of a connector. However, the process of installation is somewhat prolonged. Furthermore, several other solutions have been examined, with certain benefits and drawbacks. Nevertheless, proposed solutions do not include welded headed studs, which are characterised by good mechanical performance and which are widely used in construction. The idea of creating a connection that includes welded headed studs, but also enables reusability of the floor structure, led to an alternative demountable shear connection with two types of shear connectors, presented in the following.

A novel demountable shear connection for the implementation in steel-concrete composite beams is proposed in this thesis. The shear connection consists of two types of connectors: welded headed studs and bolts, as shown in the layout presented in Figure 1.1. The suggested connection is applicable in composite concrete slabs cast in open trough profiled steel sheeting. Welded headed studs are installed in concrete ribs, whereas bolts are placed between ribs. Two possible solutions may be applied depending on the chosen construction method, as shown in Figure 1.1: (a) composite concrete slab continuous over the supporting beam; (b) composite concrete slab discontinuous over the supporting beam. To accomplish the demountability of the shear connection with a continuous slab given in Figure 1.1.a, an additional plate placed between the concrete slab and the steel beam is required. Headed studs are welded to the plate, connecting the concrete slab and the plate, whereas the bolts' role is to connect the plate with the top flange of the steel profile. In the case of a discontinuous concrete slab presented in Figure 1.1.b, a pair of angles is used to which headed studs are welded. The connection between the angles and the steel beam is accomplished by bolts, while welded headed studs connect the angles and the concrete slabs. In both cases shown in Figure 1.1, the longitudinal shear force transfer is indirect, passing through two shear planes: "plate/angle-concrete slab" and "steel profile-plate/angle".
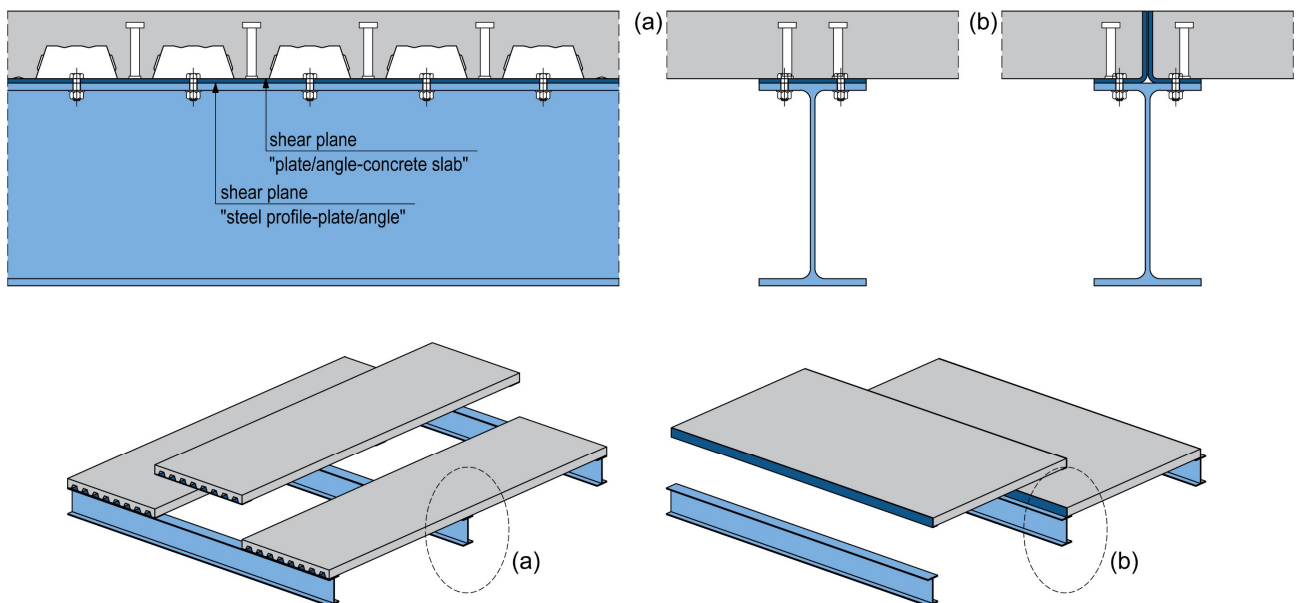
Figure 1.1: Layout of the demountable connection with welded headed studs and bolts:
(a) continuous slab over the beam, (b) discontinuous slab over the beam.

When it comes to building deconstruction, bolts need to be removed and the composite concrete slab is easily separated from the steel beam with the possibility of being installed again. In that manner, no destruction methods are applied during deconstruction. In the second life cycle of the building, the entire floor structure including concrete slabs and steel beams may be reused in the same configuration as during the first life cycle. In addition, if concrete slabs need to be replaced for the purpose of the structure reconstruction, it could be simply performed. Implementation of headed studs and bolts, which are broadly available, and the absence of any requirements for additional equipment for installation of connectors are considered advantages of the proposed connection.

Solutions presented in Figure 1.1 consider the example common in engineering practice when profiled steel sheeting ribs are transverse to the supporting beam. However, floors of irregular shape usually require the implementation of girders that make acute angles with each other. As a result, profiled sheeting ribs are not transverse nor parallel to the beam, instead they form the angle $0° < \alpha < 90°$ with the beam axis, as shown in Figure 1.2. The behaviour of welded headed studs in metal decking parallel or transverse to the beam has been broadly experimentally investigated. However, the lack of available experimental results covering headed studs in alternative profiled sheeting configurations has been observed. In addition, design codes do not give directions for calculating the

resistance of headed studs in profiled sheeting with the angle between ribs and the beam $0° < \alpha < 90°$. Investigations and discussions of the influence of the angle between profiled sheeting ribs and the beam on the response of non-demountable and demountable connections with continuous slabs over the support are covered by this thesis.
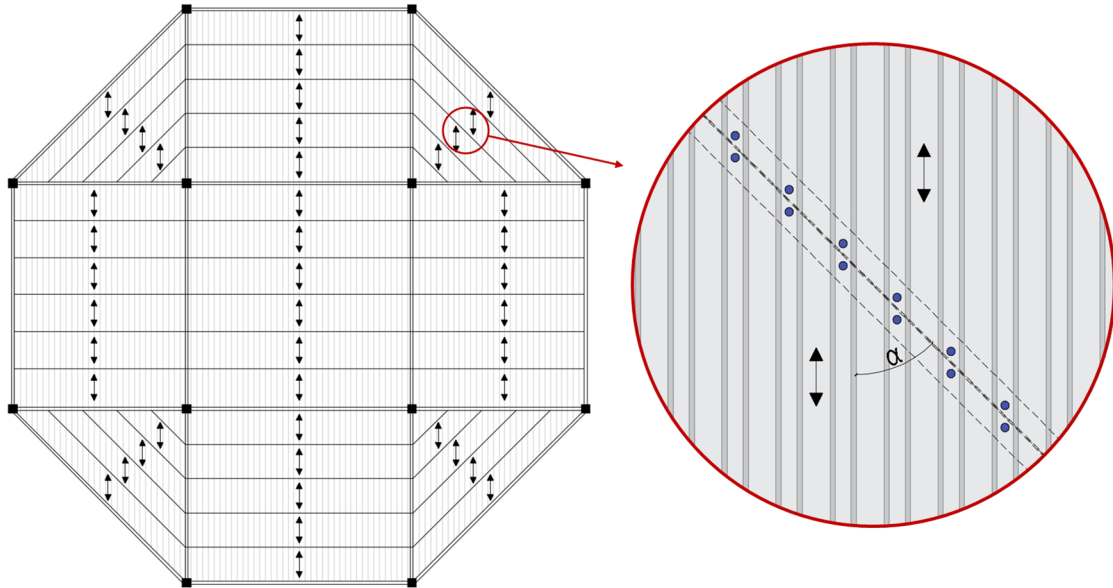
Figure 1.2: Example of the building floor layout with various profiled sheeting orientations.

1.2 Objectives of the Research

The aim of the research presented in the thesis is the realisation and promotion of the novel demountable connection with bolts and welded headed studs applicable in steel-concrete composite structures. The objectives of the research are to describe the connection response to the shear load at the point of resistance and ductility, to identify failure mechanisms and propose instructions for the design. To achieve the objectives, the following tasks are defined:

- In the beginning, an analysis of the results of other research into different demountable shear connections is conducted. A review of the design rules and recent research outcomes in the field of non-demountable connections with welded headed studs in profiled steel sheeting is given.

- Preliminary design of the demountable connection with welded headed studs and bolts is suggested and presented through the case study of a multi-storey car park building. Detailing of the shear connection is discussed and parameters that are analysed in the experimental and numerical studies are introduced.

- The experimental investigation of the novel demountable shear connection with welded headed studs and bolts, as well as the corresponding non-demountable connection with headed studs, is conducted. Therefore, the correlation between two solutions regarding stiffness, resistance and ductility is analysed. The experimental investigation covers different configurations of the demountable steel-concrete connections: connections with continuous and discontinuous slabs over the support, connections with and without stirrup reinforcement around headed studs.

- Furthermore, the experimental investigation includes specimens of demountable and non-demountable connections with different angles between profiled sheeting ribs and the beam. Comparisons are made between the structural response of connections with angles between profiled sheeting ribs and the beams of 90°, 60° and 45°.

- Results of the experimental investigation enable the development of the appropriate numerical finite element models, which are used for a detailed analysis of the connection response and further parametric studies.

- Parametric studies are performed to cover a range of parameters that might influence the connection response, including headed stud diameter and height, bolt grade and diameter, concrete class, plate and angle thickness, the distance between the headed stud and slab edge, stirrup reinforcement diameter and position, the angle between sheeting ribs and the beam, etc. The key influential parameters are identified and their effects on the connection performance are quantified.

- After the analysis of the wide set of data obtained through the parametric studies, conclusions regarding the connection behaviour are drawn and design recommendations are given.

1.3 Methodology of the Research

To reach the described objectives, the following research methodology is applied. A review of the available literature is conducted to present the current state regarding demountable steel-concrete composite floor solutions and welded headed studs in profiled steel sheeting. Experimental research covers 20 push-out tests on demountable and non-demountable specimens, followed by standard tests for obtaining material properties of concrete and steel components. Numerical finite element models developed in software Abaqus [9] are calibrated with experimental results, simulating the quasi-static analysis performed in the explicit solver. By changing the key parameters in the developed numerical models, a parametric analysis is conducted. Results are statistically processed and analytically interpreted, and discussions and conclusions are made.

1.4 Outline of the Thesis

The thesis is organised into eight chapters.

In Chapter 2, the state of the art in the developments in the field of demountable steel-concrete composite floor systems is presented. Wide literature research is conducted to collect data on various suggested and investigated solutions regarding demountable shear connectors. The main results of experimental and numerical studies of push-out and beam tests published in the past years are presented, compared and discussed. Moreover, in Chapter 2, a review of the design rules and recent research results regarding welded headed studs installed in a composite slab with profiled steel sheeting is given. New approaches for the calculation of headed stud resistance are presented. Suitable push-out test set-ups and the influence of the reinforcement arrangement are discussed.

In Chapter 3, a preliminary design of the demountable connection with welded headed studs and bolts is proposed through the case study of a multi-storey car park building. The adoption of geometric parameters and connection detailing are discussed, announcing further experimental and numerical investigations.

In Chapter 4, experimental research consisting of push-out tests and tests for obtaining material properties is presented. The experimental programme including eight different push-out specimen series is described, as well as the push-out test set-up. Experimental results are presented, compared and discussed.

In Chapter 5, the focus is put on the numerical research performed using finite element analysis. Developed numerical models are presented and validated through comparison with experimental results. The behaviour of models is discussed.

In Chapter 6, parametric studies including a variety of different parameters regarding the connection geometry, the angle between ribs and the beam and concrete class are conducted. The effects of varied parameters on the connection behaviour are presented and discussed. Numerically obtained ultimate loads for welded headed studs in profiled steel sheeting with ribs transverse to the supporting beam are compared with analytical predictions.

In Chapter 7, recommendations for the design of demountable shear connections are proposed. Directions for the selection of the plate and angle thickness, stirrup bar diameter, the distance between

the headed stud and angle leg, etc. are listed. The expression for obtaining shear resistance of welded headed studs in profiled steel sheeting with the angle between ribs and the beam smaller than 90° is suggested.

In Chapter 8, conclusions drawn from the experimental and numerical analyses are listed and directions for future investigations are proposed.

2 Literature Review

This chapter is divided into two subchapters, presenting the literature review in two different areas. Firstly, the state of the art in the demountable steel-concrete composite floor systems is presented. The review provides valuable background for further studies in that field, including the research presented in this thesis. Secondly, a summary of the codified design rules, recent research results and new analytical procedures regarding welded headed studs in the composite slab with profiled steel sheeting is given. The presented review is the basis for the experimental and numerical studies presented within this thesis.

2.1 Demountable Steel-Concrete Composite Floor Systems[1]

In this subchapter, an overview of different systems for accomplishing composite action in demountable steel-concrete composite floors is given. The main results of experimental and numerical research of the push-out and beam tests published in past years are presented, compared and discussed. Shear connectors are classified by their geometry and load-carrying mechanisms, and each type is briefly presented in a separate subchapter.

2.1.1 Friction-Grip Bolts

Friction-grip bolts are the most widely studied and analysed demountable shear connectors. These bolts are preloaded, hence shear force in the connection is transferred through friction between the concrete slab and the top flange of a steel beam. In literature, they are often referred to as high-strength friction-grip bolts.

Initial publications on the experimental beam and push-out tests on friction-grip bolts appeared in the late 1960s [15]–[17]. Experimental investigations covered various parameters, such as concrete strength, beam span, load geometry, bolt diameter, and in-situ and prefabricated concrete slabs. Main conclusions were made on the observed full interaction between a concrete slab and a steel beam in the serviceability load range.

A few years later, some of the research results were implemented in the British standard for bridge design [18]. The mentioned standard requires compliance with the following condition when designing bridges with friction-grip bolts: longitudinal shear resistance developed by friction should be greater than the longitudinal shear force in the serviceability limit state. The equation for obtaining frictional resistance is prescribed as:

$$F_{u,f} = \mu \cdot F_{p,C} / 1.2 \tag{2.1}$$

where $F_{p,C}$ is the preloading force and μ is the slip factor that should be taken as 0.45. The standard refers to the loss of preloading force in bolts over time due to concrete creep and shrinkage effects but does not specify a method to account for these effects.

The research on friction-grip bolts has regained popularity in recent years. Three different types of shear connectors, including friction-grip bolts, have been tested with the purpose of creating a composite action in the existing non-composite bridges by post-installation of bolts [19]–[21]. The research included single bolt shear tests under static and fatigue loading, experimental large-scale beam tests, and finite element numerical simulations of beam tests. Bolts were inserted in the holes predrilled in a concrete slab, pretension force was applied, and the holes were filled with high-strength grout, as shown in Figure 2.1.
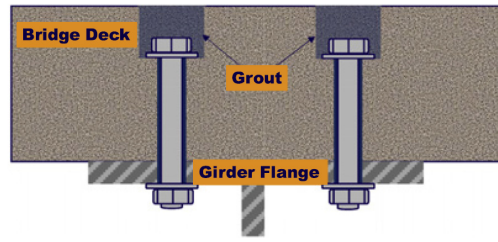
Figure 2.1: Shear connection with friction-grip bolts in bridge rehabilitation work [19].

It was reported that high-tension friction-grip bolts showed notably higher fatigue resistance than conventional welded shear studs, as a result of the elimination of weld between the flange and connector, which turned out to be an important advantage in the design of composite bridges. Beam specimens with post-installed shear connectors showed up to 50% increase in stiffness and resistance compared with non-composite beams, although they were designed with the 30% shear connection ratio only. Authors [21] suggested calculation of static resistance of post-installed shear connectors using the following equation:

$$F_u = 0.5 \, A_s f_u \tag{2.2}$$

where A_s is the effective shear area of the shear connector and f_u is the ultimate tensile strength of the shear connector material.

Another contribution to this field of study was made through the implementation of friction-grip bolted shear connectors in precast geopolymer concrete slabs [22]–[25]. Push-out and beam tests were performed and the corresponding numerical models were developed, according to the arrangement presented in Figure 2.2. Beams with post-installed friction-grip bolts in prefabricated slabs showed lower ultimate capacity, but larger deformations than the beam with embedded bolts inside the monolithic slab, which was also experimentally tested. The general weakness of the analysed system was attributed to the clearances between precast concrete slabs that led to a considerable reduction of the initial stiffness. To demonstrate the system's demountability, during both push-out and beam tests, after loading within serviceability range, some specimens were reassembled and then loaded again until failure, resulting in load-slip behaviour similar to that of specimens that were not demounted. A slight modification of Eq. (2.2) for shear resistance of friction-grip bolts in geopolymer concrete slabs was suggested [22]:

$$F_u = 0.66 \, A_s f_u \tag{2.3}$$
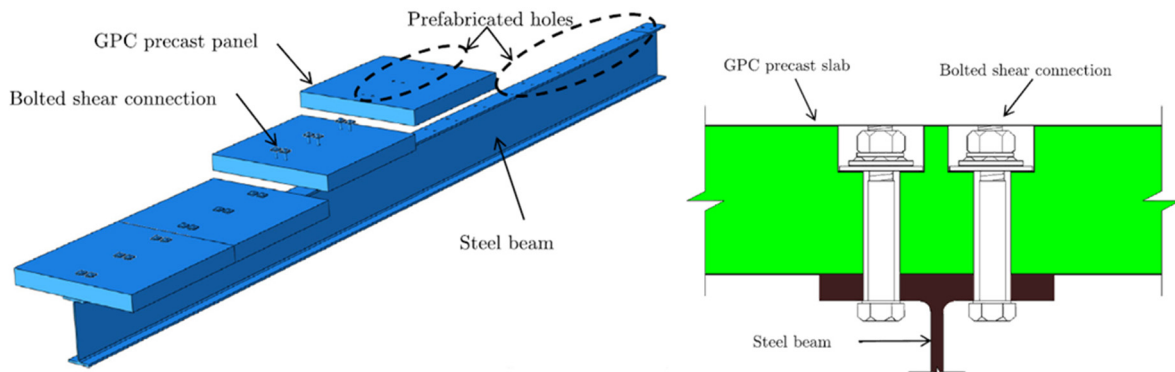
Figure 2.2: Implementation of friction-grip bolts in precast slabs [24].

A proposed simplified load-slip relationship typical for friction-grip bolts, including a linear and nonlinear part, is presented in Figure 2.3 [22]. Three regimes of shear connector behaviour can be observed. In the first regime, slip is almost negligible because of the applied pretension. Then, once the friction at the steel-concrete interface induced by preload is overcome, some slip occurs due to clearance between prefabricated holes and bolts. The slip is close to the sum of the clearance between

a steel flange hole and a bolt and the clearance between a concrete slab hole and a bolt. In the third part, a nonlinear relation between the load and slip can be observed. The analytical formulation for modelling shear connection in composite beams using pretensioned bolts was suggested, including the mentioned three stages of bolt behaviour [26].
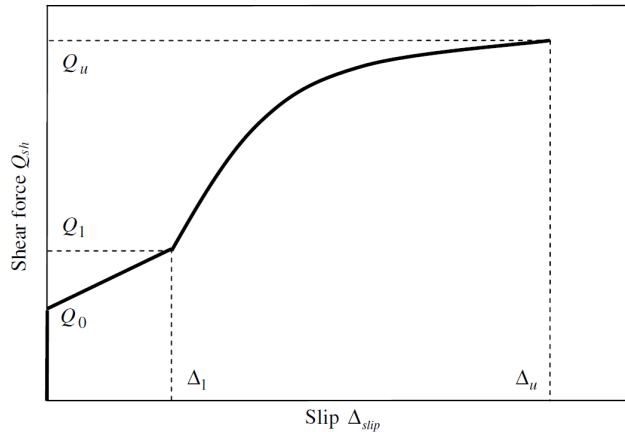
Figure 2.3: Design recommendation of load-slip relationship for friction-grip bolts [22].

In further experimental work, some refined solutions were proposed in order to improve the deformation response and decrease the maximum slip value. The use of the so-called through-bolts in steel-precast composite bridges was suggested [27], [28]. Bolt holes were formed using PVC pipes, which were placed at specified places along the concrete slab so that the space inside pipes was left unfilled after concrete casting, as shown in Figure 2.4.a. The research covered push-out and beam tests, and focused on several parameters influencing the connection behaviour: contact surface, bolt diameter, and pretension load level.

Another solution applicable to building construction was proposed, involving friction-grip bolts that were cast in steel cylinders, which were welded to the top plate and L profile, as presented in Figure 2.4.b [29], [30]. The suggested shear connection was tested by push-out tests in solid concrete slabs and composite slabs with profiled steel sheeting, while the beam test was performed on the composite slab only. A comparison between connections with galvanised and non-galvanised steel elements was made, showing that the galvanised connection changes its behaviour after reassembling, with regards to slip increase and reduction of friction resistance due to fading of the coating layer and decrease of the friction coefficient.
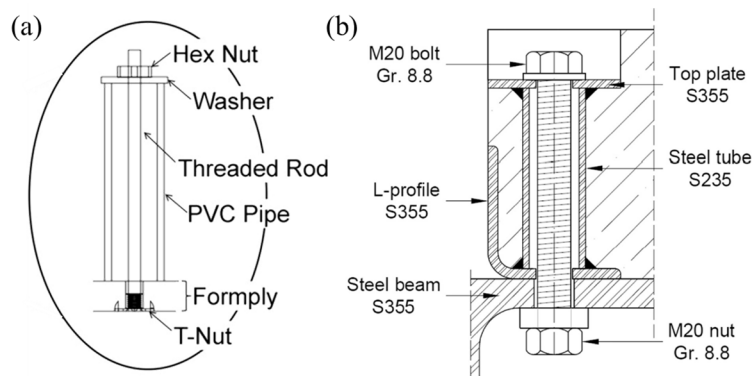
Figure 2.4: (a) Through-bolt [28], (b) Friction-grip bolt cast in steel cylinder [29].

A database showing the results of push-out tests conducted on friction-grip bolts subjected to full pretension force is presented in Table 2.1. As can be observed from the results, the maximum slip value, corresponding to the ultimate load level, varies from 10 mm to nearly 30 mm. The smallest slip of 9.7 mm is observed in the case of bolts cast in steel cylinders, which can be explained by the rigidity of the steel tube. On the other hand, the solution without any additional cylinders leads to the final slip that is up to three times larger.

9

Table 2.1: Experimental results of a push-out test conducted on friction-grip bolts in solid slabs.

Reference	Bolt diameter	Slab hole or cylinder diameter	Steel flange hole diameter	Bolt material grade	Bolt tensile strength	Concrete compressive strength	Ultimate load per connector	Maximum slip	Remark
	[mm]	[mm]	[mm]		[MPa]	[MPa]	[kN]	[mm]	
[27]	19.05	25	-	ASTM A325*	-	49.65 (cylinder)	128.1	11.1	bolts cast in PVC cylinders
	15.88	25	-	ASTM A325*	-	49.65 (cylinder)	82.5	11.7	
	12.70	25	-	ASTM A325*	-	49.65 (cylinder)	53.8	11.1	
[22]	20.00	24	24	8.8	1020	47.00 (cylinder)	219.5	24.8	geopolymer concrete slabs
	20.00	28	24	8.8	1020	47.00 (cylinder)	216.0	27.5	
	16.00	24	24	8.8	1020	47.00 (cylinder)	153.0	29.5	
[29]	20.00	-	24	8.8	-	59.40 (cube)	141.0	9.7	bolts cast in steel cylinders

*minimum yield strength f_y = 660 MPa, minimum tensile strength f_u = 830 MPa

Even though the friction-grip bolt is the most widely investigated type of demountable shear connector in composite floor structures, complete regulations in design codes considering friction-grip bolts are still lacking. The main shortcoming of this connector could be attributed to durability issues, keeping in mind the losses of pretension force over time, usually influenced by the fading of the coating layer applied to the steel flange [31]. As a result, after friction is overcome, certain slip occurs, contributing to additional deformation of the girder.

2.1.2 Bolted Shear Connectors without Embedded Nuts. Threaded Headed Studs

Compared with friction-grip bolts, bolted shear connectors without embedded nuts do not require pretension, which reduces the time of bolt installation and does not cause problems with the loss of bolt preloading force over time. Shear force is completely transferred by shear through the threaded part of the bolt and concrete bearing around the bolt. However, because of the bolt slip in the hole, lower initial stiffness is expected, which affects beam deflections and may induce serviceability issues. First studies on bolted shear connectors without embedded nuts, performed in the 1980s, revealed that the stiffness of analysed bolted connectors amounted to only 15% of the stiffness of welded headed studs, while shear resistance was about 80% of the shear resistance of welded shear connectors [32].

Another approach in accomplishing demountability of steel-concrete connections involves manufacturing a shear connector by threading the body of a headed stud, as shown in Figure 2.5. In this way, the final product has a geometry similar to the previously described bolts without embedded nuts. In past years, a series of tests followed by numerical simulations were conducted on these connectors installed in both solid slabs and composite slabs with metal decking [33]–[37]. Variations in the length of the threaded and collar part of the stud were covered by studies, which also focused on concrete strength, reinforcement arrangement in push-out test set-up, shear connector height and temperature level during loading. Compared with welded studs, the behaviour of connections achieved with threaded studs exhibited a notable difference in initial stiffness, as the outcome of the stud-to-hole clearance, although the shear resistances were almost the same for both connectors. The full-scale composite beam test demonstrated that the ultimate moment capacity of demountable beams could be well predicted by the plastic theory [35].
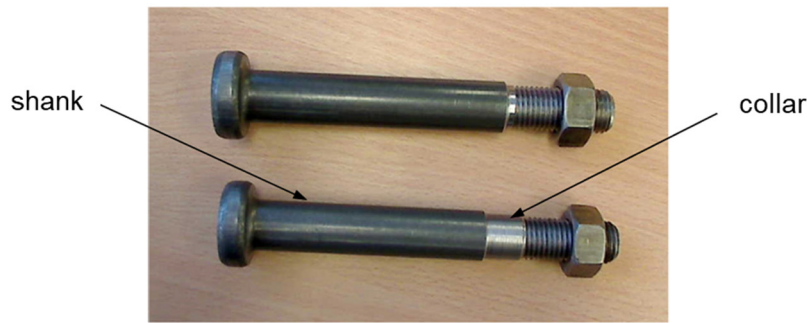
Figure 2.5: Threaded headed studs [33].

Furthermore, as push-out tests on threaded studs were conducted in both continuous and discontinuous metal decking composite slabs, it was established that connectors in continuous slabs had lower resistance, but higher load at 6 mm slip than those in discontinuous slabs [36]. It is important to note that the embedment height showed significant influence on the failure of the composite concrete slab, even though the height of both tested bolts satisfied the EN 1994-1-1:2004 request for the minimum welded stud height of $2d$ above the top of the steel deck, where d is the shank diameter [10].

The study on demountable threaded headed studs in ultra-high performance concrete, which contains evenly embedded steel fibres, is also worth mentioning [38]. To increase the slip capacities of composite shear connections achieved with this type of concrete, welded studs were replaced with threaded studs. However, although push-out tests revealed larger slip, it was still lower than 6 mm, which is required by EN 1994-1-1:2004 [10] for ductile connectors.

2.1.3 Bolted Shear Connectors with Embedded Nuts

The idea of using bolted shear connectors with nuts in their base, embedded in a concrete slab, was applied as a means of controlling bolt rotation and slip during loading. In that way, compared with bolts without embedded nuts, an increase in stiffness is expected. Another important advantage of these connectors is related to an easier mounting process than for bolts without embedded nuts, which are difficult to keep in a vertical position before and during concrete casting. Still, connections achieved with bolts with embedded nuts feature certain bolt-hole slip as a result of necessary execution tolerances, provoking additional deflections of the steel beam at the execution stage [39]. Different connection arrangements were tested in push-out and beam tests, including one or two embedded nuts, and they revealed a similar response trend.

In the 1980s, first research steps were made for implementing this type of connector in the rehabilitation of existing bridges [40]. Bolts with a single embedded nut were mounted in predrilled holes that were afterwards filled with grout, as shown in Figure 2.6.a. Authors commented on the comparable load-slip behaviour of connections made with bolts and welded studs.

Several static and fatigue push-out tests in solid slabs, involving bolts with two embedded nuts, and including a theoretical model for calculating concrete resistance to crushing and shear resistance of bolts, were conducted at the very beginning of the 21st century [41]. However, it was discovered that experimental results varied considerably from resistance calculations, and it was concluded that further investigations were necessary to make general design recommendations.

More recently, tests on double-nut bolts were performed as a part of a research study including the previously described friction-grip bolts, the purpose being to use them in bridge rehabilitation work [19]–[21]. A steel-concrete connection layout including bolts with two nuts embedded above a steel flange is presented in Figure 2.6.b. After filling the clearances with high-strength grout, a full pretension force is applied on double-nut bolts, resulting in a load-slip relationship similar in shape to the friction-grip bolt response, but with remarkably lower slip at failure.
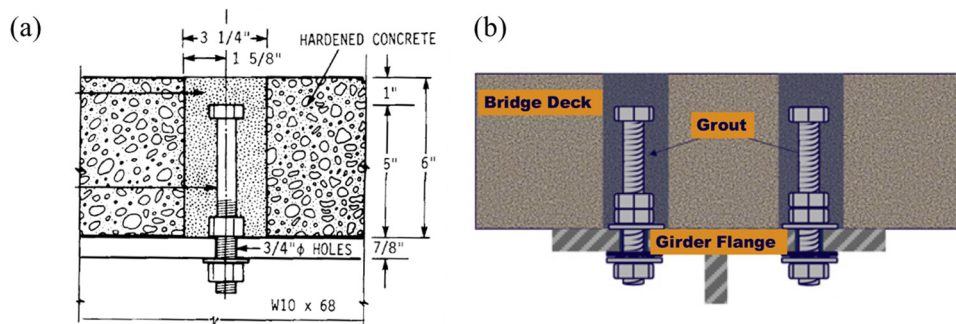
Figure 2.6: Shear connections in bridge rehabilitation work:
(a) Single-nut bolt [40], (b) Double-nut bolts [19].

Another experimental investigation showed that, in comparison with welded headed studs, the shear connection involving bolts with a single embedded nut exhibited stiffness that is as much as 50% lower for serviceability loads [42]. The phenomenon was attributed to the presence of bolt-to-hole clearances, threads-to-hole penetration, and larger contribution of shear force to the failure. Further numerical investigations helped in the formulation of the bolt failure model, including combined loading involving axial, shear and bending deformation.

A comparison of load-slip response obtained from push-out tests of bolts with a single embedded nut [42], threaded headed studs [33] and welded headed studs [33], all conducted in solid slabs, is given in Figure 2.7. Although all presented connectors reached a similar ultimate load, the shape of load-slip curves is notably different. As expected, bolts with embedded nuts show increased stiffness compared with threaded headed studs, much closer to the welded studs' stiffness. However, bolts with embedded nuts failed at a very low slip rate (< 5 mm) due to brittle bolt failure, while concrete crushing occurred for both threaded and welded stud connectors. In contrast to welded studs that exhibit ductile behaviour after the ultimate load is reached, threaded studs presented in Figure 2.7 cannot be categorised as ductile according to [12], although slip capacity is larger than 6 mm.
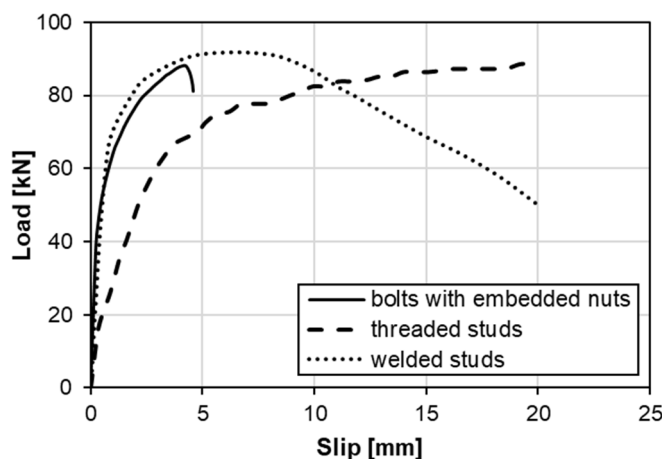
Ref.	Shear connector		Concrete cube strength [MPa]
[42]	bolts with embedded nuts	M16 8.8	40
[33]	threaded studs	18 mm*	30
[33]	welded studs	19 mm	30

*collar diameter

Figure 2.7: Comparison of shear connector behaviour.

Additional insight into the features of bolts with embedded nuts was given through experimental testing of three beams of various spans [43]. A concrete slab was cast in profiled steel decking and comparisons with previously performed tests on beams with welded headed studs were made. According to the authors, beams with bolts showed comparative resistance to beams with headed studs – moment capacities were lower in the maximum of 12%. After loading at serviceability loads, two beams were demounted, reassembled and then loaded to failure, resulting in a certain slip increase.

It should however be noted that investigations in this field are still ongoing. The cyclic behaviour of shear connections with single-nut embedded bolts in precast concrete panels has been studied

experimentally [44]. Furthermore, results of experimental and numerical research on the behaviour of bolts with a single embedded nut in continuous, partially discontinuous and separate concrete slabs with metal decking have been published [45]. It was discovered that partially and fully discontinuous slabs have higher resistance than continuous slabs. Such findings are favourable as discontinuous systems also provide for easier construction, deconstruction and repair.

2.1.4 Blind Bolts

The necessity to make the process of bolt mounting easier and faster led to the idea of using blind blots as demountable shear connectors. Blind bolts are specially designed connectors that could be installed from one side of a workpiece. Several comparative experimental and numerical analyses were performed [46]–[52] as related to two types of blind bolts, both presented in Figure 2.8. A blind bolt marked as BB2 should be put in a specialised tool that enables bolt installation, together with washers and a nut. On the other hand, bolts marked as BB1 do not have parts that need to be assembled. Instead, they have a collar that spreads open after the bolt is secured.
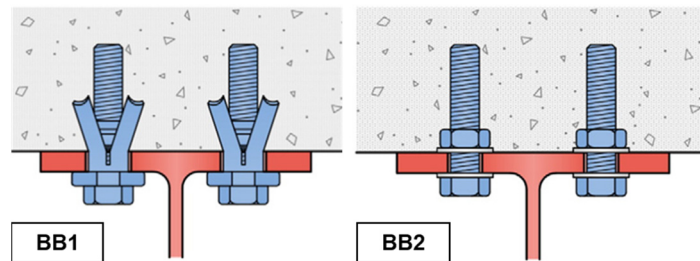
Figure 2.8: Blind bolts [48].

A comparison of load-slip curves obtained for two types of blind bolts and welded studs [51] is presented in Figure 2.9. As the results of push-out tests show, BB1 bolts have higher initial stiffness, but considerably smaller slip capacity when compared with BB2 bolts. While BB1 bolts failed due to concrete failure, bolt shear failure occurred in the push-out test of BB2 bolts. Authors suggested that an expended collar of the blind BB1 bolt provided additional inertia against slipping, but that the collar also caused damage of the concrete slab and brittle failure. On the other hand, due to oversized holes in the steel flange, the specimen with BB2 bolts had a large slip. The low ductility of welded studs was attributed to poor welding and weld failure. Beam tests confirmed bolt properties relating to ductility and resistance obtained through push-out tests. Demountability was demonstrated on beam specimens with blind BB1 bolts, proving no considerable change in the load-deflection behaviour after reassembly.

Ref.	Shear connector	Diameter	f_y/f_u	Concrete cube strength
		[mm]	[MPa]	[MPa]
[51]	blind bolts BB1	20	860/920	52.5*
[51]	blind bolts BB2	20	795/900	52.5*
[51]	welded studs	20	390/515	52.5*

*concrete cylinder strength is converted to concrete cube strength multiplying by 1.25
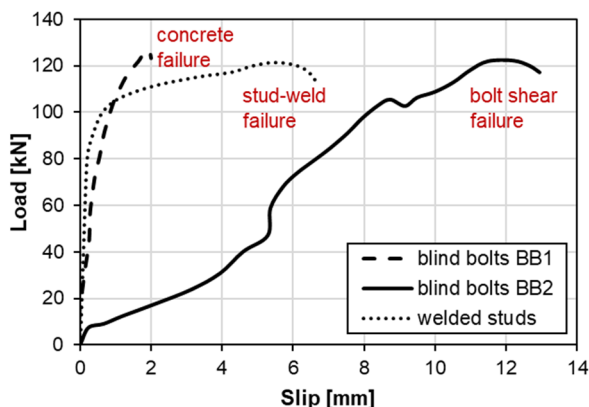
Figure 2.9: Comparison of shear connector behaviour.

In addition to the behaviour of blind bolts in solid slabs under static loading tested in push-out and beam tests, the investigation on blind bolts also covered dynamic behaviour [46], [47], time-dependent behaviour [48] and behaviour under combined shear and tension [52]. Implementation of blind bolts was suggested in both demountable composite beams [50], [51] and in bridge

rehabilitation work [49], [51], the only difference being in the mounting process: in the latter case, holes were cored in a concrete slab and drilled in a steel flange from the top side of the specimen, bolts were then fixed and holes in the concrete slab were filled with grout. Nevertheless, a different mounting process did not significantly affect bolt behaviour.

2.1.5 Bolted Shear Connectors with a Coupler System. Injection Bolts

The attempts to make the process of bolt replacement simple led to the application of bolted shear connectors with a coupler system in composite steel-concrete floors. This connector consists of a bolt that is embedded in a concrete slab, a removable bolt that is placed from below, and a coupler system that connects the two bolts, all as shown in Figure 2.10.
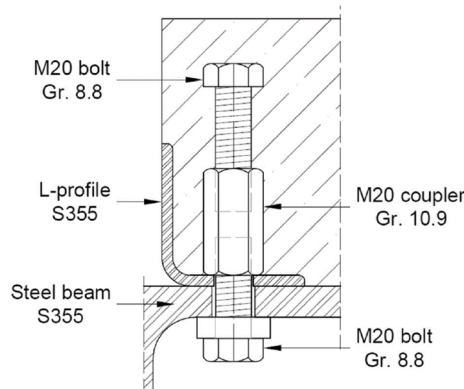
Figure 2.10: Bolted shear connector with a coupler system [29].

First analyses of this shear connector were performed by varying the geometry of bolts and by comparing their response in push-out tests with welded headed studs [53]. The observed bolt failure mode was shear through threads of the removable bolt, while no concrete damage was noticed. As the authors concluded, the stiffness of the connection was highly influenced by the clearance between the bolt and hole in the steel flange.

In subsequent studies, another research group conducted comparative investigations of bolted shear connectors with a coupler system and friction-grip bolts cast in steel cylinders [29], [30]. The benefit of bolt-coupler shear connectors over the friction-grip bolts was discussed considering the less likely bolt damage during construction and transport. As beams with the installed coupler system exhibit additional deflections in the execution stage due to bolt slip, similarly to single-nut and double-nut bolts, the authors gave suggestions for solving this issue. Two types of the coupler system were investigated: pretensioned bolts and bolts with epoxy resin injected in the hole of the steel flange. Injected epoxy resin prevents a decrease in stiffness even when the holes in the steel flange are larger, which is beneficial from the aspect of prefabrication, execution and deconstruction. For both types, a coupler was welded to the L profile. A higher grade compared with that of the bolt was selected for the coupler, because of the desired shear failure through threads of a lower bolt, which can easily be replaced. Push-out tests were conducted in solid slabs and they involved testing of both types of coupler connections, while the beam test included bolts with epoxy resin inserted in composite slab with profiled metal decking.

Recorded load-slip curves for the pretension bolt-coupler system and the bolt-coupler system with epoxy resin are compared in Figure 2.11 with the behaviour of friction-grip bolts cast in steel cylinders, tested by the same authors [29] and previously mentioned in Subchapter 2.1.1, and with welded studs of the same diameter [51]. All presented connectors have comparable initial stiffness, although a drop in stiffness is observed after friction resistance is overcome for both types of bolts with applied pretension force. The coupler system with injected resin retains higher stiffness, but it is still lower compared with welded studs. Brittle shear failure of bolts occurred in all presented connections, and no other damage patterns were noticed. The epoxy resin remained unaffected. The bolt-coupler system with resin exhibited lower slip capacity than pretensioned bolts.

Ref.	Shear connector		Concrete cube strength [MPa]
[29]	pretension coupler system	M20 8.8	44.3
[29]	coupler system with injected resin	M20 8.8	44.3
[29]	friction-grip bolts cast in steel cylinders	M20 8.8	59.4
[51]	welded studs	20 mm	52.5
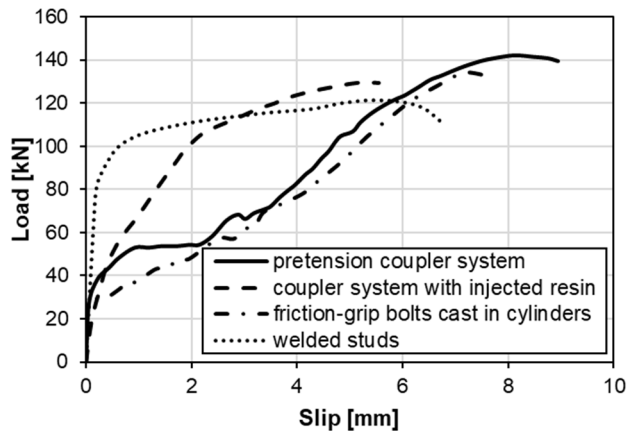
Figure 2.11: Comparison of shear connector behaviour.

Additional tests using bolt-coupler shear connectors with epoxy resin were performed on tapered composite beams, i.e. on the 90% scaled replication of a typical beam used for multi-storey car park buildings [54]. Conducted experimental work confirmed the demountability of the proposed system. However, it was shown that bolt-to-hole clearances should be increased compared to the size of normal round holes in steel-to-steel connections in order to enable convenient dismantling: for M20 bolts, holes of 32 mm in diameter were needed. In that case, the implementation of epoxy resins proved to be an effective solution to prevent the considerable initial slip of bolts. Moreover, numerical models were developed and by implementing different shear connector arrangements, it was investigated if the reduction in connectors' number and their concentration near supports could provide sufficient resistance at the serviceability load range. Conclusions regarding approximately 40–50% reduction of the number of shear connectors were made, suggesting an appropriate arrangement around the supports.

2.1.6 Friction-Based Shear Connectors and Locking Nut Shear Connectors

Although characterised by different shear force transfer mechanisms, two types of demountable shear connector systems, developed by the same authors and characterised by certain similarities in geometry, the locking nut shear connector (LNSC) [55] and the friction-based shear connector (FBSC) [56], are presented here in the same subchapter. The two systems were developed to overcome drawbacks of previously mentioned demountable shear connectors, such as the initial slip due to the bolt-to-hole clearance typical for threaded studs and bolts that are not preloaded, or a sudden slip after friction resistance is overcome in the case of preloaded bolts. LNSC and FBSC connectors were primarily developed for application in precast composite bridges, where they should be installed within pockets in the concrete slab, enabling fast assembly and disassembly. However, even though not purposely formed to be used in building floor structures, the connectors are included in this review due to their original attribute – demountability.

Both systems consist of high-strength bolts that are fastened by one nut to the upper steel flange and by another nut to the top surface of a concrete slab, as shown in Figure 2.12. The LNSC has an additional conical nut that is placed in the countersunk seat of a steel flange, and its purpose is to prevent bolt slip within the hole. Shear failure on the threaded part of the bolt is prevented by placing a conical nut in the shear plane between the steel flange and the concrete slab. In the case of the FBSC, a retaining washer is used to place the bolt in the right position. Countersunk holes are grouted to prevent a sudden slip of bolts. In both systems, bolts are placed in conical precast concrete plugs that are smaller than slab pockets, to avoid construction tolerance problems.

The typical failure mode of LNSCs and FBSCs, as observed during experimental push-out testing, was the shear fracture of a bolt just above the conical nut. Push-out tests showed very high initial stiffness of both systems, as well as large slip capacity and ultimate load. To get an insight into the benefits of the suggested systems, load-slip curves for LNSC and FBSC are presented in Figure 2.13

against the curves for bolts with embedded nuts and friction-grip bolts cast in PVC cylinders, which have a similar diameter.

(a)

LNSC

(b)
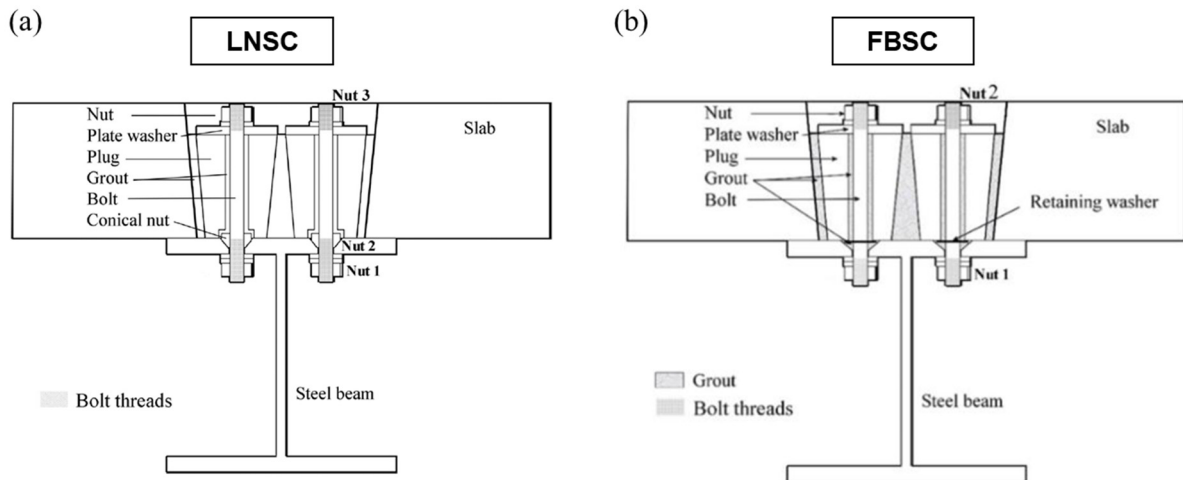
FBSC

Figure 2.12: (a) Locking nut shear connectors [55], (b) Friction-based shear connectors [56].
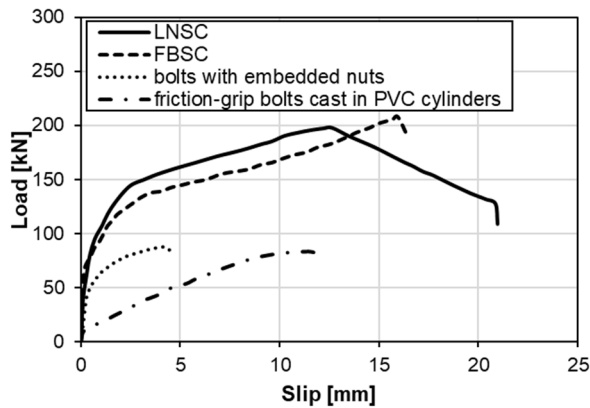
Ref.	Shear connector	Diameter	f_y/f_u	Concrete cube strength
		[mm]	[MPa]	[MPa]
[55]	LNSC	16	787/889	42.0
[56]	FBSC	16	787/889	42.0
[42]	bolts with embedded nuts	16	640/800	40.0
[27]	friction-grip bolts cast in PVC cylinders	15.88	not specified (ASTM A325)	62.1*

*concrete cylinder strength is converted to concrete cube strength multiplying by 1.25

Figure 2.13: Comparison of shear connector behaviour.

The complexity of two novel demountable systems from the aspect of geometry and requested material brings benefits such as an increase in stiffness, but also an approximately double increase in ultimate load. Hence, the application of LNSCs and FBSCs in bridge girders requires fewer slab pockets than traditional welded headed studs or bolted connectors. A comparison of the two systems shows that the LNSC exhibits an increased slip capacity in the post-ultimate domain.

2.1.7 Clamping Shear Connectors

A system with clamping connectors was developed for transferring longitudinal shear force in demountable composite steel-concrete beams [57]. As presented in Figure 2.14, connectors made of clamps and high-strength T-bolts are mounted in cast-in channels in a prefabricated concrete slab. T-bolts are pretensioned, so that shear force is transferred through friction at the contact between the concrete slab and steel girder. The advantage of the developed system is adaptability, without predefined locations of bolt holes; it can therefore be applied if flange widths are changed after deconstruction. Also, if flange thickness is being modified, clamping connectors can be reused by adding shims.

The conducted push-out tests showed high initial stiffness, but very large deformation of the analysed connection, as presented through load-slip curves in Figure 2.15. However, in contrast to friction-grip bolts and pretension double-nut bolts of comparable diameter and tensile strength, the clamping connector reaches approximately two times lower resistance at 10 mm slip. This is explained by the

specific failure mode of clamping connections, which is caused by large rotations of bolts and bolt head fracture. In order to solve this problem and limit bolt rotations, further modifications of bolts are suggested. Moreover, surface fractures due to friction were observed in concrete planks, particularly in specimens with three cast-in channels, which were characterised by deeper and wider cracks than those with two channels. The authors formulated suggestions regarding design recommendations, based on the developed numerical model [57].
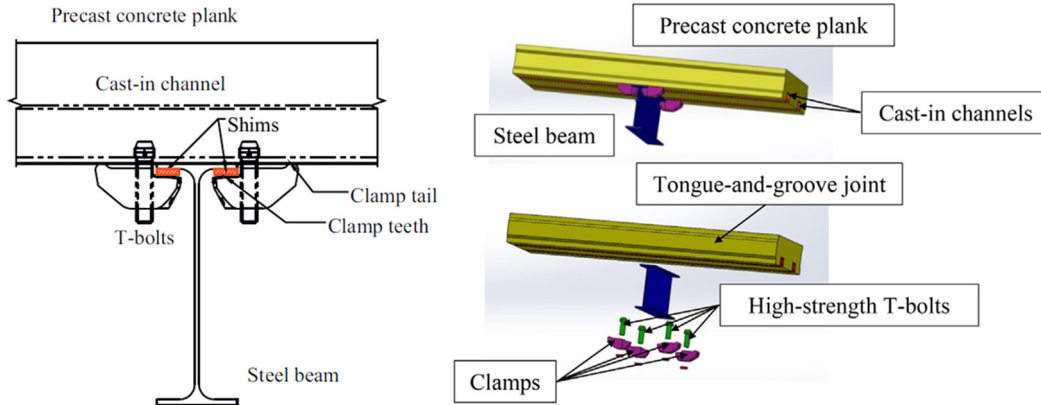
Figure 2.14: Connection with clamping shear connectors [57].
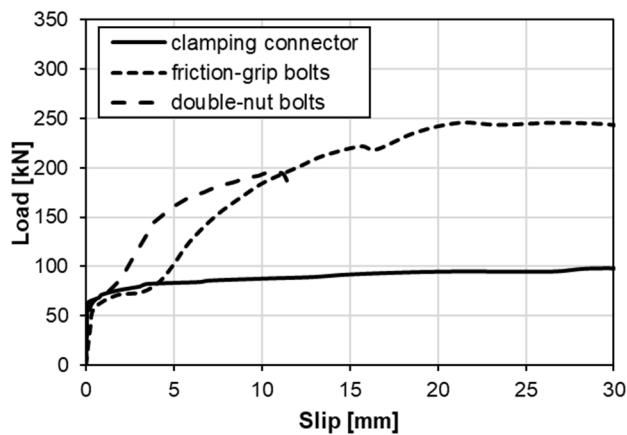
Ref.	Shear connector	Diameter	f_y/f_u	Concrete cube strength
		[mm]	[MPa]	[MPa]
[57]	clamping connector	24	759/940	36.2*
[19]	friction-grip bolts	22	-/1020	30.6*
[19]	double-nut bolts	22	-/1010	26.1*

*concrete cylinder strength is converted to concrete cube strength multiplying by 1.25

Figure 2.15: Comparison of shear connector behaviour.

2.1.8 Summary

A number of various proposed solutions for demountable connectors, investigated by different research groups, refer to the increased popularity of the specific topic of reusable steel-concrete composite floor systems. Many of the mentioned studies on the presented types of demountable shear connectors are still ongoing. The evolution of demountable shear connector systems started with basic set-ups including very few components, but in order to compensate for certain weaknesses, more complex models have been established. However, a constant balance is to be made between a proper response of the structural system, fast and simple execution, and the economic aspect.

Specific procedures in design codes for demountable steel-concrete composite structures are yet to be formulated and enacted. Some steps towards that have been made through the published "Guidance on demountable construction systems for UK practice" [12]. The suggested design rules are given considering the response of bolted shear connectors: lower stiffness compared with welded headed studs and non-ductile behaviour in the post-ultimate domain. Procedures are proposed to enable structure reuse, limiting the beam deflections and deformation of connectors. To determine the effective resistance of non-ductile bolts, the shear connector resistance is multiplied by the reduction factor k_{flex} to obtain the average load of all shear connectors along the beam span. A further calculation may be conducted according to the EN 1994-1-1:2004 procedures based on plastic analysis. The

17

abovementioned is applicable only if the slip capacity of the connectors is larger than 6 mm. Otherwise, the implementation of the elastic theory is required. Moreover, according to the publication, the end slip of a beam should be limited to 1.2 mm to prevent plastic deformation of bolted shear connectors. To obtain cross-sectional properties for the calculation of deflections and end slip, the stiffness of the shear connector should be taken into account.

Almost all of the solutions described in previous subchapters are based on the implementation of bolts on the contact between the steel beam and concrete slab. None of the previously presented connections considers the implementation of welded headed studs. By searching the available literature in this field, only one experiment on the demountable shear connection consisting of welded headed studs has been found [41]. As illustrated in Figure 2.16, the connection proposed for implementation in bridges was formed of headed studs, welded to the additional steel plate, and bolts, connecting the plate with the steel beam. As the connectors were installed in the solid concrete slab, both headed studs and bolt heads were bearing against shear on the contact between the slab and steel plate. Shear force was transferred by bolts on the contact between the steel plate and the beam. Two performed push-out tests resulted in brittle bolt failure, meaning that ductile properties of welded headed studs were not exploited. No further investigations of the connection were reported.
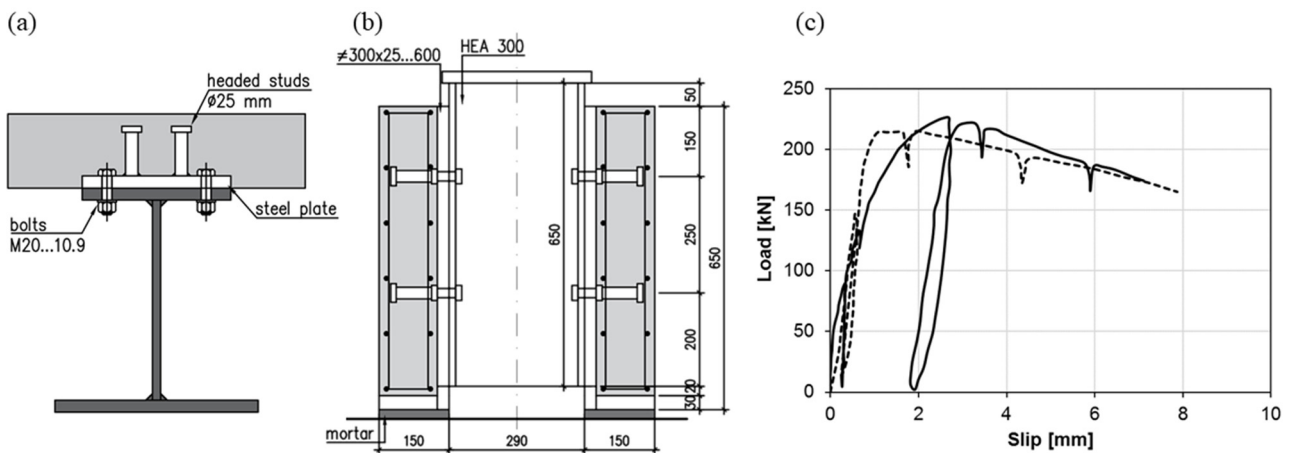
Figure 2.16: (a) Connection with welded headed studs and bolts, (b) Push-out test set-up, (c) Experimental load-slip curves [41].

The idea of implementing headed studs as widespread used connectors, featuring good mechanical performance in terms of resistance, stiffness and ductility, and not requiring additional equipment for installation such as specially designed cylinders, plugs or clamps, resulted in the demountable connection proposed and investigated within this thesis. Although non-demountable in their original form, headed studs may be part of a demountable connection if implemented in combination with bolts. In contrast to the solution with solid concrete slabs presented above, a newly suggested connection with bolts and welded headed studs is applicable in steel-concrete composite slabs with open trough profiled steel sheeting (Figure 1.1). Headed studs are welded to the additional steel plate and cast in concrete ribs, whereas bolts are placed between ribs and connect the beam and the steel plate. After the dismantling of the connection presented in Figure 2.16, bolts remain protruding from the concrete slab, which makes them susceptible to damage during transport and relocation. On the other hand, bolts in the novel connection may be completely removed after dismantling and therefore remain unaffected during the transport to another location. Moreover, unlike the solution shown in Figure 2.16, the novel connection is designed with the intention to avoid brittle failure of bolts and enable ductile shear behaviour of headed studs. The proposed demountable connection is presented and described in detail in Chapter 3.

18

2.2 Welded Headed Studs in Profiled Steel Sheeting

Welded headed studs are the most commonly used mechanical shear connectors in composite steel-concrete beams. The shear behaviour of these connectors has been widely studied since the mid-20th century. Research in this field can be divided into two parts: investigations of welded headed studs in solid concrete slabs and investigations of headed studs in composite concrete slabs cast in profiled steel sheeting. Different response trends obtained from push-out tests of shear connections in the two mentioned cases are graphically presented in Figure 2.17. The use of profiled sheeting could considerably increase ductility and develop two peaks in a load-slip curve.
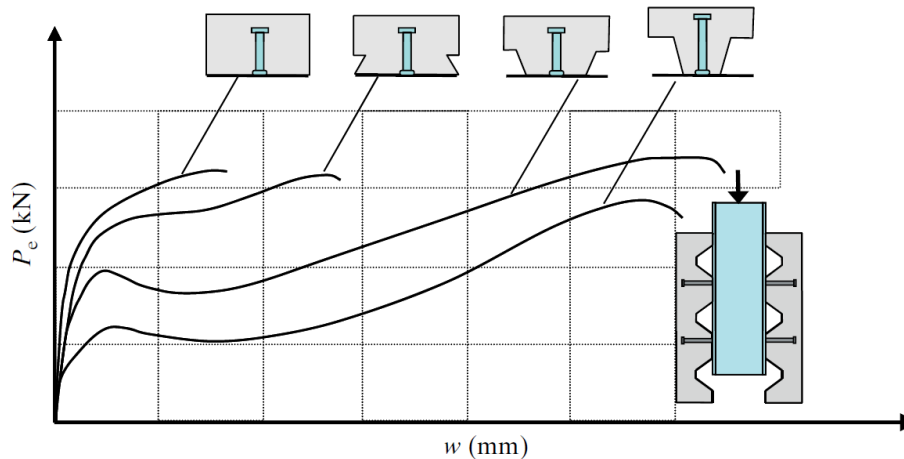
Figure 2.17: Welded headed stud shear response in solid and composite concrete slabs [58].

Hawkins and Mitchell [59] defined four types of failure in composite slabs with profiled steel sheeting: stud shearing failure, concrete pull-out, rib shearing and rib punching. Stud shearing is characterised by a plastic hinge in the stud just above the weld collar. Concrete pull-out failure occurs when the anchoring depth of a stud is too small and the concrete pyramid around the stud splits from the slab. Rib shearing is typical for edge beams where the effective width of a concrete slab is narrow, as shown in Figure 2.18. Rib punching failure may occur if a stud is placed in an unfavourable position, off-centre in a rib so that a narrow concrete layer between a rib and a stud crushes and the stud punches out of the rib wall.
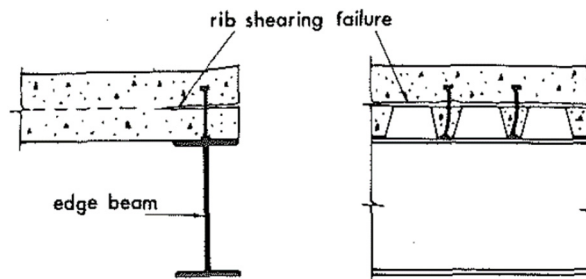
Figure 2.18: Rib shearing failure [59].

According to Johnson and Yuan [60], five failure modes in composite slabs with ribs transverse to the beam may occur: shank shearing, rib punching, rib punching with shank shearing, rib punching with concrete pull-out and concrete pull-out. When ribs are parallel to the beam, two failure modes were observed: splitting of concrete and concrete pull-out. Authors underlined that splitting of concrete is the most common mode for slabs with ribs parallel to the beam, starting with local splitting inside the rib, followed by deformation of rib walls and final failure.

Nellinger [61] distinguished four failure modes: stud failure, rib punch-through, concrete pull-out and rib pry-out. The latter two are both failures of concrete manifesting through the separation of the concrete cone from the concrete slab. Pull-out failure is characterised by high ductility and the development of two plastic hinges in the headed stud, whereas rib pry-out is a brittle failure,

commonly with only one plastic hinge formed. Therefore, pull-out is typical for beams with large stud heights above the rib, so-called embedment depths, while rib pry-out is present when headed stud embedment depth is small.

Lungershausen [62] explained differences in failure mechanisms in shear connections with solid slabs and profiled steel sheeting. In solid slabs, the shear force is acting on the weld collar of a stud, until a certain point when concrete in the stud base crushes and shear force is transferred to the stud shank. Due to stud deformation, tension force in the stud is established simultaneously with compression forces in the concrete cone. In the final stage, as cone compression forces are increasing, friction between slab and steel profile is activated and failure of the stud occurs as a result of the tension and shear interaction. The described mechanism is presented in Figure 2.19.a. For studs installed in sheeting ribs transverse to the beam, when the first peak in the load-slip curve occurs, concrete around the stud crushes and two hinges develop in the stud shank. As illustrated in Figure 2.19.b, the second peak is characterised by the development of tension force in the stud shank, followed by the final failure. However, if the stud height above the rib is too small, the second peak does not happen and brittle failure occurs, with only one plastic hinge formed at the bottom of the stud. The example is given in Figure 2.19.c, through three experimentally obtained curves for different stud embedment depths.
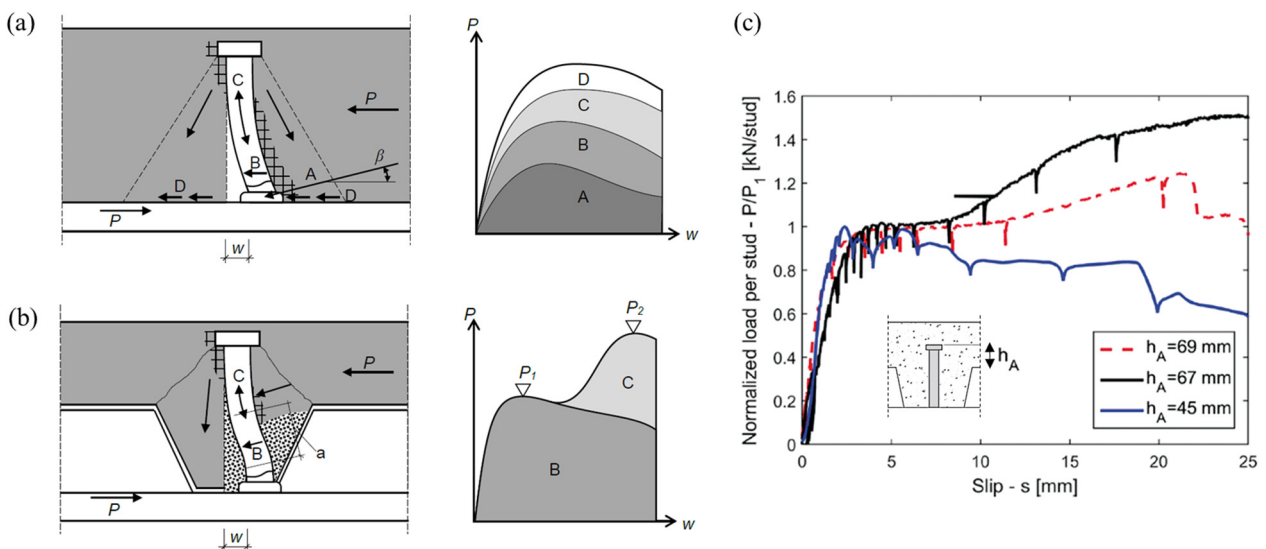
Figure 2.19: (a) Behaviour of a headed stud in a solid slab [61], (b) Behaviour of a headed stud in a composite slab [61], (c) Load-slip response for different embedment depths [63].

Vigneri [63], [64] numerically investigated failure mechanisms of headed studs in profiled steel sheeting and refined the model proposed by Lungershausen [62], suggesting the typical load-slip relationship as given in Figure 2.20. The development of the first peak is dependent on headed stud bending capacity and concrete strut resistance and it is characterised by two hinges formed in headed studs. The second peak is characterised by the start of the concrete cone failure, concrete crushing in front of the stud and a drop in the connection rotational stiffness. The third peak features certain deactivation of the upper plastic hinge in the headed stud and its movement toward the stud head. At the same time, tensile forces in connectors are activated. The final failure could be stud shear failure or concrete pull-out failure. However, if embedment depth is small or if studs are placed in a favourable position in the rib, the concrete rib starts rotating and the third peak is not achieved.
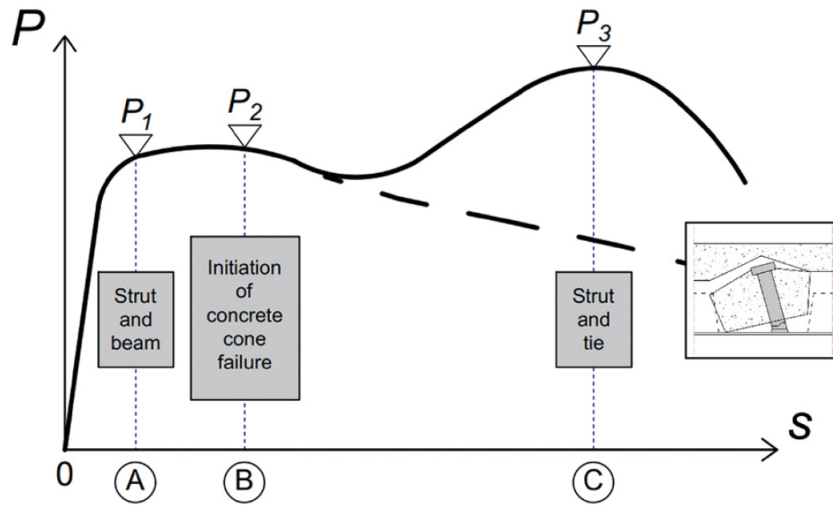
Figure 2.20: Typical load-slip curve for a headed stud in profiled steel sheeting [63].

2.2.1 Design Procedure according to EN 1994-1-1

The commonly applied approach in design codes suggests determination of headed stud resistance in composite beams with profiled steel sheeting through the reduction of headed stud resistance in solid concrete slabs. EN 1994-1-1:2004 [10] defines two reduction factors, k_t and k_l, when the ribs of the sheeting are transverse and parallel to the supporting beam, respectively. Both factors are empirically developed and based on experimental results [65].

According to EN 1994-1-1:2004, the design resistance of automatically welded headed studs in solid concrete slabs should be adopted as the minimum of Eqs. (2.4) and (2.5):

$$P_{Rd} = \frac{0.8 f_u \pi d^2 / 4}{\gamma_V} \tag{2.4}$$

and

$$P_{Rd} = \frac{0.29 \alpha d^2 \sqrt{f_{ck} E_{cm}}}{\gamma_V} \tag{2.5}$$

where:

$$\alpha = 0.2(h_{sc}/d + 1) \le 1, \text{ for } h_{sc}/d \ge 3 \tag{2.6}$$

d is the stud shank diameter;

h_{sc} is the overall shear connector height;

f_u is the characteristic stud tensile strength, which should be taken as 500 MPa at maximum;

f_{ck} is the characteristic cylinder compressive strength of the concrete;

E_{cm} is the secant modulus of elasticity of concrete;

γ_V is the partial safety factor, whose recommended value is 1.25.

Reduction factor k_l for sheeting with ribs parallel to the supporting beam is given as:

$$k_l = 0.6 \frac{b_0}{h_p} \left(\frac{h_{sc}}{h_p} - 1 \right) \le 1 \tag{2.7}$$

where b_0 and h_p are the dimensions of the rib, presented in Figure 2.21. The upper limit of the overall shear connector height is set to $h_p + 75$ mm.

21

open trough profile   re-entrant trough profile
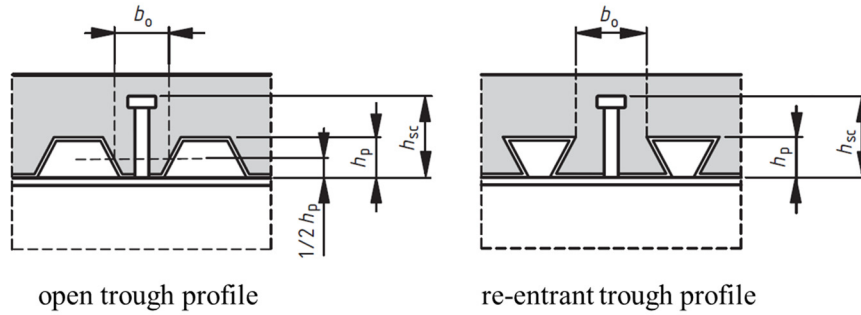
Figure 2.21: Geometric parameters according to EN 1994-1-1:2004 [10].

Reduction factor k_t for sheeting with ribs transverse to the supporting beam is given as:

$$k_t = \frac{0.7}{\sqrt{n_r}} \frac{b_0}{h_p} \left(\frac{h_{sc}}{h_p} - 1 \right) \tag{2.8}$$

where $n_r \leq 2$ is the number of stud connectors in a rib.

Eq. (2.8) is applicable in a certain scope: the diameter of the stud should not be greater than 20 mm (for through deck welding), i.e. 22 mm (when holes are provided in the sheeting), profiled steel sheeting dimensions should be $h_p \leq 85$ mm and $b_0 \geq h_p$. EN 1994-1-1:2004 also defines upper limits of reduction factor k_t depending on the number of stud connectors per rib, sheeting thickness, and installation technique (through deck welding or profiled sheeting with holes), as shown in Table 2.2. Due to the recommended connection geometry, in many cases, these upper limits are decisive in the determination of k_t, which means that the reduction coefficient is rather constant [58].

Table 2.2: Upper limits of the reduction factor k_t [10].

Number of stud connectors per rib	Profiled sheeting thickness, t [mm]	Welded through profiled sheeting and $d \leq 20$ mm	Profiled sheeting with holes and $d = 19$ mm or $d = 22$ mm
1	≤ 1	0.85	0.75
	> 1	1.00	0.75
2	≤ 1	0.70	0.60
	> 1	0.80	0.60

For any rib orientation, EN 1994-1-1:2004 requires that the height of the connector should be at least $2d$ above the rib of the profiled steel sheeting and sets the lower limit of the rib width to 50 mm. The overall slab depth should be at least 90 mm, whereas the slab depth above the sheeting rib should be at least 50 mm.

2.2.2 Weaknesses of EN 1994-1-1 Design Procedures. Alternative Approaches

Although rules considering shear connectors are covered by design codes, many research results have proven that EN 1994-1-1:2004 underestimates the welded stud resistance in profiled sheeting with ribs transverse to the supporting beam. The application of reduction factors is questionable due to differences between typical failure modes in solid slabs and slabs with profiled steel sheeting. Moreover, in the current standard, the impact of stud position inside the concrete rib is not accounted for when determining the resistance of shear connectors, even though such position is allowed: "where the sheeting is such that studs cannot be placed centrally within a trough, they should be placed alternately on the two sides of the trough, throughout the length of the span" [10]. Experimental results showed up to a 50% difference in the ultimate load when studs were placed eccentrically inside the rib on the two different sides [58], which are marked as favourable and unfavourable positions in Figure 2.22.

In contrast to EN 1994-1-1:2004, ANSI/AISC 360-16 [5] incorporates the influence of headed stud position inside the rib defining the values of reduction factor R_g when the distance e (Figure 2.22) is

smaller or greater than 50 mm. Also, ANSI/AISC 360-16 covers connections with more than two headed studs per rib through the reduction factor R_p. However, both reduction factors are given as constants depending on the number of studs and stud position, without the consideration of decking geometry and welded stud height. The headed stud shear resistance for sheeting with ribs transverse to the beam is determined as the minimum between $R_g R_p f_u d^2 \pi/4$ and $0.5 d^2 \pi/4 \sqrt{f_c'} \sqrt{E_c}$, where the first condition is commonly relevant. As well as in EN 1994-1-1:2004, reduction factors were derived by statistical evaluation of experimental results.
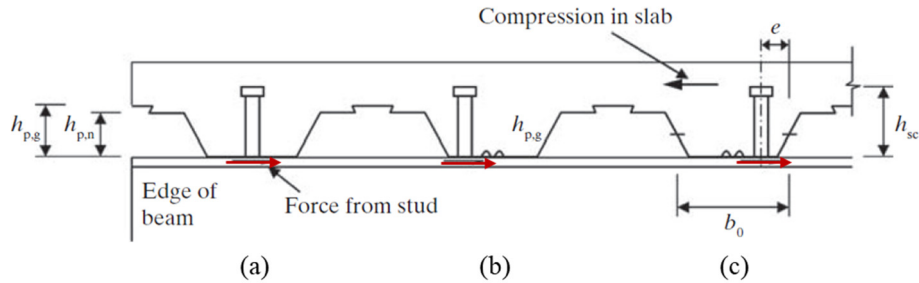
Figure 2.22: Stud position inside the rib: (a) central, (b) favourable, (c) unfavourable [66].

In addition to the codified design rules, a number of studies were conducted with the purpose of providing satisfactory predictions that cover the geometry of different types of commercially available metal decking and overcoming the weaknesses of current design codes. Many authors have developed analytical models for shear resistance of headed studs in profiled sheeting with ribs transverse to the beam based on real failure modes in composite concrete slabs. To keep the design rules simple, in some cases reduction factors have been derived from developed models, comparing results with design criteria given for solid slabs.

Table 2.3: Design models for the resistance of welded headed studs in profiled sheeting with ribs transverse to the beam.

Model	Applicable for open trough profiled sheeting	Applicable for re-entrant trough profiled sheeting	Max. number of studs per rib	Considers stud position inside the rib	Max. profiled sheeting depth [mm]	Other limits
Lungershausen [62]	yes	yes	3	no	140	$h_{sc}/d \geq 4$ $h_{sc} - h_p \geq 2d$
Johnson and Yuan [60]	yes	no	2	yes	not specified	16 mm $\leq d \leq 20$ mm $0.8 \leq b_0/h_p \leq 3.2$ $h_{sc} - h_p \geq 35$ mm
Rambo-Roddenberry [68]	yes	no	2	yes	76	$h_p = \{25; 38; 51; 76\}$ mm
Ernst [69]	yes	no	2	no	not specified	not specified
Konrad [1]	yes	yes	2	yes	not specified	16 mm $\leq d \leq 22$ mm $h_{sc}/d \geq 4$ $h_{sc}/h_p \geq 1.56$
Nellinger [67]	yes	yes	3	yes	155	16 mm $\leq d \leq 22$ mm $h_{sc} - h_p \geq d$
Vigneri [64]	yes	yes	2	no	136	19 mm $\leq d \leq 22$ mm $h_{sc} - h_p \geq 2d$

23

Several models and their scope of application are listed in Table 2.3. Models with the widest range of application are those proposed by Konrad [1] and Nellinger [67], covering both re-entrant and open trough profiled sheeting, and considering headed stud position inside the rib. The model suggested by Nellinger was the basis for the calculation models and design recommendations proposed by the working group CEN/TC250/SC4.PT3 [3]. In the next subchapters, models proposed by Konrad [1] and working group SC4.PT3 [3] are described in detail.

2.2.3 The Model according to Konrad

The model proposed by Konrad [1], [70] for ribs transverse to the supporting beam, suggests calculation of headed stud resistance through a similar algorithm as prescribed in EN 1994-1-1:2004, i.e. the headed stud resistance for solid slabs should be multiplied by a specific reduction factor, $k_\perp$. Konrad defines new expressions for the headed stud resistance inside a solid slab, which include the parameter of the effective area of the weld collar, $A_{\text{Wulst,eff}}$, but exclude the stud height. The design resistance is obtained as the minimum between Eqs. (2.9) and (2.10):

$$P_{\text{Rd,s}} = \left[313 \, A_{\text{Wulst,eff}} \left(\frac{f_{\text{ck}}}{30} \right)^{2/3} + 240 \, d^2 \left(\frac{f_{\text{u}}}{500} \right) \right] \frac{1}{\gamma_{\text{V}}} \qquad \text{[N]} \qquad (2.9)$$

and

$$P_{\text{Rd,c}} = \left[326 \, A_{\text{Wulst,eff}} \left(\frac{f_{\text{ck}}}{30} \right)^{2/3} + 220 \, d^2 \left(\frac{f_{\text{ck}}}{30} \right)^{1/3} \left(\frac{f_{\text{u}}}{500} \right)^{1/2} \right] \frac{1}{\gamma_{\text{V}}} \qquad \text{[N]} \qquad (2.10)$$

where:

$A_{\text{Wulst,eff}}$ is the effective area of the weld collar of a headed stud,

$$A_{\text{Wulst,eff}} = 0.5 \, h_{\text{Wulst}} \, d_{\text{Wulst}} \quad [\text{mm}^2] \qquad (2.11)$$

d is the headed stud shank diameter in mm;

h_{Wulst} is the height of the weld collar in mm;

d_{Wulst} is the diameter of the weld collar in mm;

f_{u} is the characteristic stud tensile strength in MPa;

f_{ck} is the characteristic cylinder compressive strength of the concrete in MPa;

γ_{v} is the partial safety factor, 1.25.

Values of the effective area of the weld collar for common headed stud shank diameters are given in Table 2.4.

Table 2.4: Effective area of the weld collar [1].

Diameter of the headed stud shank	Height of the weld collar	Diameter of the weld collar	Effective area of the weld collar
d [mm]	h_{Wulst} [mm]	d_{Wulst} [mm]	$A_{\text{Wulst,eff}}$ [mm^2]
16	4.5	21.0	47.3
19	6.0	23.0	63.0
22	6.0	29.0	87.0
25	7.0	40.0	140.0

Although Eqs. (2.9) and (2.10) might seem statistically obtained, they were developed assuming three load components that Lungershausen [62] had described: pressure on the weld collar, bending of the stud shank and horizontal component of the tensile force in the stud, whereas friction forces were not accounted for. The expressions got their final form by applying certain simplifications.

The scope of application is defined for headed stud geometry: 16 mm $\leq d \leq$ 25 mm, $h_{\text{sc}}/d \geq 4$, and material properties: 20 MPa $\leq f_{\text{ck}} \leq$ 100 MPa, $f_{\text{u}} \leq$ 740 MPa.

Konrad conducted 17 push-out tests with three types of profiled steel sheeting by varying the number of reinforcement layers, stud height and position and number of headed studs inside the rib. According to experimental results, numerical models were developed and used for the determination of the reduction factor $k_\perp$, which was defined as:

- for pre-holed steel sheeting:

$$k_\perp = k_n \left[k_e \; 0.038 \; \frac{b_m}{h_p} + 0.597 \right] \leq 1 \tag{2.12}$$

- for welded-through headed studs, with sheeting thickness $t \geq 0.75$ mm:

$$k_\perp = k_n \; k_{Tr} \left[k_e \; 0.042 \; \frac{b_m}{h_p} + 0.663 \right] \leq 1 \tag{2.13}$$

where:

$$k_n = \begin{cases} 1.0, & n_r = 1 \\ 0.8, & n_r = 2 \end{cases} \tag{2.14}$$

$$k_e = \begin{cases} 1.0, & 55 \text{ mm} \leq e \leq 100 \text{ mm} \\ 2.0, & e > 100 \text{ mm} \end{cases} \tag{2.15}$$

$$k_{Tr} = \begin{cases} 1.25, & \text{re-entrant trough profile} \\ 1.00, & \text{open trough profile} \end{cases} \tag{2.16}$$

n_r is the number of headed studs in the rib;

b_m, h_p and e are defined in Figure 2.23.

| open trough profile | re-entrant trough profile |
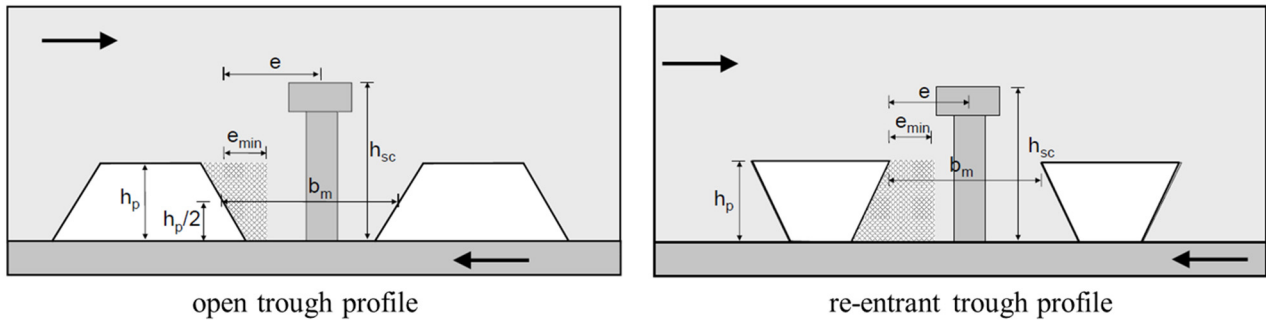
Figure 2.23: Geometric parameters according to Konrad [1].

In the case of welded-through headed studs when profiled steel sheeting thickness is $t < 0.75$ mm, Eq. (2.12) could be applied.

As shown, the reduction factors that are given by Konrad account for the geometry of profiled steel sheeting, the number of studs and their position inside the rib, presented through the distance between the rib wall and the stud in the direction of shear force, marked with e.

The design resistance of welded headed studs in ribs transverse to the beam should be obtained as:

$$P_{Rd} = k_\perp \; P_{Rd,c} \leq P_{Rd,s} \tag{2.17}$$

As well as the current design standard EN 1994-1-1:2004, Konrad's model is limited to the maximum of two headed studs per rib and connectors with a diameter between 16 mm and 20 mm for through deck welding, i.e. from 16 mm to 22 mm in the case of the pre-holed steel sheeting. The minimum anchorage depth of connectors is required to comply with the following condition $h_{sc}/h_p > 1.56$.

Eqs. (2.12) and (2.13) are not applicable when the distance e is smaller than 55 mm, which is labelled as the unfavourable position of headed studs. Even though Konrad proposed another equation for connections with $e < 55$ mm, he suggested avoiding such stud placing due to a high coefficient of

variation when comparing design predictions with experimental results. However, for some commonly applied profiled steel sheeting, for example Cofraplus 60 [71], the criteria $e > 55$ mm cannot be matched even when a headed stud is placed centrally inside the rib. For that reason, further experimental testing was conducted through the DISCCO project funded by Research Fund for Coal and Steel [72] and analysed by Eggert [73], who tested the following equation given by Konrad:

$$k_\perp = k_n \left[0.317 \frac{b_m}{h_p} + 0.06 \right] \le 0.8 \tag{2.18}$$

Eggert reported that Eq. (2.18) provides mostly safe-sided predictions when compared with experimental results of push-out tests for two analysed types of profiled steel sheeting, as presented in Figure 2.24.
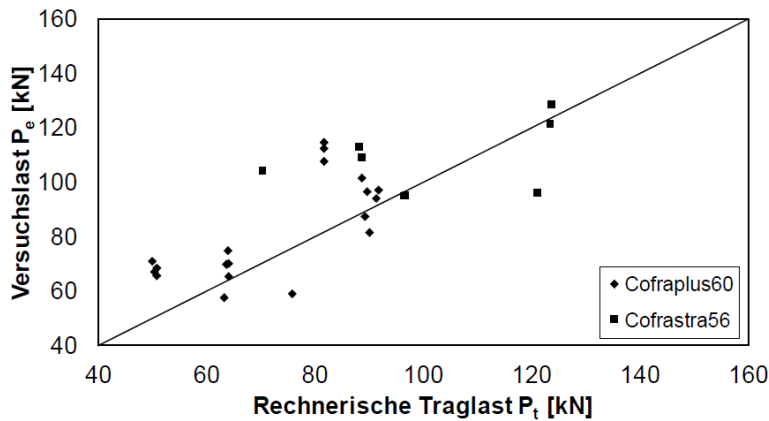
Figure 2.24: The experimental resistance vs. predicted resistance according to Konrad [73].

2.2.4 The Model according to SC4.PT3

The design procedures proposed by Nellinger [67] are based on mechanical models which describe failure modes in composite shear connections with profiled steel sheeting. Expressions cover deep steel decking, which is not the case with the current EN 1994-1-1:2004 rules, which are applicable to rib depth up to 85 mm. In total 33 push-out tests were conducted, varying the type of profiled steel sheeting, concrete strength, number of studs per rib, number of reinforcement layers, welding procedure and applied transverse loading. In the proposed equations, Nellinger included the influence of transverse loading, which was applied during experiments. However, as the calculation model [67] is complex for engineering practice, soon after Odenbreit and Nellinger [2] suggested a simplification of the model that is presented in the following.

The model is based on three load-bearing components: failure of concrete in tension during concrete cone failure, stud resistance to bending and shear failure of a stud. Simplified static schemes for concrete cone failure and headed stud bending, assuming the development of one and two plastic hinges, are presented in Figure 2.25. By superposition of these two bearing components, the first failure criterion is determined. Pure shear failure of a headed stud is assumed as the second failure criterion.
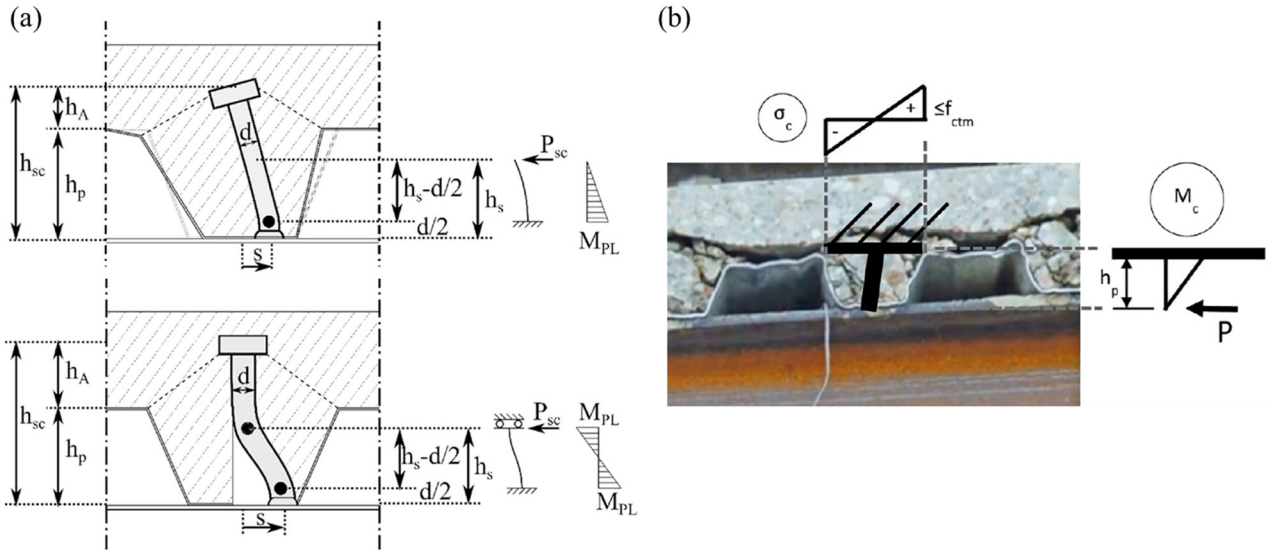
Figure 2.25: (a) Headed stud bending with one and two hinges [74], (b) Concrete cone failure [2].

According to Odenbreit and Nellinger [2], the design resistance of a shear connector should be obtained as the minimum between:

$$P_{Rd,1} = C_2 \left[\frac{\alpha_{ct} f_{ctm} W}{h_p \, n_r} + \frac{n_y \, M_{pl}}{h_s - d/2} \right] \frac{1}{\gamma_V} \tag{2.19}$$

and

$$P_{Rd,2} = C_1 f_u \pi \frac{d^2}{4} \frac{1}{\gamma_V} \tag{2.20}$$

where:

C_1 is the calibration factor, suggested value is 0.6;

C_2 is the calibration factor, suggested value is 0.9;

α_{ct} is the factor that accounts for the relaxation of concrete strength, proposed as $\alpha_{ct} = 0.85$;

f_{ctm} is the concrete tensile strength, ≥ 20 MPa;

W is the section modulus of concrete cone surface,

$$W = 0.4 \, h_{sc} \, b_{max}{}^3 / b_{top} \tag{2.21}$$

h_{sc} is the overall shear connector height;

b_{max} is the maximum width of the rib;

b_{top}, h_p and h_A are defined in Figure 2.26;

n_r is the number of headed studs in the rib;

n_y is the number of plastic hinges,

$$n_y = \begin{cases} 1, & h_A \leq 2d\sqrt{n_r} \\ 2, & h_A > 2d\sqrt{n_r} \end{cases} \tag{2.22}$$

M_{pl} is the bending resistance of a stud,

$$M_{pl} = f_u \frac{d^3}{6} \tag{2.23}$$

f_u is the characteristic stud tensile strength, ≥ 400 MPa;

d is the stud shank diameter;

h_s is the position of the upper plastic hinge,

$$h_s = \beta\, h_{sc} \leq h_p \tag{2.24}$$

$$\beta = \begin{cases} 0.45, \text{ open trough profile} \\ 0.41, \text{ re-entrant trough profile} \end{cases} \tag{2.25}$$

γ_v is the partial safety factor, 1.25.
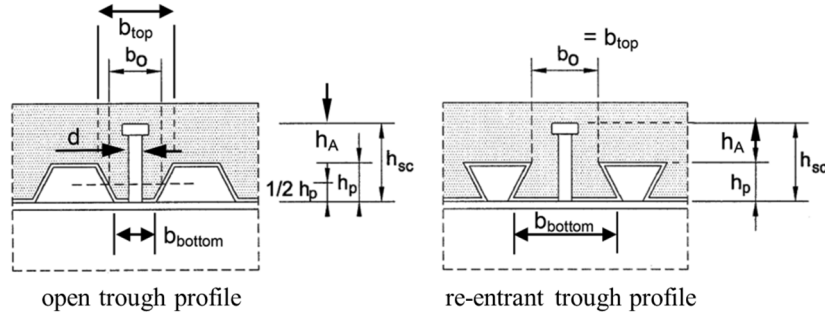
Figure 2.26: Geometric parameters according to Nellinger [67].

The described model was the base of the design procedure suggested by the working group CEN/TC250/SC4.PT3 [3]. The new model is recommended for headed studs in open trough profiled sheeting if any of the following two conditions are satisfied: $h_A \leq 2.7d$ or $e \leq 60$ mm (Figure 2.23.a). For open trough or re-entrant trough profiles that do not satisfy the requirement, the existing design procedures in EN 1994-1-1:2004 [10] are referred.

Not unlike the model proposed by Odenbreit and Nellinger [2], the model given by SC4.PT3 also considers a stud position inside a rib. New forms of Eqs. (2.19) and (2.20) are:

$$P_{Rd,1} = \alpha_N\, C_2 \alpha_{c2}\, k_u \left[\frac{f_{ctk}\, W}{h_p\, n_r} + \frac{n_y\, M_{pl}}{0.82 h_p - d/2} \right] \frac{1}{\gamma_V} \tag{2.26}$$

and

$$P_{Rd,2} = \alpha_N\, 0.58 f_u \pi \frac{d^2}{4} \frac{1}{\gamma_V} \tag{2.27}$$

where:

$$\alpha_N = \begin{cases} 1.15, \text{ for 10 or more ductile headed stud connected ribs} \\ 1.0, \text{ otherwise} \end{cases} \tag{2.28}$$

$$C_2 = 1.85\, h_p/b_0, \quad 1.0 \leq C_2 \leq 1.35 \tag{2.29}$$

α_{c2} is the factor that accounts for relaxation effects, with recommended value $\alpha_{c2} = 1.0$;

k_u is the correction factor given in Table 2.5;

f_{ctk} is the characteristic value of concrete tensile strength;

f_u is the characteristic stud tensile strength, which should be taken as 450 MPa maximum;

$$W = (2.4\, h_{sc} + (n_r - 1)\, e_t)\, b_{max}^{3} / (6\, b_{top}) \tag{2.30}$$

$$n_y = \begin{cases} 2, \; n_r = 1 \text{ or staggered position} \\ 1 + \dfrac{h_A - 2d}{0.52d} \leq 2, \; n_r = 2 \end{cases} \tag{2.31}$$

e_t is the transverse spacing between the studs inside the rib;

all the other symbols are as defined for the previous model, Eqs. (2.19) and (2.20).

Table 2.5: Correction factor k_u [3].

k_u	Profiled sheeting with holes	Welded through profiled sheeting	
		$t < 1$ mm	$t \geq 1$ mm
Centred or staggered position	1.00	1.05	1.25
Favourable position	1.10	1.16	1.38
Unfavourable position	0.80	0.95	1.00
Alternately placed studs	0.95	1.00	1.19

Proposed Eq. (2.26) includes variations in the position of headed studs inside the concrete rib through the correction factor k_u, covering possible cases presented in Figure 2.27.
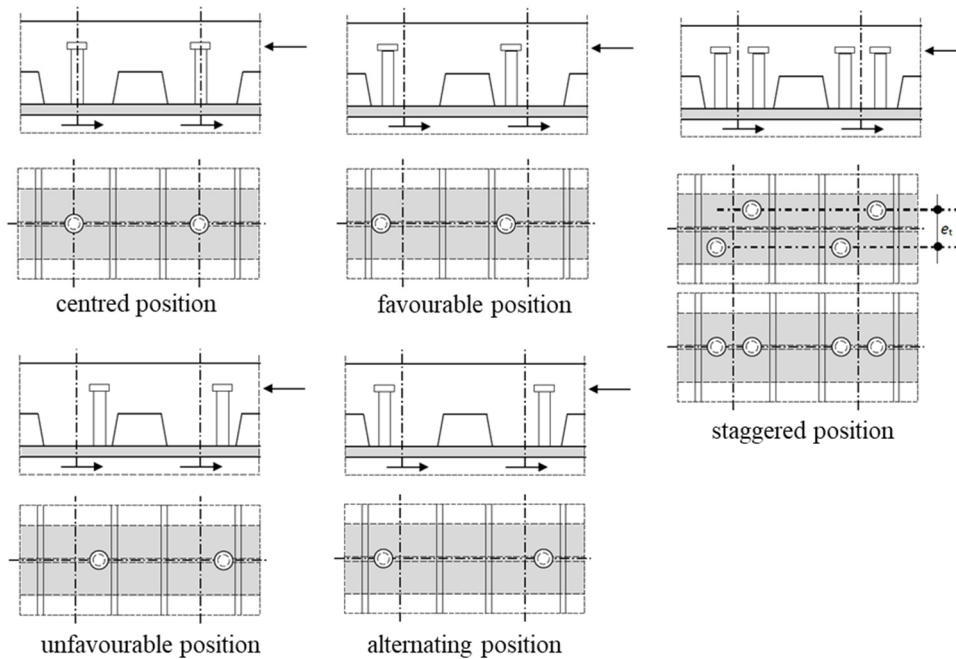
Figure 2.27: Headed stud position in the rib [3].

As well as the current EN 1994-1-1:2004 rules, the proposal suggested by SC4.PT3 is applicable if there are no more than two shear connectors per rib and the stud diameter is not greater than 20 mm when through deck welding is applied, i.e. 22 mm when holes are provided in the profiled sheeting. Moreover, it is required for the bottom reinforcement layer to be placed below the head of the stud.

2.2.5 Slip Capacity

The plastic design approach is commonly applied in steel-concrete composite beams of building structures. Development of plastic hinges and stress redistribution in the beam are followed by increased deformations of the shear connection, which needs to be adequately designed. Shear connectors should be ductile, providing sufficient slip capacity to justify the plastic distribution of shear. On the other hand, the application of partial shear connection is a common practice in composite slabs with ribs transverse to the supporting beam where the number of headed studs along the beam length is limited by the profiled sheeting geometry. In that case, the plastic capacity of the composite beam is restricted by the longitudinal shear resistance and deformation capacities of installed connectors. If the slip capacity of a connector is insufficient, premature failure of the beam may be induced. Therefore, special care should be devoted to proving the appropriate ductility of shear connectors.

Generally, slip at the beam end is larger for longer spans and lower degrees of shear connection. To apply the partial shear design approach, the degree of shear connection needs to be beyond the set limits according to EN 1994-1-1:2004 [10], depending on the effective beam span length, steel yield

strength and the ratio between areas of two steel flanges. At the same time, shear connectors need to be headed studs with $h_{sc} \geq 4d$, 16 mm $\leq d \leq$ 25 mm. If all conditions are satisfied, headed studs may be considered ductile. If the applied connection cannot fulfil the mentioned requirements, experimental push-out tests following Annex B of EN 1994-1-1:2004 need to be conducted to obtain the shear connection slip capacity. According to EN 1994-1-1:2004, "a connector may be taken as ductile if the characteristic slip capacity is at least 6 mm" [10], where the characteristic slip capacity corresponds to the minimum of all test values obtained as shown in Figure 2.28 and reduced by 10%.
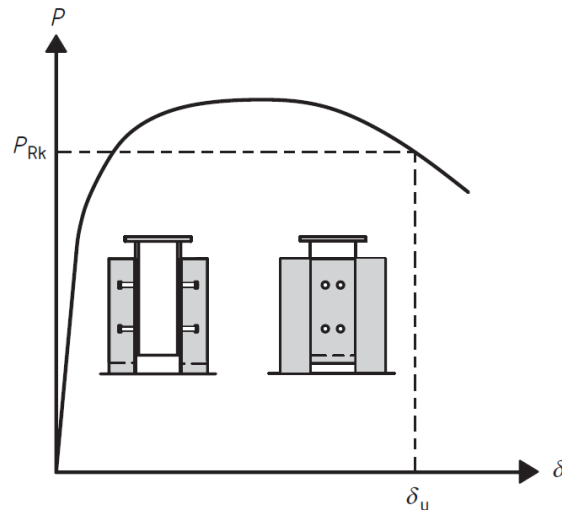
Figure 2.28: Experimental determination of slip capacity [10].

2.2.6 Push-Out Test Set-Up

Push-out tests are the most commonly performed tests for investigating composite shear connection behaviour. In EN 1994-1-1:2004, Annex B [10] directions for push-out tests for specimens with solid concrete slabs are provided. However, EN 1994-1-1:2004 does not cover a specific test set-up for composite slabs with profiled steel sheeting. Appropriate test arrangements have been widely discussed, as the geometry of specimens, boundary conditions and load application directly affect the connection response.

Hicks [66] conducted push-out and beam tests on specimens cast in open trough profiled sheeting, comparing shear connection response in two cases. He concluded that the mismatch of load-slip curves in the two cases is a result of the absence of the compression force at the steel-concrete interface in push-out tests, which is present in real composite steel-concrete beams. That compression force is essential for composite concrete slabs as it resists the tension force in headed studs, activated during pull-out failure. Hence, the lower ductility and smaller ultimate load measured during push-out tests could be explained. The application of constant concentric transverse loading during push-out tests, equal to 12% of the ultimate load, showed the best match with composite beam behaviour.

On the other hand, some authors [58] attributed differences in the shear response of push-out and beam tests to the development of friction forces. As positive effects of friction on the resistance of shear connectors are not incorporated in design codes, push-out tests were found as the relevant experimental procedure for obtaining the connector shear resistance. Although friction forces are present in the common beams, in certain cases these effects should not be taken into account, e.g. when cycle loading is applied to the beam. Therefore, the elimination of friction effects during experimental testing is recommended.

Several authors, as Ernst [69] and Qureshi [75], opted for one-side push-out tests, where the load is applied in a horizontal direction, as presented in Figure 2.29. That set-up enables easier fabrication of specimens due to the presence of only one concrete slab. In addition, results of push-out tests are expected to be closer to the beam behaviour as the slab self-weight is included.
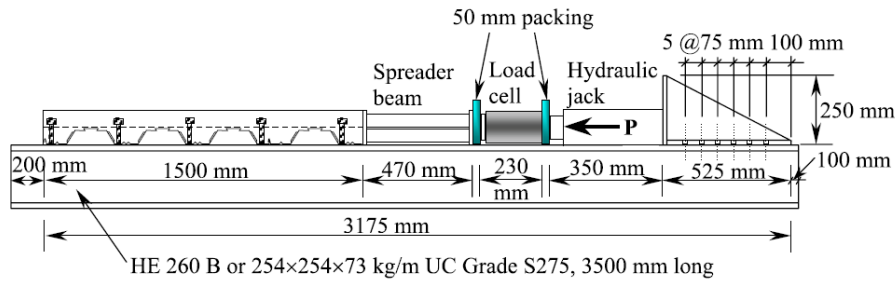
Figure 2.29: Horizontal push-out test [75].

In order to propose a standard push-out test set-up for double-symmetric specimens, experimental investigations were conducted as a part of the DISCCO project [72]. To one group of specimens, transverse loading was applied through a hydraulic jack, whereas the other group was constrained by tension ties. It was observed that tension ties were not activated during testing, except in some cases when specimens bent. Transverse loading was applied concentrically and eccentrically, as shown in Figure 2.30, and the degree of transverse loading was varied, all to simulate real loading conditions in composite beams. The results showed that the impact of the transverse load application on the results is highly dependent on the failure mode. Therefore, it was suggested to apply transverse loading of 10% of the ultimate load, if the ratio between stud height and rib height is smaller than 1.56. In those cases, it is recommended to use a hydraulic jack, whereas eccentricity is optional.
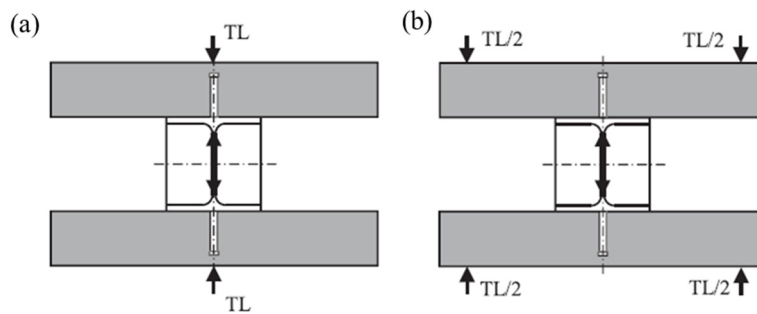
Figure 2.30: Transverse load application [61]: (a) concentric, (b) eccentric.

The recommended standard specimen geometry [72] is presented in Figure 2.31. The specimen height is dependent on the profiled sheeting geometry. Slab width should be sufficiently adopted to include the whole concrete cone that develops during a pull-out failure in push-out tests. The concrete cone width may be approximated with $e_t + 2\ h_{sc}/\tan(25^o)$, where e_t is the transverse spacing between the studs inside the concrete rib and h_{sc} is the height of the stud.
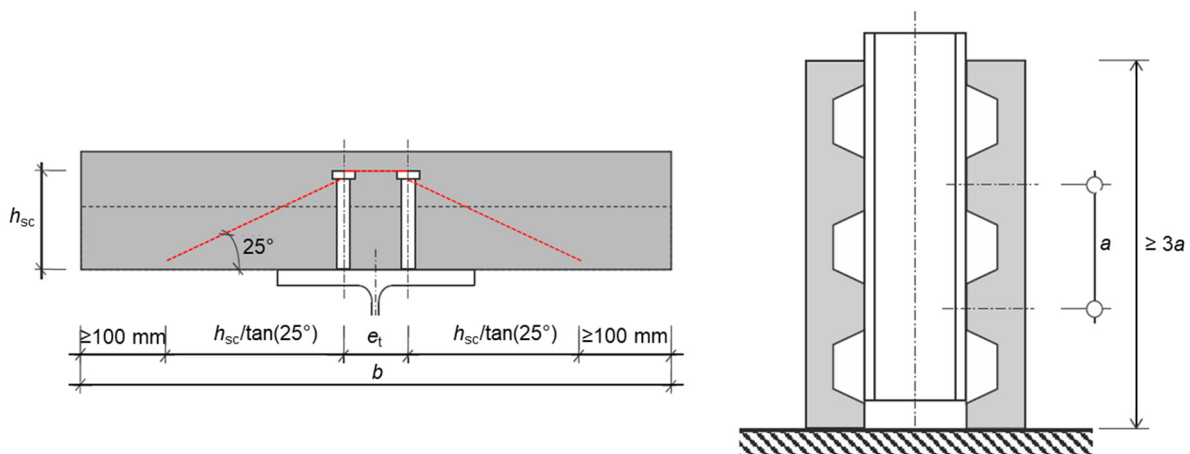
Figure 2.31: Recommended push-out test set-up [72].

According to the DISCCO project report [72], the recess at the base of the concrete slab is optional, but if it is formed, sufficient horizontal reinforcement above the recces should be provided. The recess

31

in the concrete slab was proved not to affect the shear resistance or slip capacity of the connection according to Eggert [73] and Vigneri [64].

2.2.7 Influence of the Concrete Reinforcement

According to EN 1994-1-1:2004 [10], the minimum amount of reinforcement in the concrete slab of the composite beam in both directions is 80 mm^2/m, with the shortest spacing between bars equal to double overall concrete slab depth or 350 mm, whichever is smaller. However, the position of the reinforcement inside the slab is not precisely defined for composite slabs with profiled steel sheeting. EN 1994-1-1:2004 requires that "the surface of a connector that resists separation forces (for example, the underside of the head of a stud) should extend not less than 30 mm clear above the bottom reinforcement" [10] and refers to Figure 2.32.a. On the other hand, according to Figure 2.32.b, the presence of only one reinforcement layer is allowed in slabs with profiled steel sheeting, which is inconsistent with the previous requirement [76].
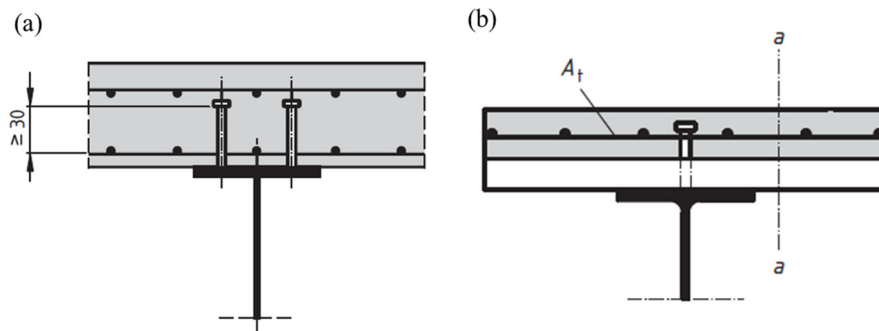
Figure 2.32: Reinforcement in composite beams according to EN 1994-1-1:2004 [10].

To increase the resistance of headed studs in profiled steel sheeting, various reinforcement arrangements have been analysed since the first studies in this field. On the one hand, the optimum position of mesh reinforcement along the concrete slab depth has been discussed, whereas, on the other hand, additional reinforcing elements placed inside the concrete rib have been developed and tested.

Konrad [58] reported that there was no considerable difference at the point of the ultimate load between the push-out specimen with one reinforcement layer in the upper zone of the concrete slab and the specimen with two reinforcement layers, where the additional layer was placed on the profiled steel sheeting. However, a notable difference in ductility was observed, as presented in Figure 2.33. The failure of the specimen with one reinforcement layer was described as a mixed failure of rib shearing, concrete pull-out and stud shearing, while rib shearing occurred for the specimen without bottom reinforcement.
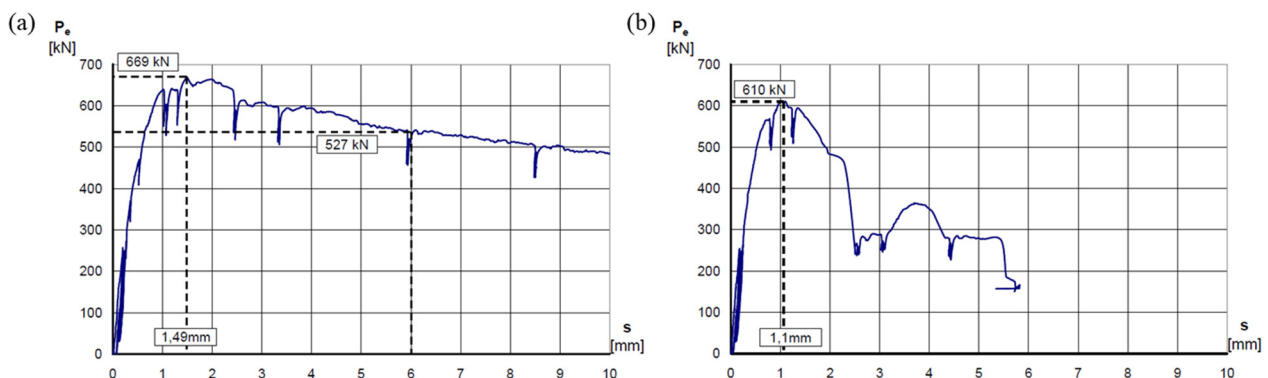
Figure 2.33: Load-slip curves obtained by Konrad [1]:
(a) specimen with bottom reinforcement, (b) specimen without bottom reinforcement.

Similar results concerning the impact of the bottom reinforcement were obtained for specimens featuring concrete pull-out failure, during experimental research conducted as a part of the DISCCO

project [72]. Nevertheless, for the specimens that failed by rib pry-out, the influence of the bottom reinforcement on the ultimate load and initial stiffness was significant, as presented in Figure 2.34. In that case, bottom bars reinforced the concrete cone around headed studs and increased the connector shear resistance by almost 50%.
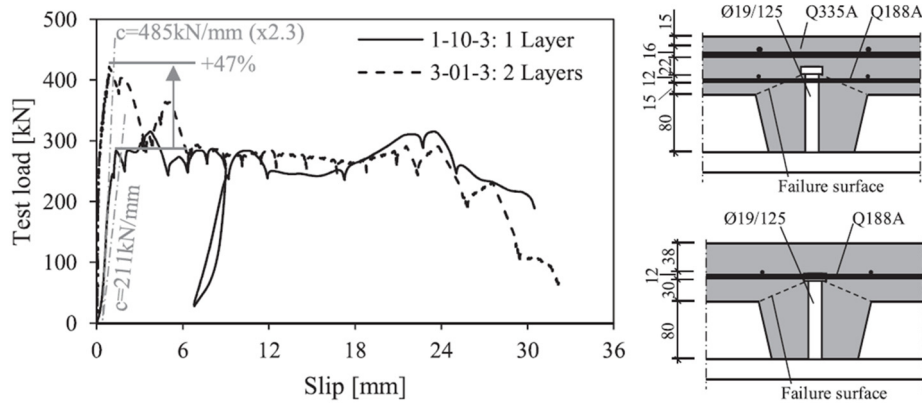
Figure 2.34: Load-slip curves for different reinforcement mesh patterns [61].

Vigneri [64] experimentally tested specimens with one layer of reinforcement mesh varying its position along the concrete slab depth: mesh above the head of the welded stud and mesh below the head of the welded stud. In both cases, pull-out failure of concrete cone occurred and similar load-slip curves were obtained, as shown in Figure 2.35.
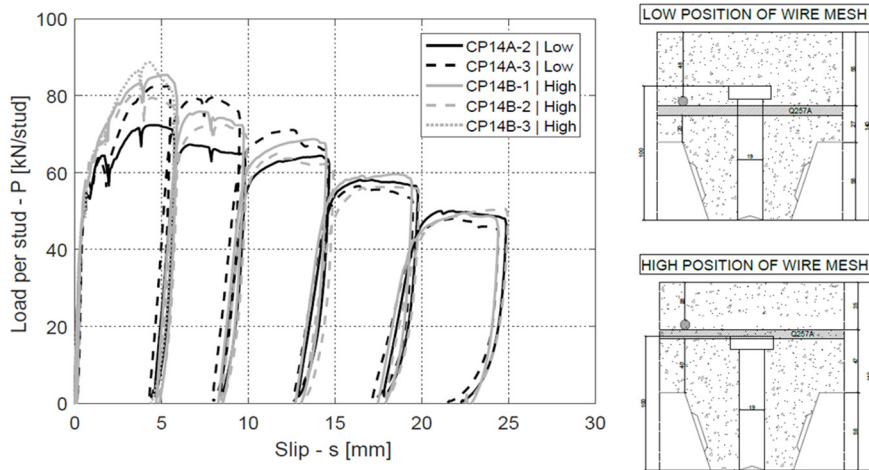
Figure 2.35: Load-slip curves for two positions of reinforcement mesh [64].

To improve headed stud performance, the implementation of an additional reinforcement inside concrete ribs has been studied. The solution with waveform reinforcement which follows the shape of open trough profiled steel sheeting was investigated by Patrick [77] (Figure 2.36.a), Ernst [76] (Figure 2.36.b) and Vigneri [64] (Figure 2.36.c). Ernst showed that reinforcement could increase ultimate loads and prevent rib-shearing and concrete pull-out failure, increasing the shear connector resistance by 20%. Specimens with waveform reinforcement showed about 80% higher load at 6 mm slip than those without it [76]. Vigneri [64] obtained similar results, showing that specimens with waveform reinforcement have approximately 26% higher shear resistance, as well as improved ductility.

Albarram [78] studied the behaviour of headed studs installed in deep steel decking, with rib depth larger than 80 mm. As these connections are characterised by brittle failure of concrete, the solution with the reinforcement grid placed inside the ribs of deep steel decking was suggested, as presented in Figure 2.36.d. The new solution affected ductility and increased the shear resistance of headed studs by 25%.
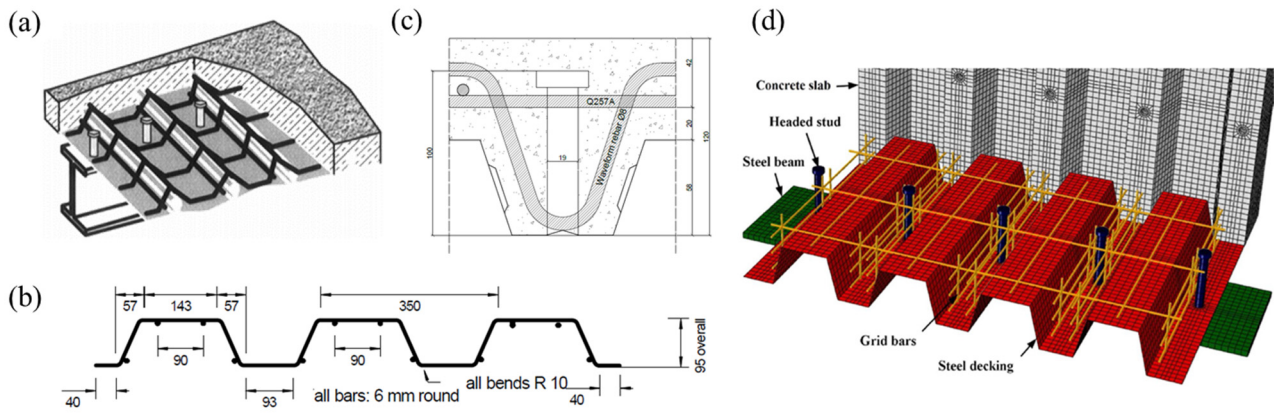
Figure 2.36: Various reinforcement arrangements [64], [77]–[79].

2.2.8 Summary

Although welded headed studs are widely used in steel-concrete composite structures, there are still certain unanswered questions considering their behaviour. Formulation of general expressions for the calculation of headed stud shear resistance when applied in composite slabs with profiled steel sheeting has been a challenge over the years. Reasons lie in a variety of profiled steel sheeting types on the construction market and different failure mechanisms depending on the connection geometry. In addition, different push-out test set-ups used in investigations complicate the manipulation of the experimental database.

Analytical procedures for calculating stud shear resistance published in the past years are mostly based on the mechanical models of failure in contrast to the design rules prescribed in EN 1994-1-1:2004 [10] which were statistically derived from experimental results. The existing design directions do not consider the headed stud position inside the rib. However, the prime drawback of the codified design rules refers to the unsafe predictions in certain cases when sheeting ribs are transverse to the supporting beam. Several studies showed a positive effect of the reinforcement installed in profiled sheeting ribs, although neither EN 1994-1-1:2004 [10] nor many proposed analytical expressions consider that parameter in headed stud resistance calculation.

Moreover, it is remarked that design procedures do not provide directions for obtaining headed stud shear resistance when profiled sheeting ribs are not transverse or parallel to the supporting beam. Reviewing the available literature in this field, studies investigating the response of welded headed studs for different profiled sheeting configurations with the angle between ribs and the beam in the range between 0° and 90° have not been found. Nevertheless, the angle between ribs and the beam smaller than 90° is not uncommon in practice, especially when building floors are of irregular shape. Therefore, the parameter of the angle between profiled sheeting ribs and the beam has been found appealing for research, and it is varied in the experimental and numerical studies of this thesis.

34

3 Connection Design

There are more than a few examples in construction where the application of demountable steel-concrete composite structures is highly favourable and beneficial. For instance, those are buildings that are subjected to changes over time (e.g. industrial buildings in which production processes are developing and changing, business parks with changing market requirements), different short-term structures and buildings that require relocation (e.g. multi-storey car park buildings, educational buildings) [12].

In this chapter, the proposed demountable shear connection is presented through the case study of a multi-storey car park building, as a typical example of a structure that may be subjected to deconstruction, relocation and multiple uses. The preliminary design is described, analysing the effects of the connection implementation in the car park building. Detailing of the shear connection is discussed and key parameters that are analysed in the experimental and numerical works are introduced.

3.1 Case Study

The multi-storey car park building "Obilićev venac" in Belgrade was designed and built in the 1970s as a demountable steel-concrete composite structure. The main bearing structure consisted of steel frames. The floor was formed of prefabricated solid concrete slabs, connected to steel beams by high-strength friction-grip bolts. However, over the course of 40 years, the serviceability of the building became considerably affected by significant deformations of the floor structure. The conducted monitoring showed a progressive increase in beam deflections over time as a result of the composite action loss between steel beams and concrete slabs. Friction-grip bolts were subjected to corrosion, influencing the significant reduction of the bolt cross-sectional area and decrease of the connector shear resistance, inducing the final failure of the shear connection. During the reconstruction, friction-grip bolts were replaced by welded headed studs as a work- and cost-effective repair solution, providing better durability than the original design. However, the installation of stud connectors transformed the floor structure into a non-demountable system.

As an alternative demountable solution for application in the car park building "Obilićev venac", the implementation of a new floor structure is proposed and discussed. Design is based on the input parameters according to the original car park building project: beams' spans, spacing, beam profiles, steel grade and concrete class. In addition to the structure self-weight, the following loads have been adopted for design: live load during construction 0.75 kN/m^2, installations 1.0 kN/m^2 and live load in garage 2.5 kN/m^2 [80].

To connect steel beams and concrete slabs, a demountable connection with headed studs and bolts is applied. The requested material for the two different beams in the building structure, spanning 15 m and 10 m, is summarised in Table 3.1. Three different types of open trough profiled metal decking commercially available in Europe are analysed: Cofraplus 60 [71], ComFlor 60 [81] and Multideck 60-V2 [82]. All three selected types have an overall depth of approximately 60 mm, which is considered an optimum solution for the analysed composite concrete slabs spanning 2.3 m.

The proposed floor structure consists of composite concrete slabs of the overall depth of 120 mm, cast in open trough profiled steel sheeting. Slabs are discontinuous over the support, with the installed angles on the edges in contact with the beam, according to the connection layout presented in Figure 3.1. Headed studs are welded to angles and bolts connect angles with the beam top flange. To dismantle the structure, bolts should be removed and concrete slabs separated from the steel beam. In the second life cycle of the structure, slabs may be reused, as well as beams. As bolts are entirely removed during deconstruction, they are not affected during transportation to another location. To accomplish convenient transportation, slab segments 5.0×2.3 m, weighing 2.7 tonnes are suggested.

Table 3.1: Proposed solutions for two analysed beams of the car park building.

Beam span	15 m			10 m		
Beam spacing	2.3 m			2.3 m		
Steel grade	S355			S235		
Beam profile	IPE 400			IPE 360		
Concrete class	C30/37			C30/37		
Concrete slab depth	120 mm			120 mm		
Profiled steel sheeting	Cofraplus 60	ComFlor 60	Multideck 60-V2	Cofraplus 60	ComFlor 60	Multideck 60-V2
Concrete volume per 1 m^2	0.085 m^3	0.088 m^3	0.085 m^3	0.085 m^3	0.088 m^3	0.085 m^3
Headed studs	d = 16 mm, h_{sc}=100 mm	d = 16 mm, h_{sc}=100 mm	d = 16 mm, h_{sc}=100 mm	d = 16 mm, h_{sc}=100 mm	d = 16 mm, h_{sc}=100 mm	d = 16 mm, h_{sc}=100 mm
Bolts	M16 8.8	M20 8.8	M20 8.8	M16 8.8	M20 8.8	M20 8.8
Longitudinal spacing between headed studs [mm]	207	300	332	207	300	332
Longitudinal spacing between bolts [mm]	414	600	664	414	600	664
Number of connectors per cross-section	2	2	2	2	2	2
Total number of headed studs	146	100	90	96	66	60
Total number of bolts	72	50	44	48	32	30
Additional elements	steel angles t_p = 8 mm			steel angles t_p = 8 mm		
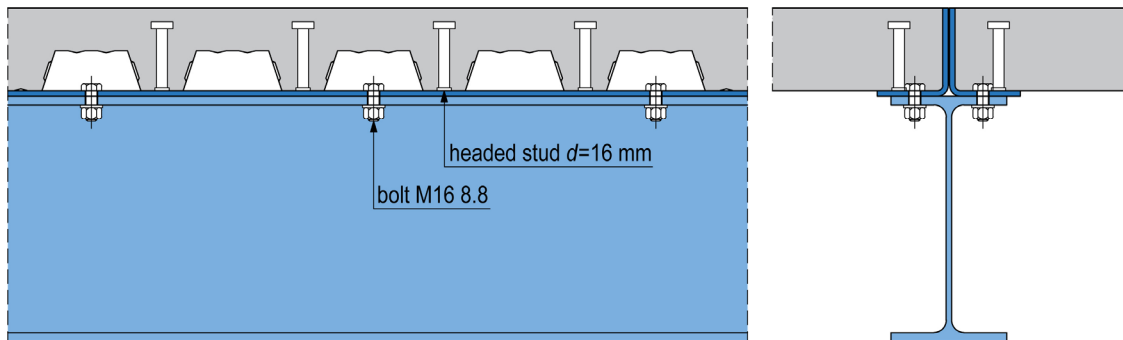
Figure 3.1: Layout of the demountable shear connection with profiled steel sheeting Cofraplus 60.

The proposed demountable shear connection contains headed studs of 16 mm in diameter and 100 mm in height, and M16 or M20 bolts of grade 8.8. A pair of headed studs is set in each sheeting rib, whereas a pair of bolts is set between every second rib. For the beams spanning 15 m and 10 m, the total number of headed studs is in the range of 90–146 and 60–96, respectively, depending on the selected metal decking. The total number of bolts is approximately two times smaller. Prediction for bolts in the longitudinal spacing twice longer than the spacing between headed studs leads to savings in execution time and costs.

The number of connectors and their diameters are adopted according to design rules in EN 1993-1-8:2005 [7] and EN 1994-1-1:2004 [10], with the initial assumption of keeping the bolts' resistance greater than headed studs' and therefore avoiding large bolt deformations and failure. In other words, it is presumed that bolts' response is elastic at ultimate loads, whereas headed studs' deformation is in the plastic domain. Therefore, simple dismantling of bolts is assured, whereas good mechanical performance of headed studs is exploited. Design resistance of headed studs used with different metal decking, calculated according to EN 1994-1-1:2004 [10], and design shear resistance of bolts,

calculated according to EN 1993-1-8:2005 [7], are given and compared in Table 3.2. Nevertheless, findings presented in Chapter 2 indicate that the design rules given in EN 1994-1-1:2004 overestimate the shear resistance of headed studs for profiled sheeting with narrow ribs, as Cofraplus 60. Hence, it may be expected that the real ratio between headed stud and bolt resistance is even smaller.

Table 3.2: Design shear resistance of headed studs and bolts.

Headed stud	Design shear resistance of the headed stud	Bolt	Design shear resistance of the bolt	Ratio	Ratio
	P_{Rd} [kN]		F_{Rd} [kN]	P_{Rd} / F_{Rd}	$2P_{Rd} / F_{Rd}$
d = 16 mm in Cofraplus 60	29.16	M16 8.8	77.21	0.38	0.75
d = 16 mm in ComFlor 60 or Multideck 60-V2	34.74	M20 8.8	120.64	0.29	0.58

It should be emphasised that the design resistance of headed studs presented in Table 3.2 is calculated assuming the position of a continuous slab over the beam. However, as the proposed design includes a discontinuous slab, effects of the slab discontinuity on the connection response should be determined and the validity of the initial assumption should be tested. The actual resistance of the demountable connection is analysed through the experimental and numerical analyses in the thesis. Connection stiffness and ductility are also examined, comparing the responses of demountable and corresponding non-demountable connections.

The total number of connectors implemented in the demountable connection is larger in comparison with the other demountable steel-concrete composite solutions with bolts. However, this system does not require special tools and additional parts, such as steel/PVC cylinders and helical reinforcement, which are needed for shear connections with friction-grip bolts. Moreover, both types of connectors, headed studs and bolts, are commercially available standard products commonly used in construction.

The described system with headed studs and bolts features two shear planes: (1) on the contact between angles and the top flange, and (2) on the contact between angles and the concrete slab. As a consequence, the transfer of shear force is indirect, with the force passing through the angles. The presence of two shear planes affects the total connection slip, which is dependent on the slip of headed studs in the shear plane "angle-concrete slab", and bolts in the shear plane "steel profile-angle". As bolts are installed in holes with adequate bolt-to-hole clearances, it is assumed that bolts slip inside holes after the mounting. The initial slip of bolts leads to incomplete interaction between the concrete slab and steel beam, inducing additional deflections of the steel beam. This deflection may be calculated according to the equation based on the initial bolt-to-hole clearances [39] or considering the stiffness of a shear connector and the effect of its flexibility on the bending stiffness of a composite beam [12]. The average initial clearance of the adopted M16 bolt is 1 mm, assuming a bolt hole diameter of 18 mm. According to [39], the initial clearance induces additional deflections of steel beams: 18.6 mm for the beam of the profile IPE 400, spanning 15 m, and 13.6 mm for the beam of the profile IPE 360, spanning 10 m. In other words, according to the case of un-propped construction given in Table 3.3, for the first beam, additional deflection equals 23% of the deflection induced by dead weight in the first phase of construction, whereas for the second beam, it is 61% of the dead weight deflection (results are presented for profiled steel sheeting Cofraplus 60, as no significant differences in deflections between three proposed solutions with different types of analysed metal decking are observed). It is clear that for longer beam spans, application of propping is necessary to decrease deflections due to structure dead weight.

Nevertheless, the exact values of the required execution tolerances and bolt hole diameters should be defined, preferably by conducting full-scale beam tests and demonstrating assembling and disassembling of the system. Although bolt holes on beam flange and L profiles are cut by CNC machines, accomplishing very high precision, bolt mounting could be affected by girder

deformations, meaning that execution tolerances are highly dependent on the beam span. Again, the application of propping is suggested to minimise those effects. If oversized holes are designed, problems of the incomplete slab-beam interaction and initial deflections could be exceeded by implementing preloaded bolts or injecting resin in bolt holes.

Table 3.3: Deflections in the beam mid-span.

| Span | Beam profile | Mid-span deflection | | | | |
| | | Execution stage | | | Composite stage | |
		dead weight	initial slip	imposed load	dead weight	imposed load
[m]	-	[mm]	[mm]	[mm]	[mm]	[mm]
15	IPE 400	80.8	18.6	23.4	10.1	23.2
10	IPE 360	22.3	13.6	6.6	2.6	6.0

3.2 Detailing of the Shear Connection

Special attention should be devoted to the detailing of the demountable connection, with the accent on the connection between the composite concrete slab and angles, accomplished by headed studs. Detailing parameters should be carefully selected to provide the appropriate connection response. Parameters are discussed in the following, initial assumptions on their adoption are elaborated and further experimental and numerical investigations are announced.

The suggested connection includes cold-formed steel angles to which headed studs are welded, whereas bolts are used for connecting angles with the beam top flange. The thickness of the steel angle should be suitably adopted to avoid deformation of the bolt holes and plate beneath headed studs. EN 1994-1-1:2004 [10] requires the following: "except when the studs are located directly over the web, the diameter of a welded stud should be not greater than 2.5 times the thickness of that part to which it is welded, unless test information is provided to establish the resistance of the stud as a shear connector". In other words, the thickness of the component to which the stud is welded should be at least $0.4d$, where d is the diameter of the shank of a headed stud. For studs of 16 mm in diameter, the minimum thickness is $0.4d = 6.4$ mm; therefore, the adopted value is rounded and set to 8 mm. Bearing resistance at bolt holes for the angle thickness of 8 mm is greater than bolt shear resistance; hence, it is not considered critical. The validity of the selected thickness is examined through the experimental work. The optimum thickness is investigated in parametric analysis.

The proposed solution with headed studs of 16 mm in diameter and 100 mm in height, embedded in the concrete slab of 120 mm in thickness, satisfies all requirements given in EN 1994-1-1:2004 [10] considering a minimum total slab depth, minimum slab depth and minimum connector height above the top of the sheeting rib, and minimum concrete cover above the connectors.

The exact position of headed studs in the cross-section should be carefully adopted. According to EN 1994-1-1:2004 [10] when the distance between the edge of a concrete slab and a row of shear connectors of the diameter d is smaller than 300 mm, three requirements need to be satisfied: (1) U-bars should be placed around the studs and as low as possible accounting for the concrete cover layer, (2) the minimum distance between the slab edge and headed studs should be $6d$, and (3) U-bars should have the diameter of at least $0.5d$. However, meeting the criteria considering the transverse distance between the headed stud and the slab edge is problematic, as in this particular case, the connector is not placed right above the steel flange if the space of $6d$ is selected. Therefore, the distance between the stud connector and the slab edge is reduced to $4d = 64$ mm and the connection response is examined in the experimental work. The problem of the optimum stud position is studied through parametric analysis.

The effects of the U-bars with the diameter of $0.5d = 8$ mm on the connection behaviour are studied through the experimental program of the thesis, comparing the response of connections with and without stirrup reinforcement. Position of U-bars along stud height and U-bar diameter are varied as parameters in numerical studies.

The layout of the proposed connection including the adopted detailing is presented in Figure 3.2. The proposed connection design is experimentally tested.
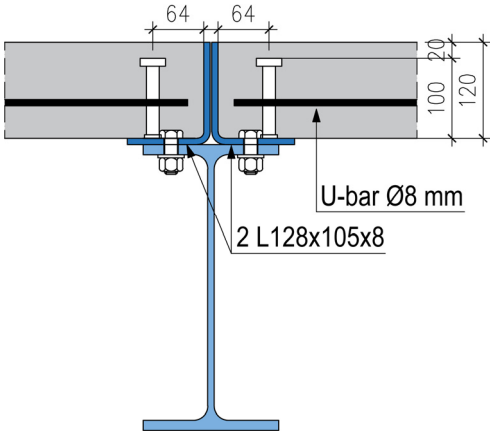
Figure 3.2: Detailing of the demountable shear connection.

4 Experimental Work

To investigate the behaviour of the proposed demountable shear connection with welded headed studs and bolts, experimental research was conducted through static push-out tests. In that way, information on the connection response to shear was collected, load-slip curves were obtained and failure modes were detected. Furthermore, experimental testing of material was performed to obtain the mechanical properties of the connection components.

Push-out tests were conducted on three different configurations of the demountable shear connection with sheeting ribs transverse to the supporting beam. Varied parameters included slab discontinuity and stirrup reinforcement. In addition, the corresponding non-demountable connection with welded headed studs was experimentally tested and used for comparison. Special attention was directed to the examination of the connection performance when the angle between profiled sheeting ribs and the beam is smaller than 90°. Therefore, demountable and non-demountable specimens with angles between ribs and the beam of 45° and 60° were tested.

4.1 Experimental Program and Specimen Preparation

Experimental work covers 20 push-out tests in total, divided into the following series:

- Series S (3 specimens) – non-demountable steel-concrete composite connection with welded headed studs installed in a composite slab with an open trough profiled steel sheeting (Figure 4.1);

- Series D (3 specimens) – demountable steel-concrete composite connection with bolts and welded headed studs applied to a composite slab with an open trough profiled steel sheeting; headed studs are welded to the steel plate, and bolts connect the plate and the flange of a steel profile (Figure 4.2);

- Series DL (2 specimens) – demountable connection with bolts and welded headed studs, but contrary to series D, the concrete slab is discontinuous over the steel profile and a pair of angles is applied instead of the steel plate (Figure 4.3);

- Series DLU (2 specimens) – connection identical to series DL with the difference of added stirrup U-bars passing around the headed studs (Figure 4.4);

- Series S45 (3 specimens) – non-demountable connection with the angle between ribs of the profiled steel sheeting and the steel beam of 45° (Figure 4.5);

- Series D45 (2 specimens) – demountable connection with the angle between ribs of the profiled steel sheeting and the steel beam of 45° (Figure 4.6);

- Series S60 (3 specimens) – non-demountable connection with the angle between ribs of the profiled steel sheeting and the steel beam of 60° (Figure 4.7);

- Series D60 (2 specimens) – demountable connection with the angle between ribs of the profiled steel sheeting and the steel beam of 60° (Figure 4.8).

A summary of the specimen properties and varied parameters is given in Table 4.1. Series S, the non-demountable solution with ribs transverse to the beam, widely present in building constructions, served as a control series for comparison with the proposed demountable connections with ribs transverse to the beam, and other connections with the angle between profiled sheeting ribs and the beam smaller than 90°. Demountable shear connections with continuous slabs over the beam were examined through series D, while demountable shear connections with discontinuous slabs over the beam were examined through series DL. Series DLU was used to determine the influence of the stirrup reinforcement around headed studs in connections with discontinuous slabs over the support. Series S45 and S60 were tested to examine the influence of the angle between profiled sheeting ribs

41

and the beam on the shear behaviour of a non-demountable connection, while series D45 and D60 were used to analyse the same effect in demountable connections.

Table 4.1: Summary of the push-out tests.

Series	Number of specimens	Headed studs	Bolts	Plate/angle thickness	Slab	Angle between ribs and the beam	Remark
S	3		/	/	continuous	90°	/
D	3						/
DL	2		M12 8.8	8 mm	discontinuous		/
DLU	2	$d = 16$ mm $h_{sc} = 100$ mm					U-bars Ø 8 mm
S45	3		/	/		45°	/
D45	2		M16 8.8	8 mm	continuous		/
S60	3		/	/		60°	/
D60	2		M16 8.8	8 mm			/
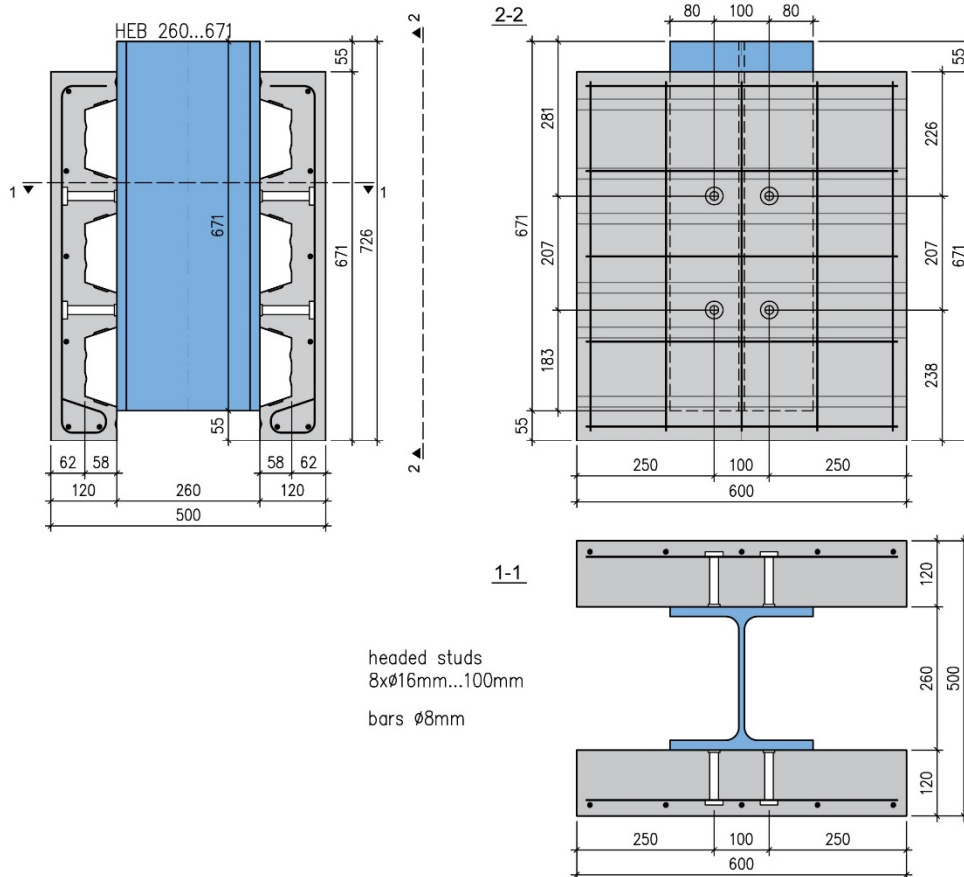
Figure 4.1: Test specimen layout: series S.
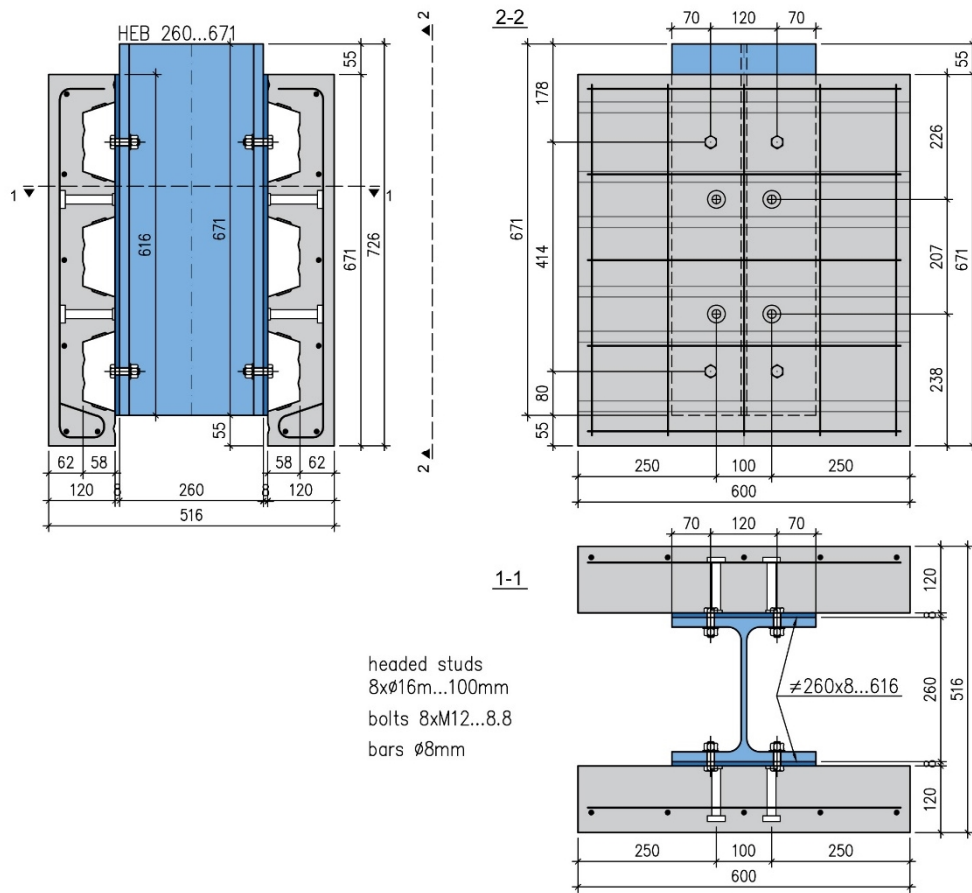
Figure 4.2: Test specimen layout: series D.
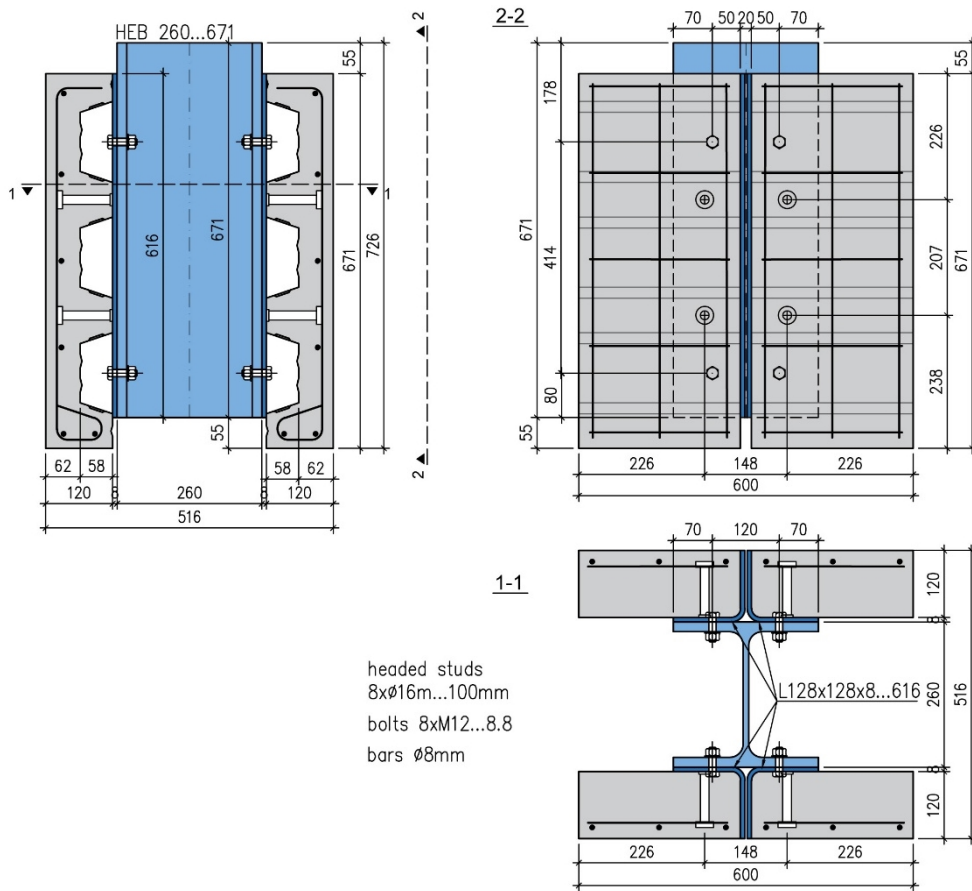
Figure 4.3: Test specimen layout: series DL.
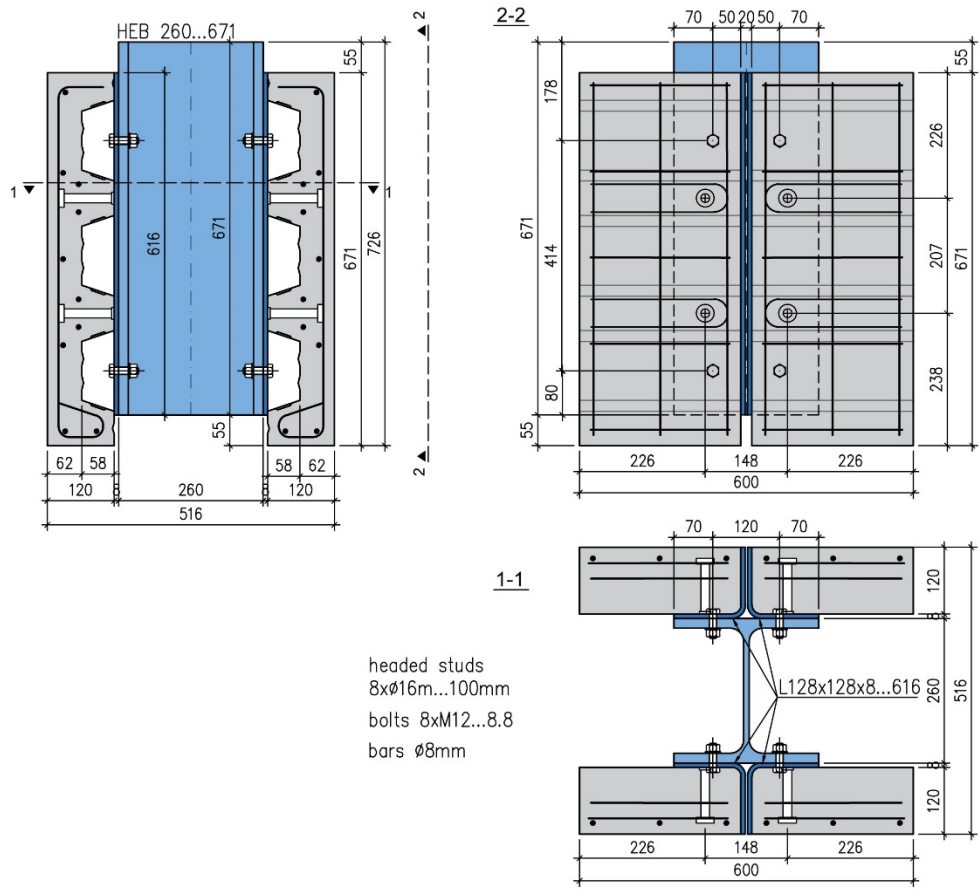
Figure 4.4: Test specimen layout: series DLU.
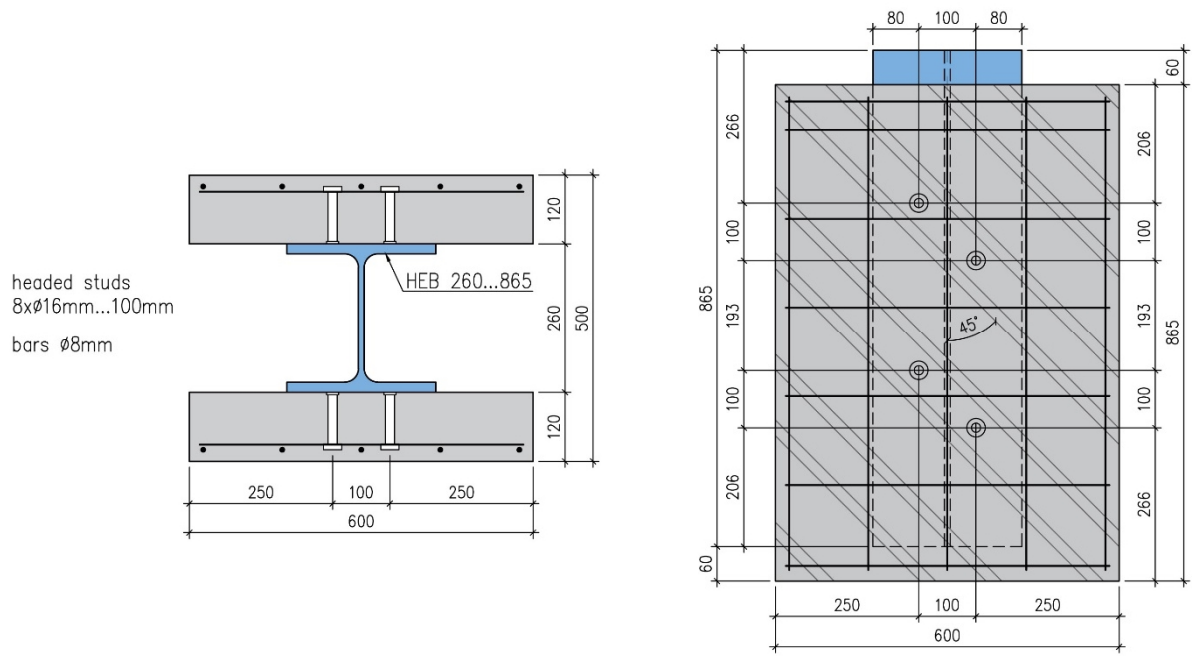
Figure 4.5: Test specimen layout: series S45.
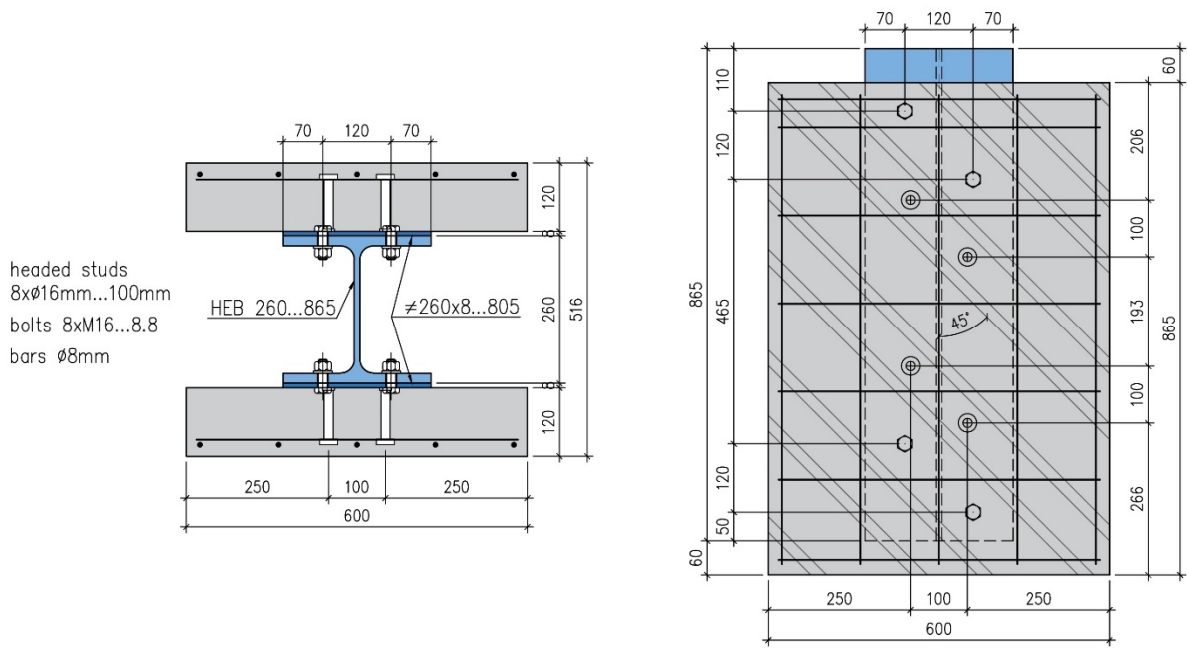
Figure 4.6: Test specimen layout: series D45.
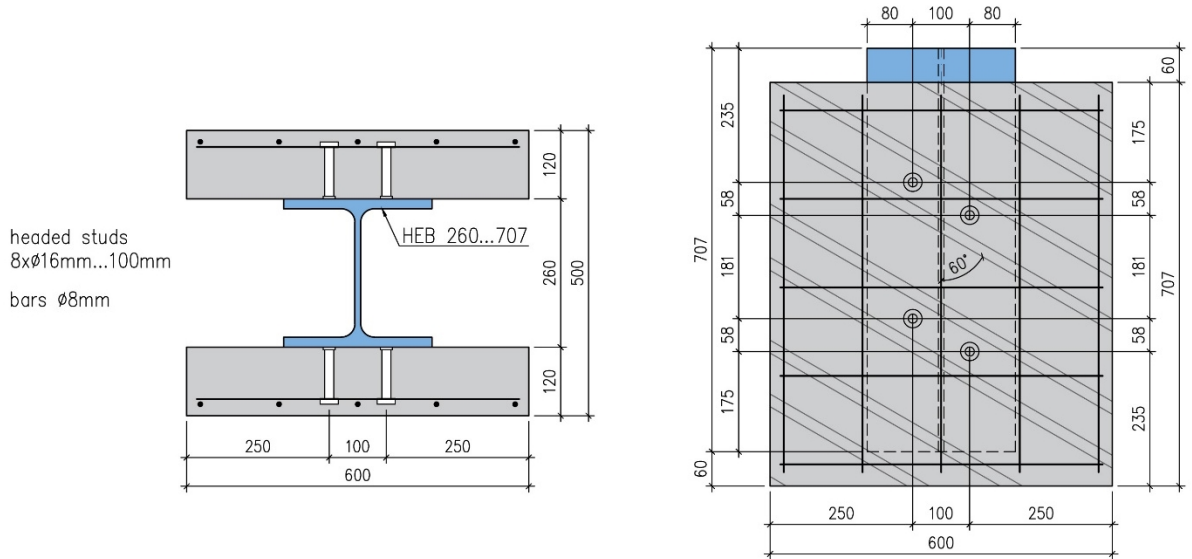
Figure 4.7: Test specimen layout: series S60.
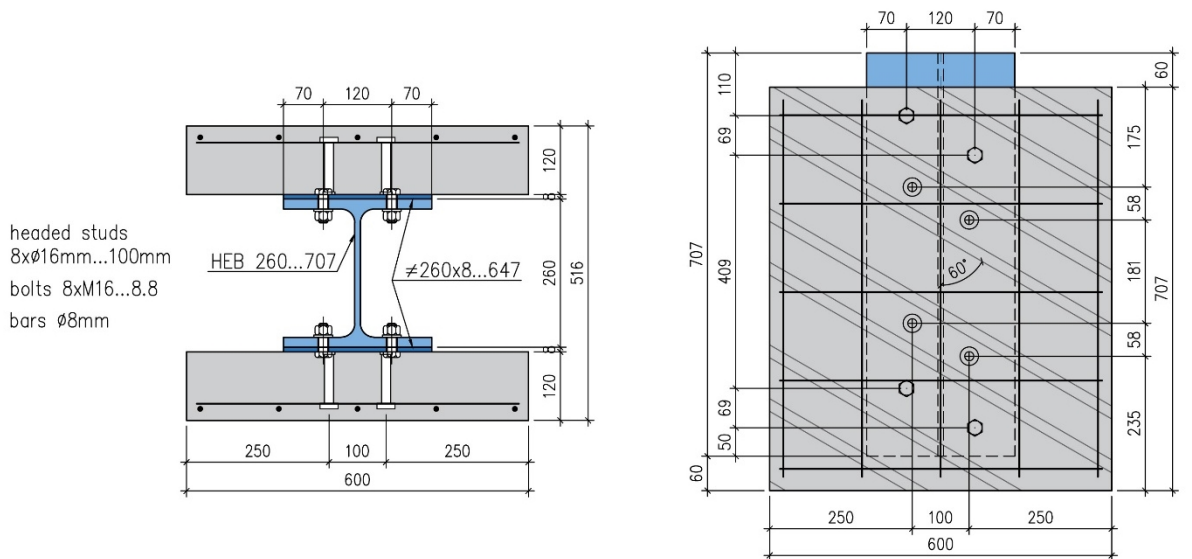
Figure 4.8: Test specimen layout: series D60.

45

All specimens were made with the open trough profiled steel sheeting Cofraplus 60 [71], commercially available in Europe. For specimens S45, D45, S60 and D60, pairs of concrete slabs connected to the steel profile were developed as mirror reflections, as shown in Figure 4.9.

Figure 4.9: Specimens D45 and D60 before concrete casting.

Each specimen consisted of eight headed studs of 16 mm in diameter. A headed stud height of 100 mm and concrete slab depth of 120 mm were kept constant in all tests. Headed studs were welded to the steel profile flange, plate or angle, whereas profiled steel sheeting with pre-punched holes was placed over before concrete casing, as shown in Figure 4.10.

Demountable specimens contained eight M12 or M16 bolts of grade 8.8. Bolt diameter and grade were chosen to keep bolt shear resistance higher than that of the headed stud and therefore accomplish similar behaviour of demountable and non-demountable connections, as previously discussed in Chapter 3. M12 bolts were applied to models with ribs orthogonal to the steel profile (series S, D, DL, DLU), whereas M16 bolts were applied to the specimens with the angle between profiled sheeting ribs and the steel beam smaller than 90° (series S45, D45, S60, D60) since larger resistance of headed studs was expected in those connections.
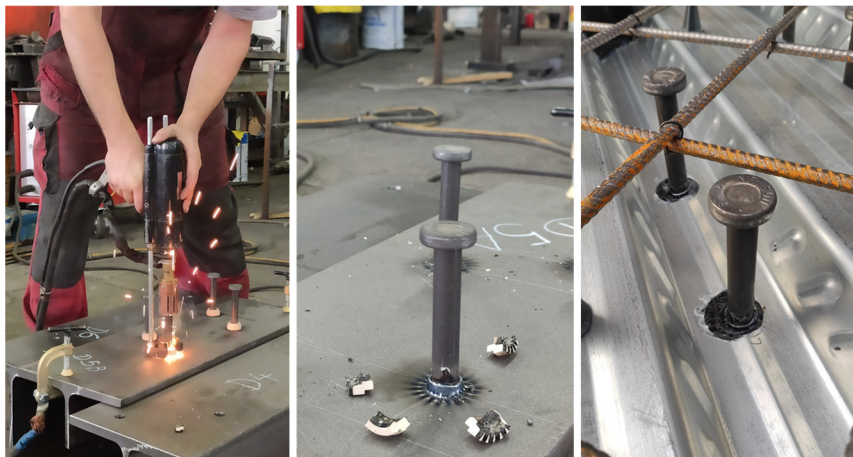
Figure 4.10: Headed studs during welding and placed in the profiled sheeting.

In specimens with continuous concrete slabs over the steel profile (series S and D), the distance between the headed studs was set to 100 mm (Figure 4.1 and Figure 4.2) to satisfy the detailing demands given in EN 1994-1-1:2004 [10]. At the same time, the headed studs in discontinuous slabs (series DL and DLU) were placed at a distance of $4d = 64$ mm in the transverse direction from the vertical angle leg, where d is the diameter of the headed stud (Figure 4.3 and Figure 4.4). The adopted length is smaller than $6d$, which is required according to EN 1994-1-1:2004 [10] as the minimum stud-to-edge distance. However, by choosing shorter distance, it is possible to keep a headed stud right above a steel flange, as explained in Chapter 3. The effects of the selected stud-to-edge distance on the connection damage are discussed throughout the study.

In specimens with the angle between profiled sheeting ribs and the beam of 45° and 60° (series S45, S60, D45, D60), the distance between headed studs in the concrete rib in the direction transverse to the steel beam was 100 mm, while the distance in the direction parallel to the steel beam depended on the adopted angle (Figure 4.5–Figure 4.8).

The bolt position was chosen according to the predefined hole position for the profile HEB 260. Bolt hole diameters were selected to comply with the requested execution tolerances. Bolt holes cut in the profile flange, plates and angles had a diameter of 13 mm in specimens with ribs transverse to the steel beam (series S, D, DL, DLU), while a diameter of 18 mm was applied to specimens with the angle between profiled sheeting ribs and the steel profile smaller than 90° (series S45, D45, S60, D60).

The thickness of the steel plate and angles at which the headed studs were welded was set to 8 mm. As explained in Chapter 3, the plate and angle thickness should be selected to avoid the deformation of the bolt holes and the plate beneath the headed studs. According to EN 1994-1-1:2004 [10], the thickness of the part to which the stud is welded should be greater than $0.4d$. As the limiting value of $0.4d$ equals 6.4 mm in the case of the tested connection, the plate thickness was rounded and set to 8 mm. The same thickness was selected for angles, which were made using the plate by cutting and cold forming the material. Design bearing resistance at bolt holes for the plate thickness of 8 mm is greater than bolt shear resistance; hence, it was not considered critical. The validity of the adopted thickness is examined throughout the study.

A recess in the concrete slab base, marked as optional according to EN 1994-1-1:2004, Annex B [10], was avoided during fabrication to accomplish easier specimen preparation. According to several research results, the absence of the recess is not expected to influence experimental results [64], [73]. A slab width of $b = 600$ mm was adopted to satisfy the condition $b > e_t + 2\ h_{sc}/\tan(25°)$ [72], where e_t is the transverse spacing between the studs inside the concrete rib and h_{sc} is the height of the stud. Therefore, it was intended to fully include a concrete cone that develops during a failure of headed studs in push-out tests.

One layer of reinforcement of 8 mm in diameter was placed in the top zone of the slab. For series S, D, DL and DLU longitudinal bars were bent on one side into a hook to reinforce the supporting rib of the concrete slab, as suggested by several authors [34], [36]. Stirrup bars applied in specimens of series DLU were formed in a U-shape to pass around the headed stud. The U-bar diameter was adopted as $0.5d = 8$ mm. U-bars were placed at the level of the top surface of profiled sheeting ribs and oriented in the transverse direction, as shown in Figure 4.11.
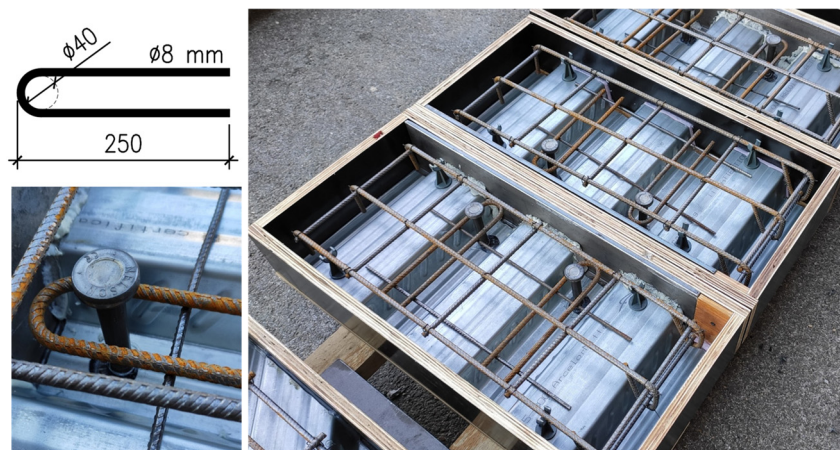
Figure 4.11: U-bar geometry and specimens with stirrups before concrete casting.

Specimen preparation was performed in two phases. In the first phase, the pilot specimens of series S were made and tested, whereas in the second phase, concrete casting was simultaneously done for all the other specimens (Figure 4.12), and push-out tests were conducted subsequently. In both cases, concrete with a maximum aggregate size of 16 mm was used, to comply with the EN 1994-1-1:2004

[10] demand considering the relations between the nominal aggregate size and connection geometry. To minimise initial shrinkage cracks, specimens were kept in wet conditions during the first three days.

Specimens were assembled for push-out testing 28 days after concrete casting. Demountable specimens were assembled by connecting concrete slabs and steel profiles with bolts. Nuts were tightened without the application of pretension force. For specimens of non-demountable shear connections S45 and S60 (except series S), HEB 260 profiles had been longitudinally cut in two segments before concreting and afterwards welded to each other before push-out testing. The aim was strictly practical as it was intended to perform all concrete castings at once, accomplishing the same material properties of the concrete on both sides of each specimen.

Figure 4.12: Concrete casting.

4.2 Experimental Testing of Material

For components that form push-out specimens, material properties were obtained through standardised testing procedures:

- tensile tests were conducted on steel coupons to obtain stress-strain curves and measure steel yield strength, ultimate tensile strength and modulus of elasticity;

- compression and splitting tests were conducted on concrete cubes and cylinders to obtain concrete compressive strength, tensile strength and modulus of elasticity.

Statistical evaluation was conducted according to directions provided in Annex D of EN 1990:2010 [83].

The geometry of steel coupons was adopted in compliance with the requirements given in EN ISO 6892-1 [84]. The testing procedure was performed as strain control, applying the uniform displacement rate of 0.1 mm/min up to 1% strain and setting the displacement rate of 2.2 mm/min afterwards [85]. All specimens were tested in the servo-hydraulic testing machine with the capacity of 300 kN in the Laboratory for Materials at the Faculty of Civil Engineering, University of Belgrade.

The results of the material testing of steel components (steel profile, steel plate, profiled steel sheeting, headed studs and bolts) and concrete cubes and cylinders are given in the following. Reinforcement bars were not tested, as it is assumed that during push-out testing stress in bars is below the yield strength and material behaviour is elastic, which is later confirmed through numerical analysis.

4.2.1 Steel Profiles and Plates

To investigate the material properties of steel profiles, plates and angles, coupons were taken from the profile flange and steel plate. Considering that angles were made of the same material as plates, coupons from angles were not taken.

Coupons made from the flange of the steel profile had a round cross-section of 10 mm in diameter, whereas coupons taken from the plate were cut by a water jet cutter and had a rectangular cross-section, 12.5×8 mm. Coupons' geometries are given in Figure 4.13.a. All coupons were tested using the digital extensometer, with the gauge length $L_0 = 50$ mm. Tensile test set-ups are shown in Figure 4.13.b, while the appearance of coupons after the testing is presented in Figure 4.13.c.
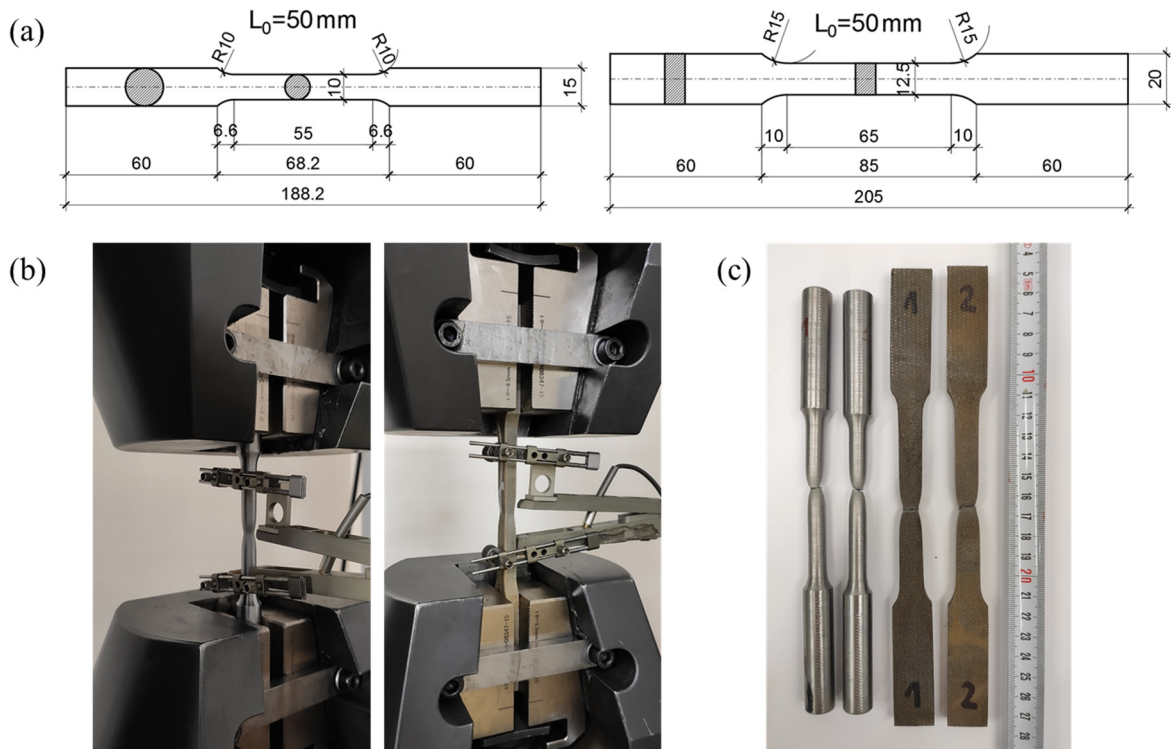
Figure 4.13: (a) Geometry of coupons, (b) Coupon testing, (c) Coupons after the testing.

Mechanical properties of both materials were obtained by means of experimental testing of three coupons. Test results are summarised in Table 4.2 and Table 4.3, whereas stress-strain curves are graphically presented in Figure 4.14. The average values of yield strength and ultimate tensile strength are 297.3 kN and 418.6 kN for the steel profile flange, and 357.1 kN and 520.7 kN for the steel plate, respectively.
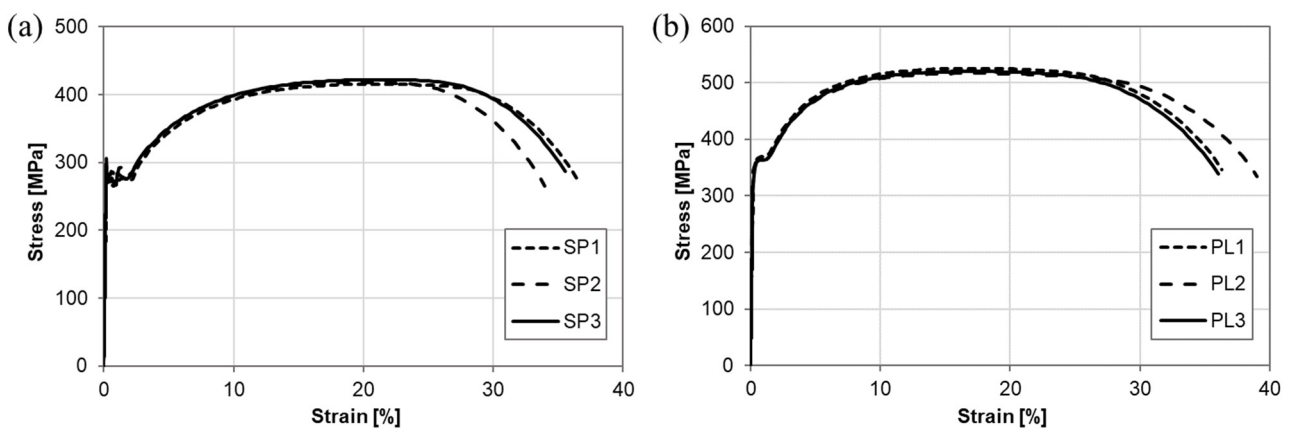
Figure 4.14: Stress-strain curves: (a) steel profile, (b) steel plate.

Table 4.2: Steel profile material properties.

Specimen	Test coupon geometry		Material mechanical properties			
	Diameter	Cross-sectional area	Yield strength	Ultimate tensile strength	Modulus of elasticity	Strain at ultimate strength
	d [mm]	A [mm^2]	f_y [MPa]	f_u [MPa]	E [GPa]	ε_u [%]
SP1	10.00	78.50	282.1	415.7	198.0	21.04
SP2	10.00	78.50	312.3	418.0	198.0	20.13
SP3	10.00	78.50	297.7	422.1	197.0	21.00
Mean			297.3	418.6	197.7	20.72
St. deviation			15.10	3.22		
CoV [%]			5.08	0.77		
Characteristic			246.45	407.75		

Table 4.3: Steel plate material properties.

Specimen	Test coupon geometry			Material mechanical properties			
	Thickness	Width	Cross-sectional area	Yield strength	Ultimate tensile strength	Modulus of elasticity	Strain at ultimate strength
	t [mm]	b [mm]	A [mm^2]	f_y [MPa]	f_u [MPa]	E [GPa]	ε_u [%]
PL1	8.20	12.60	103.32	358.1	525.4	200.0	17.03
PL2	8.20	12.60	103.32	359.5	516.8	207.0	17.23
PL3	8.20	12.60	103.32	353.7	519.9	195.0	16.93
Mean				357.1	520.7	200.7	17.06
St. deviation				3.03	4.35		
CoV [%]				0.85	0.84		
Characteristic				346.90	506.04		

4.2.2 Profiled Steel Sheeting

Coupons taken from profiled steel sheeting were cut by a water jet cutter to minimise the coupon deformation and generation of additional stress. The coupon of a width of 12.5 mm and gauge length $L_0 = 50$ mm is presented in Figure 4.15.a. To precisely obtain the sheeting thickness, the ultrasonic measurement was performed as shown in Figure 4.15.b. All four coupons were tested using the digital extensometer. For two coupons, strain gauges were added to precisely obtain the elastic modulus. The tensile test set-up is shown in Figure 4.15.c, while the appearance of coupons before and after the testing is presented in Figure 4.15.d.
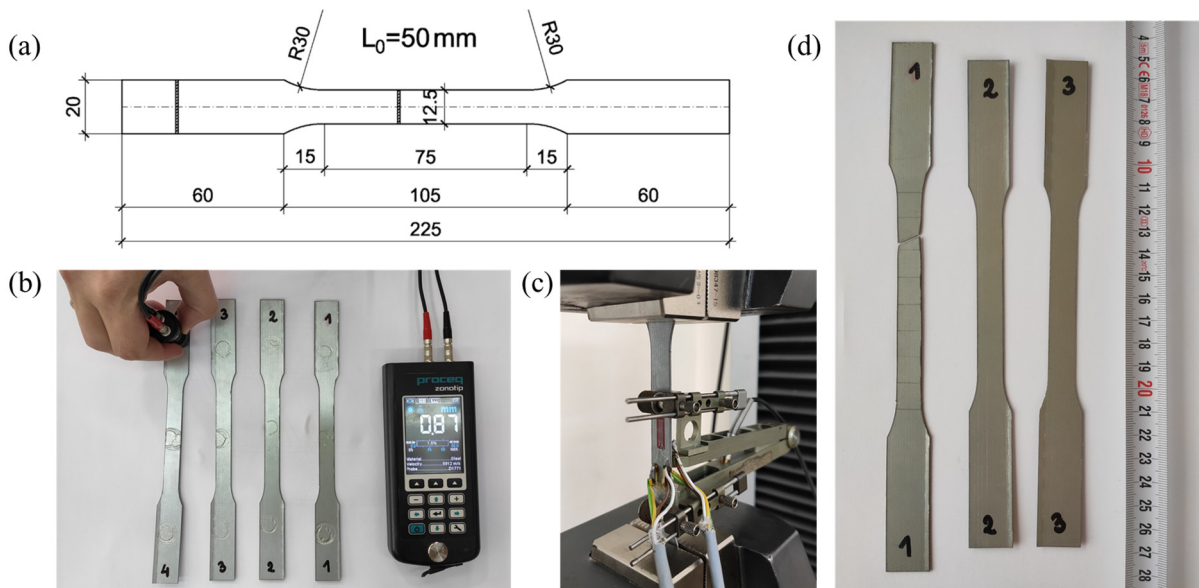
Figure 4.15: (a) Coupon geometry, (b) Ultrasonic thickness measurement, (c) Coupon testing, (d) Coupons before and after the testing.

Stress-strain curves are given in Figure 4.16, whereas a summary of profiled steel sheeting material properties is given in Table 4.4. The average values of yield strength and ultimate tensile strength are 347.7 kN and 408.2 kN.
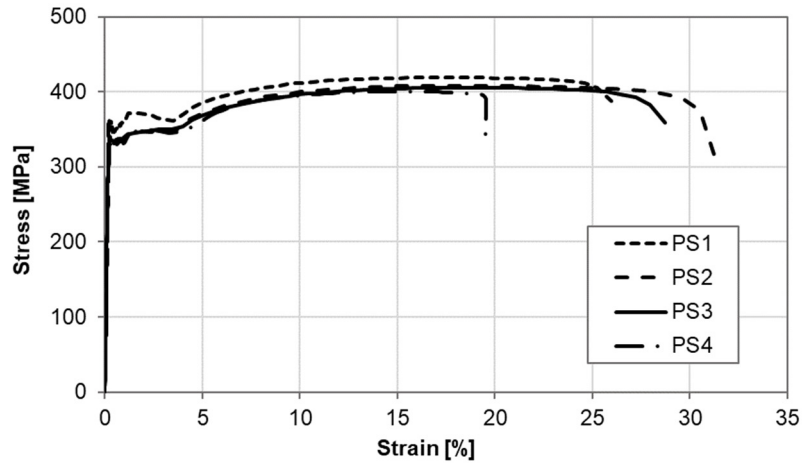
Figure 4.16: Stress-strain curves for profiled steel sheeting coupons.

Table 4.4: Profiled steel sheeting material properties.

Specimen	Test coupon geometry			Material mechanical properties			
	Thickness	Width	Cross-sectional area	Yield strength	Ultimate tensile strength	Modulus of elasticity	Strain at ultimate strength
	t [mm]	b [mm]	A [mm²]	f_y [MPa]	f_u [MPa]	E [GPa]	ε_u [%]
PS1	0.85	12.58	10.693	361.5	418.9	-	17.87
PS2	0.86	12.54	10.784	358.1	408.2	-	17.80
PS3	0.85	12.60	10.710	334.7	405.3	196.0	18.17
PS4	0.87	12.61	10.971	336.3	400.4	193.0	15.57
Mean				347.7	408.2	194.5	17.35
St. deviation				14.1	7.8		
CoV [%]				4.06	1.92		
Characteristic				310.5	387.6		

4.2.3 Headed Studs

Round coupons made from headed studs were 5 mm in diameter and the gauge length was $L_0 = 50$ mm, as shown in Figure 4.17.a. The strain was measured by a digital extensometer, as presented in Figure 4.17.b. The comparison between specimens before and after the testing is given in Figure 4.17.c. In total, three coupons were tested.
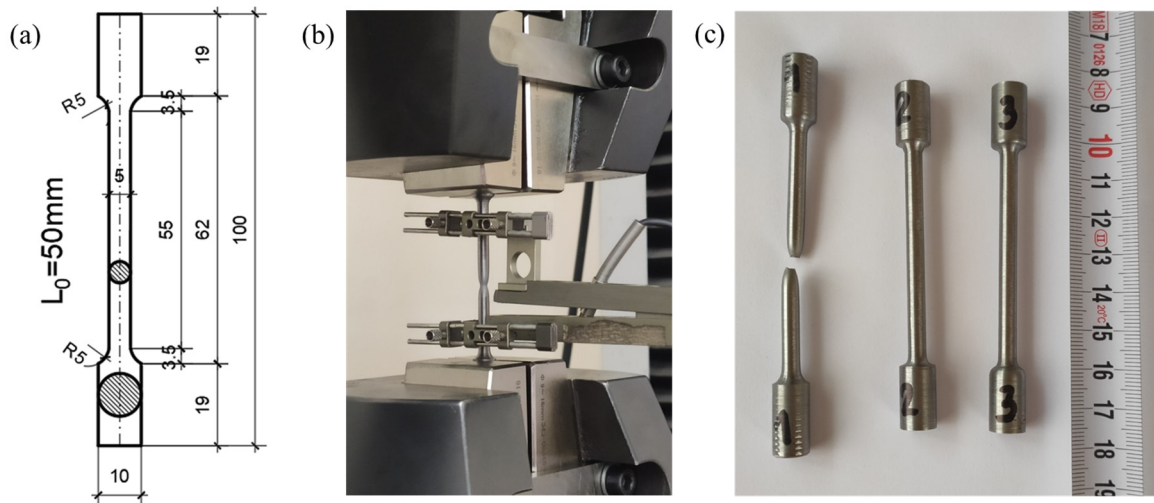
Figure 4.17: (a) Coupon geometry, (b) Coupon testing, (c) Coupons before and after the testing.

51

Stress-strain curves are presented in Figure 4.18, showing the dominant nonlinear behaviour of the material without the distinct yield point. Therefore, the yield strength was obtained as the 0.2% proof stress $f_{0.2}$ and the results are summarised in Table 4.5. The average values of yield strength and ultimate tensile strength are 421.0 kN and 509.0 kN. Compared with the response of steel coupons taken from the profile flange and plate, the strain at ultimate stress of headed stud material is 4–5 times smaller, whereas the strain at fracture is approximately three times smaller.
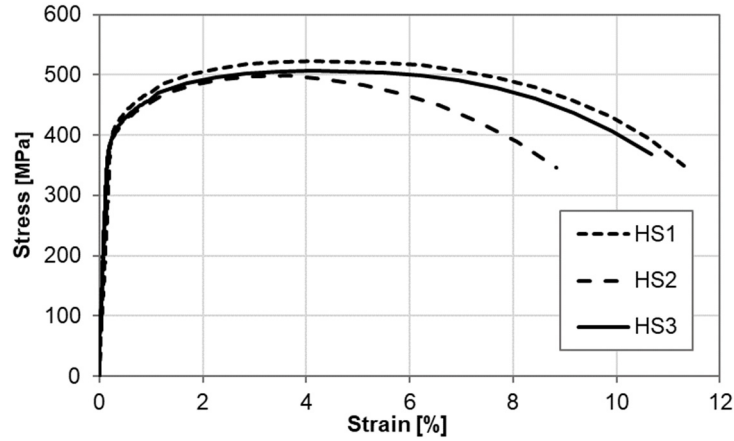
Figure 4.18: Stress-strain curves for headed stud coupons.

Table 4.5: Headed stud material properties.

Specimen	Test coupon geometry		Material mechanical properties			
	Diameter	Cross-sectional area	Yield strength	Ultimate tensile strength	Modulus of elasticity	Strain at ultimate strength
	d [mm]	A [mm^2]	f_y [MPa]	f_u [MPa]	E [GPa]	ε_u [%]
HS1	5.00	19.625	427.6	522.2	196.0	4.34
HS2	5.00	19.625	415.8	498.6	193.0	3.31
HS3	5.00	19.625	419.5	506.2	211.0	4.06
Mean			421.0	509.0	200.0	3.90
St. deviation			6.0	12.0		
CoV [%]			1.43	2.37		
Characteristic			400.6	468.4		

4.2.4 Bolts

Round coupons of 5 mm in diameter were made from M12 and M16 bolts, as presented in Figure 4.19.a. Due to the small size of coupons, the application of a digital extensometer during testing was not possible, so in order to measure strains, two strain gauges were glued around the coupon diameter, as shown in Figure 4.19.b. The comparison between M16 coupon specimens before and after the testing is given in Figure 4.19.c. Altogether, two coupons made from M16 bolts and two coupons made from M12 bolts were tested.

Stress-strain curves based on the measurement of strain gauges are presented as black lines in Figure 4.20. Strains were recorded until a certain dilatation when glue used for strain gauge fixation broke. The initial part of the stress-strain curve enabled the determination of the 0.2% proof stress $f_{0.2}$ and modulus of elasticity. To provide a better graphical presentation of bolt ductility, stress-strain curves were extended according to the measurement of the elongation obtained from the testing machine (grey lines in Figure 4.20). Results are summarised in Table 4.6. The average values of yield strength and ultimate tensile strength are 928.9 kN and 966.5 kN.
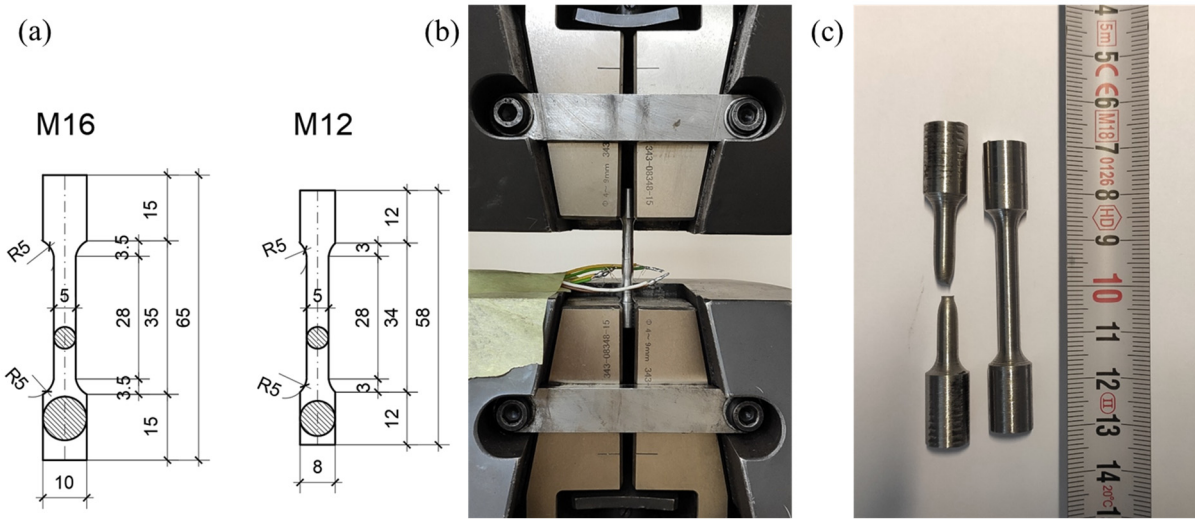
Figure 4.19: (a) Geometry of coupons, (b) Coupon testing, (c) Coupons before and after the testing.
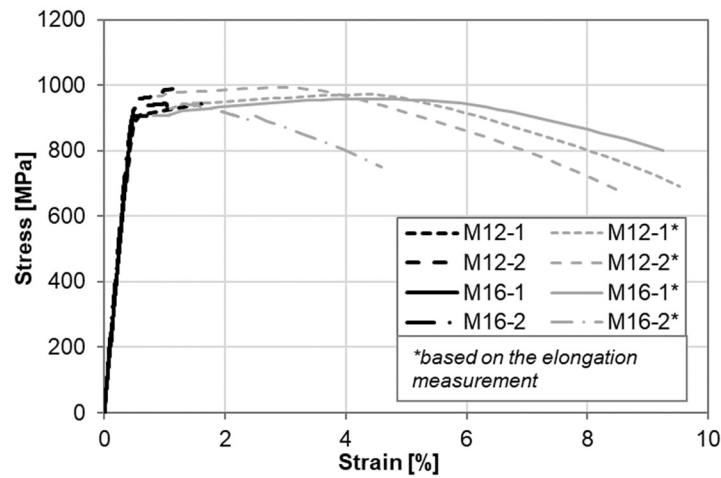
Figure 4.20: Stress-strain curves for bolt coupons.

Table 4.6: Bolt material properties.

Specimen	Test coupon geometry		Material mechanical properties		
	Diameter	Cross-sectional area	Yield strength	Ultimate tensile strength	Modulus of elasticity
	d [mm]	A [mm^2]	f_y [MPa]	f_u [MPa]	E [GPa]
M12-1	4.95	19.234	911.3	971.5	210.0
M12-2	4.95	19.234	959.4	992.3	205.0
M16-1	4.95	19.234	906.9	958.4	207.0
M16-2	4.71	17.414	938.1	943.6	201.0
Mean			928.9	966.5	204.0
St. deviation			24.6	20.7	
CoV [%]			2.64	2.14	
Characteristic			864.3	912.1	

4.2.5 Concrete

In each phase of concrete casting, cubes 15×15×15 cm were made to obtain the concrete compressive strength $f_{c,cube}$. Cubes were kept in a wet environment for the first 28 days. Push-out testing of specimens started 28 days after the specimen fabrication and continued in the next five weeks in irregular intervals. Cubes were tested at the time of push-out specimen testing to obtain precise information on the concrete cube strength at that moment. Results corresponding to the specific push-out test series are presented in Table 4.7. Mean values of the concrete compressive strengths are in the range of 38.3 MPa to 46.6 MPa.

Table 4.7: Compressive strength of concrete.

Phase	Specimens	Compressive strength of concrete cubes, $f_{c,cube}$ [MPa]				
		Measured	Mean	St. deviation	CoV [%]	Characteristic
1	S-01	36.1 42.4 35.2 39.5	38.3	3.3	8.60	29.6
1	S-02, S-03	42.3 40.5 43.7 43.6 45.0 44.1 46.3 43.8	43.7	1.7	3.96	40.2
2	D	40.8 44.2 43.8 43.4	43.1	1.5	3.51	39.1
2	S45, S60, D45, D60	43.8 44.9 45.3 47.1	45.3	1.4	2.98	41.7
2	DL, DLU	48.5 45.4 47.0 45.6	46.6	1.5	3.13	42.8

In the second phase of concrete casting, besides cubes, concrete cylinders Ø15×30 cm and Ø15×15 cm were made to obtain the elastic modulus E_{cm} and concrete tensile strength f_{ctm}, respectively. By performing splitting tests on concrete cylinders, concrete splitting tensile strength $f_{ct,sp}$ was measured and then converted to concrete axial tensile strength f_{ctm} by multiplying by 0.9 [6]. Results are given in Table 4.8 and Table 4.9. Comparing experimental results with predictions given in EN 1992-1-1:2004 [6] based on relations between elastic modulus and concrete tensile strength and concrete compressive strength, a good match was observed.

Table 4.8: Modulus of elasticity of concrete.

Phase	Modulus of elasticity of concrete, E_{cm} [MPa]				
	Measured	Mean	St. deviation	CoV [%]	Characteristic
2	30 383 31 658 33 534 34 296 32 107	32 396	1548	4.78	28 789

Table 4.9: Axial tensile strength of concrete.

Phase	Axial tensile strength of concrete, f_{ctm} [MPa]				
	Measured	Mean	St. deviation	CoV [%]	Characteristic
2	2.85 3.01 2.96 3.31 3.18 2.55	2.98	0.27	8.97	2.39

Further in the thesis, when comparing and discussing experimental and numerical push-out test results, the mean value of concrete cylinder compressive strength f_{cm} is assigned to each test series.

Cylinder compressive strength was calculated by multiplying the mean value of cube compressive strength by 0.8. All necessary values for developing numerical models and testing analytical expressions as modulus of elasticity and concrete tensile strength were derived from the cylinder compressive strength f_{cm} using the expressions given in EN 1992-1-1:2004 [6].

4.3 Push-Out Test Set-Up and Measurement Procedure

Experimental testing was performed in the Laboratory for Materials at the Faculty of Civil Engineering, University of Belgrade. Push-out tests were conducted following instructions given in EN 1994-1-1:2004, Annex B [10]. The vertical load was applied on steel profile HEB 260 through the thick steel plate to provide a uniform pressure distribution in the cross-section. Concrete slabs were placed on the layer of fresh gypsum to accomplish good contact with the support. According to recommendations given in the DISCCO report [72], no transverse loading was applied as the ratio between the stud and rib height was larger than 1.56.

For each specimen from series S, S45 and S60, a total of eight displacement transducers were installed:

- four for measuring the horizontal separation between the concrete slab and steel profile (H1–H4 in Figure 4.21);

- four for measuring the vertical slip between the concrete slab and steel profile (V1–H4 in Figure 4.21).

Test set-up for non-demountable specimens is presented in Figure 4.21, using the example of series S. The vertical slip between the concrete slab and steel profile was measured at the top of the specimen. To measure the horizontal separation between the concrete slab and steel profile, profiled steel sheeting was locally cut on the rib as close as possible to headed studs, and a glass plate was glued to the concrete to provide a smooth surface for sensor movement.
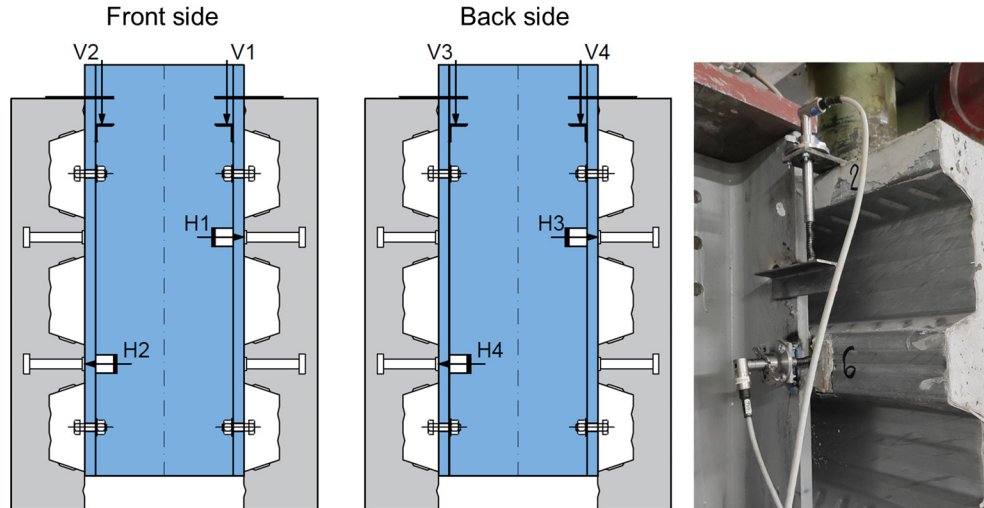
Figure 4.21: Test set-up for non-demountable specimens.

For specimens from series D, DL, DLU, D45 and D60, 12 displacement transducers were installed:

- four for measuring the horizontal separation between the concrete slab and steel profile (H1–H4 in Figure 4.22);

- four for measuring the vertical slip between the concrete slab and steel profile (V1–V4 in Figure 4.22);

- four for measuring the vertical slip between the concrete slab and steel plate/angle (V5–V6 in Figure 4.22).

In that way, recorded information on the slip of demountable specimens includes not only displacement between the concrete slab and steel profile but also the slip in two shear planes: "steel plate/angle-concrete slab" and "steel profile-steel plate/angle". Test set-up for demountable specimens is shown in Figure 4.22, using the example of series D, DL and DLU. Vertical and horizontal displacements were measured at the top of the specimen and in the area near headed stud connectors, respectively, in accordance with the non-demountable specimens as previously described.
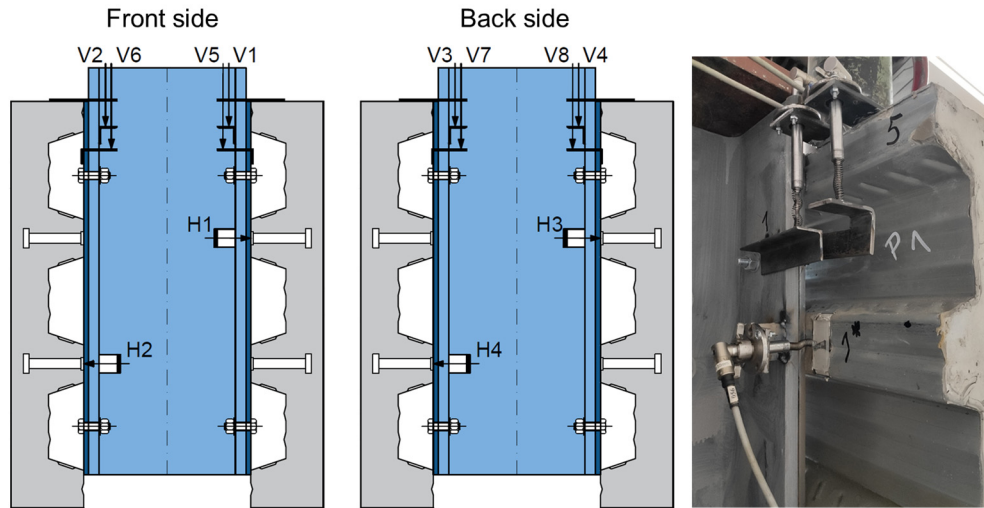
Figure 4.22: Test set-up for demountable specimens.

The exception from the listed measured values was made in the case of the specimen DLU-01, where two additional displacement transducers for measuring the lateral horizontal separation between two slabs were used. Sensors were placed at the top of the specimen, as shown in Figure 4.23. However, the displacement remained negligible during the experiment (less than 0.5 mm) and therefore, it was not measured in further testing.
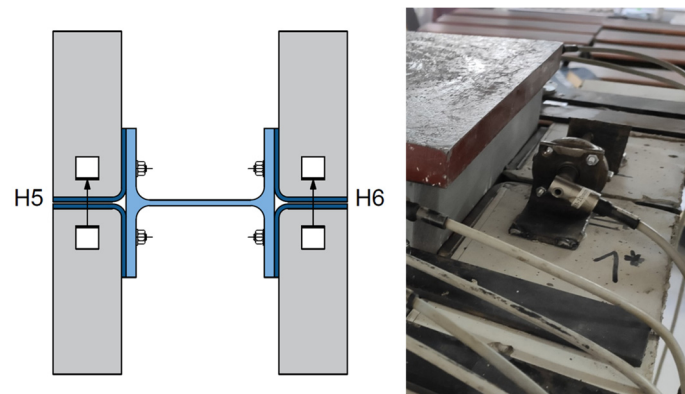
Figure 4.23: Measurement of lateral displacement between two slabs.

The applied force was measured by a load cell of the capacity of 1000 kN placed at the top. Data recording was performed at a frequency of 1 Hz using the multichannel acquisition devices.

The loading regime, shown in Figure 4.24, was adopted following propositions given in EN 1994-1-1:2004, Annex B [10]. Firstly, the load was applied in three steps up to 40% of the expected ultimate load. Then, the specimen was unloaded to 5% of the expected ultimate load and cycles ranging from 5% to 40% of the assumed shear resistance were repeated 25 times. In the last phase, loading was applied in one step, minding that failure does not appear in less than 15 minutes. Data were recorded until the load dropped to 20% below the maximum load. The only exception of the described regime was made for specimens S-02 and S-03 (Figure 4.25), which were unloaded at 70% of the expected ultimate load and then loaded again, in order to observe the connection's initial stiffness.
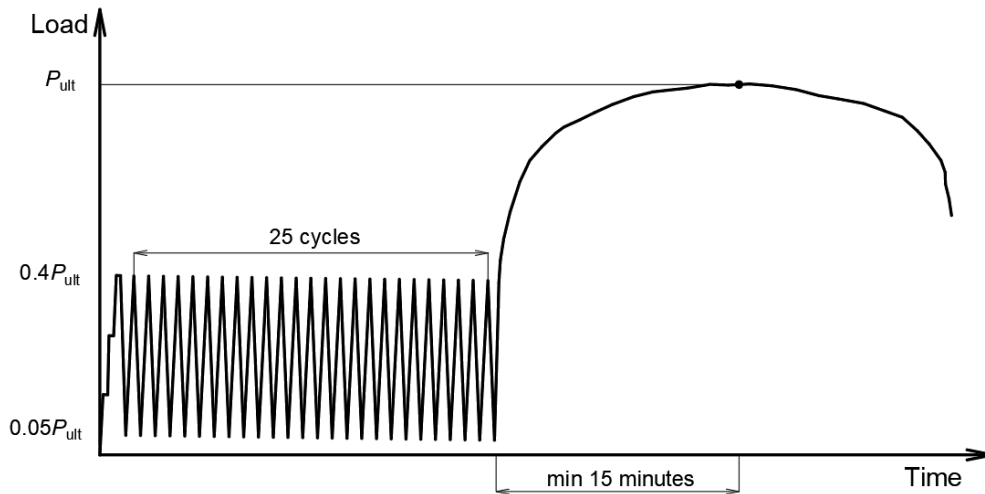
Figure 4.24: Loading regime.

4.4 Push-Out Test Results

Load-slip curves obtained during push-out testing are presented in Figure 4.25–Figure 4.32. For demountable specimens, load-slip curves are given for the overall slip between the concrete slab and steel profile and the slip in the plane "steel plate/angle-concrete slab".
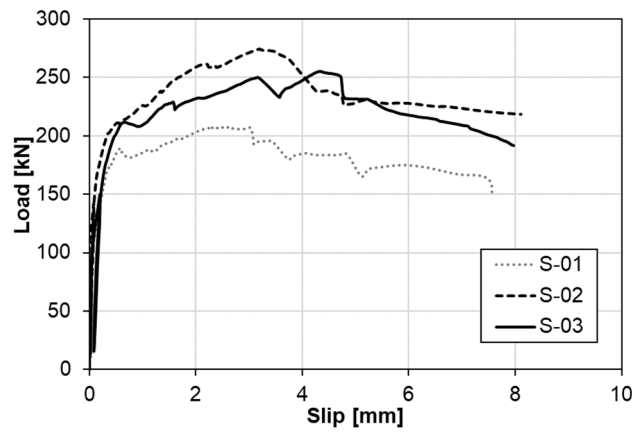
Figure 4.25: Load-slip curves for series S.
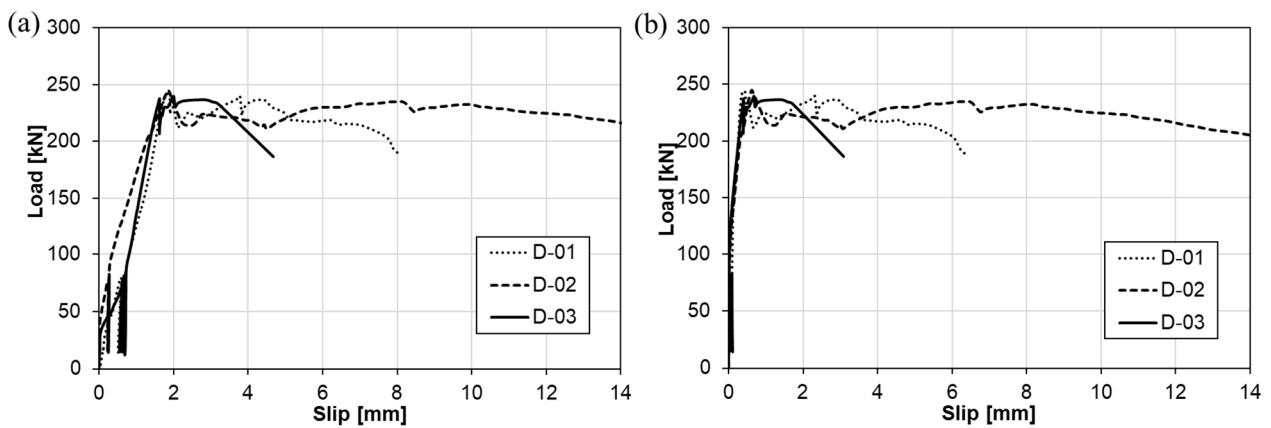
Figure 4.26: Load-slip curves for series D:
(a) steel profile-concrete slab, (b) steel plate-concrete slab.

57
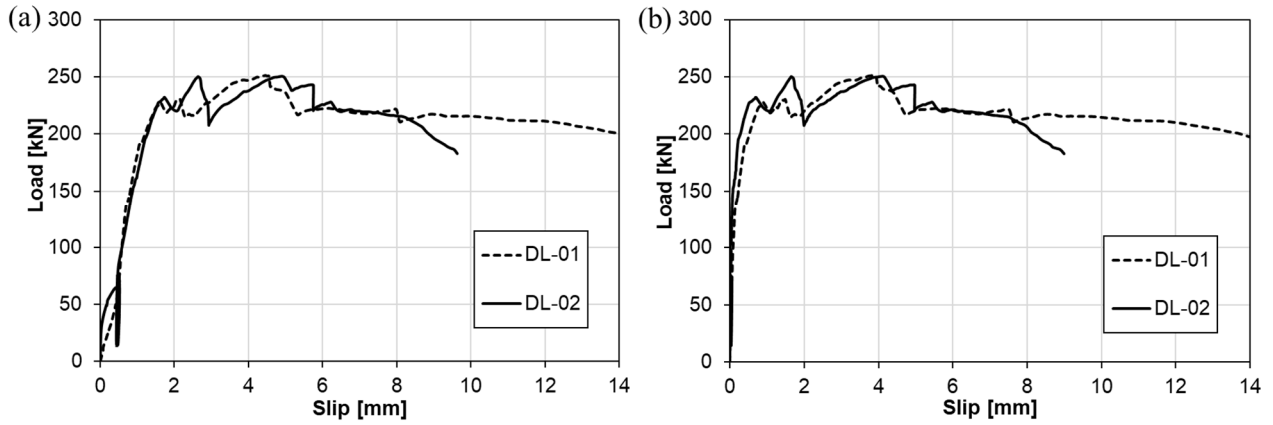
Figure 4.27: Load-slip curves for series DL:
(a) steel profile-concrete slab, (b) steel angle-concrete slab.
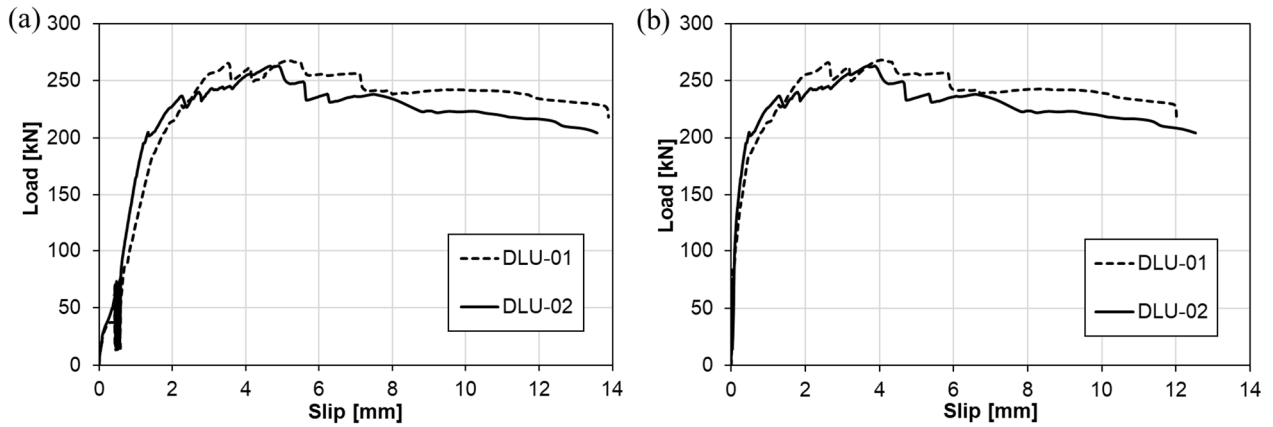
Figure 4.28: Load-slip curves for series DLU:
(a) steel profile-concrete slab, (b) steel angle-concrete slab.
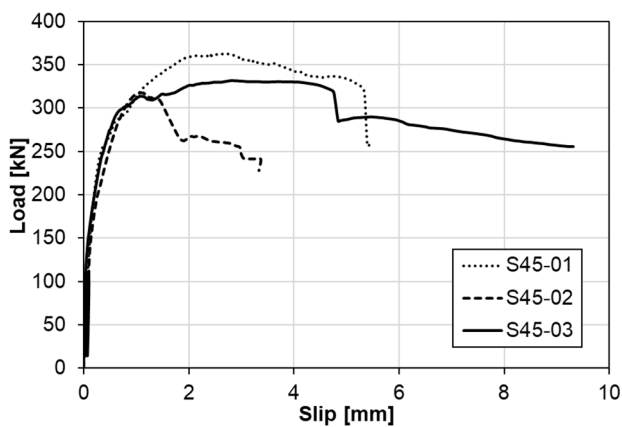
Figure 4.29: Load-slip curves for series S45.
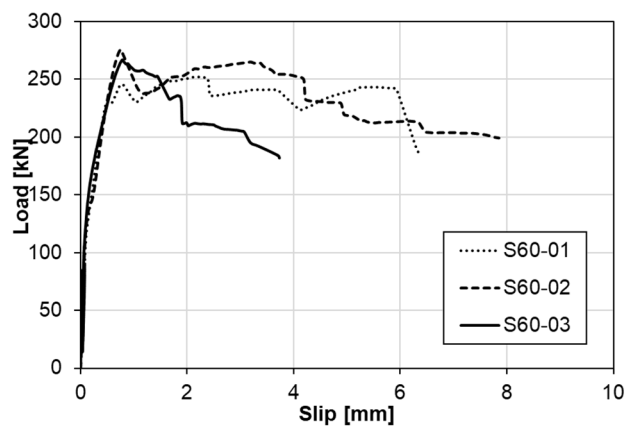
Figure 4.30: Load-slip curves for series S60.
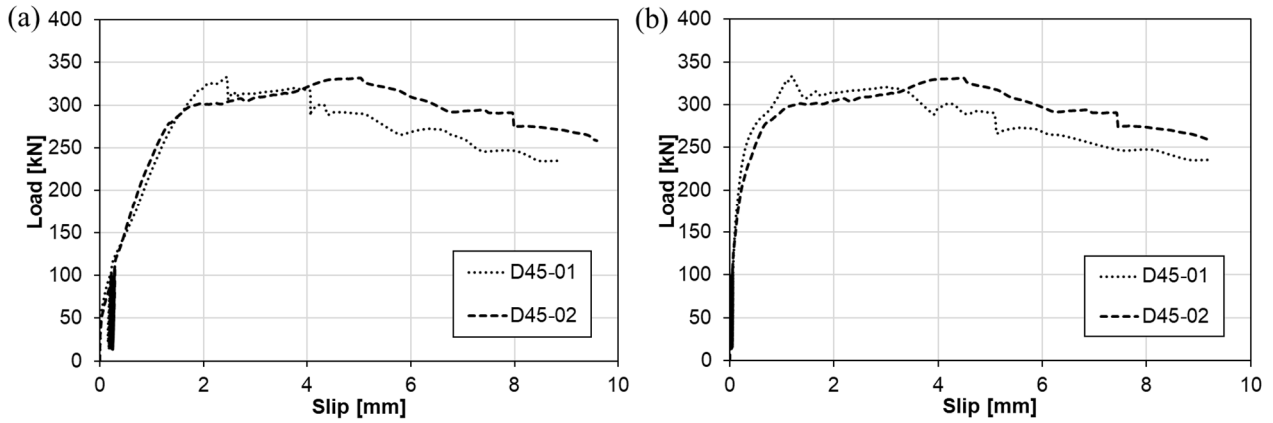
Figure 4.31: Load-slip curves for series D45:
(a) steel profile-concrete slab, (b) steel plate-concrete slab.
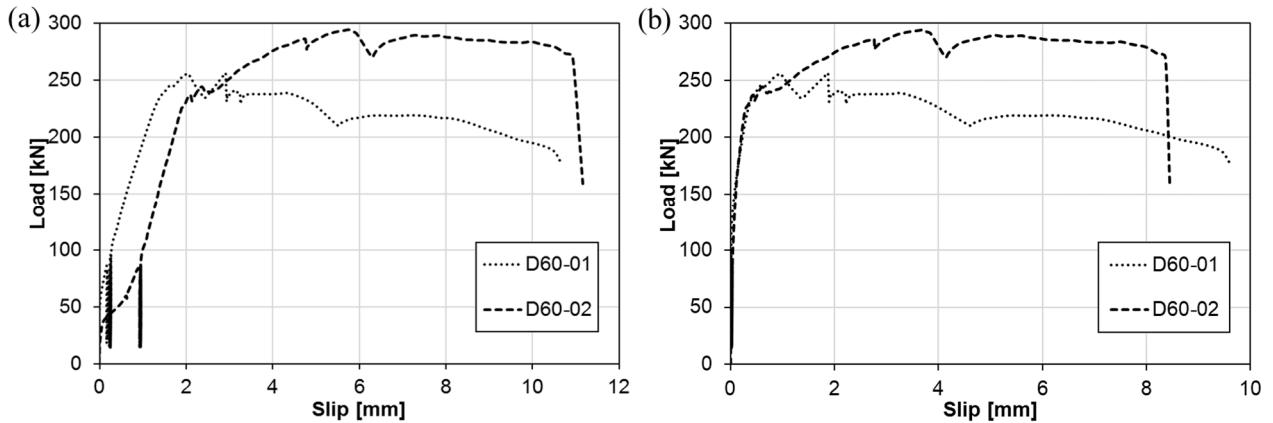
Figure 4.32: Load-slip curves for series D60:
(a) steel profile-concrete slab, (b) steel plate-concrete slab.

The ultimate load, stiffness at serviceability loads, slip and transverse separation between a concrete slab and a steel profile are summarised in Table 4.10 and Table 4.11. For demountable specimens, the slip is also presented for the shear plane on the contact between the steel plate/angles and the concrete slab.

Ultimate load $P_{ult,exp}$ is defined as the maximum measured load of the specimen, as shown in Figure 4.33. The characteristic load is calculated according to statistical evaluation procedures given in Annex D of EN 1990:2010 [83] and the alternative method provided in Annex B of EN 1994-1-1:2004 [10], which defines characteristic resistance as the minimum failure load reduced by 10%. Stiffness at serviceability loads is obtained per headed stud connector, i.e. bolt, at the load of $0.7P_{ult,exp}$ (Figure 4.33).

The load-slip curves shown in Figure 4.25–Figure 4.32 are characterised by several local peaks developed in the pre-ultimate and post-ultimate domains. Due to local peaks, the load drop is sometimes greater than 10% of the ultimate load, causing the load equal to 90% of the failure load to be reached several times during testing. To obtain the slip capacity according to Annex B of EN 1994-1-1:2004 [10], the maximum slip in the post-ultimate domain corresponding to 90% of the failure load is determined (Figure 4.33) and the characteristic value is calculated.
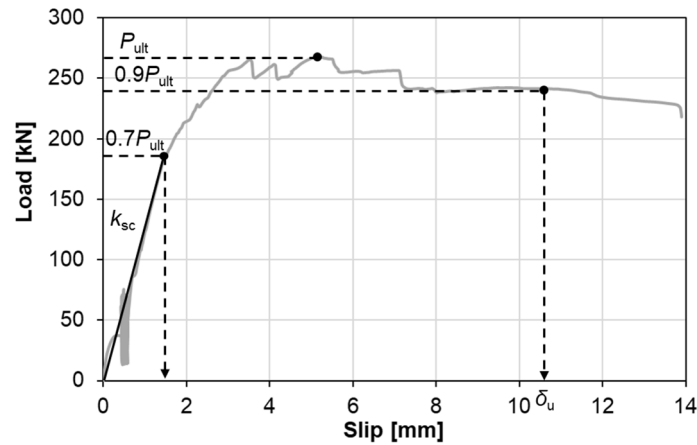
Figure 4.33: Load-slip curve and definition of the main parameters.

Table 4.10: Results of the push-out test: series S, S45 and S60.

Series	Specimen	Ultimate load	Stiffness	Transverse separation at $P_{ult,exp}$	Max. slip at $0.9P_{ult,exp}$
		$P_{ult,exp}$ [kN]	k_{sc} [kN/mm]	[mm]	$\delta_{u,exp}$ [mm]
S	S-01	207.7*	95*	0.31*	3.59*
	S-02	274.0	80	0.36	4.09
	S-03	255.1	70	0.59	5.30
	Mean	264.6	75	0.42	4.70
	St. deviation	13.36			
	CoV [%]	5.05			
	Characteristic	- [1] / 229.6 [2]			3.68 [2]
S45	S45-01	362.3	89	0.63	5.25
	S45-02	318.1	78	0.34	1.63
	S45-03	331.6	98	0.80	4.82
	Mean	337.3	88	0.59	3.90
	St. deviation	22.65			
	CoV [%]	6.71			
	Characteristic	261.0 [1] / 286.3 [2]			1.47 [2]
S60	S60-01	251.8	76	0.45	6.03
	S60-02	275.4	66	0.28	4.20
	S60-03	267.0	82	0.25	1.58
	Mean	264.7	75	0.33	3.94
	St. deviation	11.96			
	CoV [%]	4.52			
	Characteristic	224.4 [1] / 226.6 [2]			1.42 [2]

* not included in statistical evaluation
[1] according to EN 1990:2010, [2] according to EN 1994-1-1:2004

Results obtained for specimen S-01 were excluded from the statistical evaluation given in Table 4.10. It is assumed that that specimen, which was the first one prepared, had an asymmetric set-up during the testing, caused by uneven lengths of two concrete slabs. In addition, it is suspected that concrete around headed studs may not have been sufficiently consolidated because hand compaction was applied by rodding. For concrete compacting of all the other specimens, a needle vibrator was used. As a consequence, specimen S-01 showed considerably lower resistance than the other specimens of the same series.

Table 4.11: Results of the push-out test: series D, DL, DLU, D45 and D60.

Series	Specimen	Ultimate load	Stiffness	Transverse separation at $P_{ult,exp}$	Max. slip at $0.9P_{ult,exp}$	
					Total slip: HEB-slab	Shear plane: plate/angle-slab
		$P_{ult,exp}$ [kN]	k_{sc} [kN/mm]	[mm]	$\delta_{u,exp}$ [mm]	$\delta_{u,ps,exp}$ [mm]
D	D-01	244.0	24	0.28	6.68	5.43
	D-02	245.0	21	0.84	13.06	-
	D-03	239.5	18	0.24	3.73	2.20
	Mean	242.8	21	0.45	7.82	3.82
	St. deviation	2.93				
	CoV [%]	1.21				
	Characteristic	233.0 [1] / 215.6 [2]			3.36 [2]	1.98 [2]
DL	DL-01	251.3	23	0.29	5.16	4.57
	DL-02	250.6	20	0.68	5.75	4.97
	Mean	251.0	22	0.97	5.46	4.77
	St. deviation	0.49				
	CoV [%]	0.20				
	Characteristic	- [2] / 225.5 [2]			4.64 [2]	4.11 [2]
DLU	DLU-01	267.8	15	0.67	10.66	9.25
	DLU-02	263.0	21	0.75	7.67	6.74
	Mean	265.4	18	0.71	9.17	8.00
	St. deviation	3.39				
	CoV [%]	1.28				
	Characteristic	- [2] / 236.7 [2]			6.90 [2]	6.07 [2]
D45	D45-01	333.2	27	0.58	4.33	4.27
	D45-02	331.6	30	0.98	6.54	5.94
	Mean	332.4	29	0.78	5.44	5.11
	St. deviation	1.13				
	CoV [%]	0.34				
	Characteristic	- [2] / 298.4 [2]			3.90 [2]	3.84 [2]
D60	D60-01	256.7	26	0.38	4.84	3.76
	D60-02	294.6	12	1.23	14.01	11.47
	Mean	275.7	19	0.81	9.43	7.62
	St. deviation	26.80				
	CoV [%]	9.72				
	Characteristic	- [2] / 231.0 [2]			4.36 [2]	3.38 [2]

[1] according to EN 1990:2010, [2] according to EN 1994-1-1:2004

Load-slip curves for shear between the steel profile and concrete slab indicate higher initial stiffness of non-demountable specimens compared with the demountable ones. All demountable specimens feature an initial slip at the beginning of loading, as presented in Figure 4.26.a–Figure 4.28.a and Figure 4.31.a–Figure 4.32.a. However, the initial slip is not present in the shear plane "steel plate/angle-concrete slab", as shown in Figure 4.26.b–Figure 4.28.b and Figure 4.31.b–Figure 4.32.b. Comparing the stiffness at serviceability loads shown in Table 4.10, it is observed that the average stiffness per stud connector is in the range of 18–29 kN/mm for demountable specimens and 75–88 kN/mm for non-demountable specimens. Hence, the stiffness of demountable connections is approximately three to four times smaller than of the corresponding non-demountable connections. According to the obtained data, most of the demountable connections feature larger slip at 90% of the ultimate load than non-demountable connections. Slip in the shear plane "steel plate/angle-concrete slab" corresponding to 90% of the maximum load is smaller than the overall slip of demountable specimens and closer to the slip of non-demountable ones.

For loads above 200 kN, curves are characterised by fluctuations that are attributed to the crack development across concrete slabs. Damage occurred in all concrete ribs containing headed studs, causing cracks to open and stabilise alternately in different ribs, inducing drops and rises in the measured load. The measured ultimate loads of demountable and non-demountable specimens with sheeting ribs transverse to the beam were in the range of 240–274 kN, while for the specimens with

the angle between sheeting ribs and the beam smaller than 90°, they were in the range of 252–362 kN, indicating the resistance increase with the decrease of the angle size. Nevertheless, for comparing maximum loads of test series, differences in the concrete compressive strengths should be accounted for.

The appearance of a specimen before and during the push-out test is shown in Figure 4.34. A considerable deformation of profiled steel sheeting and separation from the concrete slab were observed during the testing of each specimen. Furthermore, a certain outward inclination of the slabs was noticed in the later stages of loading.
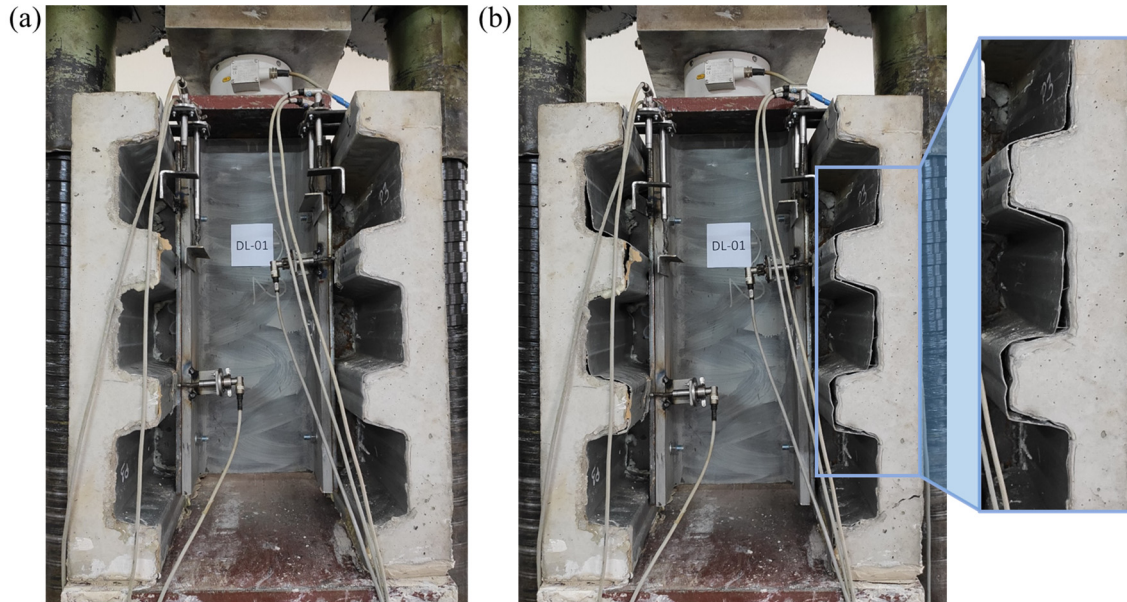
Figure 4.34: (a) Specimen before the testing, (b) Specimen during the testing.

At the top surface of concrete slabs, cracks were observed during the testing of both demountable and non-demountable specimens. Although they did not induce the specimen failure, it is interesting to note that they followed the direction of the profiled sheeting ribs. Crack patterns are presented in Figure 4.35 using the example of three specimens with different angles between ribs and the beam.
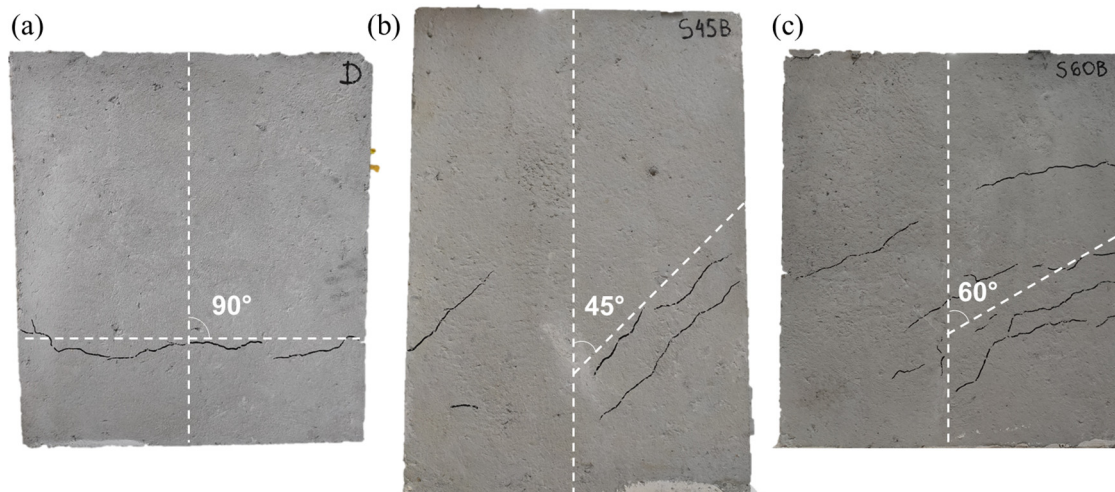
Figure 4.35: Crack pattern on the concrete slab top surface:
(a) series D, (b) series S45, (c) series S60.

After testing, specimens were demounted, and concrete failure was observed in each slab. Failure forms for different series with sheeting ribs transverse to the beam are shown in Figure 4.36. Failure modes of demountable specimens D and non-demountable specimens S are equivalent, indicating the

development of concrete cones and concrete pull-out failure. Concrete failure of the discontinuous concrete slab of the specimen DL corresponds to the failure form of the continuous slab of the specimen D. Specimens DLU reinforced with U-bars also feature concrete cone failure, as detected on the right side of the specimen presented in Figure 4.36.d. However, the left side of the specimen DLU, shown in Figure 4.36.d, indicates the separation of entire concrete ribs from the rest of the concrete slab.

Specimens with discontinuous slabs over the beam did not exhibit longitudinal concrete splitting between a headed stud and a slab edge, although the applied stud-to-edge distance had been set to 4d, which is smaller than the requested 6d according to EN 1994-1-1:2004 [10]. It might be supposed that the vertical angle leg reinforces the edge and contributes to the prevention of splitting failure.
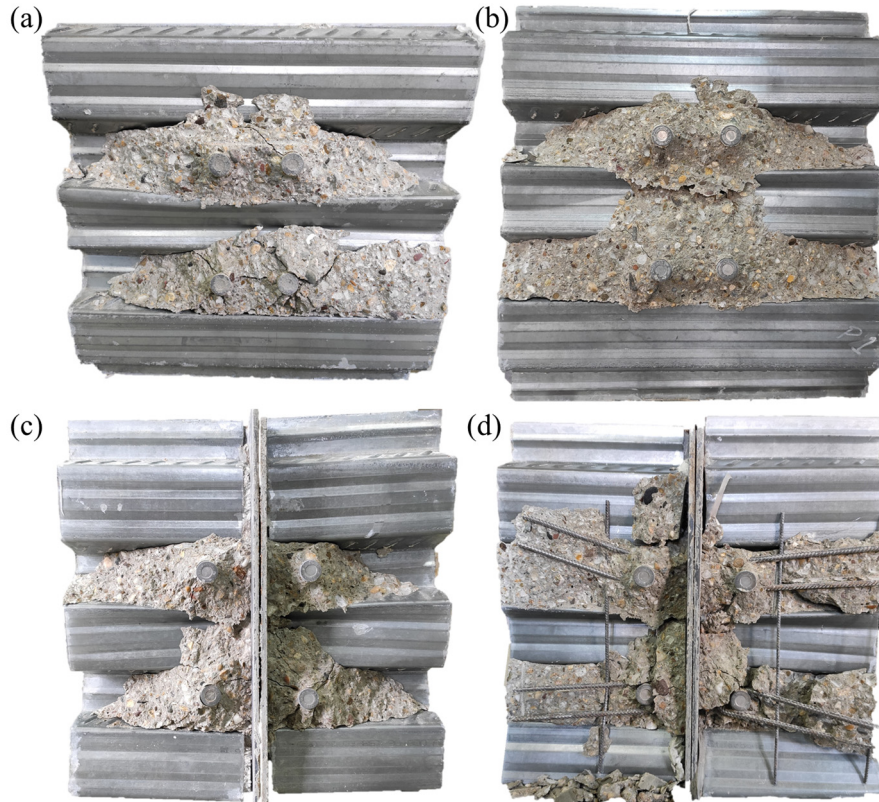
Figure 4.36: Failure forms of specimens: (a) series S, (b) series D, (c) series DL, (d) series DLU.
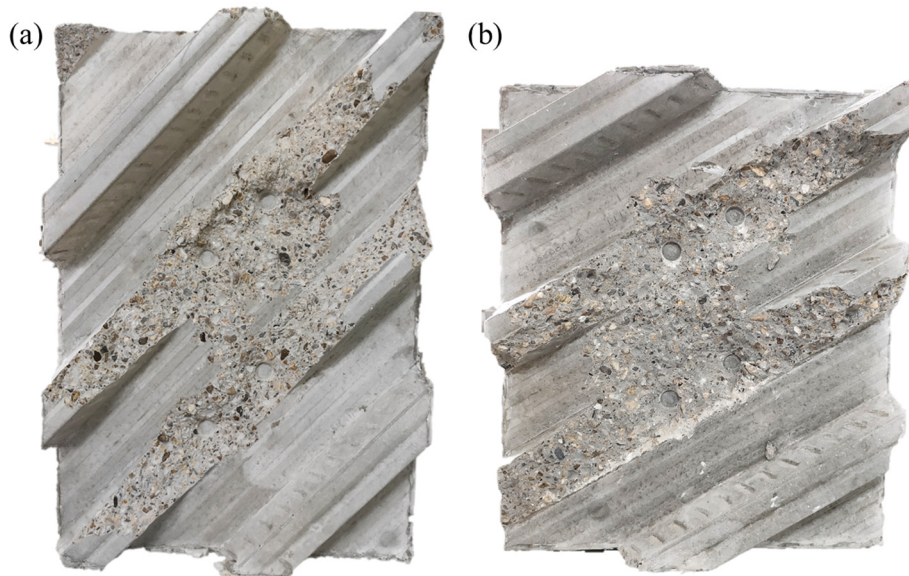
Figure 4.37: Failure forms of specimens: (a) series S45, (b) series S60.

63

Specimens with the angle between ribs and the steel profile smaller than 90° were also characterised by the development of concrete cones and pull-out failure, as shown in Figure 4.37. Concrete cones followed the concrete ribs, forming the angle of 45°, i.e. 60°, with the vertical axis.

After the removal of the surrounding concrete, a certain deformation of welded headed studs was observed, as presented in Figure 4.38. Development of a single slight curvature along stud height was noticed, but deformation was not significant. No rupture of headed studs occurred in any of the conducted push-out tests. Moreover, deformation of the plate and angles was not detected after the testing of demountable specimens, implying that plate bending on contact with headed studs did not appear for the selected plate thickness.
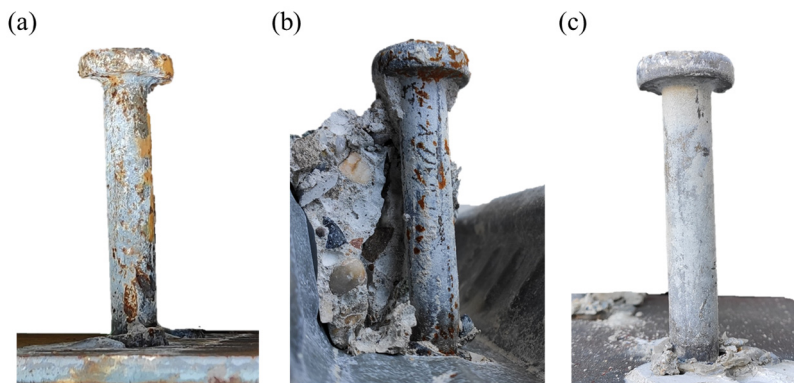
Figure 4.38: Headed studs after the testing: (a) series D, (b) series S45, (c) series S60.

To demonstrate reassembling of a demountable shear connection, bolts were dismantled after testing. Easy bolt removal proved the demountability of the proposed shear connection. Bolts and a bolt hole in the steel plate after testing of demountable specimens are presented in Figure 4.39. As there was no plastic deformation observed in M12 and M16 bolts, it could be assumed that these connectors had an elastic response during the experiment, as it was intended. Also, no deformation of the steel material around bolt holes occurred in the steel plate and angles, nor the steel profile.
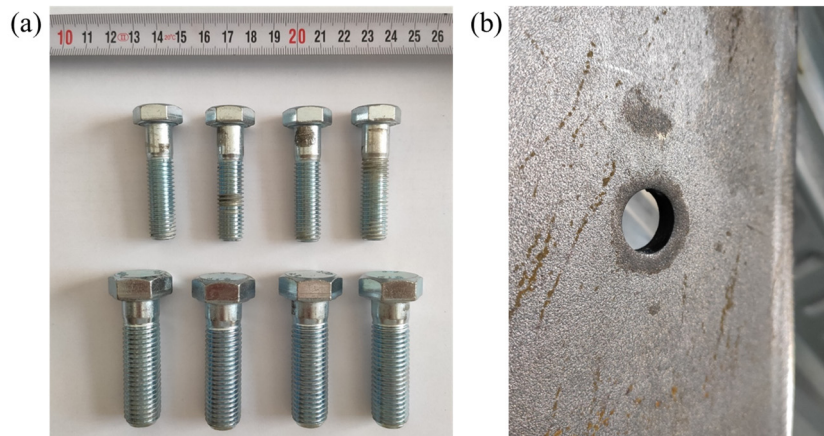
Figure 4.39: Condition of components after the testing: (a) M12 and M16 bolts, (b) steel plate.

4.5 Discussion of the Test Results

Load-slip curves obtained during push-out testing of series S and D are presented together in Figure 4.40.a. Comparing the response of the developed demountable connection with welded headed studs and bolts with the corresponding non-demountable connection with welded headed studs, it is observed that the demountable connection exhibits larger deformations due to shear load. Bolt connectors induce lower initial stiffness of the connection due to movement inside the holes. As no pretension force was applied during bolt mounting, bolt slip inside the hole starts at the early loading stage before applying loading cycles. The measured initial slip due to bolt displacement has values in the range of 0.25–0.70 mm, depending on the exact bolt position inside the holes released during

specimen mounting. For the selected bolt diameter of 12 mm and bolt hole diameter of 13 mm, a clearance between the connector and the hole is 1 mm, limiting the initial slip to that value.

Comparing the load-slip behaviour of non-demountable specimens and load-slip response in the shear plane "steel plate-concrete slab" of demountable specimens given in Figure 4.40.b, it is noticed that the curves overlap in the initial part. For the mentioned curves of series S and D, increased initial stiffness up to the load of approximately 100 kN is observed, followed by the stiffness reduction afterwards. Results suggest that at the initial loading stage, the behaviour of headed studs, welded to the steel plate with a thickness of 8 mm, corresponds to the behaviour of the stud connectors welded to the steel profile flange.
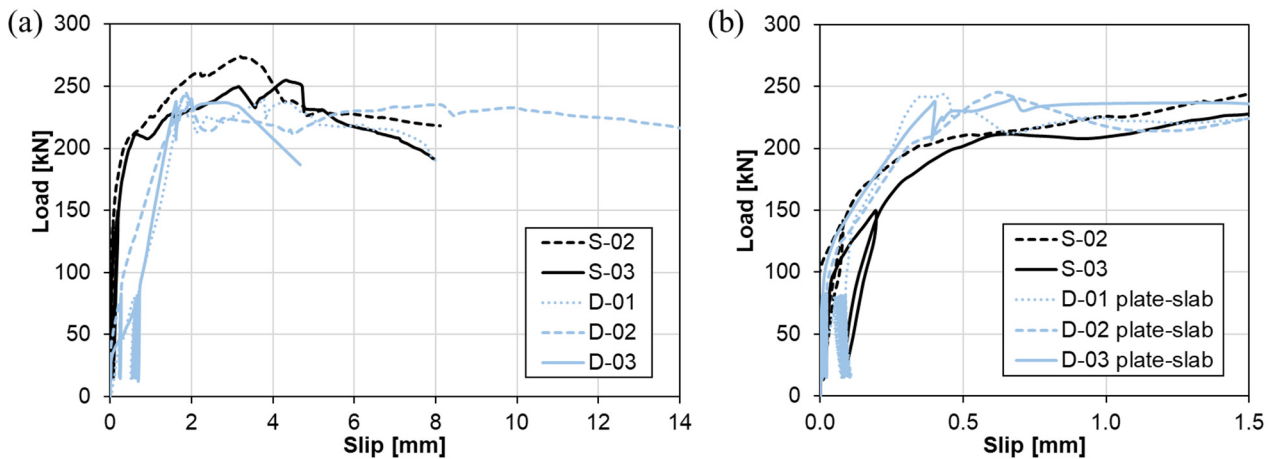
Figure 4.40: Comparison of the response of demountable and non-demountable specimens: (a) total slip, (b) slip in the shear plane with welded headed studs.

Comparing the slip capacity of demountable and non-demountable connections (Table 4.10 and Table 4.11), it is observed that the slip at load $0.9P_{ult}$ is below 6 mm for both specimens S, suggesting that connectors cannot be classified as ductile. On the other hand, two out of three tested demountable specimens D have the slip at load $0.9P_{ult}$ larger than 6 mm. Although, it is noted that the overall slip of the demountable connection contains the initial bolt slip.

Data measured during the push-out testing provide information on the slip in both shear planes of demountable specimens. The overall slip of the demountable connection is compared with the slip in planes "steel plate-concrete slab" and "steel profile-steel plate" in Figure 4.41. An exact match until the end of cyclic loading is accomplished for the load-slip curves of the overall slip and slip in the contact "steel profile-steel plate", suggesting that the shear plane with bolt shear connectors is active. For loads above 100 kN, a disagreement between the mentioned curves is present as at that stage shear plane "steel plate-concrete slab" gets activated as well. The phase between the load level of 100 kN and the first peak load is characterised by a simultaneous slip in both shear planes, i.e. the total slip is the sum of the slip of bolts and welded headed studs.

In further loading, demountable specimens feature distinct increases in the overall slip between the concrete slab and steel profile. However, the slip in the shear plane "steel profile-steel plate" becomes negligible. Almost all displacement appears on the contact between the concrete slab and steel plate, due to the slip of headed studs. Demountable specimens with discontinuous slabs over the support are characterised by a similar response, as shown in Figure 4.42.
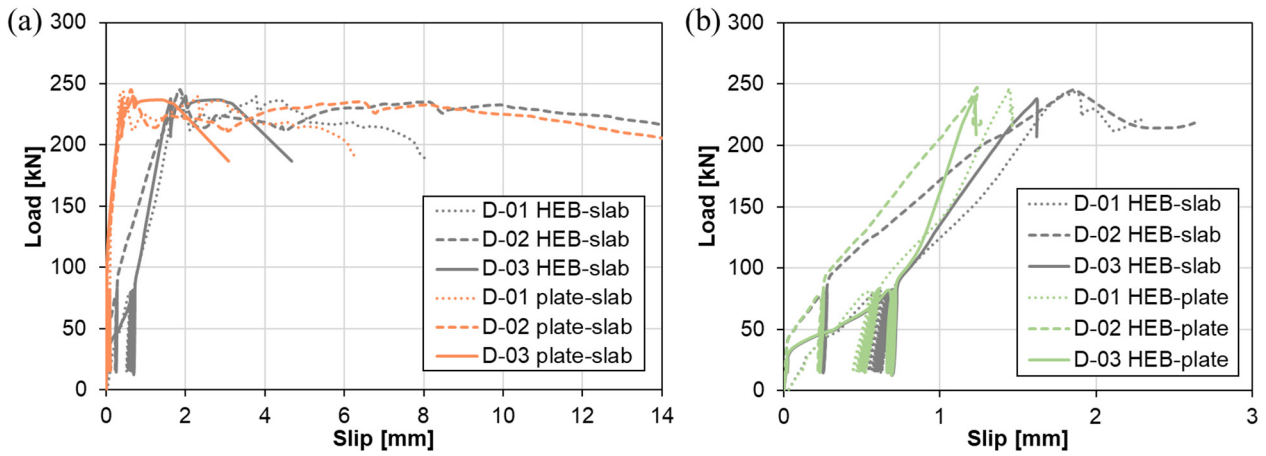
Figure 4.41: Comparison of the slip: (a) overall slip and slip on the contact "steel plate-concrete slab", (b) overall slip and slip on the contact "steel profile-steel plate".
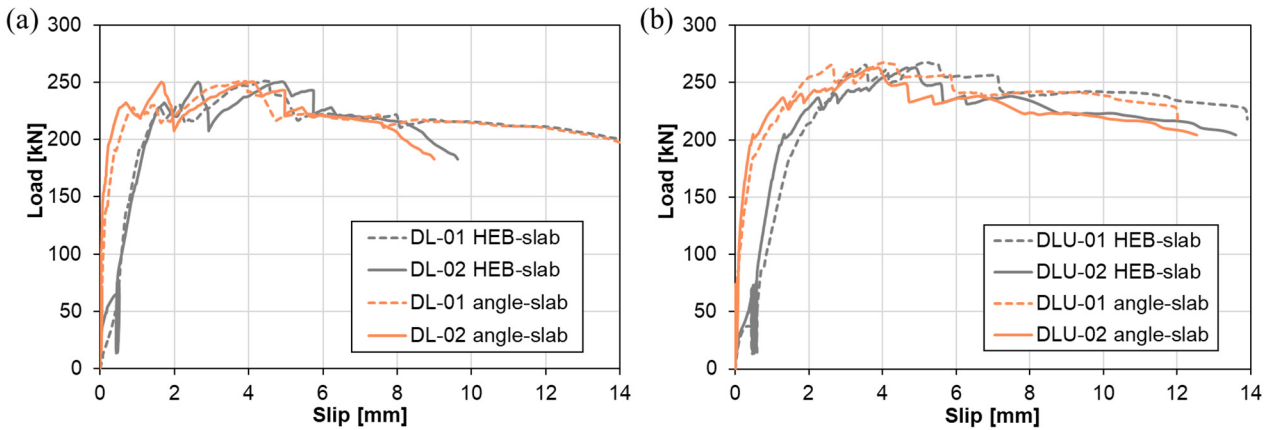
Figure 4.42: Comparison of the overall slip and the slip on the contact "steel angle-concrete slab": (a) series DL, (b) series DLU.

To observe the difference in the behaviour of demountable shear connections with continuous and discontinuous slabs over the support, load-slip curves for series D, DL and DLU are presented together in Figure 4.43. There are no significant dissimilarities in the response of demountable specimens with different configurations. Curves overlap in the initial part up to approximately 200 kN. For loads above 200 kN, curves of the specimens DL have more fluctuations in contrast to relatively smooth curves of the specimens DLU, indicating that the cracks in concrete slabs without the additional stirrup reinforcement are more pronounced. Connections with discontinuous slabs with additional U-bars have larger slip capacity (more than 6 mm) than discontinuous slabs without stirrups (less than 6 mm) (Table 4.11).
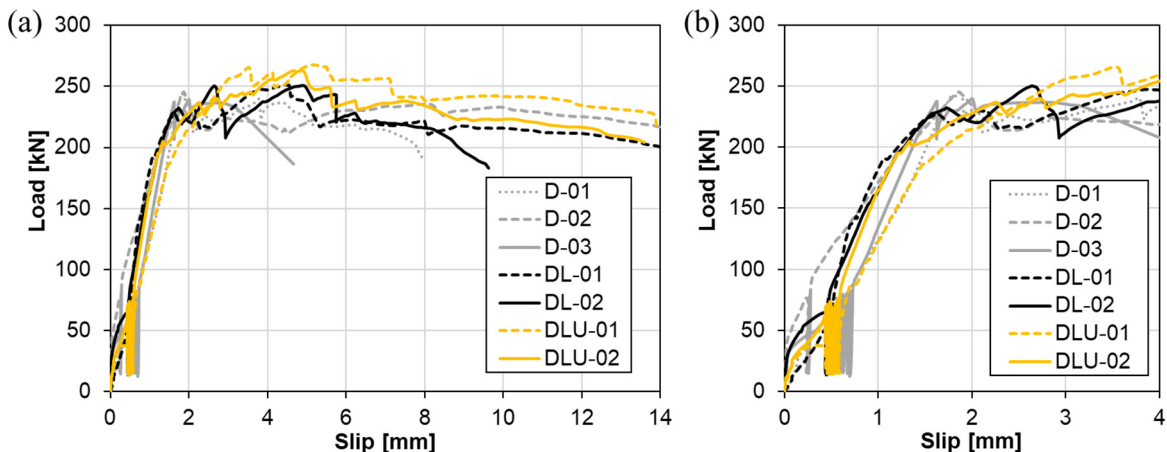
Figure 4.43: Comparison of the response of demountable specimens with continuous and discontinuous slabs: (a) total recorded data, (b) initial loading stage.

66

Comparisons of the ultimate loads of series S, D, DL and DLU are given in Table 4.12. As in all push-out tests, concrete failure occurred with no rupture in bolts nor headed studs, the experimental ultimate load for each specimen, $P_{ult,exp}$, was normalised with concrete compressive strength. For normalisation on the series S concrete strength of 35 MPa, the following relation was applied [64]:

$$P_{ult,exp,nor} = P_{ult,exp} \left(\frac{35 \, \text{MPa}}{f_{cm}} \right)^{2/3} \tag{4.1}$$

where f_{cm} is the concrete cylinder compressive strength in MPa. Normalised resistances, $P_{ult,exp,nor}$, were used for comparison of ultimate loads of different test series. Correlation between specimens' resistance is shown through the ratio $P_{ult,exp,nor}/\overline{P}_{ult,exp,nor,S}$, where $\overline{P}_{ult,exp,nor,S}$ is the mean value of the normalised ultimate load obtained for series S.

Taking into account the variation between ultimate loads of specimens from the same series, dissimilarities in the resistance of demountable and non-demountable shear connections are not significant. The lower value of the normalised ultimate load of demountable specimens D in comparison with non-demountable specimens of series S, could be assigned to differences in the stiffness of components to which the headed studs are welded: steel plate and top flange of the steel profile. This parameter is analysed through numerical analysis.

Discontinuity of the composite concrete slab over the support does not affect the resistance of the shear connection for the set distance between a headed stud and an angle leg of $4d$, as observed when comparing results shown for series D and DL. The implementation of U-bars in series DLU increases the peak load compared with the DL specimens without stirrup reinforcement. A good match between average ultimate loads obtained for series S and DLU indicates that the developed solution of a demountable shear connection with bolts and headed studs corresponds well to the non-demountable connection with welded headed studs at the point of shear resistance. The adopted distance between the headed stud and the angle leg of $4d$ seems to be sufficient for the proposed configuration of the demountable shear connection, though further conclusions regarding the exact stud-to-edge distance are made according to the results of parametric studies.

Table 4.12: Comparison of push-out test series: S, D, DL and DLU.

Series	Series	Concrete compressive strength	Ultimate load	Normalised ultimate load*	Mean value of the normalised ultimate load	Ratio	Ratio
		f_{cm} [MPa]	$P_{ult,exp}$ [kN]	$P_{ult,exp,nor}$ [kN]	$\overline{P}_{ult,exp,nor}$ [kN]	$P_{ult,exp,nor}$ /$\overline{P}_{ult,exp,nor,S}$	$\overline{P}_{ult,exp,nor}$ /$\overline{P}_{ult,exp,nor,S}$
S	S-02	35.0	274.0	274.2	264.8	1.04	1.00
	S-03	35.0	255.1	255.3		0.96	
D	D-01	34.5	244.0	246.4	245.3	0.93	0.93
	D-02	34.5	245.0	247.5		0.93	
	D-03	34.5	239.5	241.9		0.91	
DL	DL-01	37.3	251.3	240.9	240.6	0.91	0.91
	DL-02	37.3	250.6	240.3		0.91	
DLU	DLU-01	37.3	267.8	256.8	254.5	0.97	0.96
	DLU-02	37.3	263.0	252.2		0.95	

*normalised with f_{cm} = 35 MPa

Furthermore, the influence of the angle between profiled sheeting ribs and the beam is discussed through the analysis of experimental data for series S45, S60, D45 and D60. To observe differences in the response of demountable and non-demountable connections with the angle between profiled sheeting ribs and the beam smaller than 90°, load-slip curves for each specimen with the specific angle are presented in Figure 4.44. To make curves suitable for comparison, load-slip curves given for non-demountable specimens are compared with load-slip curves for the plane "steel plate-concrete slab" of demountable specimens. For both angles of 45° and 60°, a similar trend is present in the response of non-demountable and corresponding demountable connections for the shear plane "steel

plate-concrete slab". Nevertheless, comparing the overall slip between the steel profile and concrete slab at load $0.9P_{ult}$ (Table 4.10 and Table 4.11), it is noticed that the mean value of the slip for series D45 is larger than for S45, as well as that the average slip of series D60 is larger than the one of S60.
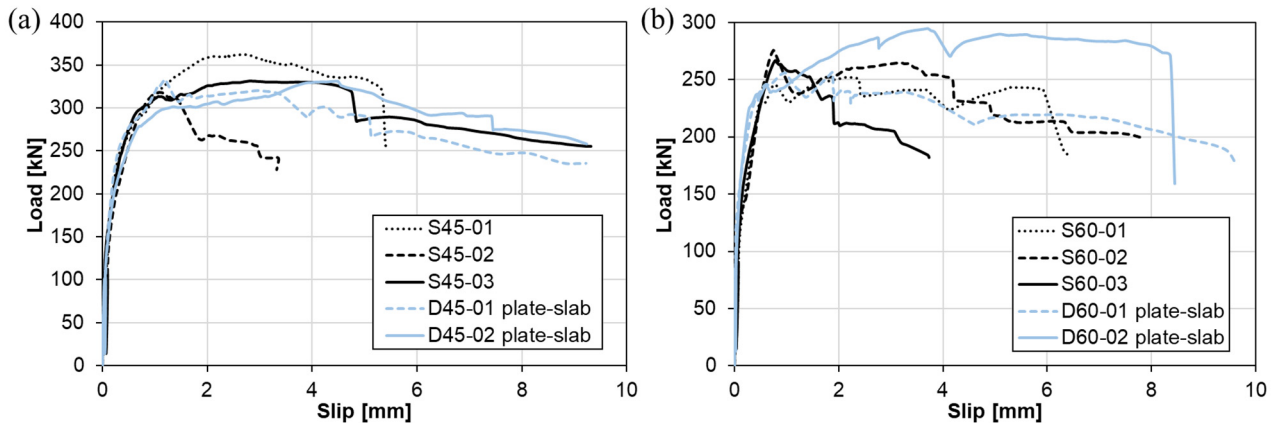
Figure 4.44: Comparison of the response of demountable and non-demountable specimens:
(a) series D45, (b) series D60.

For demountable specimens D45 and D60, the overall slip is compared with the slip in the plane "steel plate-concrete slab" in Figure 4.45. The results confirm the previously made conclusions about the behaviour of demountable connections: the slip of a demountable connection consists of the slip of welded headed studs and bolts. Firstly, the initial slip happens as the consequence of bolt displacement inside holes. The measured values of the initial slip are influenced by the position of bolts inside the holes. After the initial slip, the load-slip relationship is linear, defined by the simultaneous slips of bolts and headed studs. Finally, with the propagation of concrete cracks in the slab, the overall slip and slip in the shear plane "steel plate-concrete slab" notably increase.
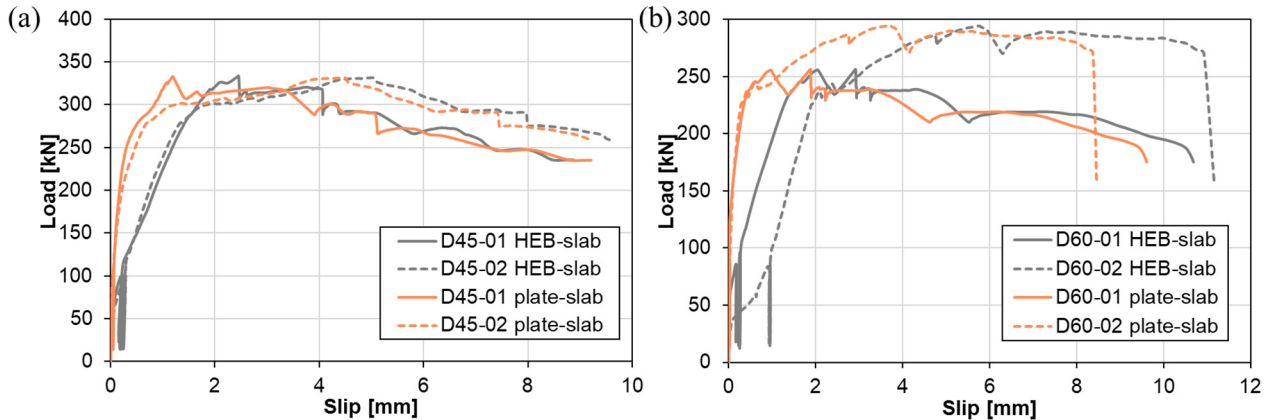
Figure 4.45: Comparison of the overall slip and the slip on the contact "steel plate-concrete slab":
(a) series D45, (b) series D60.

Comparisons of load-slip curves of the analysed non-demountable and demountable connections with continuous slabs over the support with different angles between profiled sheeting ribs and the beam are presented in Figure 4.46. In both graphs, curves corresponding to specimens with the angle between profiled sheeting ribs and the beam of 45° are distinguished by reaching the highest loads. Response of the connections with the angle between ribs and the beam of 60° is close to the one of the connections with ribs transverse to the supporting beam.
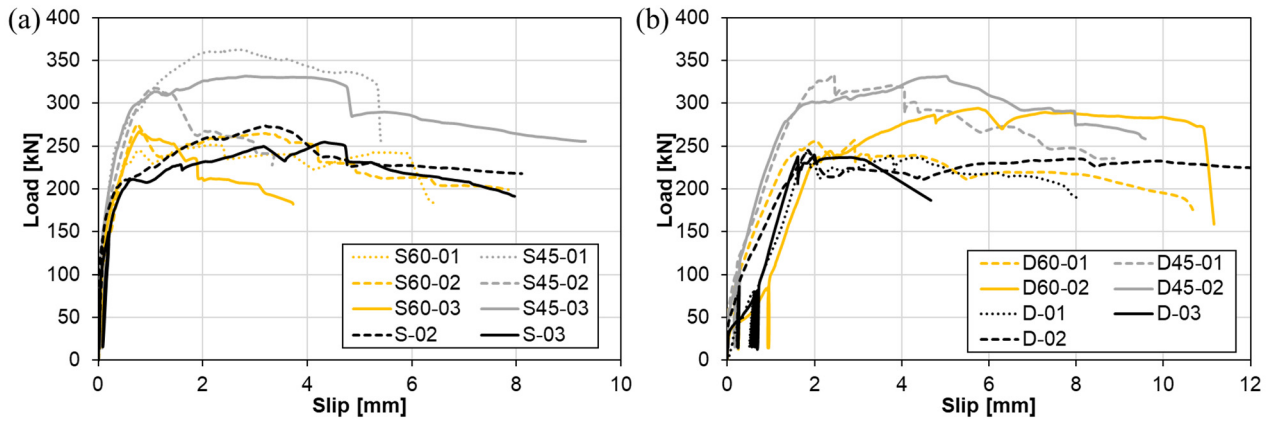
Figure 4.46: Comparison of the response of specimens with different angles between ribs and the beam: (a) non-demountable specimens, (b) demountable specimens.

In order to compare the resistance of specimens with different angles between sheeting ribs and the beam, ultimate loads are normalised on the concrete strength of 35 MPa according to Eq. (4.1) and compared in Table 4.13. Ultimate loads for series S45 and D45 match, as well as for series S60 and D60, indicating minor differences in the resistance of demountable and non-demountable series. Demountable and non-demountable connections with the angle between ribs and the beam of 45° reached the highest ultimate loads. On the other hand, connections with the angle between sheeting ribs and the beam of 60° had similar resistance as non-demountable specimens with ribs transverse to the beam. However, comparing series D and D60, somewhat higher loads are noticed for specimens with the smaller angle between ribs and the beam. To make precise conclusions and quantify the effect of the angle between ribs and the beam, finite element analysis with parametric studies is conducted.

Table 4.13: Comparison of push-out test series: S, S45, S60, D, D45 and D60.

Series	Series	Concrete compressive strength	Ultimate load	Normalised ultimate load*	Mean value of the normalised ultimate load	Ratio	Ratio
		f_{cm} [MPa]	$P_{ult,exp}$ [kN]	$P_{ult,exp,nor}$ [kN]	$\overline{P}_{ult,exp,nor}$ [kN]	$P_{ult,exp,nor}$ $/\overline{P}_{ult,exp,nor,S}$	$\overline{P}_{ult,exp,nor}$ $/\overline{P}_{ult,exp,nor,S}$
S	S-02	35.0	274.0	274.2	264.8	1.04	1.00
	S-03	35.0	255.1	255.3		0.96	
S45	S45-01	36.2	362.3	354.0	329.6	1.34	1.24
	S45-02	36.2	318.1	310.8		1.17	
	S45-03	36.2	331.6	324.0		1.22	
S60	S60-01	36.2	251.8	246.0	258.7	0.93	0.98
	S60-02	36.2	275.4	269.1		1.02	
	S60-03	36.2	267.0	260.9		0.99	
D	D-01	34.5	244.0	246.4	245.3	0.93	0.93
	D-02	34.5	245.0	247.5		0.93	
	D-03	34.5	239.5	241.9		0.91	
D45	D45-01	36.2	333.2	325.6	324.8	1.23	1.23
	D45-02	36.2	331.6	324.0		1.22	
D60	D60-01	36.2	256.7	250.8	269.3	0.95	1.02
	D60-02	36.2	294.6	287.8		1.09	

*normalised with f_{cm} = 35 MPa

69

5   Numerical Analysis

The results of the experimental work were complemented with the results of numerical analysis to gain a complete understanding of the behaviour of demountable shear connections with bolts and welded headed studs in steel-concrete composite beams. Numerical models were developed and calibrated according to the shear response of experimentally tested push-out specimens. Results of model behaviour are presented and discussed in this chapter.

Numerical analysis including geometrical and material nonlinearities was conducted in finite element software Abaqus [9]. For modelling of push-out tests, the explicit solver was used, simulating the quasi-static analysis.

5.1   Development of Finite Element Models

5.1.1   Geometry, Boundary Conditions and Loading

For the development of finite element models, all components of specimens tested in push-out tests were considered: headed studs, bolts, concrete slabs, profiled steel sheeting, steel profile, plate/angles and reinforcement bars. In addition, a supporting plate on which the concrete slab was laid was created. Components were modelled as solid parts, with two exceptions: profiled steel sheeting was modelled as a shell part and reinforcement bars were modelled as truss parts. Models of experimentally tested series are presented in Figure 5.1 and Figure 5.2.

Symmetry boundary conditions were applied where it was applicable. In models simulating specimens S, D, DL and DLU, double vertical symmetry conditions were used, whereas for specimens S45, S60, D45 and D60, a single symmetry condition was assigned, as shown in Figure 5.3. All points at the top surface of the steel cross-section were constrained to the reference point to which vertical loading was applied. Nodes at the bottom surface of the supporting plate were also constrained to the reference point setting the fully fixed boundary condition.
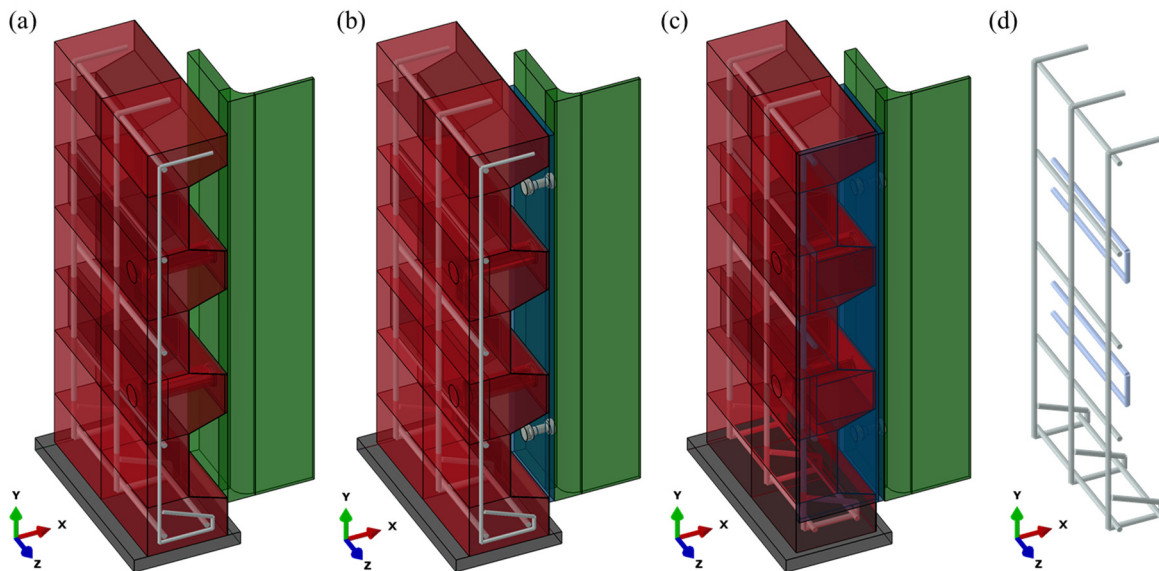
Figure 5.1: Geometry of finite element models: (a) model S, (b) model D, (c) model DL, (d) reinforcement mesh and U-bars for model DLU.
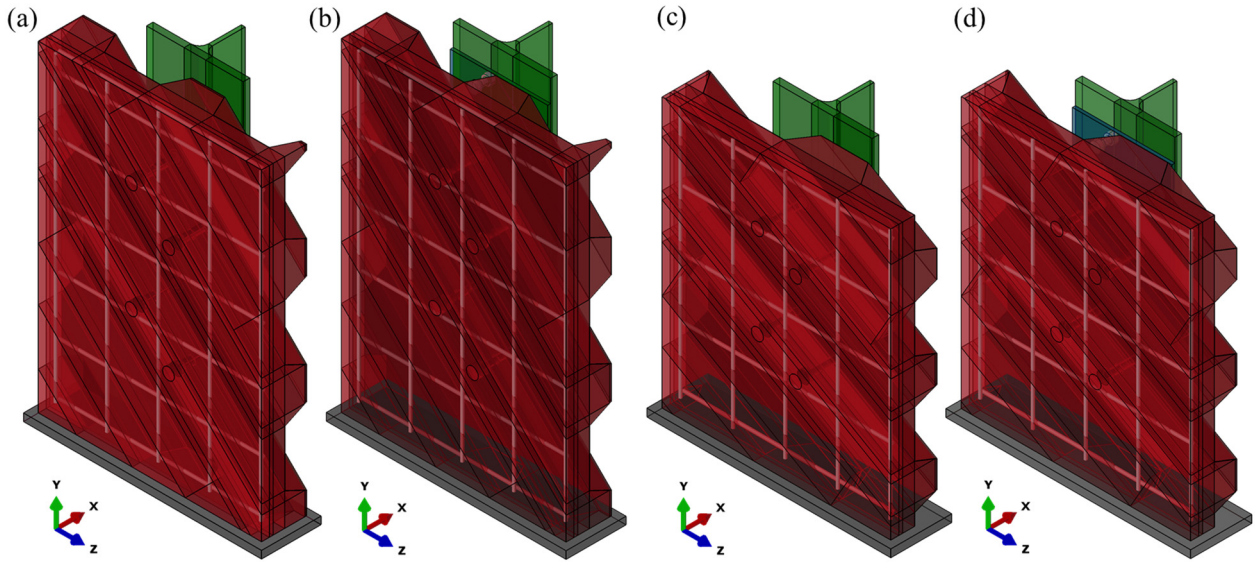
Figure 5.2: Geometry of finite element models:
(a) model S45, (b) model D45, (c) model S60, (d) model D60.
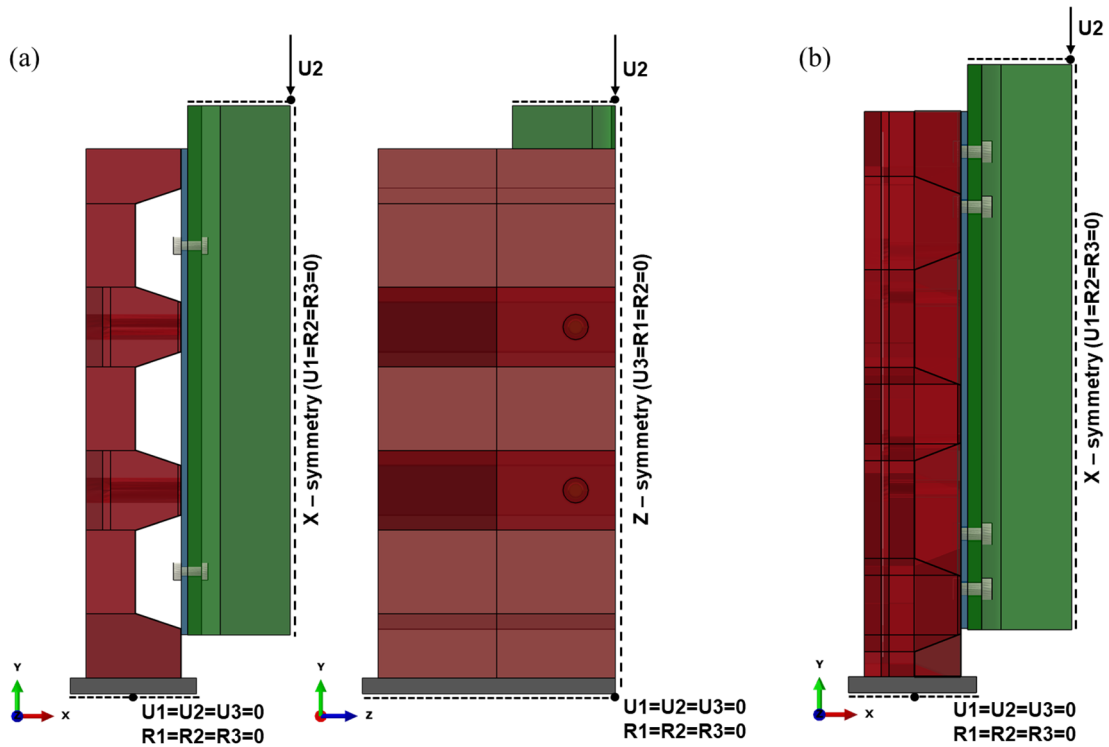
Figure 5.3: Boundary conditions: (a) double symmetry in model D, (b) single symmetry in model D60.

For connecting headed studs with the surface to which they were welded (a steel profile, plate or angles), the tie constraint was used. To set proper contact conditions between reinforcement bars and the concrete slab, the embedded constraint was applied. For the other contacts between parts, surface-to-surface contact was assigned: applying "hard" contact in the normal direction and setting different friction coefficients in the tangential direction, listed in Table 5.1.

Loading was applied as controlled displacement, using the smooth step amplitude function which showed good results for simulating quasi-static experiments [4], [86], [87]. The duration of the experiment was set to 1000 s. The mass scaling method was applied with the time increment of 0.003 s, providing a good match between numerical and experimental results.

Table 5.1: Adopted values of the friction coefficient.

Contact	Friction coefficient
concrete slab-supporting plate	0.45
concrete slab-headed studs	0.45
concrete slab-profiled sheeting	0.45
concrete slab-steel profile/plate/angle	0.30
between steel parts	0.20

5.1.2 Finite Element Mesh

The complexity of the numerical model and large zones in the concrete slab where cracks propagate influenced a large number of finite elements necessary for simulating a proper model response. Hence, a reduction of the computing time was essential. As efficient elements at the point of the computing time, 8-node linear hexahedron elements with reduced integration C3D8R were applied to solid parts. Similarly, 4-node linear quadrilateral elements with reduced integration S4R were applied to shell parts. For meshing truss parts, 2-node linear elements T3D2 were used.

Mesh size was varied throughout the model, with the smallest size of elements in headed studs and surrounding concrete (2 mm) and the largest elements in the periphery regions of the model where development of cracks and failure were not expected (10 mm). The adopted mesh was a result of the convergence study through which the size of elements on different parts had been varied to obtain the optimum mesh. To develop a mesh consisting of C3D8R elements, simple geometry of a part is required; therefore, it was necessary to divide each solid part into smaller partitions before meshing. As C3D8R elements tend to be not stiff enough in bending, the application of only one of these elements through the part thickness was avoided. Furthermore, the tendency was to use elements of the same or similar size on the contact of two surfaces. As an example of the performed meshing, the mesh applied to model D is presented in Figure 5.4. Results of the mesh sensitivity study with the size of the adopted finite elements for bolts, headed studs and surrounding concrete, and the plate, are presented in Figure 5.5.
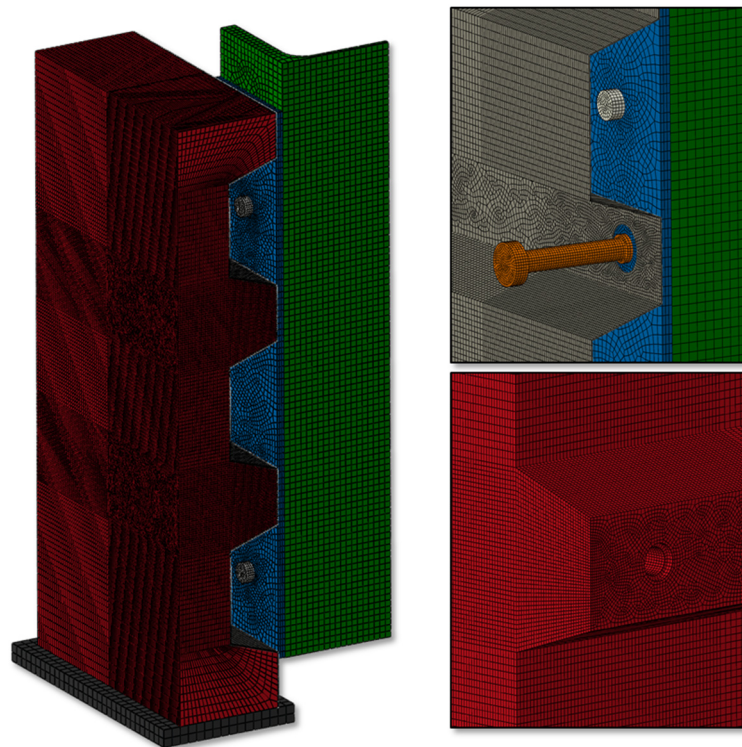
Figure 5.4: Finite element mesh for model D.
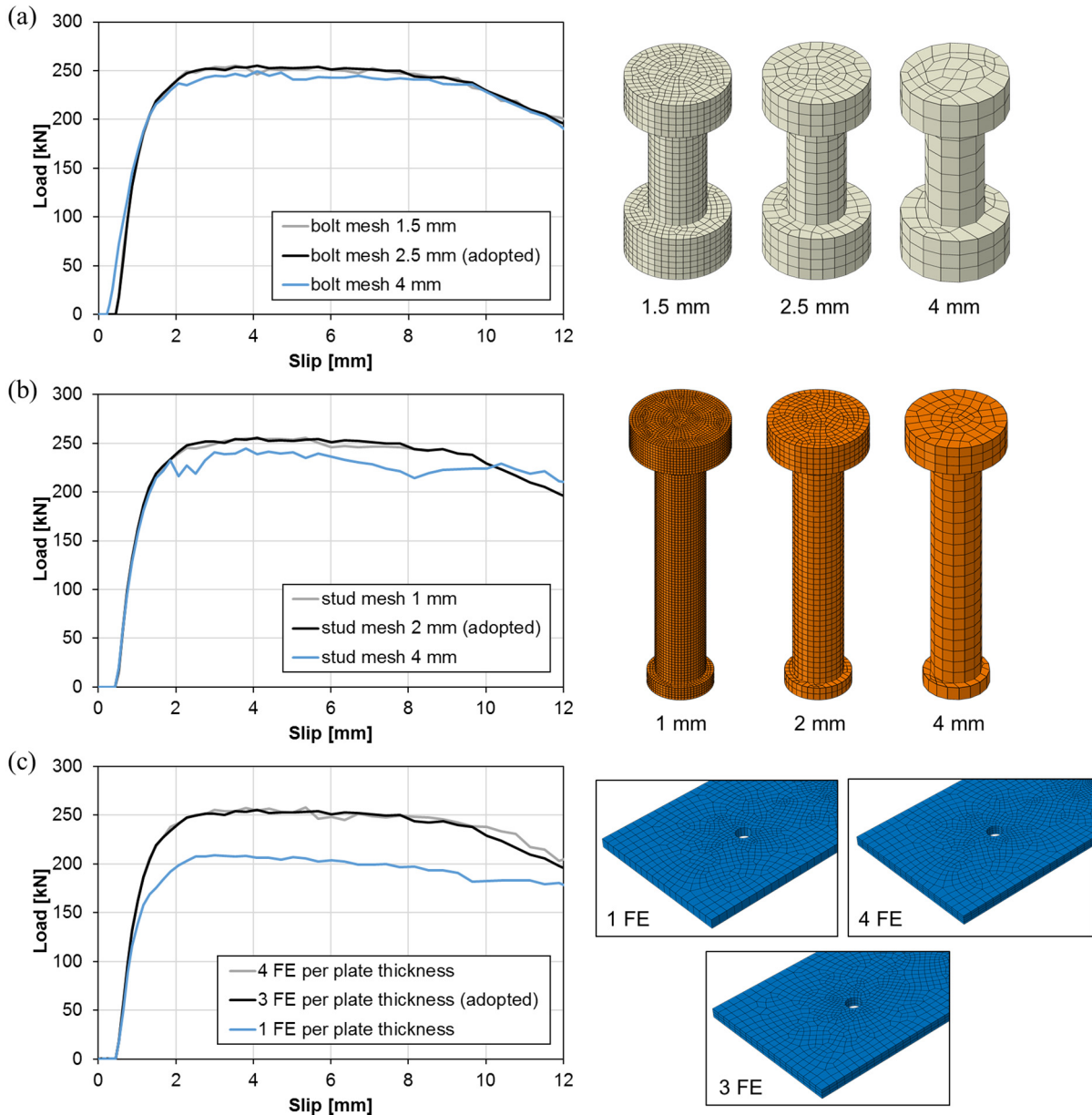
Figure 5.5: Mesh sensitivity study for model D: (a) bolt mesh,
(b) mesh for headed studs and surrounding concrete, (c) plate mesh.

5.1.3 Material Models

Material models applied in the numerical analysis were based on the experimental testing of the material. To describe the material behaviour of the steel components in the elastic domain, measured modulus of elasticity and Poisson's ratio of 0.3 were set. For defining material response in the plastic domain, true stress-strain curves were obtained from experimental stress-strain curves of coupon testing, according to Abaqus user manual [9]. True stress-plastic strain curves as implemented in the numerical model for steel profile, plate, profiled sheeting, headed studs and bolts are presented in Figure 5.6. Ductile and shear damage material models were not considered in the analysis as damage of steel components did not occur during push-out tests.

As reinforcement bars were not tested in tensile tests, the material model for reinforcement was adopted as a bilinear model, according to EN 1992-1-1:2004 [6]. Modulus of elasticity was defined and yield strength was set to 500 MPa. A top branch of the stress-strain curve was assumed to be horizontal. The adopted approximations are justified by the fact that stress in bars does not exceed 130 MPa during simulations, as later shown in Figure 5.29.

74
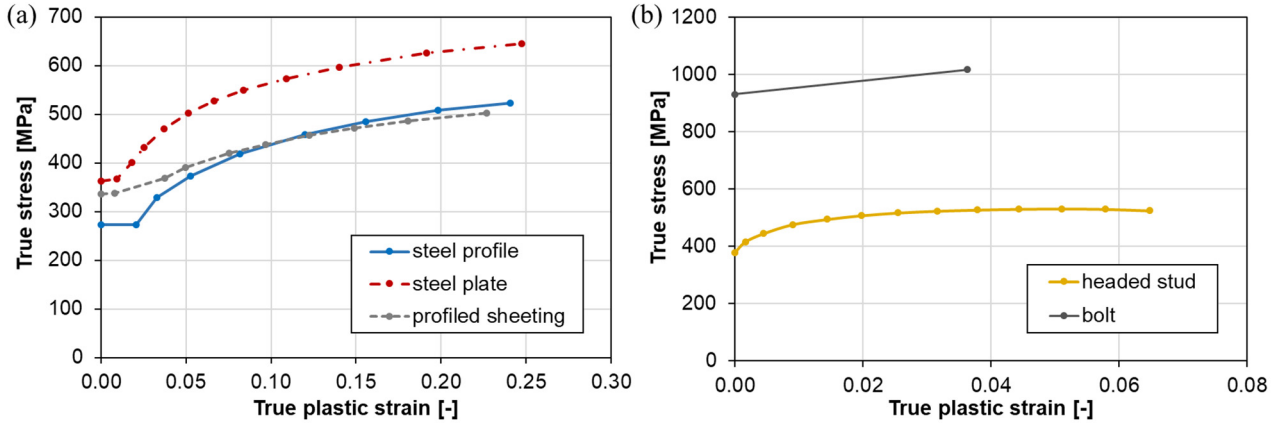
Figure 5.6: True stress-strain curves for steel components:
(a) steel profile, plate and profiled sheeting, (b) stud and bolt connectors.

As the failure of all push-out specimens was the failure of concrete, it was essential for numerical modelling to apply a material model which provides good predictions on the behaviour of composite slab cast in open trough profiled steel sheeting. Several models were considered: the model given by Carreira and Chu [13], the model suggested by Birtel and Mark [11], the model that Vigneri applied in the numerical analysis [64]. However, the best results were obtained applying the model proposed by Pavlović [4], which had been successfully implemented in several works [86], [87]. Therefore, that model was used in further numerical analysis. Comparisons of results of push-out simulations for different concrete damage plasticity models and descriptions of the considered models are given in Annex A.

For describing concrete behaviour in the elastic domain, modulus of elasticity and Poisson's ratio of 0.2 were applied. For defining compressive response in the plastic domain, the concrete stress-strain curve given in EN 1992-1-1:2004 [6] was extended by sinusoidal (from point D to E in Figure 5.7) and linear function (from point E to F in Figure 5.7), according to Pavlović [4]:

$$
\sigma_c(\varepsilon_c) = \begin{cases} f_{cm}\left[\dfrac{1}{\beta} - \dfrac{\sin(\mu^{\alpha_{tD}}\cdot\alpha_{tE}\ \pi/2)}{\beta\cdot\sin(\alpha_{tE}\ \pi/2)} + \dfrac{\mu}{\alpha}\right], \varepsilon_{cuD} < \varepsilon_c \le \varepsilon_{cuE} \\ \left[f_{cuE}(\varepsilon_{cuF} - \varepsilon_c) + f_{cuF}(\varepsilon_c - \varepsilon_{cuE})\right]/(\varepsilon_{cuF} - \varepsilon_{cuE}), \varepsilon_c > \varepsilon_{cuE} \end{cases}
\tag{5.1}
$$

where:

$$
\mu = \frac{\varepsilon_c - \varepsilon_{cuD}}{\varepsilon_{cuE} - \varepsilon_{cuD}}
\tag{5.2}
$$

$$
\beta = \frac{f_{cm}}{f_{cuD}}
\tag{5.3}
$$

$$
\alpha = \frac{f_{cm}}{f_{cuE}}
\tag{5.4}
$$

α_{tE} and α_{tE} are factors that influence the shape of the sinusoidal function.

Other symbols are defined in Figure 5.7.

The model is flexible at the point of adopting the exact shape of the sinusoidal function and stress and strain values at points E and F. Therefore, parameters were calibrated to match experimental results and to keep the curve smooth. They are presented and compared with the values suggested by Pavlović in Table 5.2.
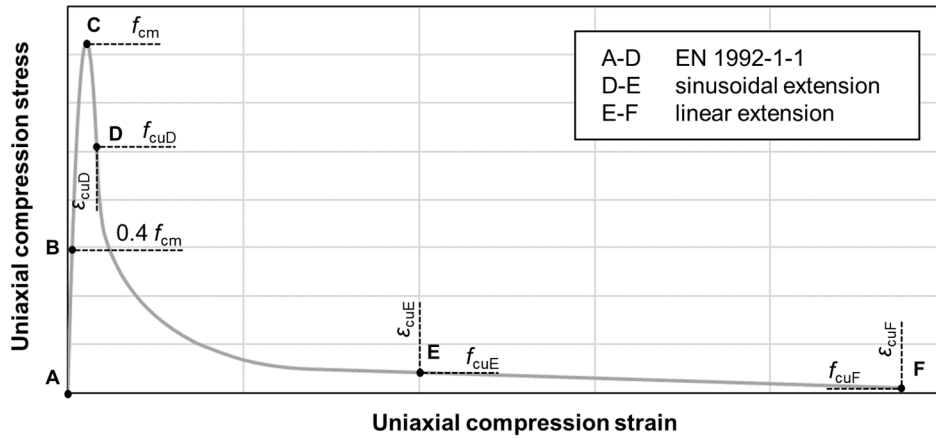
Figure 5.7: Concrete stress-strain curve in compression [4].

Table 5.2: Adopted parameters for concrete compression model.

Parameter	Pavlović [4]	FEA
α	15	8
α_{tD}	0.50	0.50
α_{tE}	0.90	0.60
ε_{cuE}	0.03	0.05
ε_{cuF}	0.10	0.20
$f_{cu,F}$ [MPa]	0.40	0.40

The adopted stress-strain curve for uniaxial compression is given in Figure 5.8.a. The implemented curve is characterised by slower descending than the original one used by Pavlović. It is important to note that Pavlović's model was originally designed for modelling push-out tests with solid concrete slabs where local concrete damage occurs in the area near shear connectors. However, different failure mechanisms present in this research, failure of concrete cone and propagation of cracks throughout the larger area of the slab, requested the adoption of the curve with higher stresses and larger strains in the post-ultimate domain.
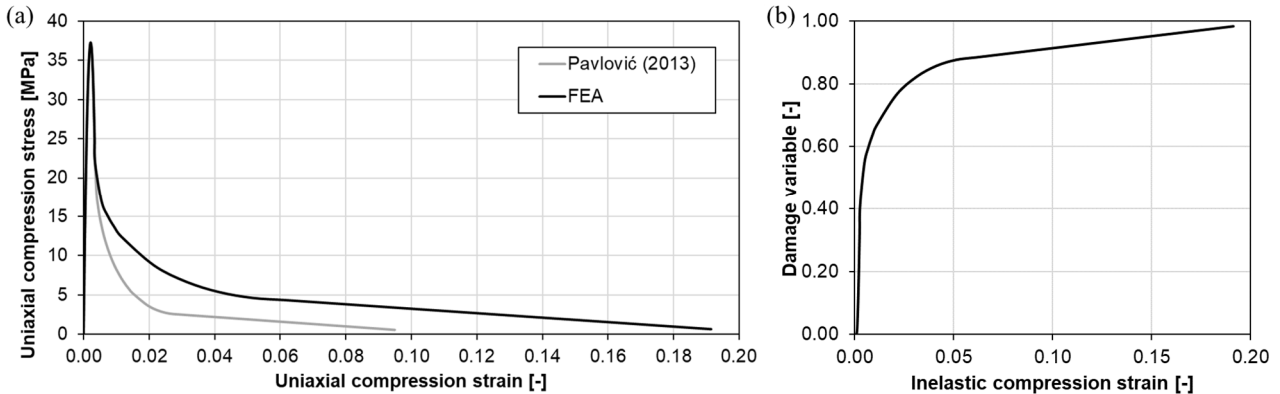
Figure 5.8: Concrete behaviour in compression (f_{cm} = 37.3 MPa):
(a) stress-strain curve, (b) compression damage.

Concrete compression damage was described using the compressive damage variable D_c, derived from the uniaxial stress-strain curve and described by Eq. (5.5). The compression damage curve is shown in Figure 5.8.b.

$$D_c = 1 - \frac{f_{cm}}{\sigma_c} \tag{5.5}$$

76

The concrete tension damage model was adopted completely according to Pavlović [4]. The stress-strain curve is given in Figure 5.9.a. Stress-strain relation in the elastic domain is linear, up to concrete tensile strength f_{ctm}. Afterwards, the sinusoidal function is used for describing tension softening until stress $f_{ctm}/20$. Concrete tension damage was described similarly as concrete compression damage using the tensile damage variable D_t, according to Eq. (5.6). The tension damage curve is shown in Figure 5.9.b.

$$D_t = 1 - \frac{f_{ctm}}{\sigma_t} \tag{5.6}$$
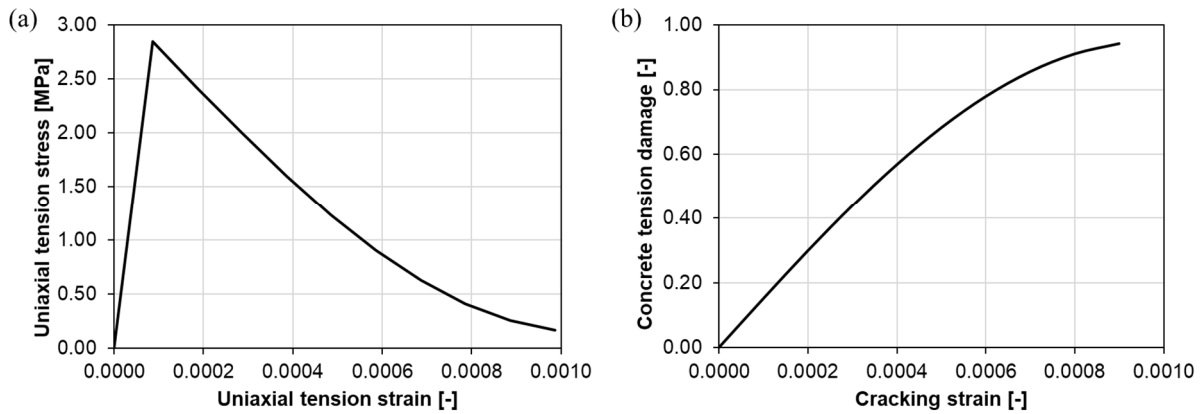
Figure 5.9: Concrete behaviour in tension (f_{cm} = 37.3 MPa): (a) stress-strain curve, (b) tension damage.

The concrete damage plasticity model in Abaqus requires a definition of plasticity parameters. The dilation angle was set to 38°, as performed in several other studies [64], [86]. Values of other parameters were set according to recommendations given in the software user manual [9]. Flow potential eccentricity was adopted as 0.1. The ratio of equibiaxial-to-uniaxial compressive strength was defined as 1.16. Parameter K which represents the ratio of the second stress invariant on the tensile meridian to that on the compressive meridian was taken as 0.67.

5.2 Validation of Finite Element Models

To validate the finite element models, their behaviour was compared with the behaviour of the experimental specimens by analysing load-slip curves, ultimate loads, crack patterns and deformations of the connection components.

Load-slip responses of developed models were compared with experimental results for each test series. All input parameters were set to be the same in all finite element models, except the geometry and concrete damage models. The concrete material model was applied according to the measured concrete compressive strength for each test series, presented in Subchapter 4.2.5. Comparisons between load-slip curves from the experimental research and numerical study are given in Figure 5.10–Figure 5.17.
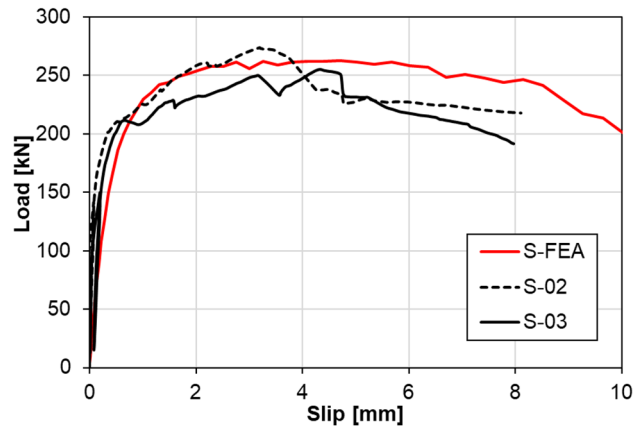
Figure 5.10: Load-slip curves for series S.
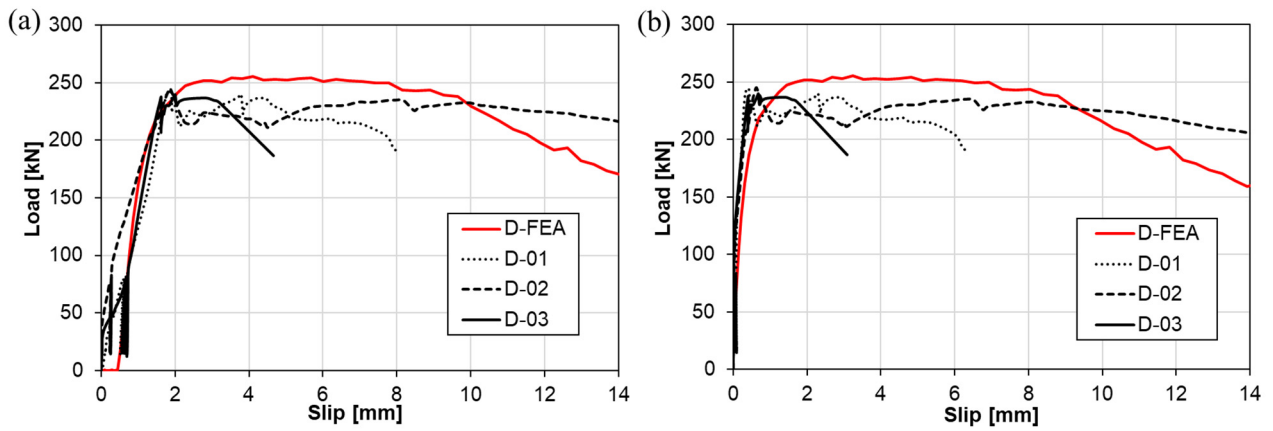
Figure 5.11: Load-slip curves for series D:
(a) steel profile-concrete slab, (b) steel plate-concrete slab.
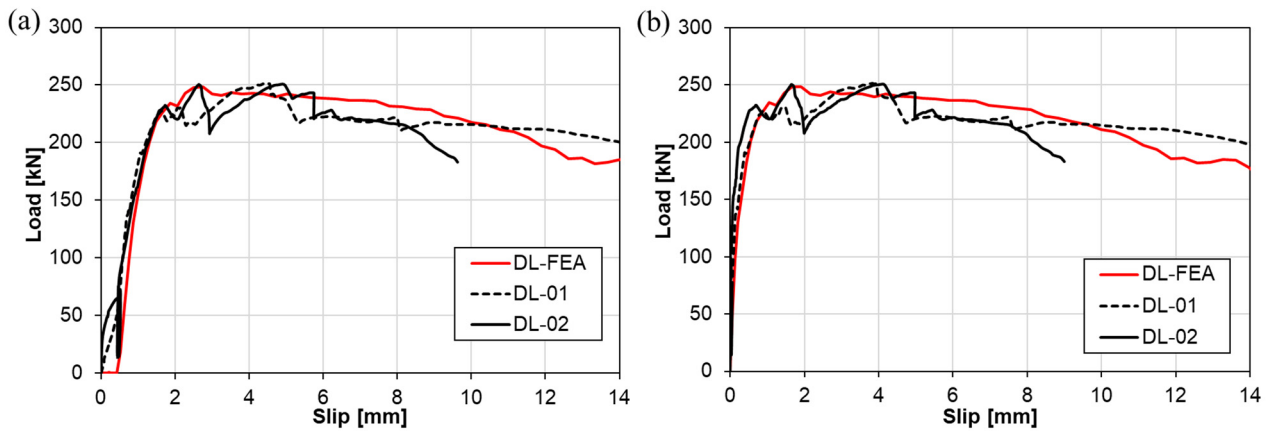
Figure 5.12: Load-slip curves for series DL:
(a) steel profile-concrete slab, (b) steel angle-concrete slab.
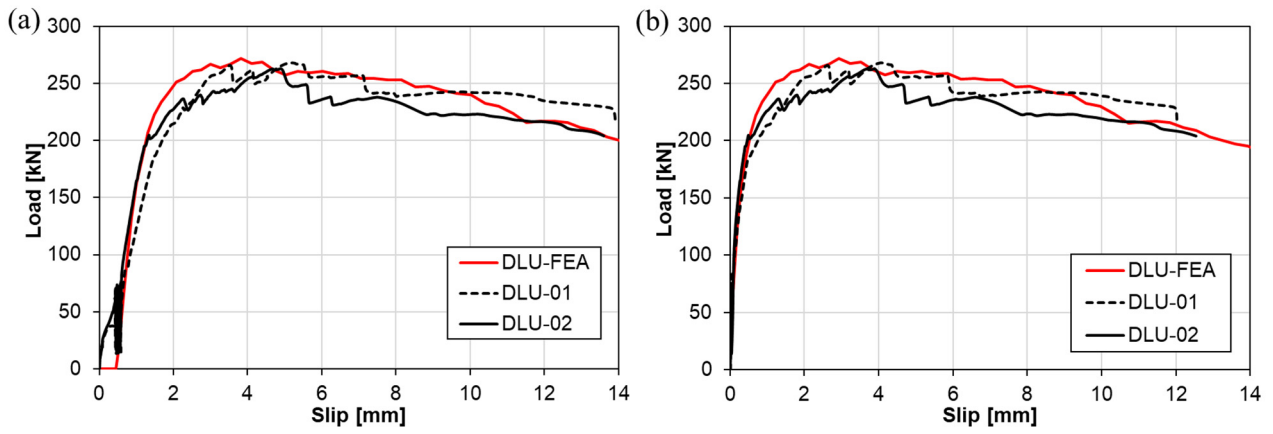
Figure 5.13: Load-slip curves for series DLU:
(a) steel profile-concrete slab, (b) steel angle-concrete slab.
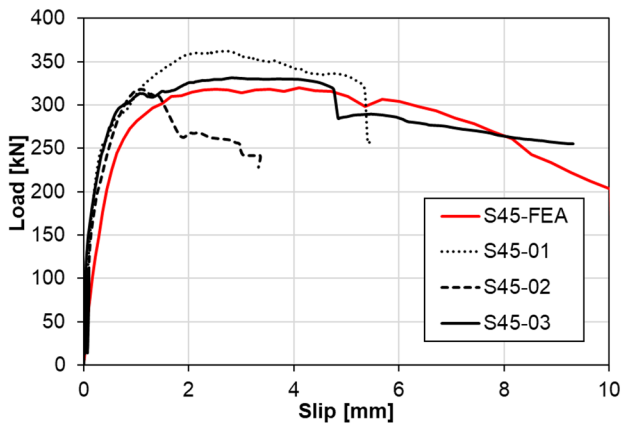
Figure 5.14: Load-slip curves for series S45.
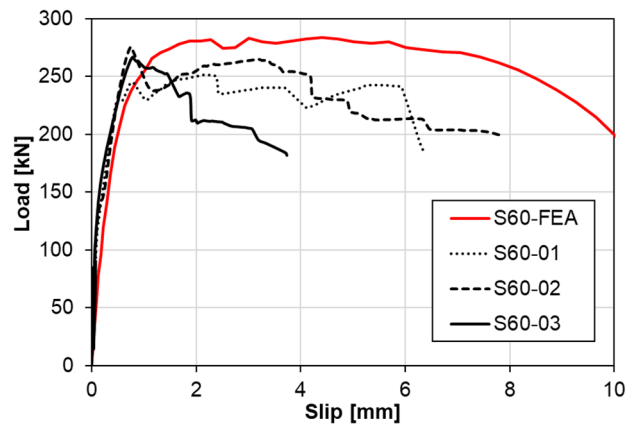
Figure 5.15: Load-slip curves for series S60.
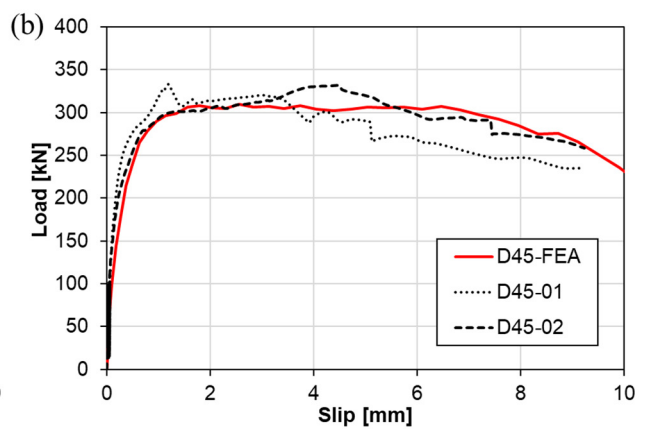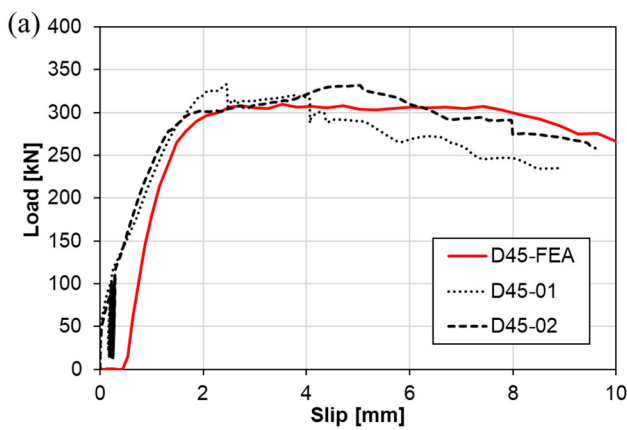
Figure 5.16: Load-slip curves for series D45:
(a) steel profile-concrete slab, (b) steel plate-concrete slab.

79
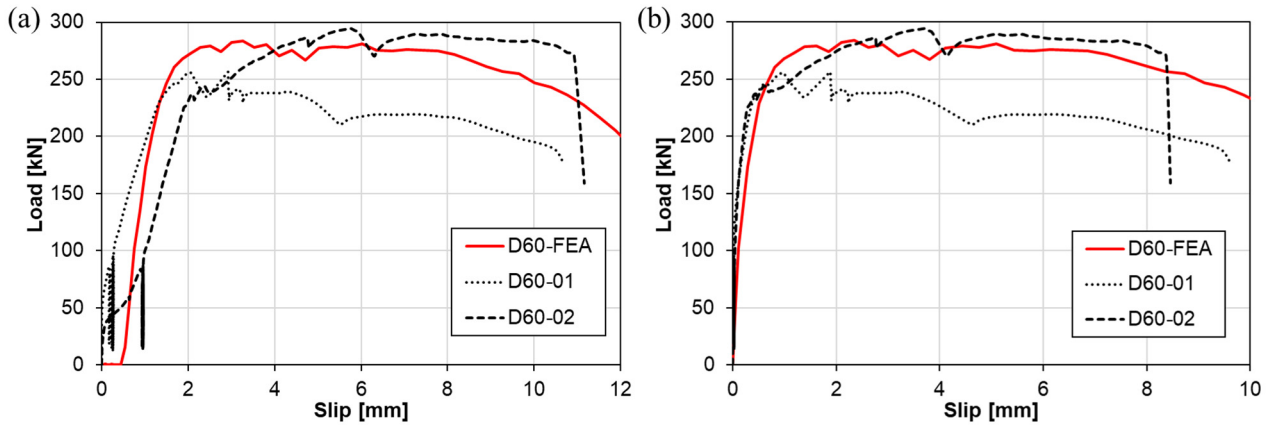
Figure 5.17: Load-slip curves for series D60:
(a) steel profile-concrete slab, (b) steel plate-concrete slab.

In general, a good match between experimentally and numerically obtained load-slip curves is accomplished. Disagreement in the initial loading stage showing the overall slip between the concrete slab and steel profile of demountable specimens may be explained. Although no additional pretension force was applied to bolts during specimen mounting, even the nut tightening induced a certain preload. However, as that variable was not measured during the experiment, it was decided to avoid numerical modelling of bolt pretension. Therefore, in numerical models, the initial slip of bolts happens at the load of 0 kN. During numerical modelling, bolts were placed in such positions in holes to simulate the average initial slip determined during the experimental testing of 0.5 mm.

The average values of ultimate loads obtained by experimental testing are compared with ultimate loads obtained through numerical simulations in Table 5.3. The relative difference in results does not exceed 7%.

Table 5.3: Comparison of experimental and numerical ultimate loads.

Series	Concrete compressive strength	Ultimate load		Ratio
		EXP	FEA	FEA/EXP
	f_{cm} [MPa]	$\overline{P}_{ult,exp}$ [kN]	$P_{ult,fea}$ [kN]	$P_{ult,fea}/\overline{P}_{ult,exp}$
S	35.0	264.6	262.5	0.99
D	34.5	242.8	255.3	1.05
DL	37.3	251.0	248.2	0.99
DLU	37.3	265.4	271.6	1.02
S45	36.2	337.3	319.8	0.95
D45	36.2	332.4	309.9	0.93
S60	36.2	264.7	283.2	1.07
D60	36.2	275.7	283.8	1.03

For the final validation of numerical results, model behaviour was inspected at the point of crack development and deformation of connectors. Cracks in the concrete slab along the rib length for models with three different angles between sheeting ribs and the beam are presented in Figure 5.18. In each of the presented models, cracks propagate downward from the welded stud head to the free concrete edge making an acute angle with the bottom slab surface. Cracks between two headed studs in the concrete rib are detected as well. The described crack pattern indicates concrete cone failure which had also been observed during the experimental testing. In addition, concrete cracks at the top surface of the slab shown in Figure 5.19 correspond to experimental findings. Cracks follow the direction of profiled sheeting ribs, making the angle of 90°, 45° or 60° with the vertical axis.
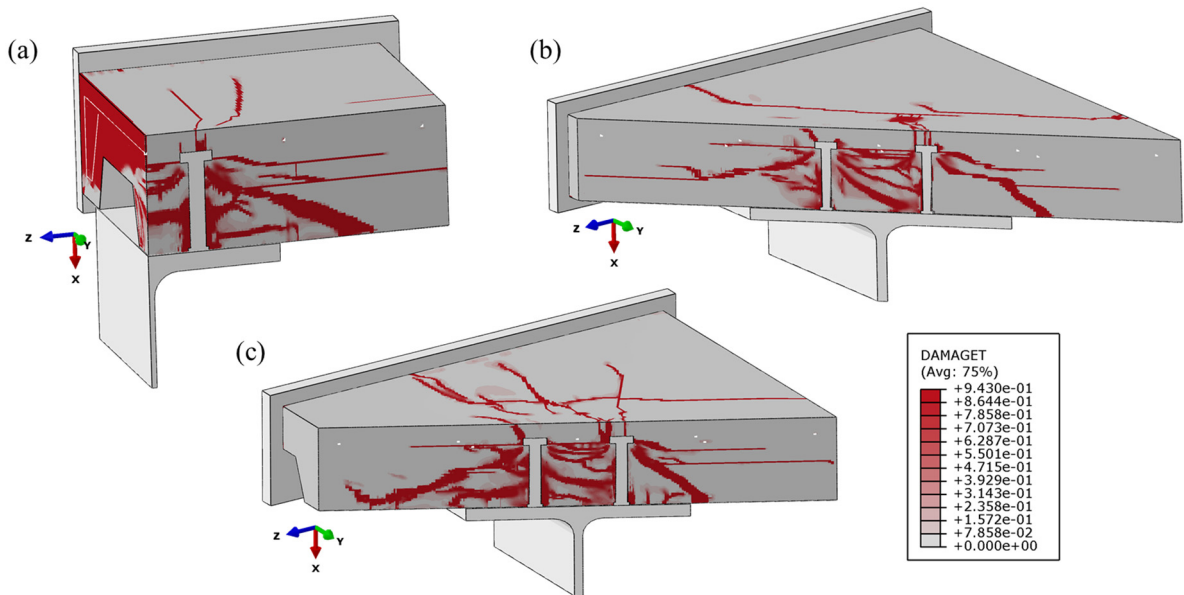
Figure 5.18: Cracks in the concrete slab indicating concrete cone failure:
(a) model S, (b) model S45, (b) model S60.

Figure 5.19: Crack pattern on the concrete slab top surface:
(a) model S, (b) model S45, (b) model S60.

In each numerical model, the deformed shape of the headed stud is characterised by a single curvature, matching the shape of headed studs observed in the experimental testing. Deformation of headed studs in the direction of shear force is presented in Figure 5.20. As observed in Figure 5.20, deformation of M12 and M16 bolts in demountable connections remains insignificant in comparison with headed studs', which is in accordance with experimental findings.
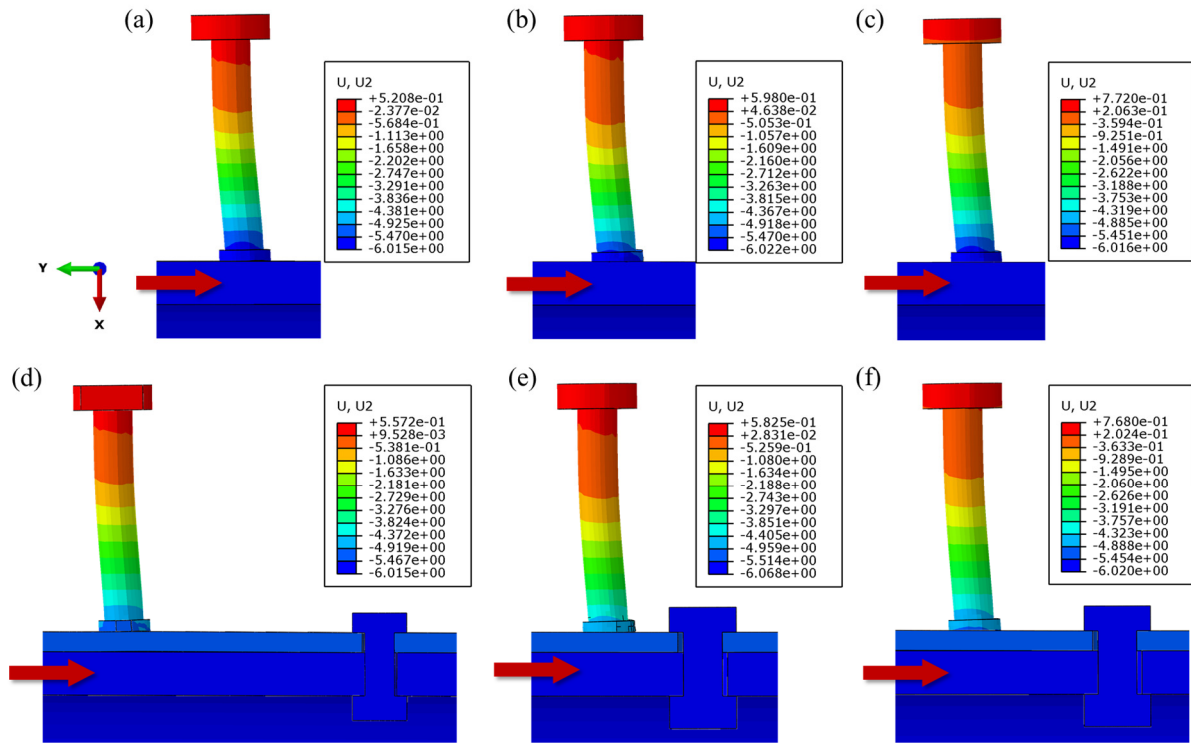
Figure 5.20: Deformed shapes of connectors:
(a) model S, (b) model S45, (c) model S60, (d) model D, (e) model D45, (f) model D60.

5.3 Results of Finite Element Analysis and Discussion

Comparisons of the performance of demountable and non-demountable numerical models were made. To provide comparable results, input parameters for the concrete material properties were set to be the same in each model, applying the concrete damage model obtained for f_{cm} = 37.3 MPa, originally corresponding to series DL and DLU. Load-slip curves are compared in Figure 5.21 and Figure 5.22. Ultimate loads and values of the maximum slip at 90% of the ultimate load, provided for the total slip and the slip in planes "plate/angle-concrete slab" and "steel profile-plate/angle", are listed in Table 5.4.
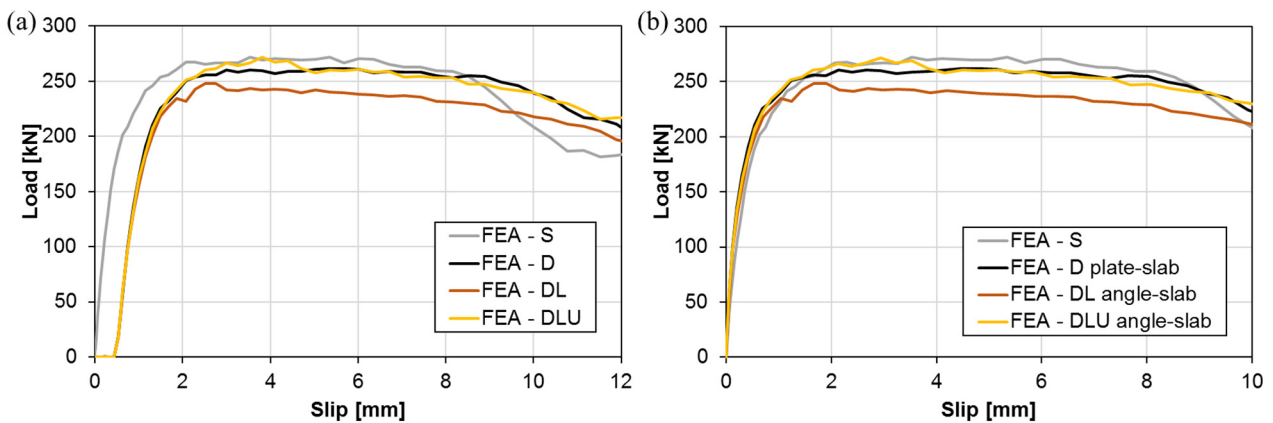
Figure 5.21: Comparison of the response of demountable and non-demountable connection models:
(a) total slip, (b) slip in the shear plane with welded headed studs.
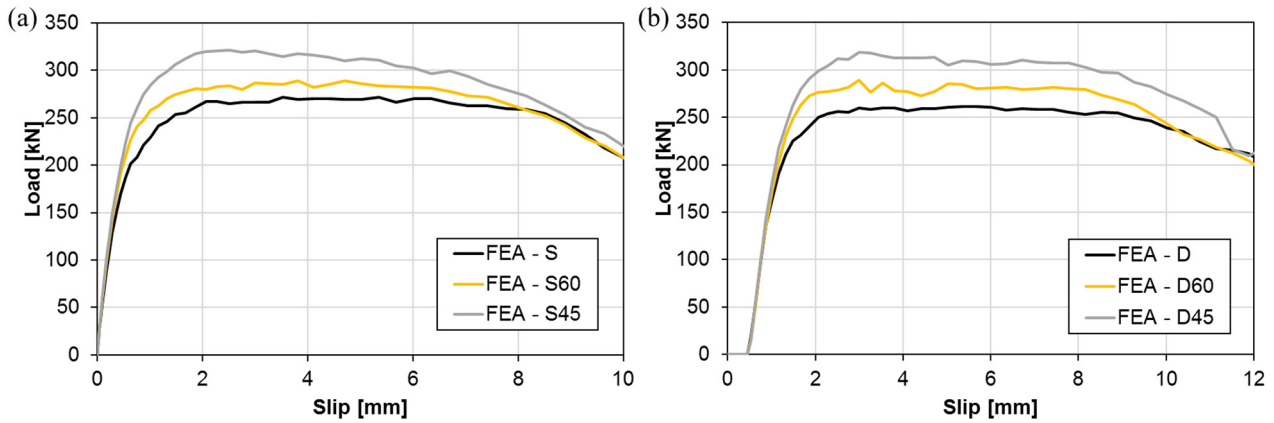
Figure 5.22: Comparison of the response of specimens with different angles between ribs and the beam:
(a) non-demountable connection models, (b) demountable connection models.

Table 5.4: Comparison between push-out test series.

| Model | Concrete compressive strength | Ultimate load | Max. slip at $0.9P_{ult,fea}$ | | | Ratio |
| | | | Total slip: HEB-slab | Shear plane: plate/angle-slab | Shear plane: HEB-plate | |
	f_{cm} [MPa]	$P_{ult,fea}$ [kN]	$\delta_{u,fea}$ [mm]	$\delta_{u,ps,fea}$ [mm]	$\delta_{u,bs,fea}$ [mm]	$P_{ult,fea}/P_{ult,fea,S}$
S	37.3	271.9	8.90	-	-	-
D	37.3	261.8	10.36	9.50	0.86	0.96
DL	37.3	248.2	9.17	8.45	0.72	0.91
DLU	37.3	271.6	9.20	8.37	0.83	1.00
S45	37.3	321.3	7.24	-	-	1.18
D45	37.3	318.7	9.30	8.29	1.01	1.17
S60	37.3	289.0	8.03	-	-	1.06
D60	37.3	289.0	9.40	8.50	0.92	1.06

According to the results of finite element analysis, each model shows a ductile response with a slip at $0.9P_{ult}$ larger than 6 mm. Demountable connections have larger slip than non-demountable ones. Values of the slip of non-demountable models are close to the slip in the shear plane "steel plate-concrete slab" of demountable models. The initial slip between the steel profile and plate in demountable models is 0.5 mm, while the slip at $0.9P_{ult}$ is in the range of 0.7–1.0 mm. Differences in ductility are not distinct between demountable models of different configurations, nor between non-demountable ones. By reducing the angle between profiled sheeting ribs and the beam from 90º to 45º, a certain decrease in the slip is present, which is more pronounced in non-demountable connections.

Model D has slightly lower resistance than the non-demountable model S. Model DL with a discontinuous slab over the support has smaller resistance than the model D with a continuous slab and almost 10% lower ultimate load than the non-demountable model S. The difference in the maximum load between models with discontinuous slabs over the beam with and without U-bars, DLU and DL, is approximately 10%. Implementation of stirrup bars around headed studs increases the resistance, resulting in the model DLU having the same resistance as the model S. It is concluded that the behaviour of the proposed demountable connection with a discontinuous slab over the beam and U-bars passing around headed studs, corresponds well at the point of resistance to the non-demountable connection.

By reducing the angle between profiled sheeting ribs and the beam from 90º to 45º, an increase in the ultimate load is present in both demountable and non-demountable connection models. Models S60 and S45 have 6% and 18% higher ultimate load than model S, respectively. For the smaller angle, the increase in the resistance is more pronounced, indicating that the rise is not a linear function of the angle.

Finite element models developed in Abaqus were used for further examination of the demountable connection response. The behaviour of bolt and stud connectors was analysed during the load application. As stress in connectors was not measured during push-out testing, numerical modelling is a useful tool for accessing that data. Stress in connectors of model D at the overall connection slip of 2 mm and 6 mm is shown in Figure 5.23. Load-slip curves on the total slip and component slip in two shear planes are also presented. The slip of bolts is pronounced at the beginning of loading. After bolt-to-hole clearances are voided, slipping in the shear plane with headed studs starts. At the total slip of 2 mm, bolt slip equals 0.82 mm, whereas the slip of headed studs is 1.22 mm. However, at the total slip of 6 mm, bolt slip remains almost the same (0.87 mm), while the slip of headed studs increases to 5.13 mm. Between the slip of 2 mm and 6 mm, the load-slip relationship is characterised by the deformation increase and almost constant load.
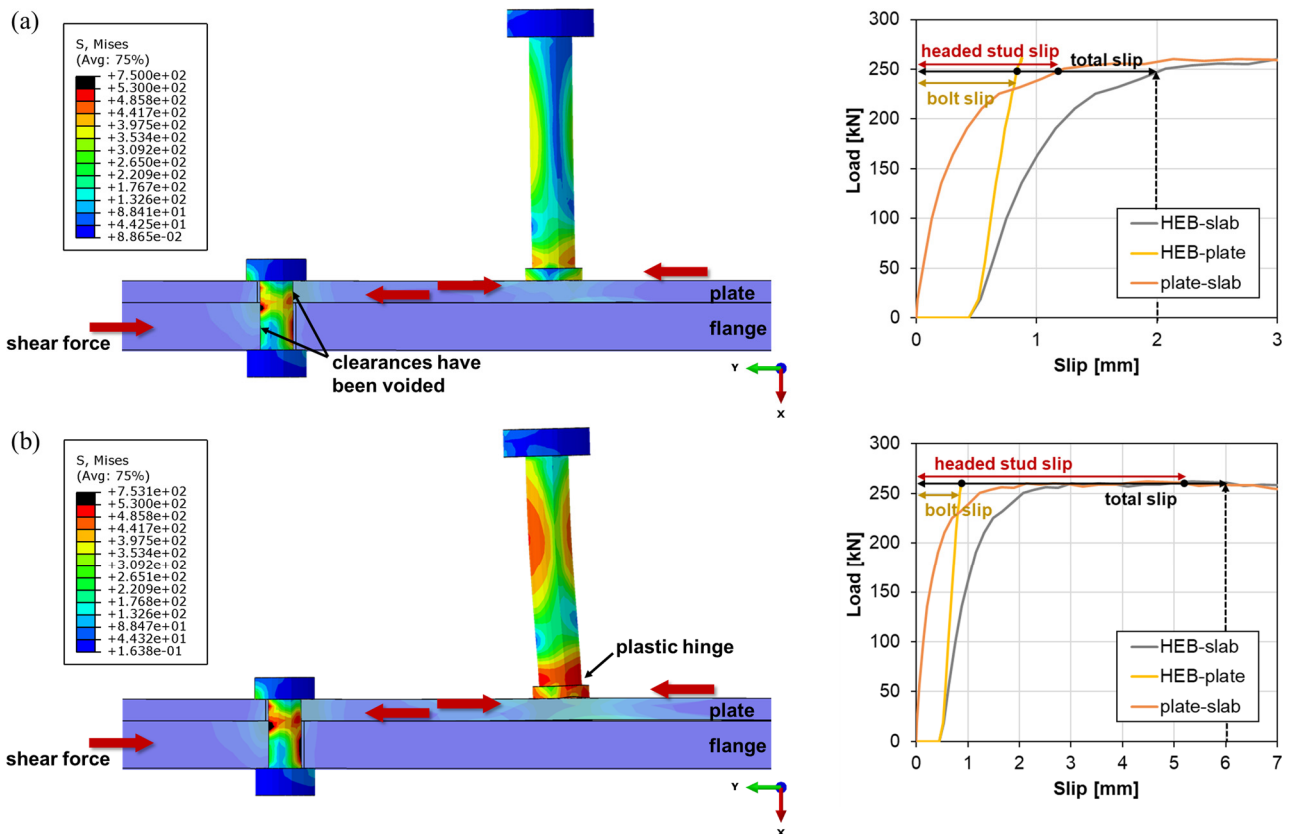
Figure 5.23: Load-slip curves and stress in shear connectors of the model D at the slip of: (a) 2 mm, (b) 6 mm.

Conclusions regarding the slip correspond to the stress distribution and deformation of connectors. In headed studs, stress is higher at the total slip of 6 mm than at the slip of 2 mm (Figure 5.23). The concentration of stress is noticed in the stud shank just above the weld collar. This stress is above the material yield strength and influences the development of a plastic hinge in the headed stud. Another concertation of stress is at the top half of the stud shank, although the hinge is not completely formed across the stud cross-section.

The highest stress in bolts is below the material yield strength both at the total connection slip of 2 mm and 6 mm. Moreover, changes in the stress in bolts are minor in the presented two moments and the bolt deformation remains insignificant. Stress in bolt holes of the plate shown in Figure 5.24 is slightly above the yield strength, though the bearing deformation is negligible.
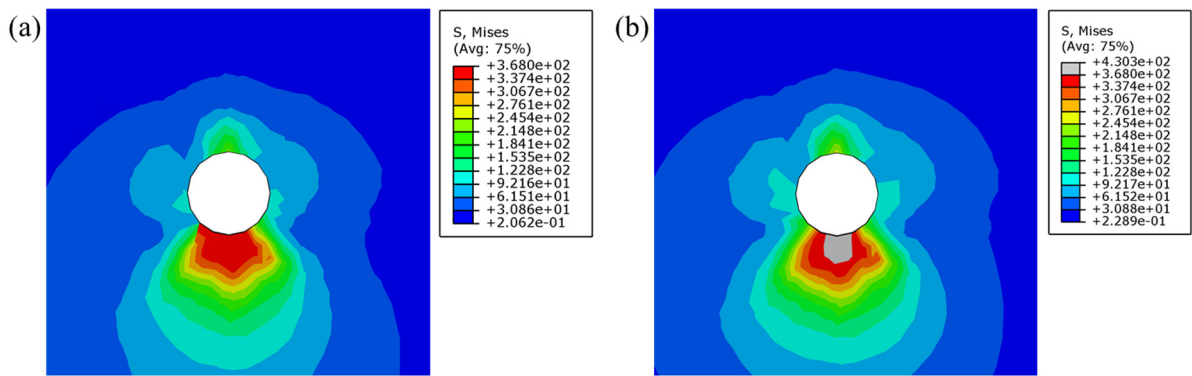
Figure 5.24: Stress in the bolt hole of the plate in the model D at the slip of:
(a) 2 mm, (b) 6 mm.

The other demountable models, DL, DLU, D45 and D60, are characterised by similar trends in the connection response as the described model D. Stress distribution in connectors of models D60 and D45 at the slip of 6 mm is presented in Figure 5.25. In all models, deformation of headed studs is followed by the development of one plastic hinge at the bottom of the stud shank. Stress in M16 bolts (Figure 5.25) is smaller than those in M12 bolts (Figure 5.23), though the deformation of all bolts is minor.
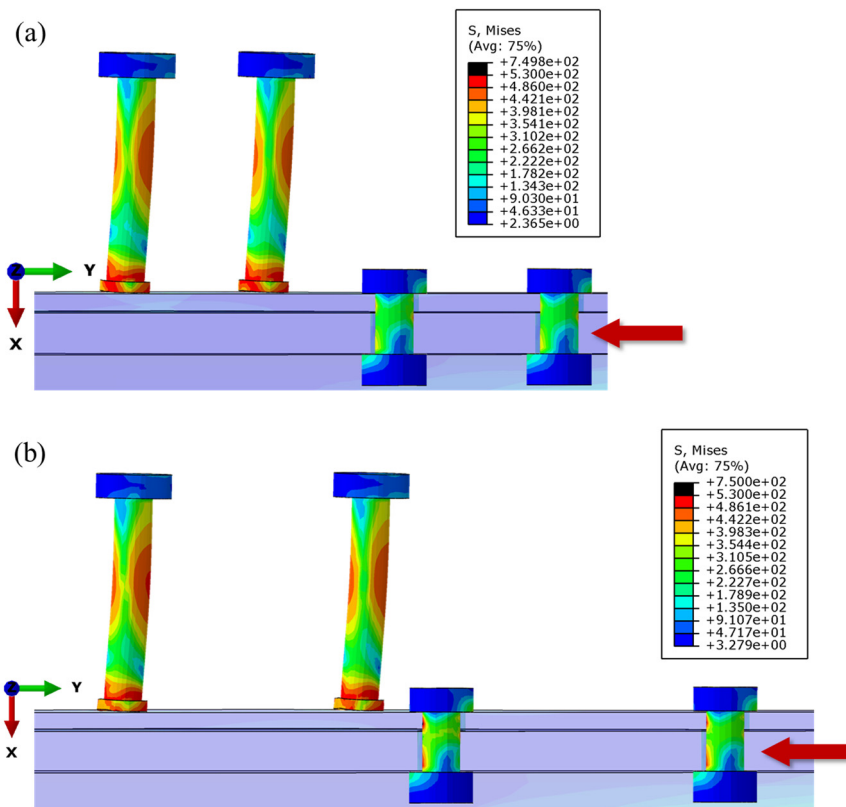
Figure 5.25: Stress distribution in headed studs and bolts at the slip of 6 mm:
(a) model D60, (b) model D45.

Moreover, the stress in headed stud connectors at the slip of 6 mm is presented for non-demountable specimens, S, S45 and S60, in Figure 5.26. Headed studs have a very similar response as in demountable models. Differences in the stress distribution in headed studs in connections with various angles between sheeting ribs and the beam are negligible.

85
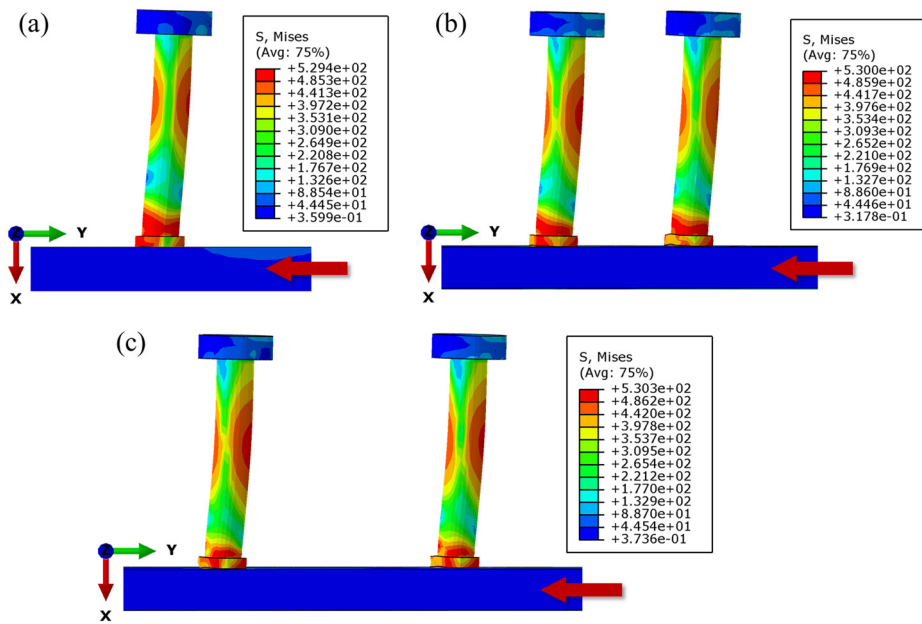
Figure 5.26: Stress distribution in headed studs at the slip of 6 mm:
(a) model S, (b) model S45, (b) model S60.

Deformation of headed studs in models with ribs transverse to the beam followed the direction of the applied shear force in push-out tests. However, numerical models showed certain deformation of headed studs in the lateral direction in models with the angle between ribs and the beam smaller than 90°. At the slip of 6 mm, the average lateral deformation of headed studs is 1.8 mm for connections with the angle between ribs and the beam of 45°, and 1.4 mm for connections with the angle between ribs and the beam of 60°. It is concluded that headed studs deform in the direction at the angle of 11–19° from the vertical axis, i.e. beam longitudinal axis, as presented in Figure 5.27. This behaviour could be explained by the asymmetric disposition of the model and the arrangement of headed studs.
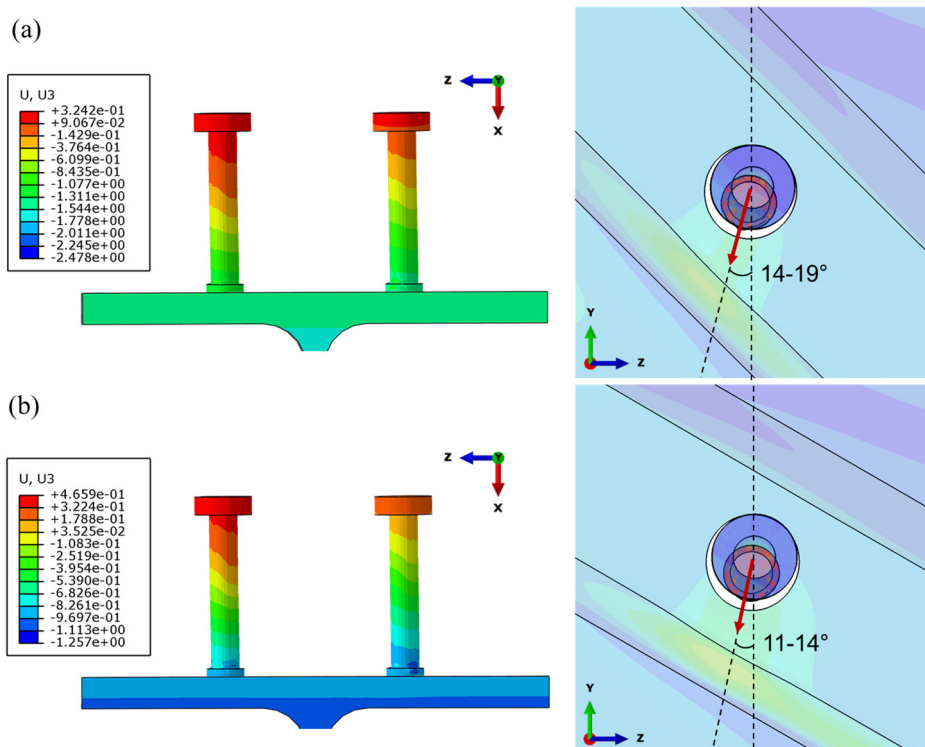
Figure 5.27: Deformation of headed studs in the lateral direction at the slip of 6 mm: (a) S45, (b) S60.

Deformation of the plate and angles was not visually observed after the experimental testing. Hence, numerical models were used to examine and quantify the deformation of steel components to which headed studs were welded. Displacements in the direction normal to the flange corresponding to the connection slip of 6 mm are presented in Figure 5.28. Flange deformation in model S is negligible. However, the deformation of thinner components than the flange – the plate in model D and the angle in model DL, is more pronounced. The maximum out-of-plane displacement in models D and DL with the amplitude of approximately 0.5 mm is beside the headed studs in the upper concrete rib of the model. The vertical leg of the angle prevents deformation in the corner, hence deformation propagates towards the edge of the horizontal leg (Figure 5.28.c). On the other hand, plate deformation is pronounced near the axis of symmetry, between two headed studs in the rib (Figure 5.28.b). To analyse the influence of different plate and angle thicknesses on the connection response, a parametric study is conducted and presented in the next chapter.
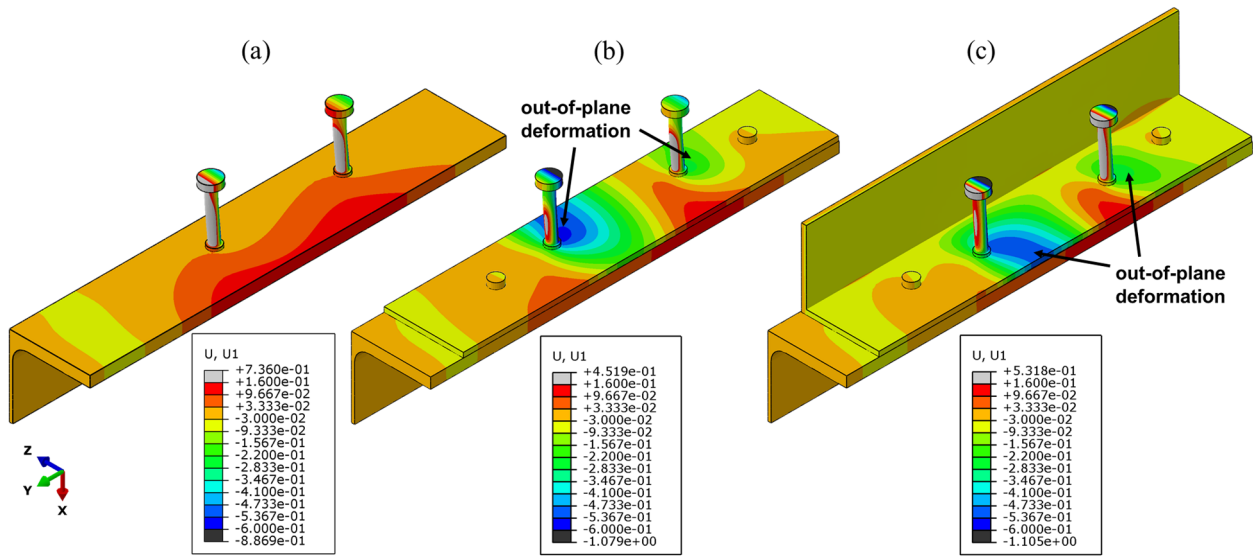
Figure 5.28: Deformation of the flange, plate and angle at the slip of 6 mm:
(a) model S, (b) model D, (c) model DL.

As another parameter that was not measured during the experiment, the normal stress in U-bars was tracked during numerical simulation. Stress in the U-bar and load plotted against slip in the plane angle-slab are shown in Figure 5.29. According to the presented, the stress increase in stirrup bars follows the loading of the specimen, indicating the activation of U-bars. The highest stress in U-bars corresponds to the moment when the ultimate load is reached. The maximum stress of 130 MPa is far below the reinforcement yield strength.
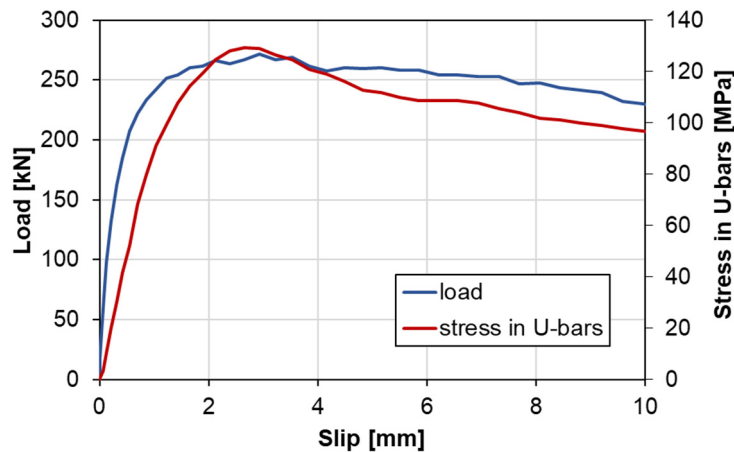
Figure 5.29: Activation of U-bars during the loading of the model DLU.

Crack patterns in concrete slabs of different models with sheeting ribs transverse to the supporting beam are compared in Figure 5.30. Fractures causing separation of the concrete cone and final pull-out failure are observed in each of the developed models in planes x-y and x-z. Moreover, in the direction of shear force, concrete damage occurs in front of the headed studs, indicating rib punching. Concrete cones of presented connections have slightly different edge slopes, from 23° to 27°. The concrete cone of the model DLU is larger than in the model DL with an edge slope of approximately 23° instead of 27°. The concrete cone developed in models with discontinuous slabs, DL and DLU, differs in its shape from the cone of models S and D, as the edge extending from the stud head to the vertical angle leg has a slope of approximately 10° instead of being horizontal.

Connections with the angle between profiled sheeting ribs and the beam of 45° and 60° are characterised by similar failure mechanisms. The formation of concrete cones is presented in Figure 5.31, through the crack pattern caused by exceeding of concrete tensile strength. Cones are formed within the rib and follow its direction. The phenomenon of local rib punching in front of the headed studs is presented in Figure 5.32, showing finite elements which exhibited compressive damage of concrete.
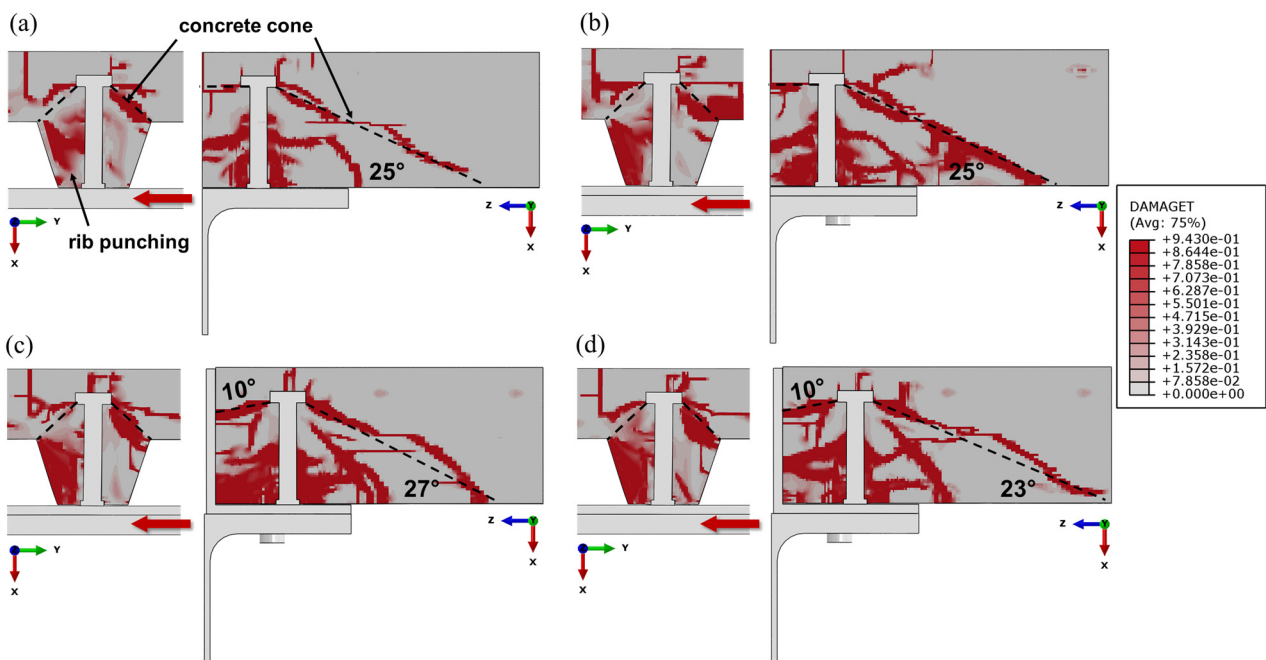
Figure 5.30: Concrete tensile damage at the slip of welded headed studs of 1 mm:
(a) model S, (b) model D, (c) model DL, (d) model DLU.
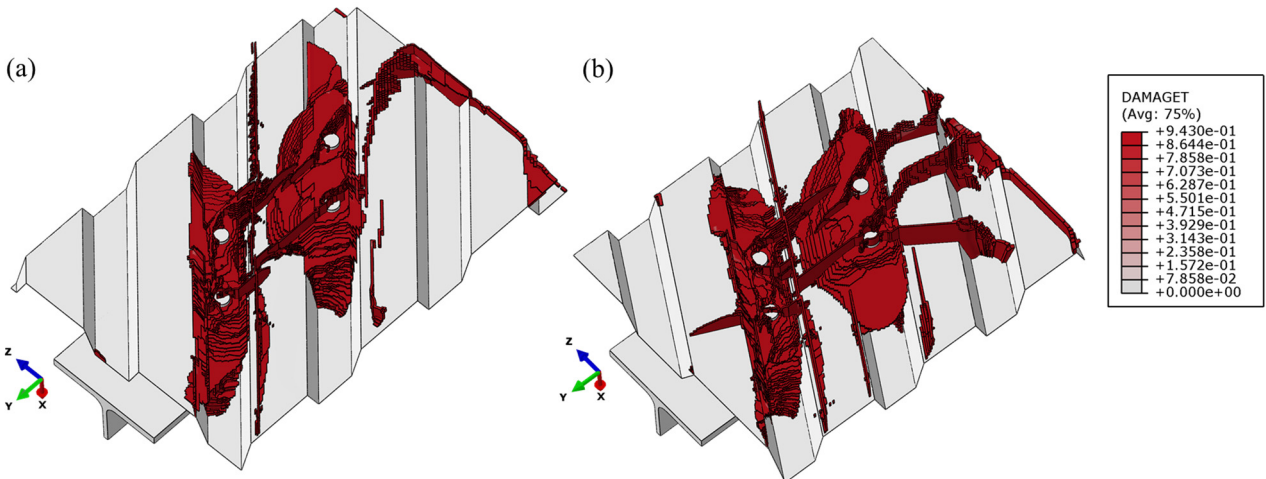
Figure 5.31: Concrete tensile damage at the slip of 1 mm: (a) model S45, (b) model S60.
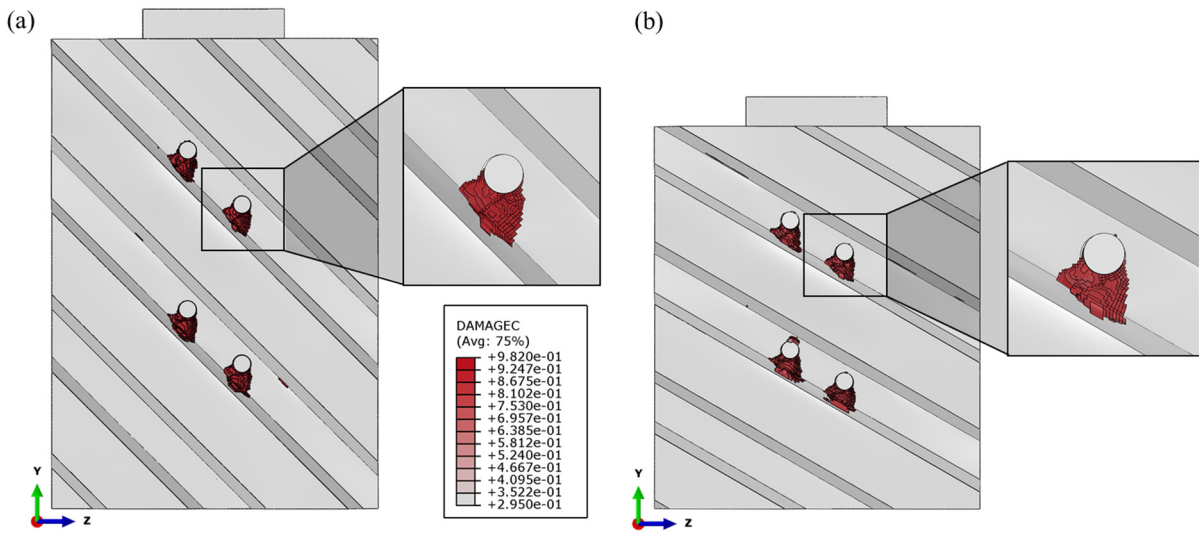
Figure 5.32: Concrete compressive damage at the slip of 6 mm: (a) model S45, (b) model S60.

6 Parametric Studies

6.1 Parametric Studies Program

Based on the validated numerical models simulating push-out tests, parametric studies were performed. Additional sets of finite element models were developed to provide further information on the demountable connection behaviour. According to the presented results, general conclusions regarding the demountable connection shear response were drawn.

Firstly, the initial parametric study was conducted analysing the parameters of the slab reinforcement and depth. Moreover, the influence of the slab width of the push-out model was examined. According to the results, decisions regarding further modelling were made.

Secondly, parametric studies were performed on demountable connections with continuous slabs over the beam. The impact of the plate thickness on the demountable connection response was examined. The proposed design of demountable shear connections with continuous slabs over the beam was tested on a set of models with different concrete classes and geometries. The behaviour of developed connections was compared to the behaviour of the corresponding non-demountable connections.

Thirdly, parametric studies covered demountable connections with discontinuous slabs over the beam. The effects of the angle thickness, stirrup diameter, stirrup position and stud-to-edge distance on the resistance of demountable connections with discontinuous slabs were studied. In order to define design proposals, a set of models with different concrete classes and geometries was analysed. Comparisons of the behaviour of demountable connections with continuous and discontinuous slabs over the support were made.

Then, the influence of the angle between profiled sheeting ribs and the beam was studied, examining the performance of shear connections with angles of 60°, 45° and 30°. A relation between the resistance of the shear connection with ribs transverse to the supporting beam ($\alpha = 90°$) and the shear connection with the angle between ribs and the beam $30° \leq \alpha < 90°$ was established.

Finally, numerically obtained resistances of different connections were compared with analytical predictions for headed stud shear resistance in profiled steel sheeting.

6.2 The Initial Parametric Study

6.2.1 Influence of the Mesh Reinforcement

As discussed in Chapter 2, slab reinforcement may affect shear connection response at the point of ductility and resistance. To draw conclusions regarding the influence of the mesh reinforcement in the specific case of the shear connection analysed within the frame of this thesis, additional models were developed: a model with reinforcement in the bottom zone of the slab and a model with reinforcement mesh in both zones of the slab, as presented in Figure 6.1. Results compared in Figure 6.2 and Table 6.1 are given for the non-demountable model, whereas similar findings were obtained for demountable models. According to the results, the reinforcement position along the slab depth does not affect the response of the connection. Similar conclusions were made by Vigneri [64] during experimental testing of headed studs in profiled steel sheeting Cofraplus 60. However, a numerical study showed that a model with two layers of reinforcement had an increase in the resistance of 9% in comparison with the original model with only one layer of reinforcement in the top zone. Nevertheless, for the selected slab depth of 120 mm, with only 60 mm concrete depth above the profiled sheeting surface, two layers of reinforcement are difficult to realise in practice, so that case is rather hypothetically analysed.
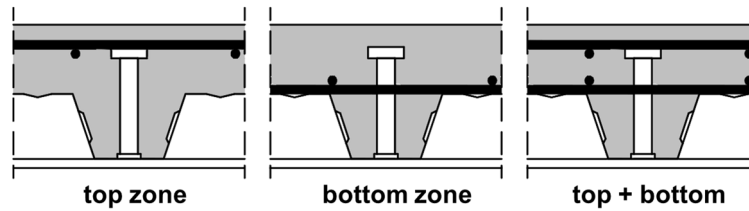
Figure 6.1: Reinforcement mesh position.
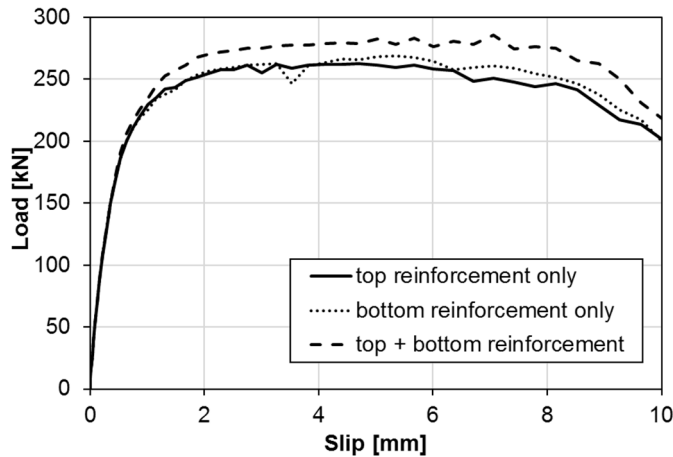
Figure 6.2: Influence of the slab reinforcement: model S.

Table 6.1: Influence of the slab reinforcement: model S.

No.	Slab reinf.	Concrete strength	Ultimate load	Ratio
		f_{cm} [MPa]	$P_{ult,fea}$ [kN]	$P_{ult,fea,(i)}/P_{ult,fea,(1)}$
(1)	top	35.0	262.5	-
(2)	bottom	35.0	268.6	1.02
(3)	top + bottom	35.0	285.5	1.09

6.2.2 Influence of the Slab Depth

The effect of the slab depth on the connection response was studied. For the constant headed stud diameter of 16 mm and height of 100 mm, slab depth was varied in the range from 120 to 180 mm. Load-slip curves presented in Figure 6.3 and ultimate loads given in Table 6.2 indicate that the increase in the slab depth leads to a certain increase in the connection shear resistance, although that rise is not very significant. The increase in the ultimate load could be attributed to the increase in the bending stiffness of the slab. Results coincide with experimental findings of Vigneri [64] obtained for slabs cast in profiled steel sheeting Cofraplus 60. In further parametric studies, connections with the smallest slab depths are analysed in order to provide safe-sided predictions.
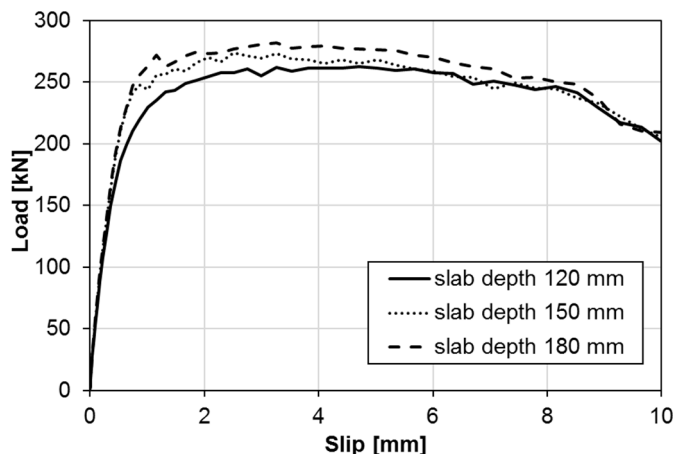
Figure 6.3: Influence of the slab depth: model S.

Table 6.2: Influence of the slab depth: model S.

No.	Slab depth	Concrete strength	Ultimate load	Ratio
	h [mm]	f_{cm} [MPa]	$P_{ult,fea}$ [kN]	$P_{ult,fea,(i)}/P_{ult,fea,(1)}$
(1)	120	35.0	262.5	-
(2)	150	35.0	273.7	1.04
(3)	180	35.0	281.8	1.07

6.2.3 Influence of the Slab Width

Additional numerical models were developed to study the impact of the slab width on the specimen resistance and verify the width adopted in experimental testing. The width of the non-demountable model S was increased from 600 mm to 700 and 800 mm. Results presented in Figure 6.4 and Table

6.3 show that there is a minor increase in the ultimate load with the increase in the slab width in the analysed range. In addition, the crack patterns of the three models compared in Figure 6.5 illustrate similar concrete cones in each case. In other words, it is confirmed that the adopted slab width of $b > e_t + 2\,h_{sc}/\tan(25^0)$ provides satisfactory results for specimens with ribs transverse to the beam.
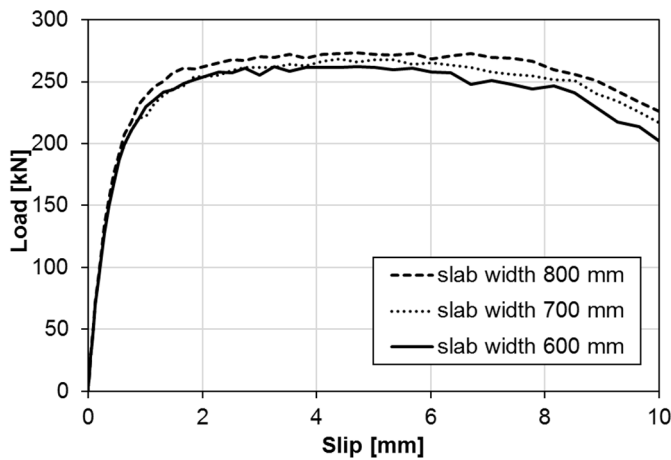
Figure 6.4: Influence of the slab width: model S.

Table 6.3: Influence of the slab width: model S.

No.	Slab width b [mm]	Concrete strength f_{cm} [MPa]	Ultimate load $P_{ult,fea}$ [kN]	Ratio $P_{ult,fea,(i)}/P_{ult,fea,(1)}$
(1)	600	35.0	262.5	-
(2)	700	35.0	268.2	1.02
(3)	800	35.0	273.6	1.04
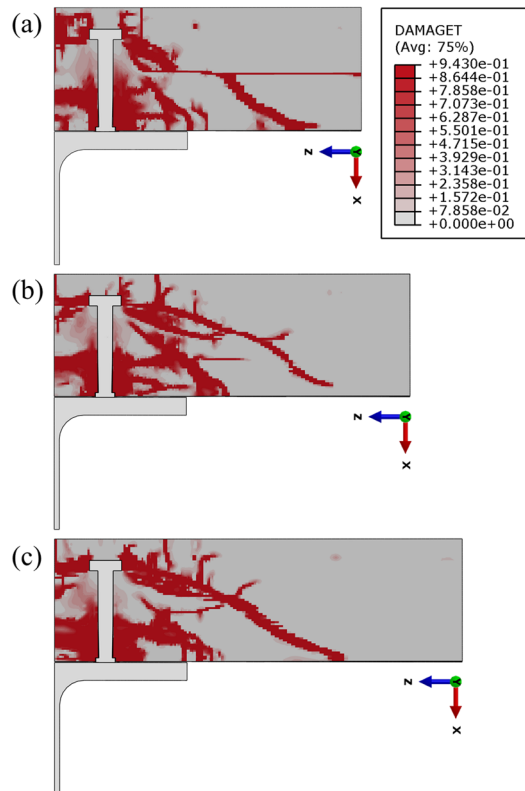
Figure 6.5: Crack pattern at the slip of 2 mm for the applied slab width:
(a) 600 mm, (b) 700 mm, (c) 800 mm.

Similarly, the specimen width was examined on models with the angle between ribs and the beam smaller than 90⁰. An increase in the slab width of the push-out model S45 negligibly affected the shear connection ultimate load as shown in Figure 6.6 and Table 6.4. In model S60, the effect of the increase in the slab width from 600 to 700 mm is more evident, as shown in Figure 6.7 and Table 6.5. The resistances of the connection S60 when slab widths of 700 mm and 800 mm were applied are the same. Therefore, in further modelling, the slab width was set to 700 mm for the connections with headed studs of 100 mm in height. The same was applied to the models with the angle between sheeting ribs and the beam of 90°, 45° and 60°. However, in the case of models S45 and S60, with

the increase in slab width, slab length was also increased to fully include concrete ribs with headed studs, as presented in Figure 6.8.
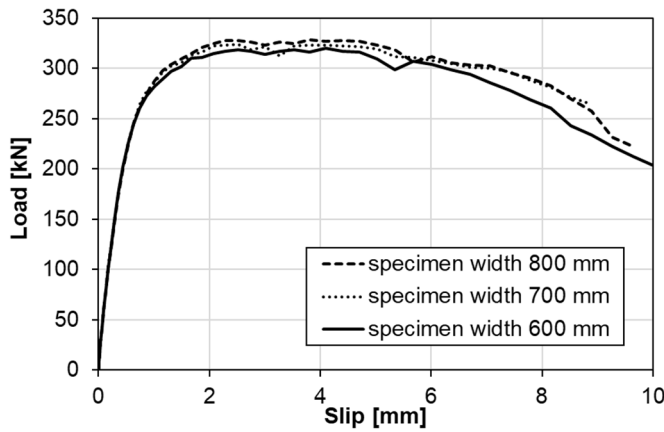
Figure 6.6: Influence of the slab width: model S45.

Table 6.4: Influence of the slab width: model S45.

No.	Slab width	Concrete strength	Ultimate load	Ratio
	b	f_{cm}	$P_{ult,fea}$	$P_{ult,fea,(i)}/P_{ult,fea,(1)}$
	[mm]	[MPa]	[kN]	
(1)	600	36.2	319.8	-
(2)	700	36.2	324.2	1.01
(3)	800	36.2	328.2	1.03
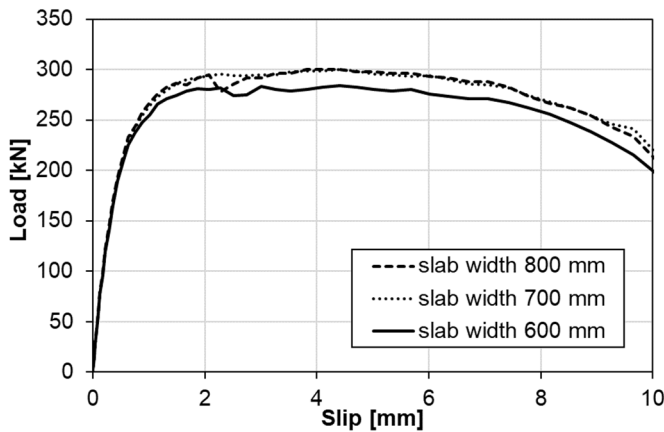
Figure 6.7: Influence of the slab width: model S60.

Table 6.5: Influence of the slab width: model S60.

No.	Slab width	Concrete strength	Ultimate load	Ratio
	b	f_{cm}	$P_{ult,fea}$	$P_{ult,fea,(i)}/P_{ult,fea,(1)}$
	[mm]	[MPa]	[kN]	
(1)	600	36.2	283.9	-
(2)	700	36.2	300.2	1.06
(3)	800	36.2	300.1	1.06
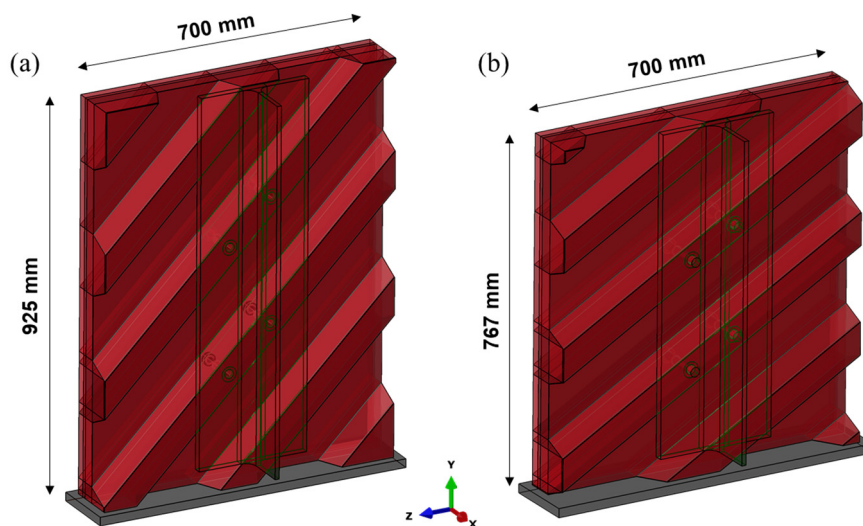
Figure 6.8: Adopted push-out models for further parametric analysis for $h_{sc} = 100$ mm: (a) S45, (b) S60.

As parametric studies presented in the following subchapters also cover headed studs of 125 mm and 150 mm in height, concrete slab width and length were suitably set, in accordance with the presented findings. For models with headed studs of 125 mm in height, the slab width was applied as 800 mm, while for the stud height of 150 mm, the slab width was set to 900 mm, as summarised in Table 6.6.

Table 6.6: Adopted slab widths for different headed stud diameters.

Headed stud height	Transverse spacing between headed studs	Predicted width of the concrete cone	Adopted slab width
h_{sc} [mm]	e_t [mm]	$e_t + 2\,h_{sc}/\tan(25^\circ)$ [mm]	b [mm]
100	100	528.9	700
125	100	636.1	800
150	100	743.4	900

6.2.4 Input Parameters for Further Parametric Studies

Considering the presented results of the initial parametric analyses, decisions regarding further parametric studies are made and listed in the following:

(1) all models have one layer of reinforcement mesh placed in the slab top zone;

(2) all models have a minimum slab depth for the selected headed stud height, respecting the minimum cover over the connector defined in EN 1994-1-1:2004 [10];

(3) the slab width is applied depending on the headed stud height:

- for h_{sc} = 100 mm, the width is b = 700 mm;
- for h_{sc} = 125 mm, the width is b = 800 mm;
- for h_{sc} = 150 mm, the width is b = 900 mm.

6.3 Demountable Shear Connections with Continuous Slabs over the Beam

One of the goals in the design of the demountable shear connection is to create a connection that has nearly the same resistance as the corresponding non-demountable connection with welded headed studs. As the demountable connection with a continuous slab over the support has additional components compared with the non-demountable connection, including bolts and the plate, it is important to choose the proper bolt diameter and plate thickness to accomplish the desired connection response.

6.3.1 Influence of the Plate Thickness

Effects of the plate thickness on the connection response were studied on the demountable connection model D, varying that dimension in the range from 4 to 10 mm. Load-slip curves presented in Figure 6.9 and comparison of ultimate loads given in Table 6.7 indicate that responses of models with the plate thickness of 8 and 10 mm do not differ. On the other hand, a decrease of the plate thickness below 8 mm induces a drop in the connection shear resistance, notably pronounced in the case of the plate thickness of 4 mm.

To explain the results, plate deformation in the area near welded headed studs was analysed. Out-of-plane deformation at the slip of 6 mm is shown in Figure 6.10. An increase in the deformation with the decrease of the plate thickness is present. For the plate thickness of 4 mm, the maximum plate deformation of 1.75 mm is evident, whereas for the plate thickness of 10 mm, it is 0.25 mm and cannot be visually noticed. Deformation of the plate induces a certain rotation of the stud connector which results in lower connection resistance to shear.
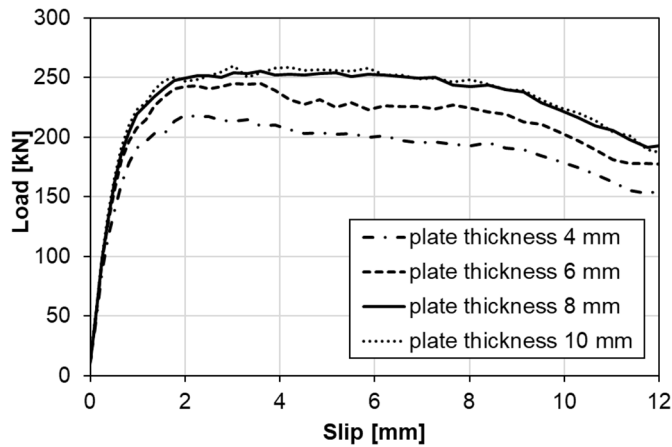
Table 6.7: Influence of the plate thickness: model D.

No.	Plate thick-ness	Concrete strength	Ultimate load	Ratio
	t_p [mm]	f_{cm} [MPa]	$P_{ult,fea}$ [kN]	$P_{ult,fea,(i)}/P_{ult,fea,(3)}$
(1)	4	34.5	218.7	0.86
(2)	6	34.5	245.4	0.96
(3)	8	34.5	255.3	-
(4)	10	34.5	259.7	1.02

Figure 6.9: Influence of the plate thickness: model D.[2]
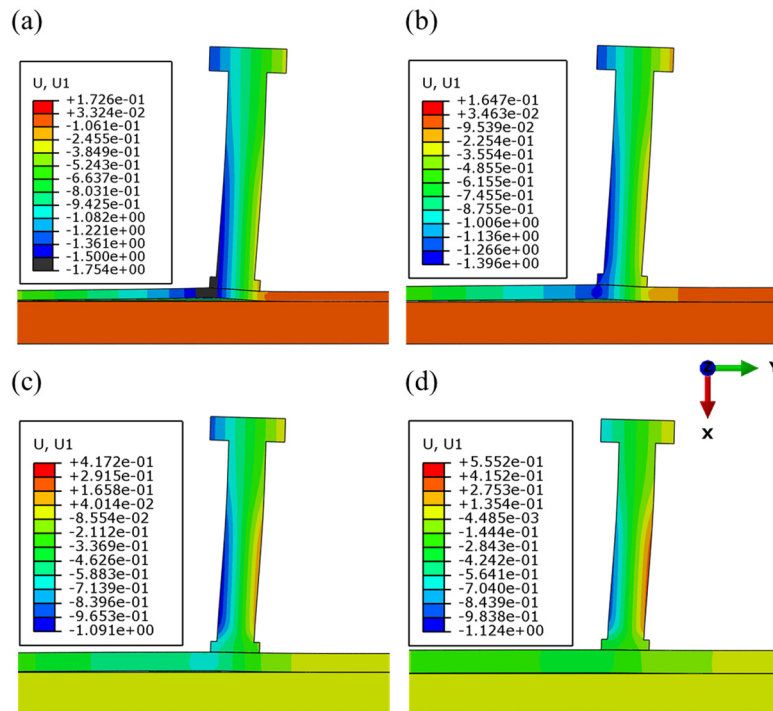
Figure 6.10: Deformed plate shape at the slip of 6 mm for the plate thickness of:
(a) 4 mm, (b) 6 mm, (c) 8 mm, (d) 10 mm.

In order to minimise the plate deformation, additional models were developed with an added pair of bolts between two pairs of headed studs in the longitudinal direction. It was tested if the additional bolt may fix the plate to the profile flange and increase the plate stiffness. However, results showed that the plate deformation has a strictly local character and consequently, the implementation of the additional bolt did not affect the connection response. The example of the 4 mm thick plate presented in Figure 6.11 shows that the deflection of the plate with the added bolt is negligibly smaller in comparison with the basic model. In terms of ultimate loads, relevant differences in the response of the two models were not noticed for any of the applied plate thicknesses, as presented in Table 6.8. Those results are advantageous as they validate the application of bolts in two times larger

---

[2] In this chapter, all load-slip curves of demountable connection models are presented without the initial bolt slip, i.e. they are shifted for the slip value of 0.5 mm or 1.0 mm, depending on the bolt hole diameter (bolt-to-hole clearance was initially set to half of the subtract between the diameter of a hole and a bolt). The reason is practical – to enable easier graph reading. Nevertheless, the initial bolt slip should be considered in a beam design.

longitudinal spacing than headed studs, leading to savings in material consumption and construction time.

(a)

(b)
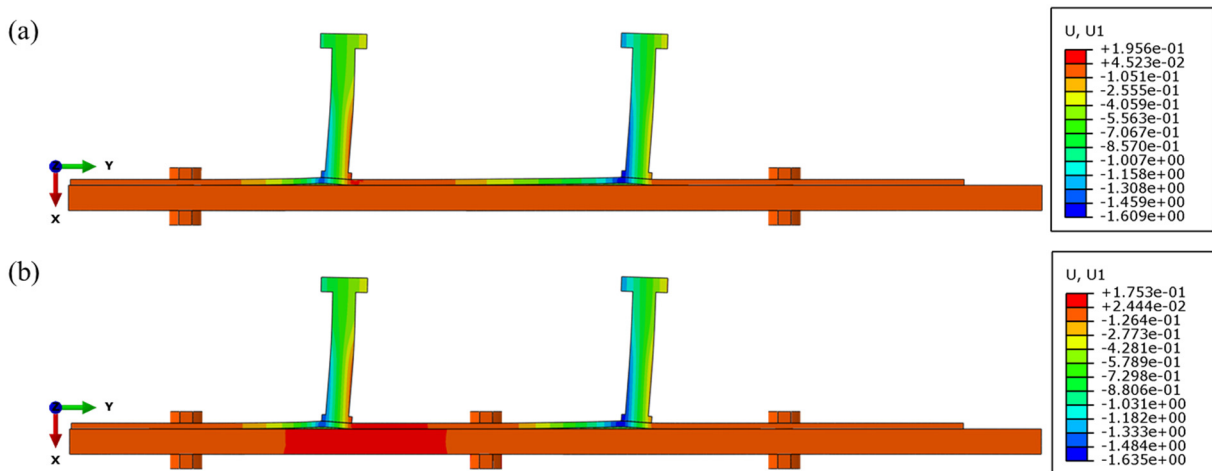
Figure 6.11: Deflection of 4 mm thick plate: (a) two bolts in the longitudinal direction, (b) three bolts in the longitudinal direction.

Table 6.8: Influence of the bolt inserted between headed studs: model D.

| Plate thickness | Concrete strength | Ultimate load | | Ratio |
		Two bolts in the long. direction	Three bolts in the long. direction	
t_p [mm]	f_{cm} [MPa]	$P_{ult,fea,2b}$ [kN]	$P_{ult,fea,3b}$ [kN]	$P_{ult,fea,3b}/P_{ult,fea,2b}$
4	34.5	218.7	219.8	1.01
6	34.5	245.4	248.5	1.01
8	34.5	255.3	257.4	1.01
10	34.5	259.7	267.7	1.03

According to the presented, the plate of 8 mm in thickness showed a satisfactory connection response to the shear, similar to the response of the connection with a 10 mm thick plate. The thickness of 8 mm was considered the most appropriate thickness of the plate in the analysed case of the demountable shear connection with the headed stud of 16 mm in diameter.

6.3.2 Comparison of the Behaviour of Non-Demountable and Demountable Shear Connections with Continuous Slabs over the Beam

Based on the presented effects of the plate thickness on the connection response, comparisons of the behaviour of the non-demountable and demountable shear connections were made. Two hypotheses regarding the adoption of the plate thickness and bolt diameter were tested through a comparison of the non-demountable and demountable connection resistance.

In total 12 demountable and 12 non-demountable models were developed varying the applied parameters: concrete class (C20/25–C50/60), stud diameter (16–22 mm) and stud height (100 and 125 mm). In that way, the spectrum of possible shear connection configurations for the selected profiled steel sheeting was covered. The slab depth and width were applied according to Subchapter 6.2.4. Bolt diameter was chosen to keep the ratio between the headed stud and bolt resistance lower than 0.70, where headed stud resistance had been derived from push-out simulations of non-demountable models. Plate thickness t_p was adopted to satisfy the condition required in EN 1994-1-1:2004 [10] regarding the relation between headed stud diameter and thickness of the component to which the stud is welded: $t_p > 0.4d$, where d is the stud shank diameter. Both bolt diameter and plate thickness were selected from the range of standard dimensions common in steel fabrication.

Load-slip curves for several demountable and non-demountable models are compared in Figure 6.12. An increase in the connection resistance with the increase in the concrete class and stud diameter is

shown. A good match in the response of demountable and non-demountable connections was accomplished.
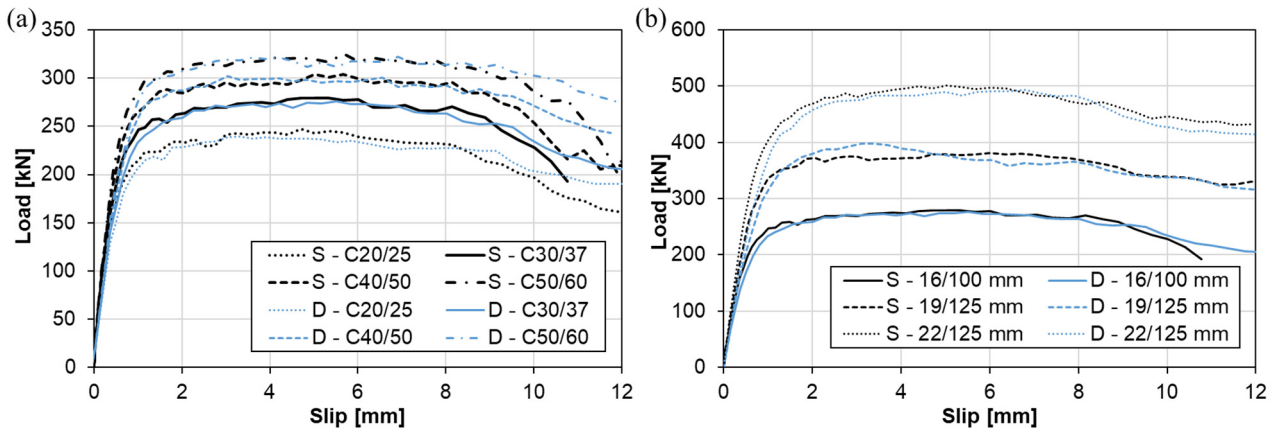
Figure 6.12: Load-slip curves for demountable and non-demountable models:
(a) varied concrete class for the headed stud diameter of 16 mm,
(b) varied headed stud geometry for the concrete class C30/37.

Ultimate loads obtained for demountable and non-demountable models are compared in Table 6.9 and Figure 6.13. The ultimate load is presented per connector, obtained by dividing the total ultimate load by the number of stud connectors in the model. The parametric analysis covered welded headed studs in profiled steel sheeting Cofraplus 60 with resistances in the range from 30 to 70 kN.

Correlation between ultimate loads of demountable and non-demountable models is strong, with the mean value of the ratio $P_{\text{ult,fea,D}}/P_{\text{ult,fea,S}}$ equal to 1 and the coefficient of variation of 2.28%. Therefore, for the analysed set of models, ultimate loads of demountable shear connections may be considered equal to the ultimate loads of non-demountable connections. The proposed design of the demountable connection including specified plate thickness and bolt diameter has been verified. It may be assumed that the shear resistance of the demountable connection with bolts and headed studs is equivalent to the shear resistance of welded headed stud connectors in profiled steel sheeting.

Table 6.9: Comparison of the resistance of demountable and non-demountable shear connections.

Stud diameter	Stud height	Slab depth	Bolt diameter	Plate thickness	Concrete class	Concrete strength	Ultimate load per connector		Ratio
							Demountable connection	Non-demountable connection	
d [mm]	h_{sc} [mm]	h [mm]	d_{b} [mm]	t_{p} [mm]	-	f_{cm} [MPa]	$P_{\text{ult,fea,D}}$ [kN]	$P_{\text{ult,fea,S}}$ [kN]	$P_{\text{ult,fea,D}}/P_{\text{ult,fea,S}}$
16	100	120	12	8	C20/25	28.0	29.98	30.91	0.97
16	100	120	12	8	C30/37	38.0	34.51	34.91	0.99
16	100	120	12	8	C40/50	48.0	37.71	38.01	0.99
16	100	120	12	8	C50/60	58.0	40.26	40.66	0.99
19	125	150	16	8	C20/25	28.0	43.51	42.15	1.03
19	125	150	16	8	C30/37	38.0	49.76	47.61	1.05
19	125	150	16	8	C40/50	48.0	53.16	52.53	1.01
19	125	150	16	8	C50/60	58.0	57.13	56.15	1.02
22	125	150	16	10	C20/25	28.0	53.28	54.61	0.98
22	125	150	16	10	C30/37	38.0	61.65	62.71	0.98
22	125	150	16	10	C40/50	48.0	66.65	66.89	1.00
22	125	150	16	10	C50/60	58.0	70.68	69.99	1.01
								Mean	1.00
								Coefficient of variation [%]	2.28
								Correlation coefficient	0.997
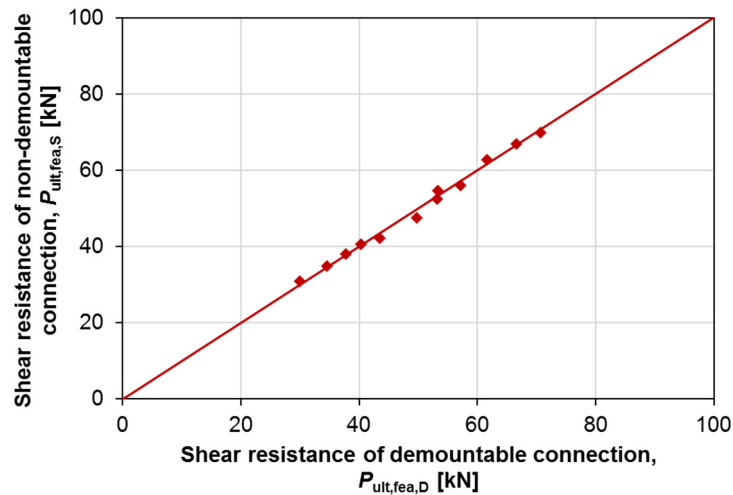
Figure 6.13: Relation between the shear resistance of demountable and non-demountable connections.

6.4 Demountable Connections with Discontinuous Slabs over the Beam

To design a demountable connection with a discontinuous slab over the supporting beam, the angle thickness and bolt diameter should be appropriately adopted, as in the case of demountable connections with continuous slabs. Moreover, the stirrup reinforcement and distance between the headed stud and slab edge should be suitably selected. The influence of these parameters on the connection shear response is discussed in the following.

6.4.1 Influence of the Angle Thickness

The angle thickness of the demountable connection with a discontinuous slab over the support was analysed on two models: DL and DLU. The angle thickness was varied from 4 to 10 mm. Results given in Figure 6.14 and Figure 6.15, i.e. Table 6.10 and Table 6.11, correspond to results shown in the previous subchapter presenting the connection response for the varied plate thickness (Figure 6.9 and Table 6.7). Nevertheless, a drop in the shear resistance when angle thickness is reduced from 8 mm to 4 mm (18–20%) is even more pronounced than a drop in the shear resistance when the plate thickness is reduced to the same value (14%). That may be attributed to the reduction of the thickness of the vertical angle leg, whose presence affects the connection behaviour as explained later in Subchapter 6.4.3.

Figure 6.14: Influence of the angle thickness: model DL.
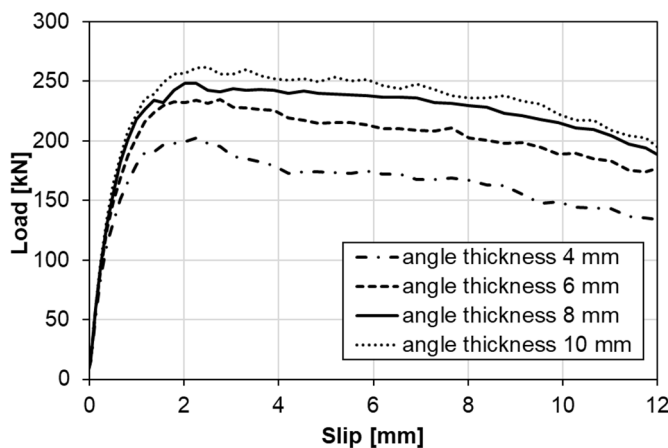
Table 6.10: Influence of the angle thickness: model DL.

No.	Angle thickness	Concrete strength	Ultimate load	Ratio
	t_p [mm]	f_{cm} [MPa]	$P_{ult,fea}$ [kN]	$P_{ult,fea,(i)}/P_{ult,fea,(3)}$
(1)	4	37.3	202.4	0.82
(2)	6	37.3	234.4	0.94
(3)	8	37.3	248.2	-
(4)	10	37.3	261.9	1.06

99
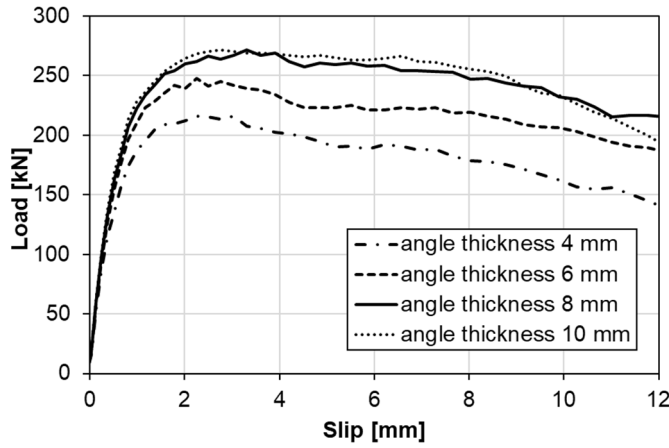
Table 6.11: Influence of the angle thickness: model DLU.

No.	Angle thick-ness	Concrete strength	Ultimate load	Ratio
	t_p [mm]	f_{cm} [MPa]	$P_{ult,fea}$ [kN]	$P_{ult,fea,(i)}/P_{ult,fea,(3)}$
(1)	4	37.3	216.2	0.80
(2)	6	37.3	247.5	0.91
(3)	8	37.3	271.6	-
(4)	10	37.3	271.3	1.00

Figure 6.15: Influence of the angle thickness: model DLU.

For the models with discontinuous slabs DL and DLU, for the angle thickness of 8 mm or larger, ultimate loads converge to a certain value. Hence, the thickness of 8 mm was confirmed to be an optimal solution in that case, as it had been previously concluded for the corresponding model with a continuous slab.

6.4.2 Influence of the Stirrup Diameter and Position

The positive effects of stirrup reinforcement on the connection resistance were shown through experimental and numerical findings. In this subchapter, the influence of the U-bar diameter and the reinforcement position along the headed stud height is analysed.

The stirrup diameter was varied from 4 to 10 mm. However, all models showed almost the same response as presented in Figure 6.16 and Table 6.12, indicating that variations in bar diameter do not affect shear resistance or ductility of the connection.

Table 6.12: Influence of the stirrup diameter: model DLU.

No.	Stirrup dia-meter	Concrete strength	Ultimate load	Ratio
	$\emptyset$ [mm]	f_{cm} [MPa]	$P_{ult,fea}$ [kN]	$P_{ult,fea,(i)}/P_{ult,fea,(3)}$
(1)	4	37.3	262.6	0.97
(2)	6	37.3	265.9	0.98
(3)	8	37.3	271.6	-
(4)	10	37.3	269.9	0.99
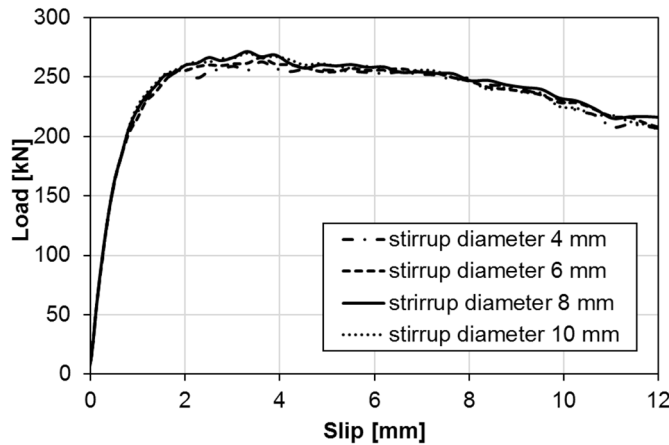
Figure 6.16: Influence of the stirrup diameter: model DLU.

To compare the activation of stirrup reinforcement in developed models, the axial force in U-bars is plotted against slip in Figure 6.17. Curves presented for models with stirrup bars of 8 mm and 10 mm in diameter coincide, and the maximum force is almost the same in those two cases. The maximum axial force is somewhat smaller for stirrups with a smaller diameter. Observing the stress in bars, it is noticed that the stress is the largest in U-bars of 4 mm in diameter, but it is still below the reinforcement yield strength.
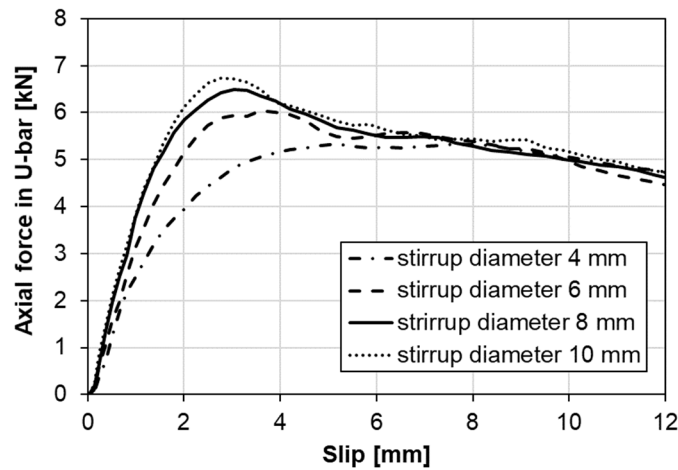
Figure 6.17: Axial force in U-bar for different bar diameters.

In the experiment, U-bars were put on the level of the top surface of profiled sheeting ribs as such position enabled simple installation. Furthermore, by avoiding the bar placement inside the rib, enough space inside the sheeting rib was provided for concrete casting. Bar position along the stud height was varied in numerical models, as shown in Figure 6.18, where the original position applied in the experiment is marked as position 1. Although EN 1994-1-1:2004 [10] suggests placing U-bars as low as possible accounting for the concrete cover layer, a change in the connection behaviour was not considerable for models with U-bars closer to the weld collar than in the basic model. Nevertheless, the resistance is decreased in the model with U-bars placed just below the stud head, as presented in Figure 6.19 and Table 6.13. Consequently, it is recommended to place U-bars at the level of the top surface of profiled sheeting ribs or within the sheeting rib if adequate concrete compaction is possible to accomplish.
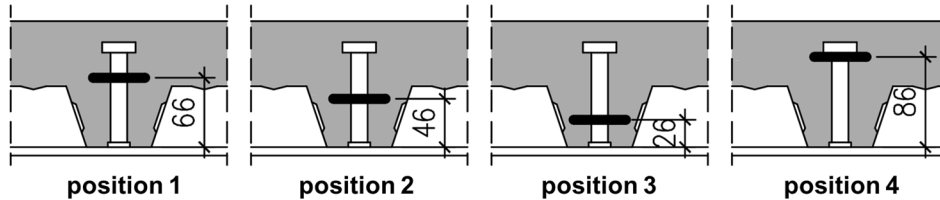
Figure 6.18: Varied stirrup position.
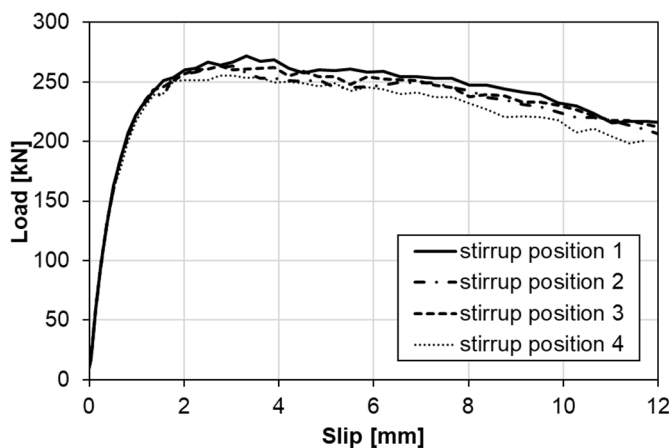
Figure 6.19: Influence of the stirrup position: model DLU.

Table 6.13: Influence of the stirrup position: model DLU.

No.	Stirrup pos.	Concrete strength f_{cm} [MPa]	Ultimate load $P_{ult,fea}$ [kN]	Ratio $P_{ult,fea,(i)}/P_{ult,fea,(1)}$
(1)	1	37.3	271.6	-
(2)	2	37.3	263.3	0.97
(3)	3	37.3	263.4	0.97
(4)	4	37.3	255.2	0.94

101

6.4.3 Influence of the Stud-to-Edge Distance

In connections with discontinuous slabs over the support, the distance between the headed stud and slab edge in the lateral direction is an important parameter that should be carefully adopted in design. EN 1994-1-1:2004 [10] requires the minimum stud-to-edge distance of $6d$ in the general case. However, experimental and numerical results proved that the developed demountable connection with the stud-to-edge distance of $4d$ has equal resistance to the non-demountable connection with a continuous slab over the beam. Therefore, the influence of the stud-to-edge distance in composite concrete slabs cast in profiled steel sheeting with installed angles on slab edges is discussed. The parametric study also covered demountable connections with discontinuous slabs without the vertical angle leg on the slab edge (Figure 6.20.b), to determine if the presence of steel angle contributes to the connection resistance. These models are labelled as NDL, i.e. NDLU, depending on whether U-bars are applied or not.
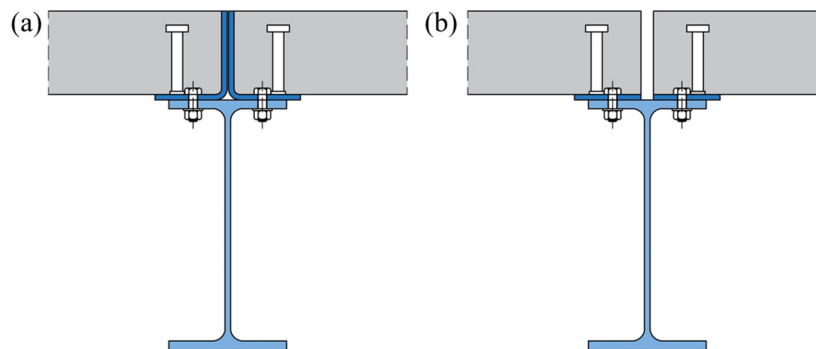
Figure 6.20: Demountable connections with discontinuous slabs over the beam:
(a) angle on the slab edge, (b) slab edge without the vertical angle leg.

The slab-to-edge distance was varied in models in the range from $3d$ to $6d$, in both models with angles (Figure 6.21.a) and without the vertical angle leg (Figure 6.21.b). Load-slip curves for the models without and with stirrup reinforcement are shown in Figure 6.22 and Figure 6.23. Distinct differences in load-slip curves are present between models with and without vertical angle legs, indicating that the steel element on the slab edge plays an important role in the shear connection response. The connection with angles and stud-to-edge distance of $3d$ has almost the same resistance as the connection with stud-to-edge distance of $6d$ without angles. However, the latter one is characterised by almost two times smaller slip capacity. It is concluded that the vertical angle leg reinforces the slab edge resulting in larger shear resistance and ductility of the connection.
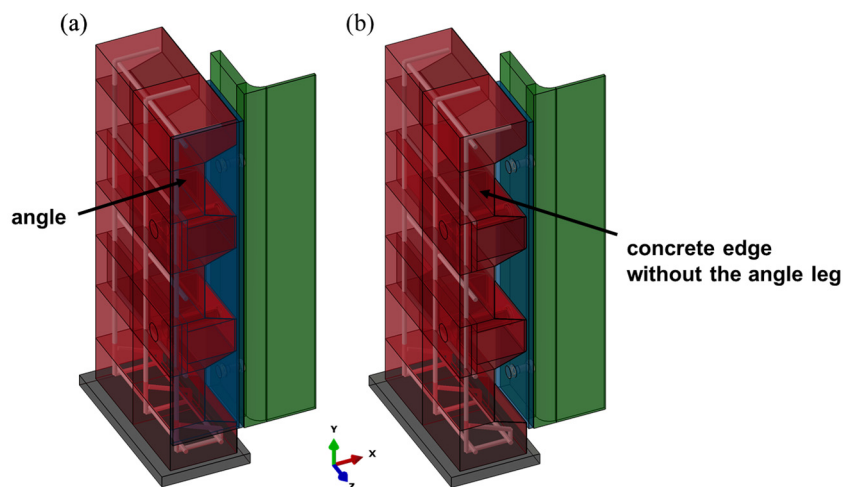
Figure 6.21: Finite element models:
(a) model with the angle (DL, DLU), (b) model without the angle (NDL, NDLU).
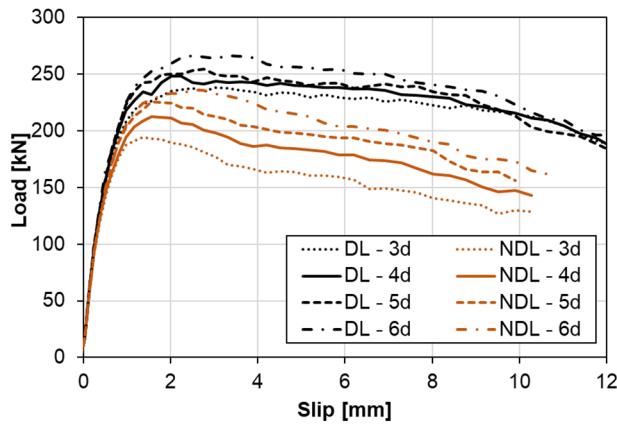
Figure 6.22: Influence of the distance between a headed stud and a slab edge: models DL, NDL.
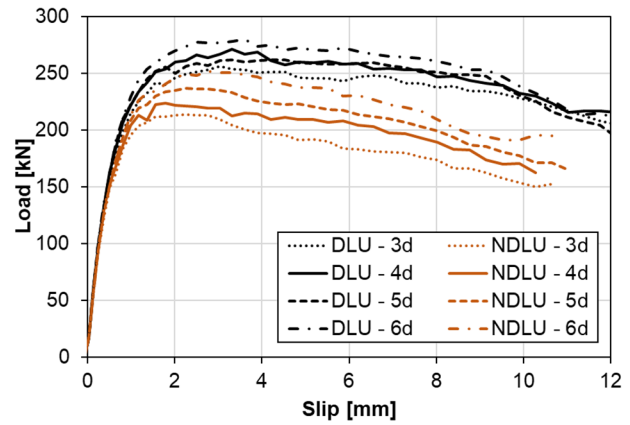
Figure 6.23: Influence of the distance between a headed stud and a slab edge: models DLU, NDLU.

Comparisons between ultimate loads for chosen different slab-to-edge distances and for models with and without angles, when stirrups are applied and when they are not, are given in Table 6.14 and Table 6.15. For both connections with and without U-bars, an increase in the ultimate load with the increase in the slab-to-edge distance is more pronounced when the slab edge is without the angle than when angles are applied. The shear resistance of the models with angles is 11–23% higher compared with the models without angles. The increase in the ultimate load when angles are applied is more distinct for smaller slab-to-edge distances. It is concluded that angles applied in the demountable connection with a discontinuous slab over the beam provide a considerable contribution to the shear connection resistance and ductility.

Table 6.14: Influence of the distance between a headed stud and a slab edge: models DL, NDL.

No.	Distance between the headed stud and slab edge	Concrete strength	With L profile		Without L profile		Ratio
			Ultimate load	Ratio	Ultimate load	Ratio	
	e_s	f_{cm}	$P_{ult,fea,DL}$	$P_{ult,fea,DL(i)}/$ $P_{ult,fea,DL(2)}$	$P_{ult,fea,NDL}$	$P_{ult,fea,NDL(i)}/$ $P_{ult,fea,NDL(2)}$	$P_{ult,fea,DL}/$ $P_{ult,fea,NDL}$
	[-]	[MPa]	[kN]		[kN]		
(1)	$3d$	37.3	238.3	0.96	194.1	0.91	1.23
(2)	$4d$	37.3	248.2	-	212.7	-	1.17
(3)	$5d$	37.3	254.3	1.02	225.2	1.06	1.13
(4)	$6d$	37.3	266.2	1.07	235.9	1.11	1.13

Table 6.15: Influence of the distance between a headed stud and a slab edge: models DLU, NDLU.

No.	Distance between the headed stud and slab edge	Concrete strength	With L profile		Without L profile		Ratio
			Ultimate load	Ratio	Ultimate load	Ratio	
	e_s	f_{cm}	$P_{ult,fea,DLU}$	$P_{ult,fea,DLU(i)}/$ $P_{ult,fea,DLU(2)}$	$P_{ult,fea,NDLU}$	$P_{ult,fea,NDLU(i)}/$ $P_{ult,fea,NDLU(2)}$	$P_{ult,fea,DLU}/$ $P_{ult,fea,NDLU}$
	[-]	[MPa]	[kN]		[kN]		
(1)	$3d$	37.3	256.5	0.94	213.5	0.95	1.20
(2)	$4d$	37.3	271.6	-	224.2	-	1.21
(3)	$5d$	37.3	262.1	0.97	237.0	1.06	1.11
(4)	$6d$	37.3	280.0	1.03	251.9	1.12	1.11

The distance between the headed stud and angle of $4d$ showed satisfactory behaviour of the demountable connection in the experimental and numerical testing presented in previous chapters, close to that of the connections with continuous slabs. Therefore, the same distance was applied to the other models for different stud diameters and varied concrete strengths. The set of developed models corresponds to models of demountable connections with continuous slabs over the support presented in Subchapter 6.3.2. However, as in some cases, the obtained ultimate loads of demountable connections with discontinuous slabs over the beam were larger than those of the corresponding connections with continuous slabs over the beam, additional models with the slab-to-edge distance of $3d$ were developed to determine the optimum design. All models included U-bars with a diameter

of at least 0.5d, placed around headed studs at the level of the top surface of profiled sheeting ribs. The bolt diameter and angle thickness greater than 0.4d were adopted as previously selected for demountable connections with continuous slabs.

All models of demountable connections with discontinuous slabs over the support were compared to corresponding models of demountable connections with continuous slabs to determine the appropriate stud-to-edge distance for which resistances of two connections are equal. Ultimate loads for connections with discontinuous slabs are shown in Table 6.16 and compared with the response of corresponding models with continuous slabs through the ratio $P_{ult,fea,DLU}/P_{ult,fea,D}$. However, a direct proportionality between the ratio and stud-to-edge distance, whether it is expressed in millimetres or as the function of the stud shank diameter, was not observed, indicating that other parameters also affect the reduction of the resistance of connections with discontinuous slabs.

Table 6.16: Comparison of the resistance of demountable shear connections with continuous and discontinuous slabs.

Stud diameter	Stud height	Slab depth	Bolt diameter	Angle thickness	U-bar diameter	Distance between the headed stud and angle		Concrete strength	Ultimate load per connector		Ratio
									Discontinuous slab over the beam	Continuous slab over the beam	
d [mm]	h_{sc} [mm]	h [mm]	d_b [mm]	t_p [mm]	Ø [mm]	e_s [-]	e_s [mm]	f_{cm} [MPa]	$P_{ult,fea,DLU}$ [kN]	$P_{ult,fea,D}$ [kN]	$P_{ult,fea,DLU}/P_{ult,fea,D}$
16	100	120	12	8	8	3d	48	28.0	26.98	29.98	0.90
16	100	120	12	8	8	3d	48	38.0	31.98	34.51	0.93
16	100	120	12	8	8	3d	48	48.0	35.69	37.71	0.95
16	100	120	12	8	8	3d	48	58.0	38.55	40.26	0.96
16	100	120	12	8	8	4d	64	28.0	29.61	29.98	0.99
16	100	120	12	8	8	4d	64	38.0	34.03	34.51	0.99
16	100	120	12	8	8	4d	64	48.0	37.06	37.71	0.98
16	100	120	12	8	8	4d	64	58.0	40.53	40.26	1.01
19	125	150	16	8	10	3d	57	28.0	42.03	43.51	0.97
19	125	150	16	8	10	3d	57	38.0	47.79	49.76	0.96
19	125	150	16	8	10	3d	57	48.0	52.01	53.16	0.98
19	125	150	16	8	10	3d	57	58.0	55.98	57.13	0.98
19	125	150	16	8	10	4d	76	28.0	45.11	43.51	1.04
19	125	150	16	8	10	4d	76	38.0	50.64	49.76	1.02
19	125	150	16	8	10	4d	76	48.0	55.25	53.16	1.04
19	125	150	16	8	10	4d	76	58.0	58.80	57.13	1.03
22	125	150	16	10	12	3d	66	28.0	53.15	53.28	1.00
22	125	150	16	10	12	3d	66	38.0	61.63	61.65	1.00
22	125	150	16	10	12	3d	66	48.0	67.09	66.65	1.01
22	125	150	16	10	12	3d	66	58.0	72.76	70.68	1.03
22	125	150	16	10	12	4d	88	28.0	56.60	53.28	1.06
22	125	150	16	10	12	4d	88	38.0	64.81	61.65	1.05
22	125	150	16	10	12	4d	88	48.0	71.01	66.65	1.07
22	125	150	16	10	12	4d	88	58.0	76.79	70.68	1.09

Analysing the set of data, an adequate correlation between the ratio $P_{ult,fea,DLU}/P_{ult,fea,D}$ and value of $e_s \cdot f_{cm}^{0.1}$ was detected, where e_s is the stud-to-edge distance and f_{cm} is the cylinder compressive strength of concrete. The ratio $P_{ult,fea,DLU}/P_{ult,fea,D}$ plotted against $e_s \cdot f_{cm}^{0.1}$ for each analysed model is presented in Figure 6.24, as well as the linear regression line. The proposed analytical relationship between ultimate loads of demountable connections with discontinuous slabs and demountable connections with continuous slabs is given as:

$$\frac{P_{ult,fea,DLU}}{P_{ult,fea,D}} = 2.2797\, e_s f_{cm}{}^{0.1} 10^{-3} + 0.7799 \qquad (6.1)$$

where:

e_s is the stud-to-edge distance in mm;

f_{cm} is the cylinder compressive strength of the concrete in MPa.

For the defined linear regression model, the coefficient of determination R^2 is 0.93.
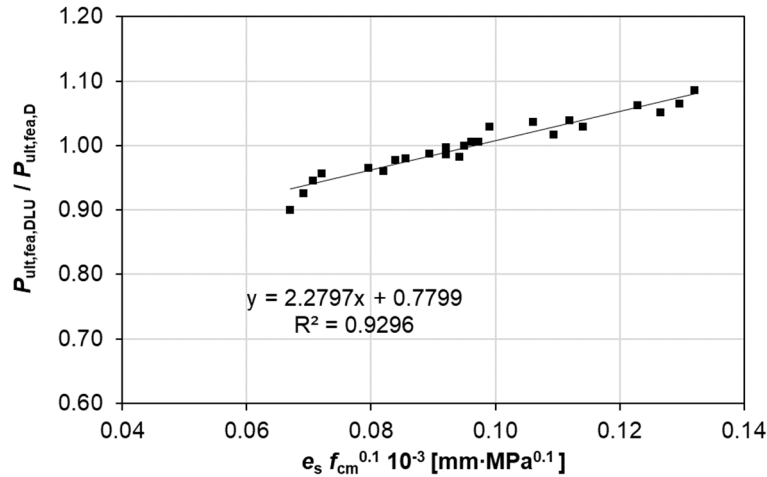
Figure 6.24: Relation between shear resistance of demountable shear connections
with discontinuous and continuous slabs.

To test the analytical prediction, comparisons between analytically and numerically obtained results are provided in Table 6.17. A low coefficient of variation of 1.24% and a high correlation coefficient of 0.964 imply that the suggested analytical equation provides satisfactory predictions.

In the end, according to the proposed equation, the appropriate stud-to-edge distance for accomplishing equal resistance of the shear connections with continuous and discontinuous composite concrete slabs was defined. As the function of the concrete strength, optimum distances are listed in Table 6.18. For the adopted stud-to-edge distance of at least 70 mm, the resistance of the connection with a discontinuous slab is not expected to be smaller than of the demountable connection with a continuous slab. Consequently, the application of analytical expressions for shear resistance of welded headed studs in profiled steel sheeting may be applicable even in the case of connections with discontinuous slabs.

Table 6.17: Reduction of the resistance of demountable shear connections with discontinuous slabs.

Stud diameter	Stud height	Distance between the headed stud and angle		Concrete strength	Ultimate load per connector		Ratio		
					Discontinuous slab over the beam	Continuous slab over the beam	Numerically obtained (1)	Analytical prediction (2)	(2) / (1)
d [mm]	h_{sc} [mm]	e_s [-]	e_s [mm]	f_{cm} [MPa]	$P_{ult,fea,DLU}$ [kN]	$P_{ult,fea,D}$ [kN]	$P_{ult,fea,DLU} / P_{ult,fea,D}$	$\dfrac{2.2797\,e_s}{f_{cm}^{0.1}}10^{-3} + 0.7799$	
16	100	3d	48	28.0	26.98	29.98	0.90	0.93	1.04
16	100	3d	48	38.0	31.98	34.51	0.93	0.94	1.01
16	100	3d	48	48.0	35.69	37.71	0.95	0.94	0.99
16	100	3d	48	58.0	38.55	40.26	0.96	0.94	0.99
16	100	4d	64	28.0	29.61	29.98	0.99	0.98	1.00
16	100	4d	64	38.0	34.03	34.51	0.99	0.99	1.00
16	100	4d	64	48.0	37.06	37.71	0.98	0.99	1.01
16	100	4d	64	58.0	40.53	40.26	1.01	1.00	0.99
19	125	3d	57	28.0	42.03	43.51	0.97	0.96	1.00
19	125	3d	57	38.0	47.79	49.76	0.96	0.97	1.01
19	125	3d	57	48.0	52.01	53.16	0.98	0.97	0.99
19	125	3d	57	58.0	55.98	57.13	0.98	0.97	0.99
19	125	4d	76	28.0	45.11	43.51	1.04	1.02	0.99
19	125	4d	76	38.0	50.64	49.76	1.02	1.03	1.01
19	125	4d	76	48.0	55.25	53.16	1.04	1.04	1.00
19	125	4d	76	58.0	58.80	57.13	1.03	1.04	1.01
22	125	3d	66	28.0	53.15	53.28	1.00	0.99	0.99
22	125	3d	66	38.0	61.63	61.65	1.00	1.00	1.00
22	125	3d	66	48.0	67.09	66.65	1.01	1.00	0.99
22	125	3d	66	58.0	72.76	70.68	1.03	1.01	0.98
22	125	4d	88	28.0	56.60	53.28	1.06	1.06	1.00
22	125	4d	88	38.0	64.81	61.65	1.05	1.07	1.02
22	125	4d	88	48.0	71.01	66.65	1.07	1.08	1.01
22	125	4d	88	58.0	76.79	70.68	1.09	1.08	0.99
								Mean	1.00
								Coefficient of variation [%]	1.24
								Correlation coefficient	0.964

Table 6.18: The distance between the headed stud and angle for accomplishing equal resistance of the shear connections with continuous and discontinuous composite concrete slabs.

Concrete strength	Distance between the headed stud and vertical angle leg
f_{cm} [MPa]	e_s [mm]
28.0	69.2
38.0	67.1
48.0	65.6
58.0	64.3

6.5 Influence of the Angle between Profiled Sheeting Ribs and the Beam

Experimental and numerical results presented in previous chapters imply that the angle between sheeting ribs and the beam influences the resistance of the shear connection. To find a correlation between the shear resistance of connections with profiled sheeting ribs transverse to the supporting beam ($\alpha = 90°$) and connections with the angle between ribs and the beam smaller than 90° ($\alpha < 90°$), a parametric study was conducted. The set of push-out models included headed studs of 16, 19 and 22 mm in diameter, concrete classes in the range C20/25–C50/60 and angles between sheeting ribs and the beam of 30°, 45° and 60°. According to previous findings, it is clear that if specific design procedures are followed, the resistance of the demountable connection with bolts and headed studs

should be equal to the resistance of the corresponding non-demountable connection with headed studs. Therefore, to analyse the effect of the angle between ribs and the beam, only non-demountable models were developed, assuming that the same conclusions may be applied in the design of demountable connections.

Load-slip curves are compared in Figure 6.25, showing the increase in the connection resistance with the increase in the concrete class and stud diameter. However, it is noticed that the connection resistance is affected more by the stud diameter than the concrete strength or angle between profiled sheeting ribs and the beam.
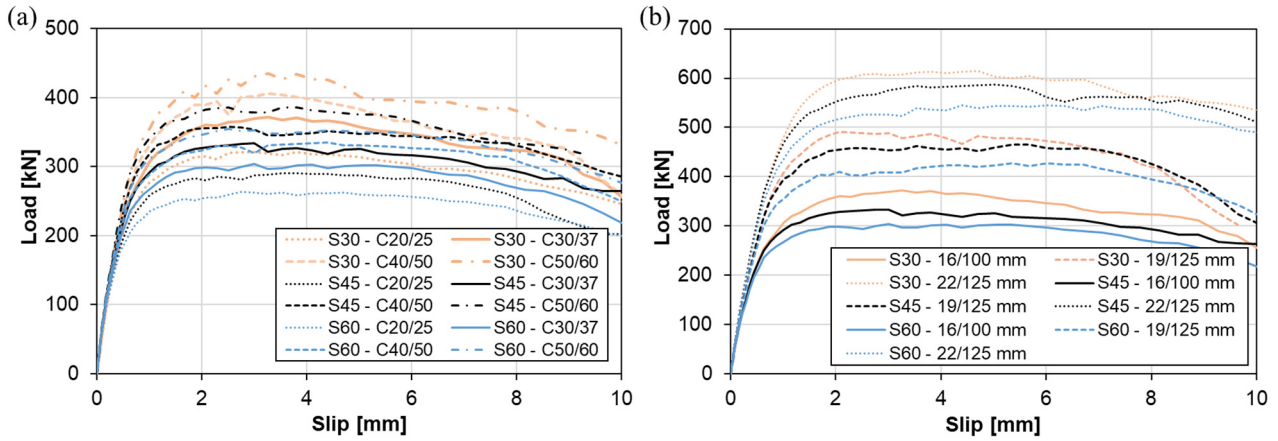
Figure 6.25: Load-slip curves for models with different angles between sheeting ribs and the beam:
(a) varied concrete class for the headed stud diameter of 16 mm,
(b) varied headed stud geometry for the concrete class C30/37.

The ultimate load per connector of each model with the angle between sheeting ribs and the beam α < 90°, $P_{ult,fea,S\alpha}$, was compared with the ultimate load per connector obtained for the corresponding connection with ribs transverse to the beam, i.e. $\alpha = 90°$, $P_{ult,fea,S}$, as presented in Table 6.19.

The set of ratios $P_{ult,fea,S\alpha}/P_{ult,fea,S}$, where $P_{ult,fea,S\alpha}$ is the resistance of the connection with the angle between profiled sheeting ribs and the beam $\alpha < 90°$, and $P_{ult,fea,S}$ is the resistance of the corresponding connection with ribs transverse to the beam, i.e. $\alpha = 90°$, is in the range of 1.06–1.30. The relation between the applied concrete strength or stud diameter and the obtained ratio was not observed. The key influential parameter is the angle between sheeting ribs and the beam. The mean values of the ratio $P_{ult,fea,S\alpha}/P_{ult,fea,S}$ for the applied angles of 60⁰, 45⁰ and 30⁰ are 1.10, 1,19 and 1.30, respectively. The maximum coefficient of variation is 2.75%.

The relation between the resistance of the connection with the angle between sheeting ribs and the beam α, and the connection with ribs transverse to the beam, was introduced through the factor k_α. In Figure 6.26, the ratio $P_{ult,fea,S\alpha}/P_{ult,fea,S}$ is plotted against $\sin(\alpha)$ and the regression line is fitted. The initial request that the ratio $P_{ult,fea,S\alpha}/P_{ult,fea,S}$ equals 1 for the angle $\alpha = 90°$ determines one point of the line. The slope of the regression line is adopted for the minimum root-mean-square error, as presented in Table 6.20. Finally, the regression line is defined as:

$$P_{ult,fea,S\alpha}/P_{ult,fea,S} = 1 + 0.61\,(1 - \sin\alpha) \tag{6.2}$$

Table 6.19: Comparison of the resistance of connections with different angles between profiled sheeting ribs and the beam.

Stud diameter	Stud height	Slab depth	Angle between sheeting ribs and the beam	Concrete class	Concrete strength	Ultimate load per connector		Ratio
						$\alpha \neq 90°$	$\alpha = 90°$	
d [mm]	h_{sc} [mm]	h [mm]	α [°]	-	f_{cm} [MPa]	$P_{ult,fea,S\alpha}$ [kN]	$P_{ult,fea,S}$ [kN]	$P_{ult,fea,S\alpha}$ / $P_{ult,fea,S}$
16	100	120	60	C20/25	28.0	32.90	30.91	1.06
16	100	120	60	C30/37	38.0	37.96	34.91	1.09
16	100	120	60	C40/50	48.0	41.88	38.01	1.10
16	100	120	60	C50/60	58.0	44.40	40.66	1.09
19	125	150	60	C20/25	28.0	49.03	42.15	1.16
19	125	150	60	C30/37	38.0	53.43	47.61	1.12
19	125	150	60	C40/50	48.0	58.30	52.53	1.11
19	125	150	60	C50/60	58.0	60.19	56.15	1.07
22	125	150	60	C20/25	28.0	60.05	54.61	1.10
22	125	150	60	C30/37	38.0	68.08	62.71	1.09
22	125	150	60	C40/50	48.0	73.39	66.89	1.10
22	125	150	60	C50/60	58.0	78.18	69.99	1.12
							Mean	1.10
							Coefficient of variation [%]	2.35
16	100	120	45	C20/25	28.0	36.34	30.91	1.18
16	100	120	45	C30/37	38.0	41.71	34.91	1.19
16	100	120	45	C40/50	48.0	44.70	38.01	1.18
16	100	120	45	C50/60	58.0	48.23	40.66	1.19
19	125	150	45	C20/25	28.0	51.96	42.15	1.23
19	125	150	45	C30/37	38.0	58.20	47.61	1.22
19	125	150	45	C40/50	48.0	61.81	52.53	1.18
19	125	150	45	C50/60	58.0	66.44	56.15	1.18
22	125	150	45	C20/25	28.0	65.65	54.61	1.20
22	125	150	45	C30/37	38.0	73.45	62.71	1.17
22	125	150	45	C40/50	48.0	78.91	66.89	1.18
22	125	150	45	C50/60	58.0	83.71	69.99	1.20
							Mean	1.19
							Coefficient of variation [%]	1.63
16	100	120	30	C20/25	28.0	40.19	30.91	1.30
16	100	120	30	C30/37	38.0	46.53	34.91	1.33
16	100	120	30	C40/50	48.0	50.71	38.01	1.33
16	100	120	30	C50/60	58.0	54.43	40.66	1.34
19	125	150	30	C20/25	28.0	56.39	42.15	1.34
19	125	150	30	C30/37	38.0	61.75	47.61	1.30
19	125	150	30	C40/50	48.0	67.00	52.53	1.28
19	125	150	30	C50/60	58.0	71.79	56.15	1.28
22	125	150	30	C20/25	28.0	67.83	54.61	1.24
22	125	150	30	C30/37	38.0	77.50	62.71	1.24
22	125	150	30	C40/50	48.0	85.44	66.89	1.28
22	125	150	30	C50/60	58.0	90.84	69.99	1.30
							Mean	1.30
							Coefficient of variation [%]	2.75

Figure 6.26: Development of the factor k_α.
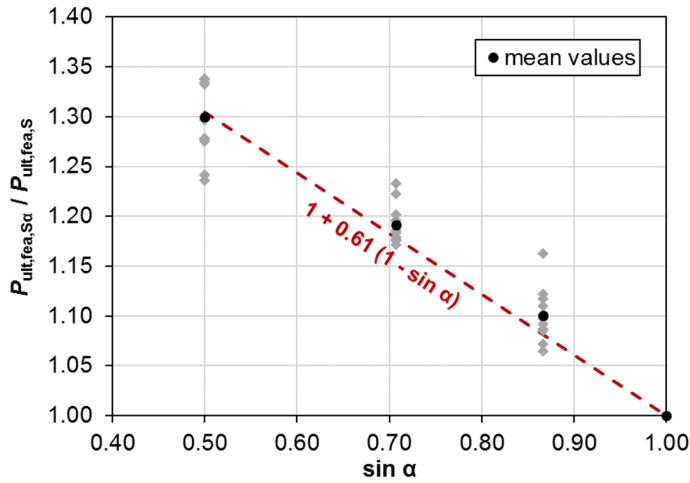
Table 6.20: Development of the factor k_α.

The slope	Root-mean-square error
0.58	0.03245
0.59	0.03136
0.60	0.03062
0.61	**0.03025**
0.62	0.03027
0.63	0.03068

The developed relation may be used to estimate the resistance of the welded headed stud in profiled steel sheeting for the angle between sheeting ribs and the beam α. The analytical prediction of the shear resistance of the welded headed stud in profiled steel sheeting with the angle between sheeting ribs and the beam $30^0 \leq \alpha < 90^0$ is given through the expression:

$$P_{ult,anl,S\alpha} = k_\alpha \cdot P_{ult,fea,S} \tag{6.3}$$

where:

$$k_\alpha = 1 + 0.61\,(1 - \sin\alpha) \tag{6.4}$$

α is the angle between profiled sheeting ribs and the beam, $30^0 \leq \alpha < 90^0$;

$P_{ult,fea,S}$ is the numerically obtained shear resistance of the welded headed stud in profiled steel sheeting for sheeting ribs transverse to the supporting beam.

The proposed equation was tested on developed numerical models. Comparisons between numerically obtained ultimate loads and analytical predictions are presented in Table 6.21 and Figure 6.27. The coefficient of variation of 2.47% indicates a good estimate of the proposed analytical expression.
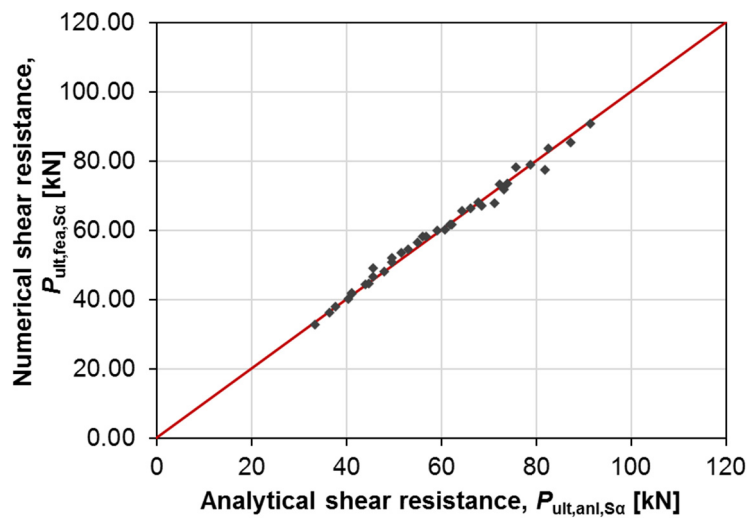
Figure 6.27: Comparison between numerically and analytically obtained shear resistance of a welded headed stud in profiled steel sheeting with $\alpha \neq 90°$.

109

Table 6.21: Relation between the shear resistance of connections with $\alpha \neq 90°$ and $\alpha = 90°$.

Stud diameter	Stud height	Slab depth	Angle between sheeting ribs and the beam	Concrete strength	Ultimate load per connector			Ratio
					FEA	FEA	Analytical prediction	
					$\alpha = 90°$	$\alpha \neq 90°$	$\alpha \neq 90°$	
d [mm]	h_{sc} [mm]	h [mm]	α [°]	f_{cm} [MPa]	$P_{ult,fea,S}$ [kN]	$P_{ult,fea,S\alpha}$ [kN]	$P_{ult,anl,S\alpha}$ [kN]	$P_{ult,anl,S\alpha}$ /$P_{ult,fea,S\alpha}$
16	100	120	60	28.0	30.91	32.90	33.44	1.02
16	100	120	60	38.0	34.91	37.96	37.77	0.99
16	100	120	60	48.0	38.01	41.88	41.12	0.98
16	100	120	60	58.0	40.66	44.40	43.99	0.99
19	125	150	60	28.0	42.15	49.03	45.59	0.93
19	125	150	60	38.0	47.61	53.43	51.50	0.96
19	125	150	60	48.0	52.53	58.30	56.82	0.97
19	125	150	60	58.0	56.15	60.19	60.74	1.01
22	125	150	60	28.0	54.61	60.05	59.08	0.98
22	125	150	60	38.0	62.71	68.08	67.84	1.00
22	125	150	60	48.0	66.89	73.39	72.35	0.99
22	125	150	60	58.0	69.99	78.18	75.71	0.97
16	100	120	45	28.0	30.91	36.34	36.44	1.00
16	100	120	45	38.0	34.91	41.71	41.15	0.99
16	100	120	45	48.0	38.01	44.70	44.80	1.00
16	100	120	45	58.0	40.66	48.23	47.93	0.99
19	125	150	45	28.0	42.15	51.96	49.68	0.96
19	125	150	45	38.0	47.61	58.20	56.12	0.96
19	125	150	45	48.0	52.53	61.81	61.91	1.00
19	125	150	45	58.0	56.15	66.44	66.18	1.00
22	125	150	45	28.0	54.61	65.65	64.37	0.98
22	125	150	45	38.0	62.71	73.45	73.92	1.01
22	125	150	45	48.0	66.89	78.91	78.84	1.00
22	125	150	45	58.0	69.99	83.71	82.49	0.99
16	100	120	30	28.0	30.91	40.19	40.34	1.00
16	100	120	30	38.0	34.91	46.53	45.56	0.98
16	100	120	30	48.0	38.01	50.71	49.61	0.98
16	100	120	30	58.0	40.66	54.43	53.06	0.98
19	125	150	30	28.0	42.15	56.39	55.01	0.98
19	125	150	30	38.0	47.61	61.75	62.13	1.01
19	125	150	30	48.0	52.53	67.00	68.55	1.02
19	125	150	30	58.0	56.15	71.79	73.28	1.02
22	125	150	30	28.0	54.61	67.83	71.27	1.05
22	125	150	30	38.0	62.71	77.50	81.84	1.06
22	125	150	30	48.0	66.89	85.44	87.29	1.02
22	125	150	30	58.0	69.99	90.84	91.33	1.01
							Mean	0.99
							Coefficient of variation [%]	2.47
							Correlation coefficient	0.995

6.6 Comparison with Analytical Predictions

In the end, numerically obtained ultimate loads for welded headed studs in profiled steel sheeting were compared with design predictions. Three different analytical procedures were used for comparison: design provisions provided in EN 1994-1-1:2004 [10] and two newly developed procedures proposed by Konrad [1] and the working group CEN/TC250/SC4.PT3 [3]. The set of numerical models included 28 models of non-demountable connections. In comparison with the models analysed in previous subchapters covering concrete classes C20/25–C50/60, headed stud diameters of 16–22 mm and heights of 100–125 mm, the set was extended to cover headed stud heights of 150 mm.

The shear resistance obtained by finite element analysis and analytical predictions of the headed stud resistance in profiled steel sheeting calculated without partial safety factors and applying the mean values of material properties are given in Table 6.22. For the analysed set of data, EN 1994-1-1:2004 and the model suggested by SC4.PT3 provide unsafe predictions with the mean value of the ratio between the numerical ultimate load per connector and analytical shear resistance of 0.82 and 0.84, respectively. On the other hand, the analytical model proposed by Konrad gives safe-sided results with an average value of 1.12. However, the highest coefficient of variation between numerical and predicted resistances is present for EN 1994-1-1:2004, while it is the smallest for the design model proposed by SC4.PT3.

Table 6.22: Comparison of numerically obtained shear resistance of a headed stud in profiled steel sheeting with the analytical predictions.

Stud diameter	Stud height	Slab depth	Concrete class	Concrete strength	Ultimate load per connector	Predicted headed stud resistance			Ratios		
						EN 1994-1-1	Konrad	SC4.PT3	$P_{ult,fea}/P_{EN}$	$P_{ult,fea}/P_{K}$	$P_{ult,fea}/P_{SC4}$
d	h_{sc}	h	-	f_{cm}	$P_{ult,fea}$	P_{EN}	P_{K}	P_{SC4}			
[mm]	[mm]	[mm]		[MPa]	[kN]	[kN]	[kN]	[kN]			
16	100	120	C20/25	28.0	30.91	34.25	28.41	34.95	0.90	1.09	0.88
16	100	120	C30/37	38.0	34.91	41.24	32.16	39.45	0.85	1.09	0.88
16	100	120	C40/50	48.0	38.01	41.24	35.40	43.47	0.92	1.07	0.87
16	100	120	C50/60	58.0	40.66	41.24	38.30	47.16	0.99	1.06	0.86
16	125	150	C20/25	28.0	36.25	40.80	28.41	37.51	0.89	1.28	0.97
16	125	150	C30/37	38.0	39.81	49.12	32.16	42.80	0.81	1.24	0.93
16	125	150	C40/50	48.0	42.69	49.12	35.40	47.53	0.87	1.21	0.90
16	125	150	C50/60	58.0	45.19	49.12	38.30	51.87	0.92	1.18	0.87
16	150	180	C20/25	28.0	37.60	40.80	28.41	40.07	0.92	1.32	0.94
16	150	180	C30/37	38.0	41.36	49.12	32.16	46.16	0.84	1.29	0.90
16	150	180	C40/50	48.0	43.88	49.12	35.40	51.59	0.89	1.24	0.85
16	150	180	C50/60	58.0	46.66	49.12	38.30	52.48	0.95	1.22	0.89
19	125	150	C20/25	28.0	42.15	57.53	39.60	52.65	0.73	1.06	0.80
19	125	150	C30/37	38.0	47.61	69.27	44.78	57.95	0.69	1.06	0.82
19	125	150	C40/50	48.0	52.53	69.27	49.26	62.67	0.76	1.07	0.84
19	125	150	C50/60	58.0	56.15	69.27	53.25	67.02	0.81	1.05	0.84
19	150	180	C20/25	28.0	46.71	57.53	39.60	55.21	0.81	1.18	0.85
19	150	180	C30/37	38.0	50.96	69.27	44.78	61.30	0.74	1.14	0.83
19	150	180	C40/50	48.0	55.36	69.27	49.26	66.74	0.80	1.12	0.83
19	150	180	C50/60	58.0	57.14	69.27	53.25	71.73	0.82	1.07	0.80
22	125	150	C20/25	28.0	54.61	77.14	53.41	74.58	0.71	1.02	0.73
22	125	150	C30/37	38.0	62.71	92.87	60.43	79.87	0.68	1.04	0.79
22	125	150	C40/50	48.0	66.89	92.87	66.50	84.60	0.72	1.01	0.79
22	125	150	C50/60	58.0	69.99	92.87	71.92	88.94	0.75	0.97	0.79
22	150	180	C20/25	28.0	61.75	77.14	53.41	77.14	0.80	1.16	0.80
22	150	180	C30/37	38.0	66.50	92.87	60.43	83.23	0.72	1.10	0.80
22	150	180	C40/50	48.0	69.63	92.87	66.50	88.66	0.75	1.05	0.79
22	150	180	C50/60	58.0	73.81	92.87	71.92	93.66	0.79	1.03	0.79
								Mean	0.82	1.12	0.84
								Coefficient of variation [%]	10.46	8.34	6.53

Numerically obtained ultimate loads are plotted against predicted resistance values in Figure 6.28–Figure 6.30. In the same graphs, experimental results of the resistance for series S and D are presented, as well as experimental results for headed studs in the profiled steel sheeting Cofraplus 60 published by Vigneri [64] and within the DISCCO project report [72]. The complete database of experimental results used for comparison is given in Annex B, with the listed connection geometry, material

properties and headed stud installation technique. The existing database for the selected profiled steel sheeting provided in the research of Vigneri and DISSCO project, including headed studs of 19 mm and 22 mm in diameter, is extended by the results of this research obtained for headed studs of 16 mm in diameter. Furthermore, most of the existing experimental push-out tests included one headed stud per concrete rib, while this research contributed with results for connections with two headed studs in the rib.

Numerically obtained data presented in graphs match some of the experimental results given by Vigneri and in the DISCCO project report. It is observed that EN 1994-1-1:2004 design procedures predict the same resistance for several different connections, meaning that they are less sensitive to mechanical and geometrical parameters of the connection than the other two design models. According to the presented, for almost all results in the database, Konrad's model gives conservative predictions, while EN 1994-1-1:2004 predictions are unsafe. For certain experimental results given by Vigneri and in the DISCCO project report, the newly developed equations by SC4.PT3 provide safe-sided predictions, whereas for the set of numerically obtained data, predictions are unsafe. However, it is remarked that analytically predicted values used for comparison are obtained without partial safety factors, applying the mean values of the measured material mechanical properties. To make general conclusions regarding the applicability and suitability of design models, a reliability analysis needs to be performed.
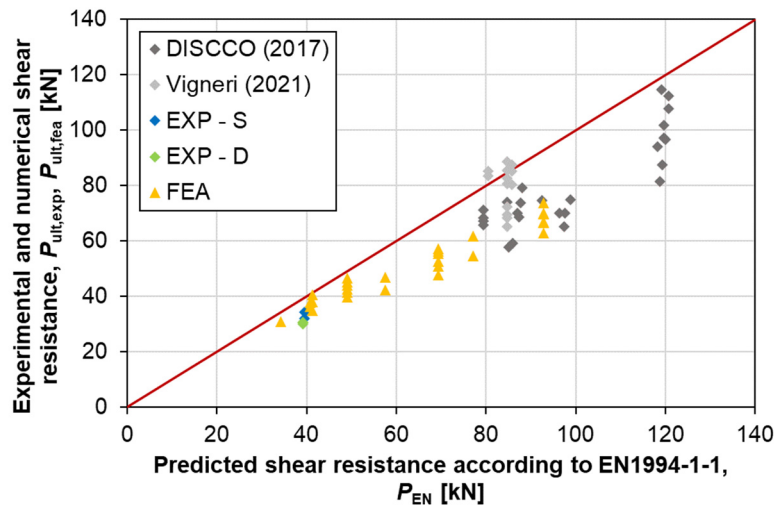
Figure 6.28: Comparison between experimental and numerical results with predicted shear resistance according to EN 1994-1-1:2004 [10].
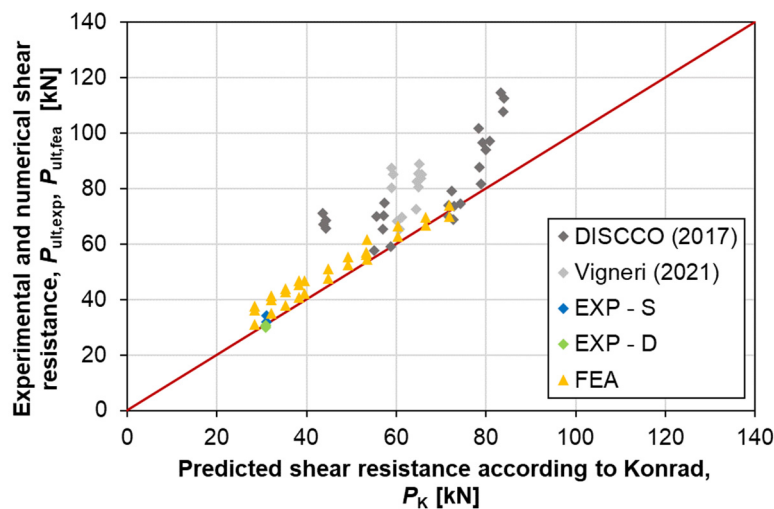
Figure 6.29: Comparison between experimental and numerical results with predicted shear resistance according to Konrad [1].

112
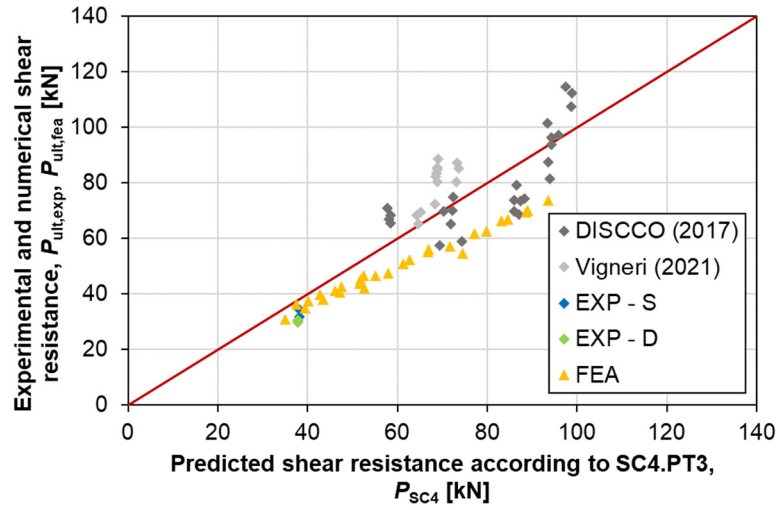
Figure 6.30: Comparison between experimental and numerical results with predicted shear resistance according to SC4.PT3 [3].

7 Design Recommendations

The results of experimental work, numerical analysis and parametric studies were used to draw general conclusions regarding the behaviour of the demountable shear connection with welded headed studs and bolts. According to concluded, recommendations for design and detailing were proposed.

Design instructions were developed for demountable shear connections with continuous and discontinuous slabs over the beam. A demountable shear connection designed following the suggested guidelines may be assumed to have equal resistance as the corresponding non-demountable shear connection with welded headed studs.

Design recommendations also include the analytical expression for obtaining the resistance of shear connections with angles between profiled sheeting ribs and the beam $30° \leq \alpha < 90°$. The expression applies to both demountable and non-demountable shear connections with welded headed studs.

7.1 Demountable Shear Connections with Continuous Slabs over the Beam

A demountable shear connection with bolts and welded headed studs with a continuous slab over the supporting beam is presented in Figure 7.1. The connection is suggested for application in composite beams consisting of a steel profile and composite concrete slab cast in open trough profiled steel sheeting. Headed studs are welded to the steel plate, while bolts connect the steel plate and profile flange. Headed studs are placed in every profiled sheeting rib, whereas bolts can be placed between every second rib.
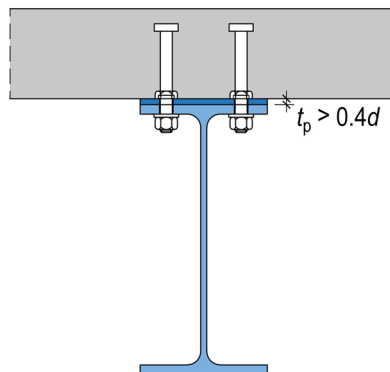
Figure 7.1: Demountable shear connection with a continuous slab over the beam.

To design a demountable shear connection with bolts and welded headed studs cast in a continuous slab over the beam, two recommendations should be followed:

(1) shear capacity of bolts should be adequate to enable the elastic behaviour of bolts at ultimate loads;

(2) plate thickness should be greater than $0.4d$, where d is the stud shank diameter.

If the listed requirements are fulfilled, the resistance of the shear connection may be calculated as for the corresponding non-demountable shear connection with welded headed studs.

7.2 Demountable Shear Connections with Discontinuous Slabs over the Beam

Demountable shear connection with bolts and welded headed studs could be implemented in slabs that are discontinuous over the supporting beam, as shown in Figure 7.2. Headed studs should be welded to steel angles, which are connected to the profile flange by bolts. As well as for connections with continuous slabs over the support, composite concrete slabs should be cast in open trough profiled steel sheeting.
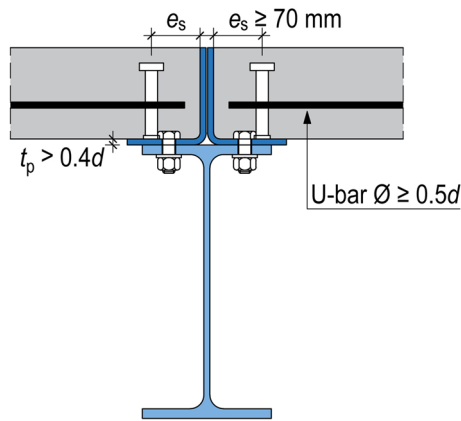
Figure 7.2: Demountable shear connection with a discontinuous slab over the beam.

Recommendations for the design of a demountable shear connection with a discontinuous slab over the supporting beam are listed:

(1) shear capacity of bolts should be adequate to enable the elastic behaviour of bolts at ultimate loads;

(2) angles of thickness greater than $0.4d$, where d is the stud shank diameter, should be used on the slab edge;

(3) U-bars with a diameter of at least $0.5d$ should be placed around headed studs at the level of the top surface of profiled sheeting ribs or lower;

(4) headed studs should be installed at a distance of at least 70 mm from the vertical angle leg in the transverse direction.

Resistance of the shear connection designed according to the proposed recommendations may be assumed to be equal to the resistance of the corresponding non-demountable shear connection with welded headed studs and continuous slab over the beam. If U-bars are not implemented or headed studs are installed at a distance smaller than 70 mm from the vertical angle leg, the resistance of the connection should be reduced.

7.3 Connections with the Angle between Profiled Sheeting Ribs and the Beam Smaller than 90°

In a general case, the presented demountable shear connection has ribs that are transverse to the supporting beam ($\alpha = 90°$). However, the angle between sheeting ribs and the beam may be smaller than 90°. In that case, the resistance of the demountable or non-demountable shear connection with welded headed studs could be obtained according to the proposed expression.

For shear connections with angles between profiled sheeting ribs and the beam in the range from 30° to 90°, shear resistance of the welded headed stud may be determined as:

$$P_\alpha = k_\alpha \cdot P_{90} \qquad (7.1)$$

where:

k_α is the factor depending on the angle α,

$$k_\alpha = 1 + 0.61\,(1 - \sin \alpha) \qquad (7.2)$$

P_α is the shear resistance of the welded headed stud for the angle between profiled sheeting ribs and the beam $30° \le \alpha < 90°$;

P_{90} is the shear resistance of the welded headed stud in profiled steel sheeting transverse to the beam.

116

It is important to emphasise that Eq. (7.1) is developed according to the results of numerical simulations of push-out tests for connections with profiled steel sheeting Cofraplus 60 [71]. However, in order to widen the application of the proposed relation to any other metal decking, additional models with varied profiled sheeting geometry need to be analysed.

8 Conclusions

The novel demountable shear connection with welded headed studs and bolts, designed for application in composite concrete slabs cast in open trough profiled steel sheeting, has been realised. The connection response to shear load has been examined by push-out tests, conducting experimental and numerical research. The connection behaviour has been analysed for different configurations, comparing the connection resistance, ductility and stiffness with corresponding non-demountable connections with welded headed studs.

The following conclusions can be drawn:

(1) The proposed solution of demountable shear connection with bolts and welded headed studs cast in profiled steel sheeting has a similar resistance and failure mode as the corresponding non-demountable shear connection with welded headed studs. The failure is characterised by the separation of the concrete cone from the rest of the slab.

(2) The main difference in the response of demountable and non-demountable connections is reflected in the slip capacity. The total slip of the demountable connection is the sum of the bolt slip and the slip of welded headed studs. Bolt slip is dominant in the initial loading stage due to the presence of bolt-to-hole clearances. In the later stages of loading, after bolt-to-hole clearances have been voided, the slip of headed studs becomes a dominant component in the total slip of the connection.

(3) As a result of the initial bolt slip inside holes, demountable connections have approximately three to four times smaller stiffness at serviceability loads than non-demountable connections.

(4) The thickness of the plate and angles affects the behaviour of the demountable shear connection. Therefore, the thickness of the plate and angles should be carefully selected to avoid plate deformation due to the shear of headed studs. The thickness of the plate and angles greater than $0.4d$ provides a satisfactory response of the connection.

(5) The relation between the resistance of the demountable connection with a discontinuous slab over the beam and the corresponding demountable connection with a continuous slab over the beam has been determined. The relation is dependent on the concrete strength and transverse distance between welded headed studs and slab edge in the demountable connection with a discontinuous slab over the support.

(6) Resistance of the demountable connection with a discontinuous slab over the supporting beam corresponds to the resistance of the demountable connection with a continuous slab over the supporting beam if proper design is performed. U-bars of $0.5d$ in diameter should be placed around headed studs at the level of the top surface of profiled sheeting ribs or lower. Angles of thickness greater than $0.4d$ should be used on the slab edge. The transverse distance between welded headed studs and angle legs should be adopted as at least 70 mm.

(7) In addition to the primary function of accomplishing connection demountability, angles applied on the edges of discontinuous concrete slabs have a reinforcing role. Connections without the vertical angle leg on the slab edge were found to have smaller resistance and ductility than those with angles. Reduction in the resistance when angles are avoided is in the range of 11–23% for the analysed connections.

(8) The position of mesh reinforcement along the slab depth does not affect the connection response. The slab depth has a minor influence on the connection shear resistance.

(9) The angle between profiled sheeting ribs and the beam affects the resistance of the connection. With the decrease of the angle, the resistance of the shear connection increases.

(10) The relation between the resistance of the connection with angles between profiled sheeting ribs and the beam in the range from 30° to 90° and the connection with ribs transverse to the beam has been proposed. According to the relation, the analytical expression for the resistance of welded headed studs for the angle between profiled sheeting ribs and the beam between 30° and 90° has been recommended.

(11) Resistance of welded headed studs in profiled steel sheeting with ribs transverse to the supporting beam has been compared with analytical design predictions. It is observed that the models proposed by Konrad and working group SC4.PT3 are more sensitive to connection geometry and material properties than the design rules given in EN 1994-1-1:2004. The model proposed by Konrad provides safe-sided predictions for the applied mean values of material properties, unlike the other two procedures. The smallest variation between calculated and obtained resistances is observed for the model proposed by SC4.PT3.

In addition, recommendations for future work may be proposed:

(1) To demonstrate the feasibility of the proposed solution and verify the shear response of the connection with bolts and welded headed studs when implemented in the girder, full-scale beam tests should be performed. Therefore, the practical requirements for bolt-to-hole clearances could be determined, and the exact deformations induced by the incomplete interaction due to the initial slip of bolts may be quantified. The use of preloaded bolts or the application of resin injected in bolt holes may be considered as two alternatives for reducing the initial bolt slip. The contribution of plates and angles to the bending resistance of the composite cross-section could be determined. In addition, beam tests could be used to observe girder behaviour in the second use, after already being loaded to a certain level before demounting and reassembling.

(2) Following concepts of sustainable construction, the application of the shear connection with bolts and welded headed studs in steel-concrete composite beams with "green" concrete could be considered. Further experiments should be performed to investigate the behaviour of headed studs when applied in different types of "green" concrete.

(3) More push-out tests should be conducted covering different profiled sheeting types to validate the proposed analytical relation for the resistance of connections with angles between profiled sheeting ribs and the beam smaller than 90°. Furthermore, the analyses may be extended to connections with one headed stud in the concrete rib and connections with headed studs welded through metal decking.

(4) Investigations of the behaviour of headed studs in connections with angles between profiled sheeting ribs and the beam smaller than 90° could be extended to beam tests. In that way, drawn conclusions regarding the response of shear connectors could be confirmed.

References

[1] M. Konrad, "Tragverhalten von Kopfbolzen in Verbundträgern bei senkrecht spannenden Trapezprofilblechen," Universität Stuttgart, 2011.

[2] C. Odenbreit and S. Nellinger, "Mechanical model to predict the resistance of the shear connection in composite beams with deep steel decking," *Steel Constr.*, vol. 10, no. 3, pp. 248–253, Aug. 2017.

[3] C. Odenbreit and V. Vigneri, "Headed studs in profiled steel sheeting transverse to the beam - Investigations on design resistance of headed stud shear connectors on the basis of the Final Draft of SC4.PT3, Rev. B," Luxembourg, 2021.

[4] M. Pavlović, "Resistance of bolted shear connectors in prefabricated steel-concrete composite decks," University of Belgrade, 2013.

[5] ANSI/AISC360-16, *Specification for Structural Steel Buildings*. Chicago: American Institute of Steel Construction, 2016.

[6] EN1992-1-1, *Eurocode 2: Design of Concrete Structures. Part 1-1: general rules and rules for buildings*. Brussels: CEN, 2004.

[7] EN1993-1-8, *Eurocode 3: Design of steel structures. Part 1-8: Design of joints*. Brussels: CEN, 2005.

[8] CEB-FIP, *Model Code for Concrete Structures 2010*. Berlin: Wilhelm Ernst & Sohn, 2010.

[9] Abaqus/CAE, *User's Guide*. Providence: DS SIMULIA Corp., 2009.

[10] EN1994-1-1, *Eurocode 4: Design of composite steel and concrete structures. Part 1-1: General rules and rules for buildings*. Brussels: CEN, 2004.

[11] V. Birtel and P. Mark, "Parameterised Finite Element Modelling of RC Beam Shear Failure," in *ABAQUS Users' Conference*, 2006, pp. 95–108.

[12] A. M. Girão Coelho *et al.*, *Guidance on demountable composite construction systems for UK practice*. Ascot: SCI, 2020.

[13] D. J. Carreira and K.-H. Chu, "Stress-strain relationship for plain concrete in compression," *ACI J.*, vol. 82, no. 6, pp. 797–804, 1985.

[14] G. Brambilla, M. Lavagna, G. Vasdravellis, and C. A. Castiglioni, "Environmental benefits arising from demountable steel-concrete composite floor systems in buildings," *Resour. Conserv. Recycl.*, vol. 141, no. 1, pp. 133–142, 2019.

[15] L. N. Dallam, "Pushout tests with high strength bolt shear connectors," Missouri State Highway Department, 1968.

[16] L. N. Dallam and J. L. Harpster, "Composite beam tests with high-strength bolt shear connectors," Missouri State Highway Department, 1968.

[17] W. Marshall, H. Nelson, and H. Banerjee, "An Experimental Study of the Use of High-Strength Friction Grip Bolts as Shear Connectors In Composite Beams," *Struct. Eng.*, vol. 49, no. 4, pp. 171–178, 1971.

[18] BS5400-5, *Steel, concrete and composite bridges Part 5: Code of practice for the design of composite bridges*. London: BSI, 1979.

[19] G. Kwon, M. D. Engelhardt, and R. E. Klingner, "Behavior of post-installed shear connectors under static and fatigue loading," *J. Constr. Steel Res.*, vol. 66, no. 4, pp. 532–541, Apr. 2010.

[20] G. Kwon, M. D. Engelhardt, and R. E. Klingner, "Experimental Behavior of Bridge Beams

Retrofitted with Postinstalled Shear Connectors," *J. Bridg. Eng.*, vol. 16, no. 4, pp. 536–545, Jul. 2011.

[21] G. Kwon, M. D. Engelhardt, and R. E. Klingner, "Parametric Studies and Preliminary Design Recommendations on the Use of Postinstalled Shear Connectors for Strengthening Noncomposite Steel Bridges," *J. Bridg. Eng.*, vol. 17, no. 2, pp. 310–317, Mar. 2012.

[22] X. Liu, M. A. Bradford, and M. S. S. Lee, "Behavior of High-Strength Friction-Grip Bolted Shear Connectors in Sustainable Composite Beams," *J. Struct. Eng.*, vol. 141, no. 6, p. 04014149, Jun. 2015.

[23] X. Liu, M. A. Bradford, Q.-J. Chen, and H. Ban, "Finite element modelling of steel-concrete composite beams with high-strength friction-grip bolt shear connectors," *Finite Elem. Anal. Des.*, vol. 108, no. 1, pp. 54–65, Jan. 2016.

[24] A. Ataei, M. A. Bradford, and X. Liu, "Experimental study of composite beams having a precast geopolymer concrete slab and deconstructable bolted shear connectors," *Eng. Struct.*, vol. 114, no. 1, pp. 1–13, May 2016.

[25] X. Liu, M. A. Bradford, and A. Ataei, "Flexural performance of innovative sustainable composite steel-concrete beams," *Eng. Struct.*, vol. 130, no. 1, pp. 282–296, Jan. 2017.

[26] M. Rowe and M. A. Bradford, "Partial Shear Interaction in Deconstructable Steel-Concrete Composite Beams with Bolted Shear Connectors," in *Design, Fabrication and Economy of Metal Structures - International Conference Proceedings*, 2013, pp. 585–590.

[27] Y.-T. Chen, Y. Zhao, J. S. West, and S. Walbridge, "Behaviour of steel–precast composite girders with through-bolt shear connectors under static loading," *J. Constr. Steel Res.*, vol. 103, no. 1, pp. 168–178, Dec. 2014.

[28] K. D. Balkos, M. Sjaarda, J. S. West, and S. Walbridge, "Static and Fatigue Tests of Steel-Precast Composite Beam Specimens with Through-Bolt Shear Connectors," *J. Bridg. Eng.*, vol. 24, no. 5, p. 04019036, 2019.

[29] A. Kozma, C. Odenbreit, M. V. Braun, M. Veljkovic, and M. P. Nijgh, "Push-out tests on demountable shear connectors of steel-concrete composite structures," *Structures*, vol. 21, no. April, pp. 0–1, 2019.

[30] C. Odenbreit and A. Kozma, "Dismountable Flooring Systems for Multiple Use," in *IOP Conference Series: Earth and Environmental Science*, 2019, vol. 225, no. 1, p. 012028.

[31] N. Fric, "Theoretical and experimental research of losses of pretension force in high strength bolts," University of Belgrade, 2015.

[32] N. M. Hawkins, "Strength in Shear and Tension of Cast-in-Place Anchor Bolts," *Spec. Publ.*, vol. 103, no. 1, pp. 233–256, Sep. 1987.

[33] X. H. Dai, D. Lam, and E. Saveri, "Effect of Concrete Strength and Stud Collar Size to Shear Capacity of Demountable Shear Connectors," *J. Struct. Eng.*, vol. 141, no. 11, p. 04015025, 2015.

[34] N. Rehman, D. Lam, X. Dai, and A. F. Ashour, "Experimental study on demountable shear connectors in composite slabs with profiled decking," *J. Constr. Steel Res.*, vol. 122, no. 1, pp. 178–189, 2016.

[35] N. Rehman, D. Lam, X. Dai, and A. Ashour, "Testing of composite beam with demountable shear connectors," *Proc. Inst. Civ. Eng. - Struct. Build.*, vol. 171, no. 1, pp. 3–16, 2018.

[36] J. Yang, D. Lam, X. Dai, and T. Sheehan, "Experimental study on demountable shear connectors in profiled composite slabs," in *Proceedings 12th international conference on Advances in Steel-Concrete Composite Structures - ASCCS 2018*, 2018, pp. 115–121.

[37] R. M. Sencu, Y. C. Wang, J. Yang, and D. Lam, "Performance evaluation of demountable shear connectors with collar step at ambient and elevated temperatures," *Eng. Struct.*, vol. 194, no. May, pp. 94–105, 2019.

[38] J. Y. Wang, J. Y. Guo, L. J. Jia, S. M. Chen, and Y. Dong, "Push-out tests of demountable headed stud shear connectors in steel-UHPC composite structures," *Compos. Struct.*, vol. 170, no. 1, pp. 69–79, 2017.

[39] M. Todorović, S. Kovačević, M. Pavlović, M. Spremić, and Z. Marković, "Behaviour of prefabricated steel-concrete composite bridge decks with grouped headed studs and bolted shear connectors," in *Proceedings of Eurosteel 2014*, 2014, pp. 1–6.

[40] D. J. Dedic and F. W. Klaiber, "High-strength bolts as shear connectors in rehabilitation work," *Concr. Int.*, vol. 6, no. 7, pp. 41–46, 1984.

[41] G. Sedlecek, B. Hoffmeister, H. Trumpf, and B. Kühn, "EUR 20583 - Steel structures: Composite bridge design for small and medium spans," Luxembourg, 2003.

[42] M. Pavlović, Z. Marković, M. Veljković, and D. Buđevac, "Bolted shear connectors vs. headed studs behaviour in push-out tests," *J. Constr. Steel Res.*, vol. 88, no. 1, pp. 134–149, Sep. 2013.

[43] M. C. Moynihan and J. M. Allwood, "Viability and performance of demountable composite connectors," *J. Constr. Steel Res.*, vol. 99, no. 1, pp. 47–56, Aug. 2014.

[44] A. Ataei, M. Zeynalian, and Y. Yazdi, "Cyclic behaviour of bolted shear connectors in steel-concrete composite beams," *Eng. Struct.*, vol. 198, no. November 2018, p. 109455, 2019.

[45] X. Dai, D. Lam, T. Sheehan, J. Yang, and K. Zhou, "Use of bolted shear connectors in composite construction," in *Proceedings 12th international conference on Advances in Steel-Concrete Composite Structures - ASCCS 2018*, 2018, pp. 475–482.

[46] I. E. J. Henderson, X. Q. Zhu, B. Uy, and O. Mirza, "Dynamic behaviour of steel-concrete composite beams with different types of shear connectors. Part I: Experimental study," *Eng. Struct.*, vol. 103, no. 1, pp. 298–307, 2015.

[47] I. E. J. Henderson, X. Q. Zhu, B. Uy, and O. Mirza, "Dynamic behaviour of steel-concrete composite beams with different types of shear connectors. Part II: Modelling and comparison," *Eng. Struct.*, vol. 103, no. 1, pp. 308–317, 2015.

[48] H. Ban, B. Uy, S. W. Pathirana, I. Henderson, O. Mirza, and X. Zhu, "Time-dependent behaviour of composite beams with blind bolts under sustained loads," *J. Constr. Steel Res.*, vol. 112, no. 1, pp. 196–207, 2015.

[49] S. W. Pathirana, B. Uy, O. Mirza, and X. Zhu, "Strengthening of existing composite steel-concrete beams utilising bolted shear connectors and welded studs," *J. Constr. Steel Res.*, vol. 114, no. 1, pp. 417–430, 2015.

[50] S. W. Pathirana, B. Uy, O. Mirza, and X. Zhu, "Flexural behaviour of composite steel-concrete beams utilising blind bolt shear connectors," *Eng. Struct.*, vol. 114, no. 1, pp. 181–194, 2016.

[51] S. W. Pathirana, B. Uy, O. Mirza, and X. Zhu, "Bolted and welded connectors for the rehabilitation of composite beams," *J. Constr. Steel Res.*, vol. 125, no. 1, pp. 61–73, 2016.

[52] E. L. Tan, H. Varsani, and F. Liao, "Experimental study on demountable steel-concrete connectors subjected to combined shear and tension," *Eng. Struct.*, vol. 183, no. 1, pp. 110–123, 2019.

[53] F. Yang, Y. Liu, Z. Jiang, and H. Xin, "Shear performance of a novel demountable steel-concrete bolted connector under static push-out tests," *Eng. Struct.*, vol. 160, no. August 2017, pp. 133–146, 2018.

[54] M. P. Nijgh, I. A. Gîrbacea, and M. Veljkovic, "Elastic behaviour of a tapered steel-concrete composite beam optimized for reuse," *Eng. Struct.*, vol. 183, no. 1, pp. 366–374, Mar. 2019.

[55] A. S. H. Suwaed and T. L. Karavasilis, "Novel Demountable Shear Connector for Accelerated Disassembly, Repair, or Replacement of Precast Steel-Concrete Composite Bridges," *J. Bridg. Eng.*, vol. 22, no. 9, p. 04017052, 2017.

[56] A. S. H. Suwaed and T. L. Karavasilis, "Removable shear connector for steel-concrete composite bridges," *Steel Compos. Struct.*, vol. 29, no. 1, pp. 107–123, 2018.

[57] L. Wang, M. D. Webster, and J. F. Hajjar, "Pushout tests on deconstructable steel-concrete shear connections in sustainable composite beams," *J. Constr. Steel Res.*, vol. 153, no. 1, pp. 618–637, 2019.

[58] M. Konrad and U. Kuhlmann, "Headed Studs Used in Trapezoidal Steel Sheeting According to Eurocode 4," *Struct. Eng. Int.*, vol. 19, no. 4, pp. 420–426, Nov. 2009.

[59] N. M. Hawkins and D. Mitchell, "Seismic Response of Composite Shear Connections," *J. Struct. Eng.*, vol. 110, no. 9, pp. 2120–2136, Sep. 1984.

[60] R. P. Johnson and H. Yuan, "Models and design rules for stud shear connectors in troughs of profiled sheeting," *Proc. Inst. Civ. Eng. - Struct. Build.*, vol. 128, no. 3, pp. 252–263, 1998.

[61] S. Nellinger, C. Odenbreit, R. Obiala, and M. Lawson, "Influence of transverse loading onto push-out tests with deep steel decking," *J. Constr. Steel Res.*, vol. 128, pp. 335–353, Jan. 2017.

[62] H. Lungershausen, "Zur Schubtragfähigkeit von Kopfbolzendübeln," Ruhr-Universität Bochum, 1988.

[63] V. Vigneri, C. Odenbreit, and D. Lam, "Different load bearing mechanisms in headed stud shear connectors for composite beams with profiled steel sheeting," *Steel Constr.*, vol. 12, no. 3, pp. 184–190, Aug. 2019.

[64] V. Vigneri, "Load bearing mechanisms of headed stud shear connections in profiled steel sheeting transverse to the beam," University of Luxembourg, 2021.

[65] J. Grant, J. Fisher, and R. Slutter, "Composite beams with formed steel deck," *Eng. J.*, vol. 14, no. 1, 1977.

[66] S. J. Hicks and A. L. Smith, "Stud Shear Connectors in Composite Beams that Support Slabs with Profiled Steel Sheeting," *Struct. Eng. Int.*, vol. 24, no. 2, pp. 246–253, May 2014.

[67] S. Nellinger, "On the behaviour of shear stud connections in composite beams with deep decking," University of Luxembourg, 2015.

[68] M. Rambo-Roddenberry, "Behavior and Strength of Welded Stud Shear Connectors," Virginia Polytechnic Institute and State University, 2002.

[69] S. Ernst, "Factors Affecting the Behaviour of the Shear Connection of Steel-Concrete Composite Beams," University of Western Sydney, 2006.

[70] M. Konrad, F. Eggert, U. Kuhlmann, and J. Schorr, "New approach for the design shear resistance of headed studs in profiled steel sheeting with ribs transverse to supporting beam," *Steel Constr.*, vol. 13, no. 4, pp. 252–263, 2020.

[71] ArcelorMittal, "Cofraplus® 60." [Online]. Available: https://construction.arcelormittal.com/fr-en/product/floors/composite-floors/cofraplus-60. [Accessed: 01-Aug-2021].

[72] R. M. Lawson *et al.*, "Development of Improved Shear Connection Rules in Composite Beams (DISCCO)," Luxembourg, 2017.

[73] F. Eggert, "Einfluss der Verdübelung auf das Trag- und Verformungsverhalten von Verbundträgern mit und ohne Profilblech," Universität Stuttgart, 2019.

[74] V. Vigneri, C. Odenbreit, and M. Braun, "Numerical evaluation of the plastic hinges developed in headed stud shear connectors in composite beams with profiled steel sheeting," *Structures*, vol. 21, pp. 103–110, Oct. 2019.

[75] J. Qureshi, D. Lam, and J. Ye, "Effect of shear connector spacing and layout on the shear connector capacity in composite beams," *J. Constr. Steel Res.*, vol. 67, no. 4, pp. 706–719, 2011.

[76] S. Ernst, M. Patrick, R. Bridge, and A. Wheeler, "Reinforcement Requirements for Secondary Composite Beams Incorporating Trapezoidal Decking," in *Composite Construction in Steel and Concrete V*, 2006, pp. 236–246.

[77] M. Patrick, "Experimental investigation and design of longitudinal shear reinforcement in composite edge beams," *Prog. Struct. Eng. Mater.*, vol. 2, no. 2, pp. 196–217, Apr. 2000.

[78] A. Albarram, J. Qureshi, and A. Abbas, "Effect of Rib Geometry in Steel-concrete Composite Beams with Deep Profiled Sheeting," *Int. J. Steel Struct.*, no. 0123456789, 2020.

[79] S. Ernst, R. Q. Bridge, and A. Wheeler, "Push-out tests and a new approach for the design of secondary composite beam shear connections," *J. Constr. Steel Res.*, vol. 65, no. 1, pp. 44–53, Jan. 2009.

[80] EN1991-1-1, *Eurocode 1: Actions on structures - Part 1-1: General actions - Densities, self-weight, imposed loads for buildings*. Brussels: CEN, 2002.

[81] Tata Steel, "ComFlor® 60." [Online]. Available: https://www.tatasteelconstruction.com/en_GB/Products/structural-buildings-and-bridges/Composite-floor-deck/Comflor®-60. [Accessed: 26-Apr-2021].

[82] Kingspan, "Multideck 60-V2." [Online]. Available: https://www.kingspan.com/gb/en-gb/products/structural-steel-solutions/structural-steel-products/multideck. [Accessed: 26-Apr-2021].

[83] EN1990:2002, *Eurocode - Basis of structural design*. Brussels: CEN, 2002.

[84] ISO6892-1:2009, *Metallic materials - Tensile testing - Part 1: Method of test at room temperature*. Brussels: CEN, 2009.

[85] I. Arrayago, E. Real, and L. Gardner, "Description of stress-strain curves for stainless steel alloys," *Mater. Des.*, vol. 87, pp. 540–552, Dec. 2015.

[86] M. Spremić, "Analiza ponašanja grupe elastičnih moždanika kod spregnutih nosača od čelika i betona," University of Belgrade, 2013.

[87] N. Gluhović, "Behaviour of shear connections realised by connectors fastened with cartridge fired pins," University of Belgrade, 2019.

[88] W. B. Krätzig and R. Pölling, "An elasto-plastic damage model for reinforced concrete with minimum number of material parameters," *Comput. Struct.*, vol. 82, no. 15–16, pp. 1201–1215, 2004.

[89] X. Xu, Y. Liu, and J. He, "Study on mechanical behavior of rubber-sleeved studs for steel and concrete composite structures," *Constr. Build. Mater.*, vol. 53, pp. 533–546, 2014.

Annex A: Concrete Damage Plasticity Models

To develop finite element models that realistically simulate the conducted push-out tests, several concrete damage models were considered. Besides the model proposed by Pavlović [4] described in Subchapter 5.1.3, models given by Carreira and Chu [13], Birtel and Mark [11] and Vigneri [64] were analysed. Different concrete damage material models and obtained results are presented in the following.

A.1 Model according to Carreira and Chu

Carreira and Chu [13] described concrete compression behaviour using a stress-strain curve according to the following equation:

$$\sigma_c(\varepsilon_c) = f_{cm} \frac{\beta \, (\varepsilon_c/\varepsilon_{c1})}{\beta - 1 + (\varepsilon_c/\varepsilon_{c1})^\beta} \tag{A.1}$$

where:

$$\beta = \left(\frac{f_{cm}}{32.4 \text{ MPa}}\right)^3 + 1.55 \tag{A.2}$$

f_{cm} is the mean value of the cylinder compressive strength of concrete in MPa;

ε_{c1} is the compressive strain in the concrete at f_{cm}.

This stress-strain relation was applied to the numerical model to simulate concrete compression behaviour for strains larger than ε_{c1}. For strains smaller than ε_{c1}, the stress-strain curve given in EN 1992-1-1:2004 [6] was implemented. Concrete compression damage was introduced using the damage variable D_c, according to Eq. (5.5). In numerical simulations, this compressive model was applied in combination with the tensile model presented in Subchapter 5.1.3.

A.2 Model according to Birtel and Mark

Birtel and Mark [11] used the following stress-strain relation, previously elaborated by Krätzig and Pölling [88] for strains larger than ε_{c1}:

$$\sigma_c(\varepsilon_c) = \left(\frac{2 + \gamma_c f_{cm}\varepsilon_{c1}}{2f_{cm}} - \gamma_c\varepsilon_c + \frac{\gamma_c\varepsilon_c^2}{2\varepsilon_{c1}}\right)^{-1} \tag{A.3}$$

where γ_c is the parameter that defines the area under the stress-strain curve. Xu et al. [89] adopted this parameter as 1.7 for modelling shear connection with headed studs. The same value was used in this study.

Furthermore, Birtel and Mark proposed the expression for obtaining the compressive damage variable D_c:

$$D_c = 1 - \frac{\sigma_c/E_{cm}}{\varepsilon_c^{pl}(1/b_c - 1) + \sigma_c/E_{cm}} \tag{A.4}$$

where:

ε_c^{pl} is the plastic strain defined as inelastic strain multiplied by the factor b_c, $0 < b_c \leq 1$,

$$\varepsilon_c^{pl} = b_c(\varepsilon_c - \sigma_c/E_{cm}) \tag{A.5}$$

E_{cm} is the secant modulus of elasticity of concrete.

The proposed value of the factor b_c is 0.7.

Instead of applying the stress-strain curve to define the tensile behaviour of concrete, Birtel and Mark used the following relation between the stress and crack opening:

$$\sigma_t(w) = f_{ctm}\left[g(w) - \left(\frac{w}{w_c}\right)g(w_c)\right]$$ (A.6)

where:

$$g(w) = \left[1 + \left(\frac{3w}{w_c}\right)^3\right]e^{\left(-\frac{6.93w}{w_c}\right)}$$ (A.7)

w is the crack opening,

$$w = 5.14\frac{G_F}{f_{ctm}}$$ (A.8)

w_c is the critical value of the crack opening at which tensile stress cannot be transferred;

f_{ctm} is the mean value of the concrete tensile strength;

G_F is the fracture energy, which is the function of the concrete compressive strength according to Model Code 2010 [8].

Similarly to compressive damage, Birtel and Mark defined the tensile damage variable D_t:

$$D_t = 1 - \frac{\sigma_t/E_{cm}}{\varepsilon_t^{pl}(1/b_t - 1) + \sigma_t/E_{cm}}$$ (A.9)

where ε_t^{pl} is the plastic strain defined as inelastic strain multiplied by the factor b_t, $0 < b_t \leq 1$,

$$\varepsilon_t^{pl} = b_t(\varepsilon_t - \sigma_t/E_{cm})$$ (A.10)

The proposed value of the factor b_t is 0.1.

A.3 Model according to Vigneri

Vigneri [64] used the following relation to simulate concrete compressive response:

$$\sigma_c(\varepsilon_c) = f_{cm}\frac{n\left(\frac{\varepsilon_c}{\varepsilon_{c1}}\right)}{(n-1) + \left(\frac{\varepsilon_c}{\varepsilon_{c1}}\right)^n}$$ (A.11)

where:

$$n = 1.25\left(0.058f_{cm} + 1 \text{ MPa}\right)$$ (A.12)

f_{cm} is the mean value of the cylinder compressive strength of concrete in MPa;

ε_{c1} is the compressive strain in the concrete at f_{cm}.

Eq. (A.11) was used to describe the total stress-strain curve. Concrete compressive damage was applied according to Eq. (A.4).

To model concrete tensile behaviour, Vigneri implemented the same procedure as proposed by Birtel and Mark through Eq. (A.6)–(A.8). However, Vigneri did not use Eq. (A.9) to define tensile damage variable; instead, Eq. (5.6) was applied.

A.4 Comparisons between Concrete Damage Plasticity Models

Different stress-strain curves for concrete response under uniaxial compression and corresponding concrete damage-inelastic strain relations are compared in Figure A.1. Besides models presented in this Annex, the model proposed by Pavlović with the originally selected parameters and those adopted in this research (Table 5.2) is given in the graph. Furthermore, stress-crack opening and tensile damage-crack opening curves according to Vigneri are presented in Figure A.2.
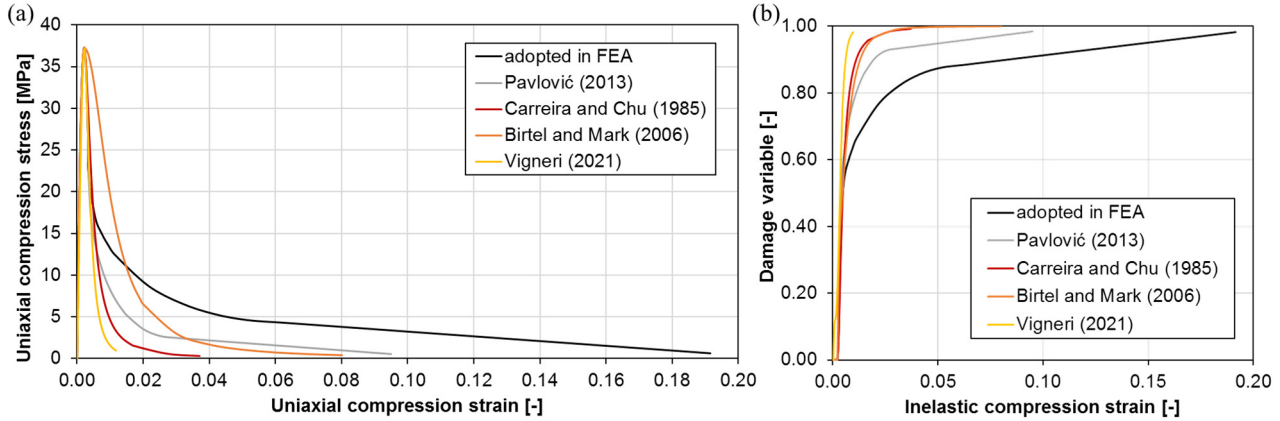
Figure A.1: Concrete behaviour in compression (f_{cm} = 37.3 MPa):
(a) stress-strain curves, (b) compression damage.
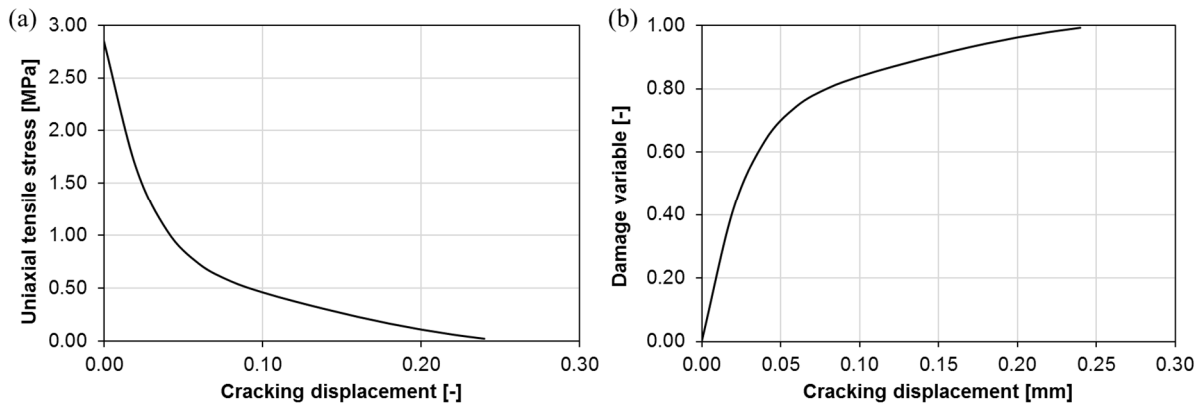
Figure A.2: Concrete behaviour in tension according to Vigneri (f_{cm} = 37.3 MPa):
(a) stress-crack opening curve, (b) tension damage.

Listed concrete material models are applied to push-out models and load-slip curves are compared to the experimental ones. As shown in Figure A.3.a, the model given by Birtel and Mark [11] overestimates the connection resistance and the load-slip curve does not follow the shape of experimental results for the specimen DLU. The model according to Carreira and Chu [13] predicts lower shear resistance and slip capacity than experimentally obtained. Similar results are observed applying the model proposed by Pavlović with the originally selected parameters [4].

Best matches between experimental and numerical results for model DLU are observed for the concrete damage model used by Vigneri [64] and the final adopted concrete damage model described in Subchapter 5.1.3. However, the model according to Vigneri does not provide good predictions for connections with angles between profiled sheeting ribs and the beam smaller than 90°. An example is specimen S45 where a considerable decrease in the connection stiffness is noticed for loads above 200 kN, as presented in Figure A.3.b. Therefore, the model proposed by Pavlović with the calibrated parameters listed in Table 5.2 is used in all numerical simulations of push-out tests.

Figure A.3: Load-slip curves for different concrete damage plasticity models:
(a) model DLU, (b) model S45.

Annex B: Database of Experimental Push-Out Tests with Cofraplus 60

Table B.1: Database of experimental results of push-out tests with profiled steel sheeting Cofraplus 60.

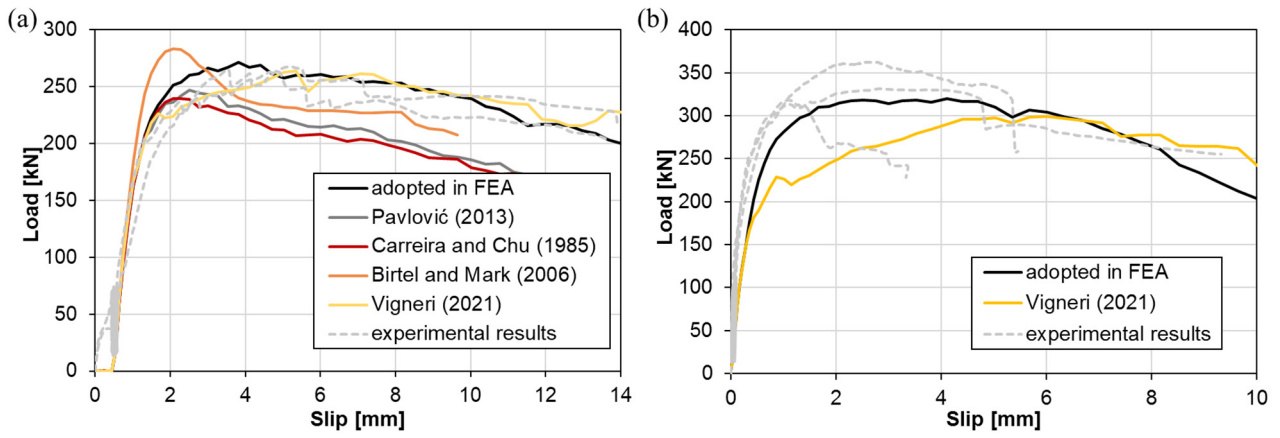| Resource	Specimen	Stud diameter d [mm]	Stud height h_{sc} [mm]	Slab depth h [mm]	Transverse spacing between studs e_t [mm]	Number of studs in a rib -	Stud tensile strength f_u [MPa]	Concrete compressive strength f_{cm} [MPa]	Concrete modulus of elasticity E_{cm} [GPa]	WT – welded through profiled sheeting PP – profiled sheeting with pre-punched holes	T – only top reinforcement B – only bottom reinforcement TB – top + bottom reinforcement	Ultimate load per connector $P_{ult,exp}$ [kN]
DISCCO report [72]	1.04.1*	22.16	124.3	150	-	1	551.0	30.1	20.90	PP	TB	73.91
	1.04.2*	22.24	124.0	150	-	1	551.0	30.9	21.50	PP	TB	73.61
	1.04.3*	22.20	123.9	150	-	1	551.0	30.9	21.50	PP	TB	68.66
	1.05.1*	22.16	124.0	150	-	1	551.0	30.0	22.10	PP	TB	69.95
	1.05.2*	22.17	123.8	150	-	1	551.0	30.7	22.10	PP	TB	79.15
	1.05.3*	22.20	123.9	150	-	1	551.0	32.6	22.80	PP	TB	74.43
	1.03.1	22.14	123.3	150	-	1	514.0	41.0	33.59	PP	TB	81.50
	1.03.2	22.10	122.0	150	-	1	514.0	42.5	33.96	PP	TB	93.88
	1.03.3	22.22	122.7	150	-	1	514.0	42.9	34.05	PP	TB	97.13
	2.01.1	19.10	121.7	150	-	1	467.0	42.4	33.93	WT	T	65.25
	2.01.2	19.12	121.7	150	-	1	467.0	42.6	33.98	WT	T	70.13
	2.01.3	19.23	122.0	150	-	1	467.0	41.8	33.79	WT	T	74.88
	2.02.1	19.00	122.5	150	-	1	467.0	40.7	33.52	WT	TB	69.88
	2.03.1	19.00	121.7	150	-	1	467.0	39.7	33.27	PP	T	57.63
	2.04.1	19.00	120.6	150	100	2	467.0	40.3	33.42	WT	T	68.38
	2.05.1	19.00	121.0	150	100	2	467.0	40.2	33.40	WT	TB	65.63
	2.05.2	19.00	121.7	150	100	2	467.0	38.6	32.99	WT	TB	71.06
	2.05.3	19.00	121.7	150	100	2	467.0	39.2	33.14	WT	TB	67.06
	2.06.1	22.20	122.2	150	-	1	514.0	40.1	33.37	PP	T	87.50
	2.06.2	22.22	122.2	150	-	1	514.0	39.6	33.25	PP	T	101.60
	2.06.3	22.25	122.2	150	-	1	514.0	40.6	33.50	PP	T	96.50
	2.07.1	22.17	121.7	150	-	1	514.0	46.4	34.86	PP	TB	114.60
	2.07.2	22.32	122.2	150	-	1	514.0	46.3	34.84	PP	TB	112.40
	2.07.3	22.33	122.2	150	-	1	514.0	46.0	34.77	PP	TB	107.60
	2.08.1	19.09	122.0	150	-	1	467.0	45.8	34.73	PP	TB	59.10
Vigneri [64]	CP12A.1	19.00	98.0	120	-	1	551.0	42.2	33.89	PP	B	68.31
	CP12A.2	19.00	98.0	120	-	1	551.0	42.9	34.05	PP	B	65.25
	CP12A.3	19.00	98.0	120	-	1	551.0	44.0	34.31	PP	B	69.48
	CP14A.2	19.00	98.0	140	-	1	551.0	49.7	35.59	PP	B	72.35
	CP14A.3	19.00	98.0	140	-	1	551.0	50.2	35.70	PP	B	82.47
	CP14B.1	19.00	98.0	140	-	1	551.0	50.7	35.80	PP	T	85.46
	CP14B.2	19.00	98.0	140	-	1	551.0	50.8	35.82	PP	T	80.45
	CP14B.3	19.00	98.0	140	-	1	551.0	51.1	35.89	PP	T	88.70
	CP14D.1	19.00	125.0	140	-	1	504.3	43.5	34.20	PP	B	80.33
	CP14D.2	19.00	125.0	140	-	1	504.3	43.7	34.24	PP	B	87.31
	CP14D.3	19.00	125.0	140	-	1	504.3	44.2	34.36	PP	B	85.19
	CP14C.2	19.00	94.0	140	-	1	551.0	51.9	36.06	WT	T	83.54
	CP14C.3	19.00	94.0	140	-	1	551.0	52.0	36.08	WT	T	85.08
Jakovljević	S-02	16.00	100.0	120	100	2	509.0	35.0	32.03	PP	T	34.25
	S-03	16.00	100.0	120	100	2	509.0	35.0	32.03	PP	T	31.89
	D-01**	16.00	100.0	120	100	2	509.0	34.5	31.89	PP	T	30.50
	D-02**	16.00	100.0	120	100	2	509.0	34.5	31.89	PP	T	30.63
	D-03**	16.00	100.0	120	100	2	509.0	34.5	31.89	PP	T	29.94

*transverse loading was applied during the testing; **demountable specimens with bolts and welded headed studs

Curriculum Vitae

Isidora Jakovljević was born in Belgrade, Serbia, on February 7th, 1993. She completed elementary and high school in Belgrade. While attending high school, she also attended educational programs at Petnica Science Centre in Serbia.

She enrolled at the University of Belgrade, Faculty of Civil Engineering in 2012. After completing her undergraduate studies, she started her master studies in the field of Structural Engineering in 2016. She participated in several student conferences and competitions. In the summer of 2015, she did an internship at the University of Exeter, UK, at the Vibration Engineering Research Section. In September and October 2016, she worked as an intern at the Federal Institute for Materials Research and Testing in Berlin, Germany, in Division 7.4, Technology of Construction Materials. She won several awards and scholarships, including the award received from the Prof. Milan Đurić Fund for the outstanding results in the Theory of Structures courses in 2015, the award for the best student graduating from the Faculty of Civil Engineering in 2016, and the award received from the Prof. Branko Zarić Fund for the best master's thesis in the field of Steel Structures in 2017.

In 2017, she started her PhD studies at the University of Belgrade, Faculty of Civil Engineering in the field of Steel Structures. She is the author and co-author of several journal papers and papers in international conference proceedings. In 2018, she participated in the Training School Advances in Wind Energy Technology in Bratislava, Slovakia, under COST Action TU1304. In the same year, she attended the Bauhaus Summer School of Forecast Engineering in Weimar, Germany. She received an award from the Serbian Association of Structural Engineers for the best scientific paper authored by a young researcher in 2018.

Since 2018, she has worked as a teaching assistant at the University of Belgrade, Faculty of Civil Engineering. She participates in the preparation and implementation of undergraduate courses in the field of Steel Structures. She attended two training programs for the teaching staff of the University of Belgrade: TRAIN – Training and Research for Academic Newcomers (2018–2019) and EMI – English as a Medium of Instruction (2019–2020). As part of her professional work, she participated in the preparation of several projects involving industrial steel structures.

Изјава о ауторству

Име и презиме аутора: Исидора Јаковљевић

Број индекса: 902/17

Изјављујем

да је докторска дисертација под насловом

DEMOUNTABLE SHEAR CONNECTIONS WITH BOLTS AND WELDED HEADED STUDS IN STEEL-CONCRETE COMPOSITE STRUCTURES

наслов на српском језику:

ДЕМОНТАЖНИ СМИЧУЋИ СПОЈЕВИ ОСТВАРЕНИ ЗАВРТЊЕВИМА И МОЖДАНИЦИМА СА ГЛАВОМ КОД СПРЕГНУТИХ КОНСТРУКЦИЈА ОД ЧЕЛИКА И БЕТОНА

- резултат сопственог истраживачког рада;
- да дисертација у целини ни у деловима није била предложена за стицање друге дипломе према студијским програмима других високошколских установа;
- да су резултати коректно наведени и
- да нисам кршио/ла ауторска права и користио/ла интелектуалну својину других лица.

Потпис аутора

У Београду, април 2022.

_____

Изјава о истоветности штампане и електронске верзије докторског рада

Име и презиме аутора: Исидора Јаковљевић

Број индекса: 902/17

Студијски програм: Грађевинарство

Наслов рада:

DEMOUNTABLE SHEAR CONNECTIONS WITH BOLTS AND WELDED HEADED STUDS IN STEEL-CONCRETE COMPOSITE STRUCTURES

Наслов на српском језику:

ДЕМОНТАЖНИ СМИЧУЋИ СПОЈЕВИ ОСТВАРЕНИ ЗАВРТЊЕВИМА И МОЖДАНИЦИМА СА ГЛАВОМ КОД СПРЕГНУТИХ КОНСТРУКЦИЈА ОД ЧЕЛИКА И БЕТОНА

Ментори: проф. др Златко Марковић, дипл. грађ. инж.

в. проф. др Милан Спремић, дипл. грађ. инж.

Изјављујем да је штампана верзија мог докторског рада истоветна електронској верзији коју сам предао/ла ради похрањена у **Дигиталном репозиторијуму Универзитета у Београду.**

Дозвољавам да се објаве моји лични подаци везани за добијање академског назива доктора наука, као што су име и презиме, година и место рођења и датум одбране рада.

Ови лични подаци могу се објавити на мрежним страницама дигиталне библиотеке, у електронском каталогу и у публикацијама Универзитета у Београду.

Потпис аутора

У Београду, април 2022.

_____

Изјава о коришћењу

Овлашћујем Универзитетску библиотеку „Светозар Марковић" да у Дигитални репозиторијум Универзитета у Београду унесе моју докторску дисертацију под насловом:

DEMOUNTABLE SHEAR CONNECTIONS WITH BOLTS AND WELDED HEADED STUDS IN STEEL-CONCRETE COMPOSITE STRUCTURES

Наслов на српском језику:

ДЕМОНТАЖНИ СМИЧУЋИ СПОЈЕВИ ОСТВАРЕНИ ЗАВРТЊЕВИМА И МОЖДАНИЦИМА СА ГЛАВОМ КОД СПРЕГНУТИХ КОНСТРУКЦИЈА ОД ЧЕЛИКА И БЕТОНА

која је моје ауторско дело.

Дисертацију са свим прилозима предао/ла сам у електронском формату погодном за трајно архивирање.

Моју докторску дисертацију похрањену у Дигиталном репозиторијуму Универзитета у Београду и доступну у отвореном приступу могу да користе сви који поштују одредбе садржане у одабраном типу лиценце Креативне заједнице (Creative Commons) за коју сам се одлучио/ла.

1. Ауторство (CC BY)

2. Ауторство – некомерцијално (CC BY-NC)

③. Ауторство – некомерцијално – без прерада (CC BY-NC-ND)

4. Ауторство – некомерцијално – делити под истим условима (CC BY-NC-SA)

5. Ауторство – без прерада (CC BY-ND)

6. Ауторство – делити под истим условима (CC BY-SA)

(Молимо да заокружите само једну од шест понуђених лиценци.
 Кратак опис лиценци је саставни део ове изјаве).

Потпис аутора

У Београду, април 2022.

_____

1. **Ауторство**. Дозвољавате умножавање, дистрибуцију и јавно саопштавање дела, и прераде, ако се наведе име аутора на начин одређен од стране аутора или даваоца лиценце, чак и у комерцијалне сврхе. Ово је најслободнија од свих лиценци.

2. **Ауторство – некомерцијално**. Дозвољавате умножавање, дистрибуцију и јавно саопштавање дела, и прераде, ако се наведе име аутора на начин одређен од стране аутора или даваоца лиценце. Ова лиценца не дозвољава комерцијалну употребу дела.

3. **Ауторство – некомерцијално – без прерада**. Дозвољавате умножавање, дистрибуцију и јавно саопштавање дела, без промена, преобликовања или употребе дела у свом делу, ако се наведе име аутора на начин одређен од стране аутора или даваоца лиценце. Ова лиценца не дозвољава комерцијалну употребу дела. У односу на све остале лиценце, овом лиценцом се ограничава највећи обим права коришћења дела.

 4. **Ауторство – некомерцијално – делити под истим условима**. Дозвољавате умножавање, дистрибуцију и јавно саопштавање дела, и прераде, ако се наведе име аутора на начин одређен од стране аутора или даваоца лиценце и ако се прерада дистрибуира под истом или сличном лиценцом. Ова лиценца не дозвољава комерцијалну употребу дела и прерада.

5. **Ауторство – без прерада**. Дозвољавате умножавање, дистрибуцију и јавно саопштавање дела, без промена, преобликовања или употребе дела у свом делу, ако се наведе име аутора на начин одређен од стране аутора или даваоца лиценце. Ова лиценца дозвољава комерцијалну употребу дела.

6. **Ауторство – делити под истим условима**. Дозвољавате умножавање, дистрибуцију и јавно саопштавање дела, и прераде, ако се наведе име аутора на начин одређен од стране аутора или даваоца лиценце и ако се прерада дистрибуира под истом или сличном лиценцом. Ова лиценца дозвољава комерцијалну употребу дела и прерада. Слична је софтверским лиценцама, односно лиценцама отвореног кода.